A HARDWARE-BASED TRANSIENT CHARACTERIZATION OF ELECTROCHEMICAL START-UP IN AN SOFC/GAS TURBINE HYBRID ENVIRONMENT USING A 1-D REAL TIME SOFC MODEL

A Dissertation
Presented to
The Academic Faculty

by

Dimitri O. Hughes

In Partial Fulfillment
of the Requirements for the Degree
Doctor of Philosophy in the
School of Mechanical Engineering

Georgia Institute of Technology
August 2011

A HARDWARE-BASED TRANSIENT CHARACTERIZATION OF ELECTROCHEMICAL START-UP IN AN SOFC/GAS TURBINE HYBRID ENVIRONMENT USING A 1-D REAL TIME SOFC MODEL

Approved by:

Dr. Comas L. Haynes, Co-Advisor
Center for Innovative Fuel Cell and Battery Technologies
Georgia Tech Research Institute

Dr. Sheldon Jeter
School of Mechanical Engineering
Georgia Institute of Technology

Dr. William J. Wepfer, Co-Advisor
School of Mechanical Engineering
Georgia Institute of Technology

Dr. Melin Liu
Material Science
Georgia Institute of Technology

Dr. Samuel Graham
School of Mechanical Engineering
Georgia Institute of Technology

Dr. David Tucker
Advanced Fuel Cell Division
National Energy Technology Laboratory

Date Approved: July 7th, 2011

To the SOURCE, To the CAUSE, To the VISION, To the CALLING.

Jeremiah 29:11

ACKNOWLEDGEMENTS

The utmost thanks goes to my Lord and Savior Jesus Christ. It is only through the grace and mercy of the Father that I had the adequate blessings to endeavor on this journey and I humbly acknowledge that I was merely a tool that He used to conduct the work encapsulated in this dissertation. I must also acknowledge one of the premier blessings bestowed upon me by my Lord and Savior, my mother, Wenora Hughes. Mama, your continuous words of love and encouragement, your support financial, emotional and otherwise, all played a tremendous and vital role in the navigation of this journey. I love you. You are an awesome and phenomenal woman. To all those who came before us and opened up the books of wisdom, knowledge, and experience to assist us in navigating the Ph.D. journey. To all of the C. Greens, J. Wilsons, the J.C. Fords, the O. Smarts, J. Fairleys, the S. Remys, and all the other Ph.D. pioneers. You not only paved the way but you led us down the path and let us free when we were ready to navigate alone. You also engrained in us an innate desire to embraced our responsibility to do the same for those coming after. Much appreciation to all of the journey companions, particularly the BGSA class of 2005. You all provided a myriad of support, love, friendship and understanding. You were so vital in the process and I can truly say I love each and every one of you. To all of those who didn't believe in me (and thus didn't believe in the awesomeness of God), who didn't support me, who thought it couldn't be done. For the ones who this journey was completed in spite of. Thank you for the drive and the motivation. To all those who played a tremendous role but that I have forgotten, much thanks. So many people have played a significant role in this journey and I recognize that some may have been overlooked in the composition of this single page of acknowledgements, but understand that your contribution and commitment do not go unacknowledged or unappreciated. To my fiancee', Joyette Mitchell, I Love You. Thank you for navigating the end of this journey with me and for embarking on the lifelong one ahead. God bless.

TABLE OF CONTENTS

LIST OF TABLES

LIST OF FIGURES

LIST OF SYMBOLS AND ABBREVIATIONS

A	Area
E_{an}	Anode direct internal reformation activation energy
Q_{gen} total	Total subsystem thermal effluent
Q_{gen} local	Local solid oxide fuel cell heat generation
BA	Bleed Air
BOP	Balance of Plant
C_p	Heat capacity
CA	Cold Air
D	Diffusion coefficient
DIR	Direct Internal Reformation
F	Faraday's Constant
FC	Fuel Cell
GT	Gas Turbine
HH	Humidified Hydrogen
HS	Hybrid System
HiLS	Hardware-in-the-Loop Simulation
i	Current density
IP	Integrated Planar
K	Thermal conductivity
NETL	National Energy Technology Laboratory
p	Pressure
R_u	Universal gas constant
SECA	Solid State Energy Conversion Alliance
SOFC	Solid Oxide Fuel Cell

T	Temperature
TPB	Triple Phase Boundary
V	Voltage
β	implicit/explicit weighting factor
γ_{sr}	Pre-exponential factor for direct internal reformation of methane
δ	thickness
ΔG°	Gibbs free energy of formation
ε	Porosity
η	Polarization Loss
ρ	Electrical resistivity (ohmic loss), Density (heat diffusion equation)
τ	Tortuosity

SUMMARY

Solid oxide fuel cell/gas turbine (SOFC/GT) hybrid systems harness the capability to operate nearly 15 to 20 percentage points more efficiently than standard natural gas or pulverized coal power plants. Though the performance of these systems is quite promising, a number of system integration challenges, primarily with regards to thermal transport, still remain. Though pre-existing research efforts have attempted to address these challenges individually for each subsystem, the coupled nature of hybridization, which includes system balance of plant feedback as well as dynamic response, demands that these challenges be likewise addressed in coupled manner. It is for that reason that the HyPer facility, a Hardware-in-the-Loop SOFC/GT hybrid simulator, was built at the National Energy Technology Laboratory in Morgantown, WV. The HyPer facility couples an actual gas turbine with a combination of hardware and software that are used to simulate an actual SOFC. The facility is used to empirically address the system integration issues associated with fuel cell/gas turbine hybrids. Through this dissertation project, the software component of the SOFC simulator was upgraded from a 0-D lumped SOFC model to a 1-D, distributed, real-time operating SOFC model capable of spatio-temporal characterization of a fuel cell operating with a gas turbine in a hybrid arrangement. Once completed and verified, the upgraded HyPer facility was used to characterize the impact of cold air by-pass and initial fuel cell load on electrochemical start-up in an SOFC/GT hybrid environment. The impact of start-up on fuel cell inlet process parameters, SOFC performance and SOFC distributed behavior are presented and analyzed in comparative manner. This study represents the first time that an empirical parametric study, characterizing system operation during electrochemical start-up has been conducted. The results and findings of this study can be used to design control mechanisms for hybrid systems to ensure safe and reliable system operation during electrochemical start-up.

CHAPTER 1

INTRODUCTION

1.1: Energy Arena Overview

Given the increase in world population, the elevated per capita consumption of fossil fuels, and the apparent deleterious environmental impact of our current energy practices, development of more sustainable, reliable, and environmentally benign power producing mechanisms is paramount [1-3]. Power producing technologies that have the ability to increase operational efficiency and decrease harmful emissions, all the while utilizing fossil and other carbon-based fuels, are likely candidates to aid the transformation to a more effective energy infrastructure.

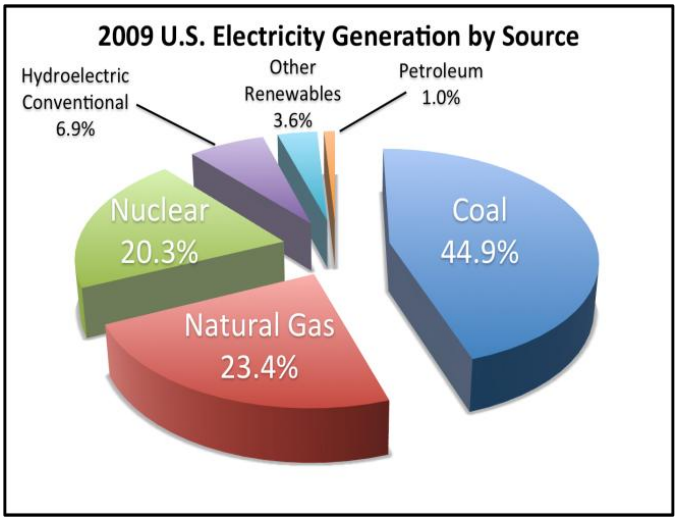

Figure 1.1: U.S. electricity generation breakdown by fuel source

Large-scale electrical power production in the United States is typically accomplished through coal and natural gas fueled power plants. As illustrated in Figure 1.1, in 2009, 44.9% and 23.4% of the electricity produced in the U.S. was done via coal and natural gas, respectively [4]. Currently, power plants operate between 35 – 40% efficiency when in the sub-critical regime, but exceptions have exhibited efficiencies

beyond 50% when employing ultra-critical operation as reported by the world coal institute [5]. Given that nearly 70% of the nation's electricity is produced from fossil fuels, there is compelling motivation to investigate and develop more highly efficient power-generating technologies within this sector.

Our current energy infrastructure is primarily dependent upon fossil fuel consuming technologies that pose significant economic and environmental threats [2, 3]. Given the inertia of fossil fuels within our society, however, fossil fuel based power systems with the potential to increase efficiency and improve environmental impact would be extremely valuable. Select fuel cell technologies, primarily characterized by elevated efficiencies and lower emissions, make them strong candidates for performance enhancement of fossil fuel based systems. To that end the development of a hybrid system that can both operate within our current energy framework but can leverage the advantages of a highly efficient, alternative power producing technology is significant in addressing the necessary dynamic change in our energy arena. This project thus focuses on enabling aids to the development of solid oxide fuel cell / gas turbine hybrid power plants.

1.2: Solid Oxide Fuel Cell / Gas Turbine (SOFC/GT) Hybrid Systems

SOFC/GT hybrid systems dynamically couple gas turbines and solid oxide fuel cells for the purpose of producing highly efficient, large scale, stationary power. Currently, most stationary power plants can be generally described by the schematic presented in Figure 1.2.

This diagram illustrates a basic open thermodynamic system used to produce rotational power via the expansion of a gaseous working fluid through a turbine. The power cycle successively includes compression, heat input, and expansion of some externally acquired working fluid. Net power output is illustrated on the schematic as well.

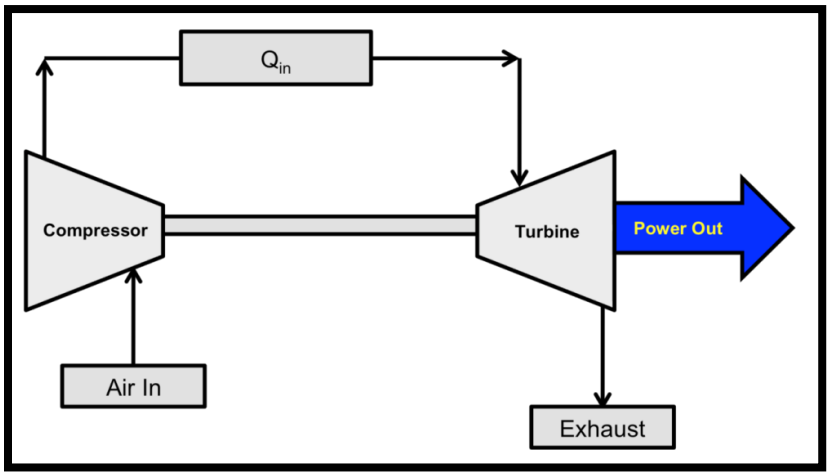

Figure 1.2: Generic open system for stationary power

Figure 1.3 illustrates a similar type of power system with the heat source replaced with a SOFC stack. As illustrated one of the key advantages of using this type of power cycle as opposed to the one illustrated in Figure 1.2 is the conversion of the heat source to a combined heat source and power source. This conversion of the standard heat source, which is typically a combustor or a high temperature heat exchanger to a joint heat and power source operating at an efficiency of over 50% is the key driver behind gains in overall system efficiency of 15-20 percentage points, as achieved through SOFC/GT hybridization [5].

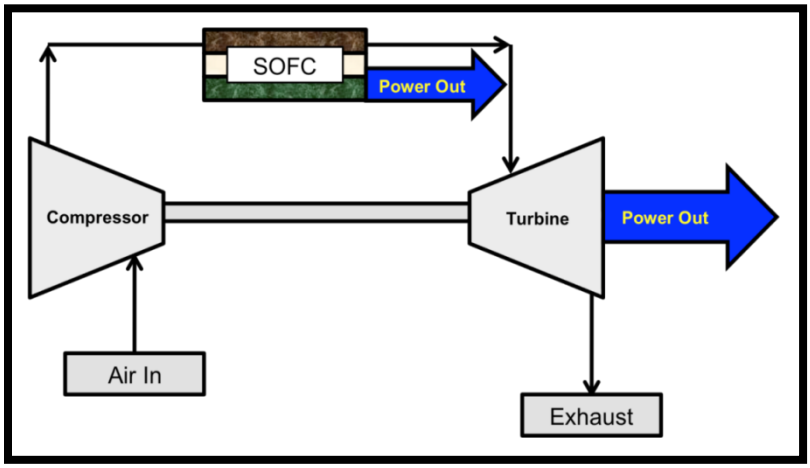

Figure 1.3: Generic SOFC/GT hybrid system for stationary power

State of the art power systems employ a number of design techniques and methodologies to increase system efficiency such as, but not limited to, waste heat recuperation and fuel recycling. Figure 1.4 illustrates a general direct fired, recuperated, SOFC/GT hybrid system.

As illustrated in the figure, the compressor exhaust recuperates heat from both the inlet and exit turbine streams, which increases the inlet temperature to the SOFC subsystem and can potentially have a positive impact on overall system efficiency. The illustrated system also includes a pre-combustor "C1" at the inlet side of the fuel cell to insure that the temperature of cathode inlet airstream is sufficient to promote and sustain electrochemical activity. Additionally, this recuperated system includes anode recycle which potentially optimizes the amount of fuel that is consumed by the SOFC which also contributes to the over-all system efficiency.

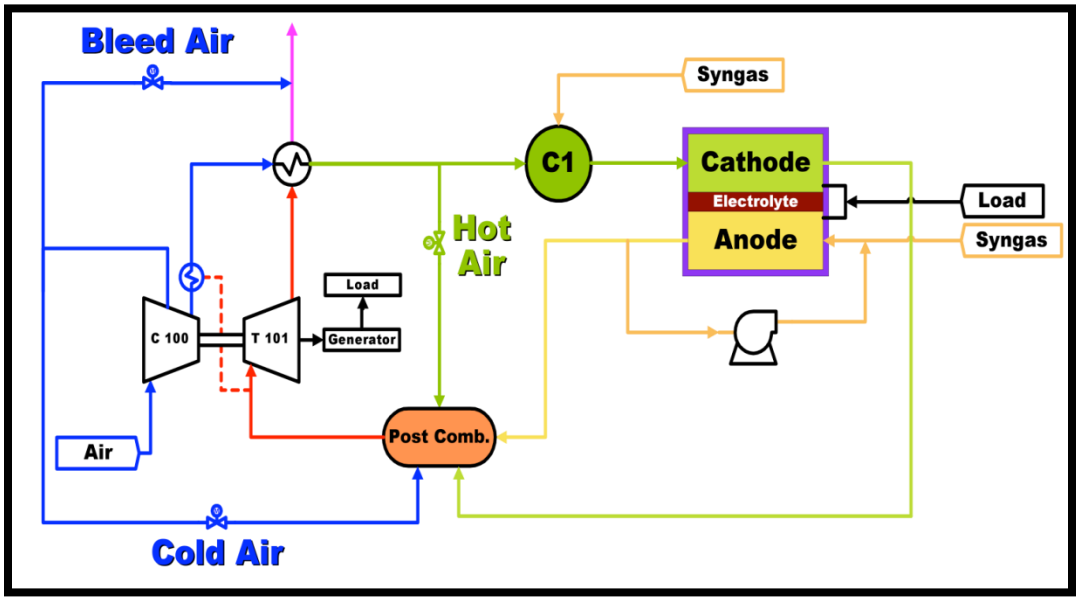

Figure 1.4: Direct fired recuperated fuel cell / gas turbine hybrid

In addition to the recycle component, the fuel cell subsystem also includes a post combustor, which produces heat from the combustion of the unutilized fuel from fuel cell operation. Extremely high fuel utilizations (above 90%) can cause a number of harmful effects within the fuel cell stack such as anode oxidation at the electrode/electrolyte

interface and potentially destructive spatial temperature gradients caused by extreme current density distributions and system dynamics [6], all of which are potentially threatening to cell reliability. This typically requires low- to moderate- fuel utilization levels which make fuel cell subsystem post combustion a necessity to ensure the elimination of combustible species in operating balance of plant.

1.2.1: Solid Oxide Fuel Cell (SOFC) Overview

A solid oxide fuel cell (SOFC) is an electrochemical energy conversion device that oxidizes fuel to generate electrical energy. SOFCs are high temperature fuel cells operating between 650°C -1000°C and harness the ability to produce power at efficiencies as high as 55% [7]. Similar to a battery, fuel cells, but more specifically SOFCs, have a negative polarity electrode known as an anode, a positive polarity electrode known as the cathode and a thin, internal electrolyte layer that allows for the necessary ionic transport to support the power producing electrochemistry of the operating SOFC. The governing electrochemical reaction for operating SOFCs results in the formation of water and the relinquishing of electrons on the anode side of the cell. Those released electrons ultimately pass through an external load and eventually arrive at the cathode, where they combine with oxygen atoms, form oxygen ions, pass through the electrolyte layer and arrive at the anode to combine with hydrogen to form water and complete the circuit as illustrated in Figure 1.5.

Given this governing electrochemical reaction, the ideal fuel for these power-generating devices is hydrogen, but given the promotion of the water gas shift reaction due to the high operating temperature and ability of nickel to serve as a catalyst for the reforming of light hydrocarbons, such as methane, SOFCs have the fuel flexibility that makes them strong candidates for a variety of light hydrocarbon and/or synthesis gas feed compositions [8].

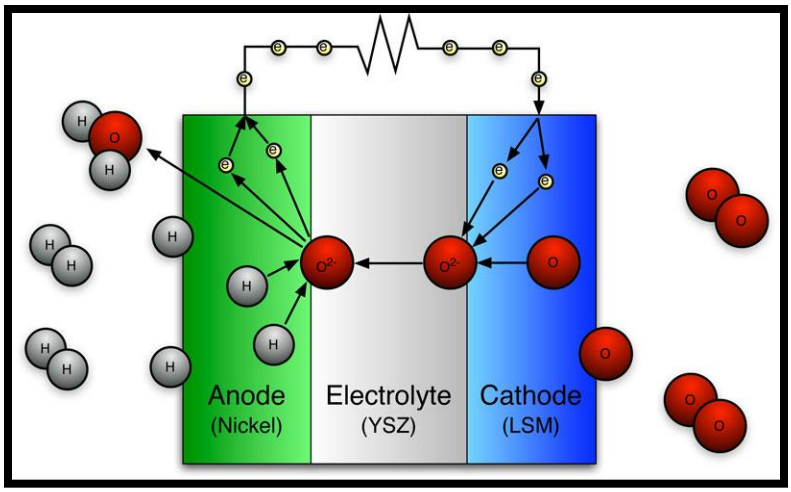

Figure 1.5: Electrochemical SOFC schematic

In addition to their relatively high operating temperature, two of the key characteristics that makes SOFCs such strong candidates for hybridization with gas turbines is their fuel flexibility and their ability to produce both electrical energy and high quality heat. As previously stated, and illustrated in Figure 1.3, the electrochemical nature of SOFC operation makes electrical power its primary output; secondarily, however, the by-product heat and residual fuel from the operating fuel cell can be used to provide the thermal energy necessary to "fire" the gas turbine in its power cycle arrangement, thus producing additional electrical power. Ultimately, SOFC subsystems serve as both a direct source of electrical power as well as thermal energy for the gas turbine power cycle. SOFC/GT hybrid power systems have theoretical efficiencies as high as 60% on a higher heating value (HHV) basis for coal syn-gas and 75% on a lower heating value (LHV) basis for natural gas [9].

Though SOFCs have a number of attributes that make hybridization and integration into the energy arena quite attractive, there also exists a number of sensitivities and design challenges that must be addressed and managed in order for these systems to operate in both a reliable and economically efficient fashion. SOFCs have both thermal and pressure sensitivities that make them very susceptible to mechanical failure. Previous studies on tolerable temperature gradients broach values of

approximately 12 K/cm [10-12] as being threatening to the mechanical integrity of the SOFC. Research also indicates that pressure imbalance or build up can have a deleterious effect on cell performance and result in mechanical failure as well [13]. Given the dynamic nature of these hybrid systems, both the thermal and pressure sensitivities of the SOFCs can be impacted by normal system dynamics and characterization and control of this dynamic behavior is essential to reliable SOFC and system operation.

1.2.2: Gas Turbine Overview

Gas turbines are energy conversion devices that produce rotational power from thermal and pressure energy in a given working fluid. The expansion and enthalpy decrease of the working fluid results in mechanical shaft energy that can then be converted to electrical energy. These devices have been used in the stationary power production arena for quite some time and the technology has been well established, developed and implemented. These devices are primarily powered by fossil fuels (coal and or natural gas) but ultimately only require a source of heat to increase the energy of the working fluid for the purpose of producing electrical power.

Though gas turbine technology is well developed, there still remain a number of challenges that pose issues in the design and operation of power plants with regards to these devices. One of the most significant of these design sensitivities is surge and stall [14, 15]. When surge and stall events occur in the turbine/compressor assembly, a transient event results in back flow of air through the compressor which ultimate causes an immediate halt in both turbine and compressor rotation and finally system shut down. Decreasing the turbines rotational speed from some nominal condition to nil has proven to have a negative impact on the operation of the gas turbine but furthermore, with regards to its applicability to SOFC/GT hybrid systems; the development of system wide pressure waves and the quick decrease in overall system pressure can cause failure in the

solid oxide fuel cells. The surge and stall phenomena is explained in more detail in subsequent sections.

1.2.3: Design Challenges Associated with SOFC/GT Hybrid Systems

Hybrid systems have numerous dynamic, operational sensitivities. As an example, a seemingly minor stimulus such as transient fuel cell stack thermal effluent, has the potential to have a cascading effect and potentially cause compressor surge and stall, which can result in system shut-down or failure [14, 16]. In short, compressor surge and/or stall is a disruption in compressor airflow that causes a flow reversal through the intake and results in an immediate shutdown of the turbine-compressor assembly. The step decrease in turbine speed from nominal operating condition (e.g., 40,500 RPM) to a non-rotational state that results from surge and stall events has proven to be harmful to the gas turbine, and in addition, the pressure waves that form from these surge and stall events travel through the system and threaten the mechanical integrity of SOFC stacks. If inappropriately managed, such changes in the heat provided to the balance-of-plant from the fuel cell subsystem, which is typically influenced by load demand and/or fuel flow, can thus cause surge and stall events in the turbine-compressor assembly [14, 17], which can result in SOFC and overall system failure.

As current demand from the SOFC stack changes, the overall thermal effluent (SOFC by-product heat generation and heat of combustion of unutilized fuel) from the SOFC subsystem will change as well. The change in SOFC subsystem thermal effluent results in a change in SOFC outlet temperature, which directly impacts turbine speed. Turbine speed impacts cathode airflow, which in turn, impacts SOFC thermal transport and turbine speed again. The direct coupling of the turbine and compressor, as illustrated in Figure 1.4, causes changes in turbine speed to effect compressor operation, thus possibly resulting in surge and/or stall which results in shutdown or failure.

In addition to SOFCs' sensitivity to pressure gradients caused by system surge and stall, they are also extremely sensitive to temperature gradients and transients (e.g., tendencies for warpage and shock); thus the ability to predict internal temperature gradients that pose threats to the mechanical integrity of the fuel cells is not only valuable, but imperative in cell and system design. Though the merger of these two power generating technologies is promising, a number of design challenges inclusive of, but not limited to, the management of spatial and temporal temperature derivatives in the SOFC to eliminate mechanical failure must be addressed and resolved in this investigative stage [18].

1.3: Hybrid Performance Project (HyPer) Facility

For the purpose of studying and developing SOFC/GT hybrid technology, a SOFC/ GT hybrid, pilot scale test facility has been constructed at the National Energy Technology Laboratory (NETL) in Morgantown, West Virginia through the Hybrid Performance (HyPer) Project. For the sake of developmental investigation and reliability, this hybrid, pilot-scale test facility utilizes a combination of hardware and software to simulate the operation of a SOFC stack in the hybrid arrangement. It uses hardware-in-the-loop simulation (HiLS) [17, 19, 20] and a SOFC software model component, which is capable of both operating in real time and capturing internal diagnostics of the simulated fuel cell. HiLS and the real-time, 1-D SOFC model provide the capability to characterize the operational design space of the system to manage potentially harmful transient effects.

The HyPer facility, illustrated in Figure 1.6, is a pilot scale SOFC/GT hybrid power plant test facility that employs the use of a SOFC model and HiLS [20, 21] to simulate an actual operating SOFC subsystem in a SOFC/GT hybrid arrangement. The HyPer facility simulates a 400kW-500kW powerplant, with the gas turbine accounting for 120kW and the simulated SOFC stacks accounting for approximately 350kW. A real-

time operating 1-D distributed fuel cell model was constructed on a Matlab-Simulink™ platform and integrated into the HyPer facility using dSpace™ controldesk software. The dSpace™ software can be coupled with Matlab-Simulink™ models and affords the user the ablity to change system inputs and observe transient changes in system operating parameters as desired. The model is built to operate in real time, and through the dSpace™ platform it can extract live inputs from the operating HyPer system and simulate and characterize fuel cell operation. The model has the capability to produce current density, cathode oxidant stream temperature, solid fuel cell temperature, and polarization profiles that have both spatial and temporal resolution.

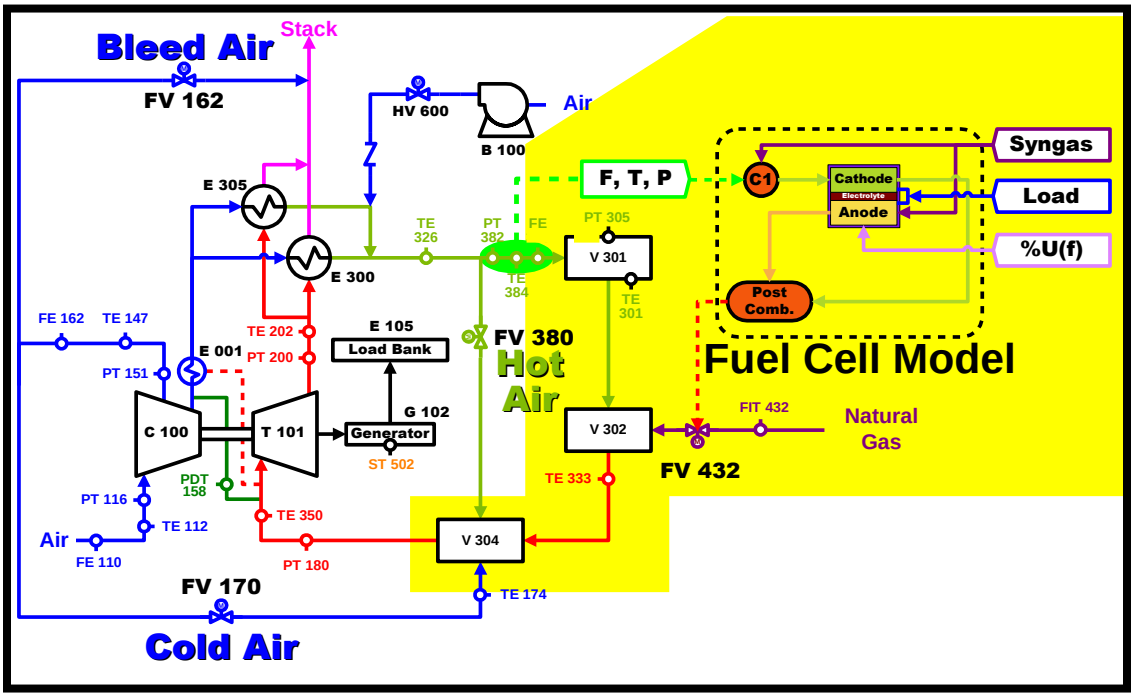

Figure 1.6: Simplified HyPer Schematic

Through the dSpace™ platform, temperature, pressure, and mass flow readings into the air plenum, which represent the cathode volume, are extracted from the operating HyPer facility (via sensors TE-326, PT-305, and FE-380, respectively) and are fed into the SOFC model as cathode air stream parameters. The operator is responsible for prescribing the operating load and fuel flow into the virtual SOFC stack. In addition to the spatio-temporal characterization of the operating fuel cell, the model also calculates a

fuel cell subsystem thermal effluent. The thermal effluent value is then fed into the fuel valve model, which adjusts the fuel valve (FV-432) position to provide the appropriate thermal effluent to the HyPer facility.

The HyPer system also provides insight regarding turbine operation. HyPer employs the use of a constant speed turbine with a synchronous generator, but is capable of variable speed operation in a small regime of ±5% of its nominal operating speed of 40,500 RPM. Significant changes in turbine speed are not tolerable; thus, significant changes in thermal effluent to the turbine subsystem must be controlled. System transients due to changes in simulated fuel cell stack thermal effluent caused by changes in current demand have also been shown to induce surge and stall events in the turbine [15]. The compressor map shown in Figure 1.7 can be used to illustrate the phenomena of compressor surge and stall. The figure plots the compressor pressure ratio with respect to air flow through the compressor. During start-up, and throughout system operation, the system must operate in a regime to the right of the "Stall Line" to avoid surge and stall.

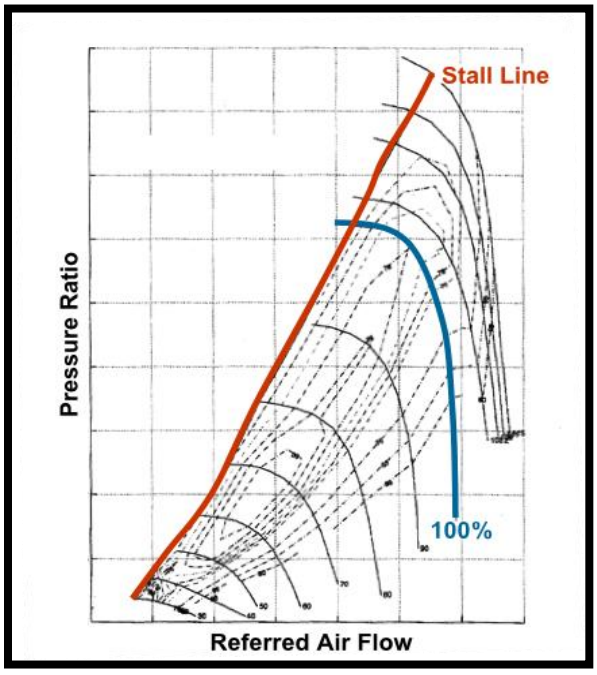

Figure 1.7: Compressor Map

The blue line represents operation at 100% nominal speed. During system operation, the system can operate anywhere on this line, but again, crossing over the "stall line" will result in surge and stall and ultimately system shutdown. As illustrated in Figure 1.7, when the system is operating at nominal speed, decreases in airflow result in increases in compressor pressure ratio. As airflow continues to decrease, the increase in pressure begins to level off and the operating point begins to approach the stall line. Once the operating point crosses the stall line, surges begin to occur which cause uncontrollable pressure waves in the system and eventually result in compessor stall. Given the impact of SOFC thermal effluent on system operating parameters, thorough investigations on the impact of thermal transients can provide insight regarding the needed heat generation or heat sinking to aid turbine and SOFC safety and reliability. The robustness of control mechanisms that need to be designed to control turbine speed is influenced by thermal transients as well.

1.4: SOFC/GT System Start-Up

Coupling SOFCs and gas turbines into a hybrid arrangement for large-scale power production appears to possess tremendous promise for increasing system efficiency, decreasing emissions, and assisting a more sustainable power-generating infrastructure. The sensitivity to thermal transients that the SOFC and gas turbine share, both individually and collectively, poses a significant design challenge that requires a viable and sound solution before these hybrid systems can be integrated into the existing energy framework. The importance of managing thermal transients with respect to the SOFCs is especially significant due to the threat of cracking and mechanical failure from spatial gradients and thermal shock, and creep from extreme temporal derivatives as well [22-24]. Changes in SOFC operating conditions affect internal SOFC thermal transport, turbine speed, pressure ratio, and cathode airflow; and this occurs in related transient manner. The ability to analyze the impact of fuel cells (and thus thermal effluent)

transients on significant operational process variables is essential to reliable system operability.

With regards to SOFCs, a number of studies have been conducted to thermally characterize them during steady state operation [25-29] and have been supplemented by some investigations on the impact of operational transients (i.e. load changes) [30-36]. Transient models simulating tubular SOFC operation on one- and two- dimensional bases have been developed by Jiang et. al. [34] and Mollayi Barzi et. al. [35] respectively. Both models are capable of capturing internal transport phenomena but neither exhibits the capability to account for either balance of plant or hardware facility transient feedback. Salogni et. al. [36] present a dynamic model of a planar SOFC stack designed for simulations of integrated systems. Although it is capable of accounting for system wide transient effects, its design allows for coupling with other dynamic models and not with actual operating facility hardware. Much like the other models presented, it does not have the necessary real-time operating capabilities for hardware-based simulation. Significant work has been done characterizing SOFC/GT hybrids in a global manner [14, 15, 37-41]; however, the majority of this work characterizes the global hybrid system and analyzes the impact of thermal transients on system performance, but does not offer detailed characterization of the internal dynamics of the operating fuel cells in the hybrid arrangement. The model presented in this dissertation harnesses the capability to internally characterize SOFC operation while operating in-the-loop in an SOFC/GT hybrid system; and the accompanying study presented characterizes the impact of system-wide, real-time feedback during system operation.

The capability of integrating a SOFC model into the HyPer facility was first presented by Smith et al. [20]. This work demonstrated the ability to use HiLS to characterize fuel cell operation in the hybrid arrangement in real-time by intricately coupling a computational model with the appropriate hardware to simulate fuel cell operation. The model used in this study was of the 0-D or “lumped” type, and though it

demonstrated the HiLS capability, it failed to provide high fidelity spatio-temporal data about the simulated fuel cells, which is necessary for performance and development of design methodologies for these hybrid systems. A recent study presented by Hughes et al. [18] illustrated the initial capability of the 1-D, distributed fuel cell model to provide these necessary internal diagnostics while operating in real-time.

As previously stated, transient events are of particular interest in the investigation and development of fuel cell/gas turbine hybrid systems. One of the most significant transient events associated with any power system, but particularly in SOFC systems, is start-up. SOFCs are intermediate to high temperature fuel cells that must be heated to a moderately high temperature (e.g., 700°C), known as the electrochemical light-off (ELO) temperature, before they can begin operating [42]. The existence of this ELO temperature subsequently partitions the start-up process into two inherent phases. The first of these phases is the sensible heating required to increase the fuel cell stack temperature to ELO temperature from its initial ambient temperature. The second start-up phase involves placing load on the fuel cell. During start-up, once ELO temperature is reached, the current demand must be increased from an un-loaded condition to some final operating load. As previously stated, changes in current demand directly impact thermal transport throughout the system and can potentially have a cascading effect, which must be suitably managed for the sake of reliability and system integrity.

The majority of the literature that has involved investigating the start-up and shut-down components of transient SOFC operation has primarily focused on start-up With regards to the first (inert) component of the start-up phase, Tucker et al. [11] utilized a 1-D distributed model to study the initial thermal transient fuel cell response to turbine start-up. The investigation showed promise to manage both spatial and temporal gradients in the SOFC during rapid turbine start-up, and also illustrated that the use of the cold air bypass valve (FV-170 in Figure 1.6), a concept developed at NETL, creates the most favorable thermal scenario for the SOFC during turbine start-up. The second

(electrochemically active) component of the start-up phase has yet to be characterized and developed; Chyou et al. [43] however, has conducted a study to optimize the start-up scenario from un-loaded conditions to operating load at ELO temperature. The examination broaches the balancing of current density step sizes and wait times to optimally minimize both internal temperature gradients and start-up time. Since this study only examined a fuel cell not coupled with a gas turbine or additional balance of plant components, feedback effects from the balance-of-plant were not considered.

The completed 1-D SOFC model is being used to characterize the electrochemical phase of these start-up scenarios, placing load on the virtual SOFC at ELO temperature while coupled in the HyPer facility. As previously stated, changes in thermal effluent from the fuel cell affect pressure, temperature, and flow through the cathode, which conversely affects SOFC and balance-of-plant operations and dynamics. Using this distributed model, the impact of electrochemical start-up (i.e., applying load to the SOFC from an unloaded state while at ELO temperature) on SOFC and system operating conditions will be investigated with specific emphasis placed on characterization of the evolution of temperature gradients and temporal derivatives within the SOFC.

1.4.1: Gas Turbine / SOFC Inert Heating – Phase I Start-Up

One of the most significant issues with regards to SOFC/GT hybrid system start-up is the disparity between the SOFC and gas turbine operational time scales [18, 21]. Furthermore, gas turbine start-up is comprised of a single, short, 2-5 minute timeframe [11, 16], whereas SOFC start-up is comprised of two separate phases with notably different time scales. The disparity in operational time scales of the two power systems coupled with the difference in steps in the individual start-up procedures creates a significant level of complexity with regards to transitioning SOFC/GT hybrid systems towards an operational condition. The dual phased nature of SOFC system start-up governs the start-up of the entire system and compartmentalizes the process into 2

phases; the first of these phases is herein termed gas turbine / SOFC inert heating start-up. During this phase, the rotational speed of the gas turbine is increased from 0, at its stationary "at rest" condition to its nominal operating speed, which for the HyPer facility is 40,500 RPM. This is achieved through the combustion of natural gas in the system combustor (V-302) and the expansion of hot, pressurized combustion gases passing through the turbine.

In unison with the start-up of the compressor-turbine assembly is the inert heating of the SOFC. In most SOFC systems (including hybrids), the cathode inlet air stream serves as the primary thermal management mechanism and consequently is the primary means for fuel cell preheat. As illustrated in Figure 1.6, heat is exchanged from the turbine exhaust to the compressor exhaust and this heated stream is then fed into the cathode side of the fuel cell. This use of turbine exhaust to pre-heat the cathode inlet stream directly couples gas turbine start-up with SOFC inert heating and ultimately requires characterization and development of control strategies to ensure efficient and safe start-up. Research investigating the impact of turbine speed ramp rate and cold air by-pass flow on SOFC thermal dynamics has been conducted [11]. Although the results show that both decreasing ramp rate and decreasing cathode airflow by increasing cold air by-pass both have a beneficial impact on spatial gradients and temporal rates of change in the SOFC, with increased cold air by-pass flow having a more significant and notable impact, none of the case-studies conducted presented values that fell outside of the tolerable regime. Though further investigation in this area is necessary to develop a broad scoping operating envelope and to establish strong quantitative conclusions on the impact of turbine start-up on SOFC thermal transport, preliminary studies tend to support that the presence of harmful SOFC spatial gradients and temporal rates of change will be very manageable through phase I hybrid system start-up [11].

1.4.2: Electrochemical – Phase II Start-Up

Once the turbine has gone through its start-up phase and has reached its nominal operating speed and the SOFC has gone through its inert heating phase and has arrived at electrochemical light-off (ELO) temperature, phase I start-up is complete. The second phase of start-up, herein referred to as electrochemical start-up, refers to the transition associated with taking the SOFC from an unloaded, electrochemically inactive state to an electrochemically active state, during which electrical power is being drawn from the cell. Figures 1.8 and 1.9 illustrate the internal SOFC dynamics on both a thermal and electrochemical basis respectively when the SOFC is taken from an unloaded state to 200A of nominal load in stepwise manner with 40A steps.

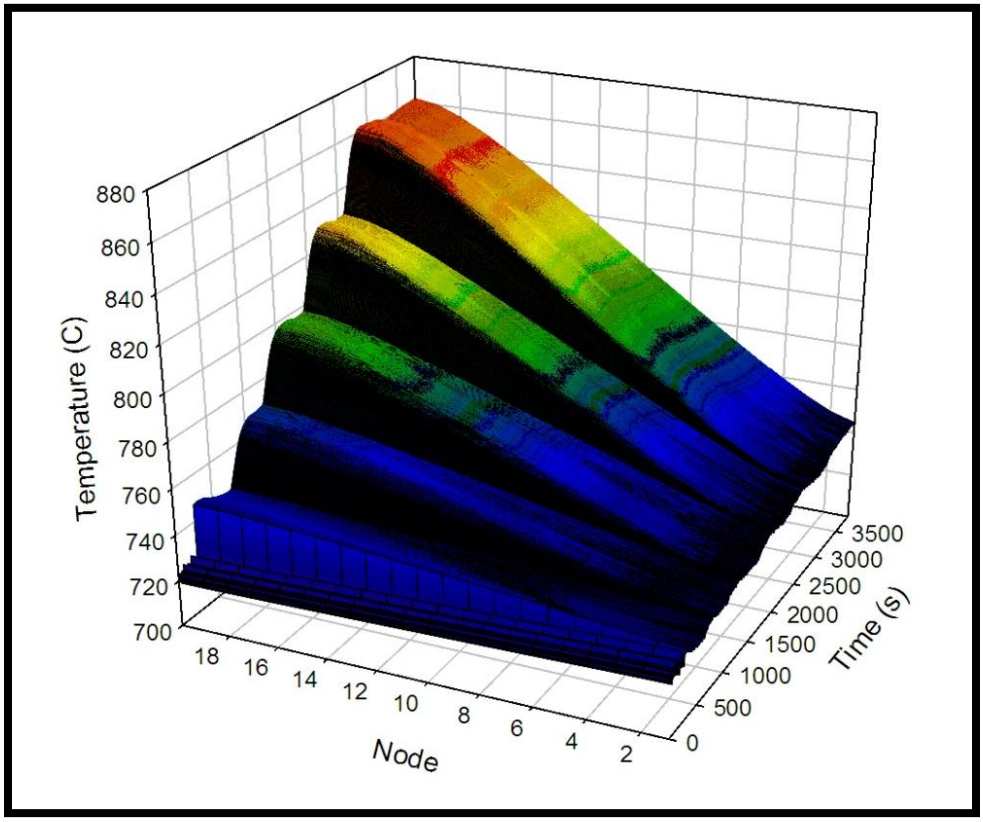

Figure 1.8: SOFC solid temperature spatio-temporal profile during electrochemical start up to 200A of fuel cell load

The data presented was collected from a preliminary experiments during which the SOFC was taken from an unloaded condition up to a nominal load of 200A while the HyPer facility was in an open loop configuration which allowed the turbine speed to vary through the electrochemical start-up period. As illustrated in Figure 1.8, the overall temperature profile of the SOFC increases throughout electrochemical start-up. This is due to by-product heat generation caused by electrochemistry in the SOFC. Figure 1.9 illustrates the evolution of the current density profiles in the SOFC during phase II start-up.

As illustrated, the current density increases throughout the start-up phase until the nominal 200A condition is reached. As the current demand on the SOFC is increased, the distribution of the current density changes, ultimately resulting with some local maxima inside the SOFC. The increased electrochemical activity results in by-product heat generation, which contributes to the elevated temperatures seen at higher current demand. Figure 1.10 presents cathode inlet pressure, temperature and flow throughout the start-up phase.

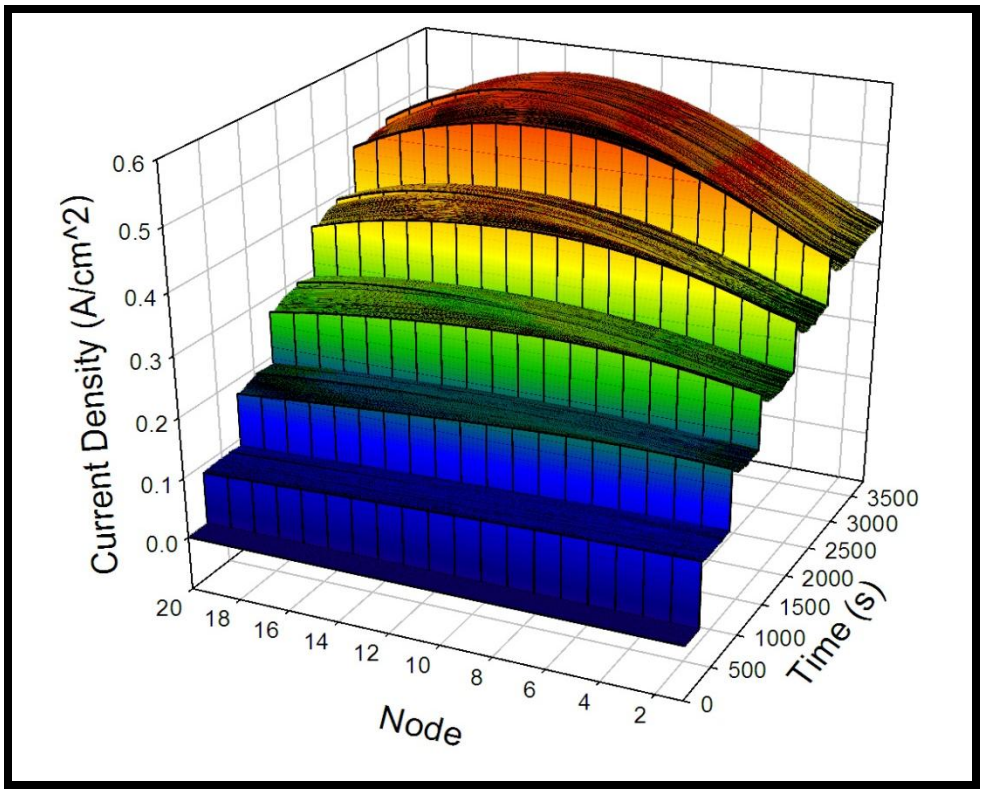

Figure 1.9: SOFC current density spatio-temporal profile during electrochemical start-up to 200A

The cathode inlet parameters demonstrate dynamic behavior throughout the start-up phase. As illustrated all three parameters exhibit modulating behavior that aligns with the SOFC thermal and electrochemical dynamics. As fuel cell load is increased, the overall thermal effluent from the SOFC subsystem that provides thermal energy to the balance of plant decreases. The decrease in thermal effluent results in a decrease in turbine speed which causes the decrease in cathode inlet parameters exhibited in Figure 1.10. Increases in cathode inlet parameters can be attributed to the addition of fuel for the purpose of returning the turbine to its nominal operating speed of 40,500 RPM.

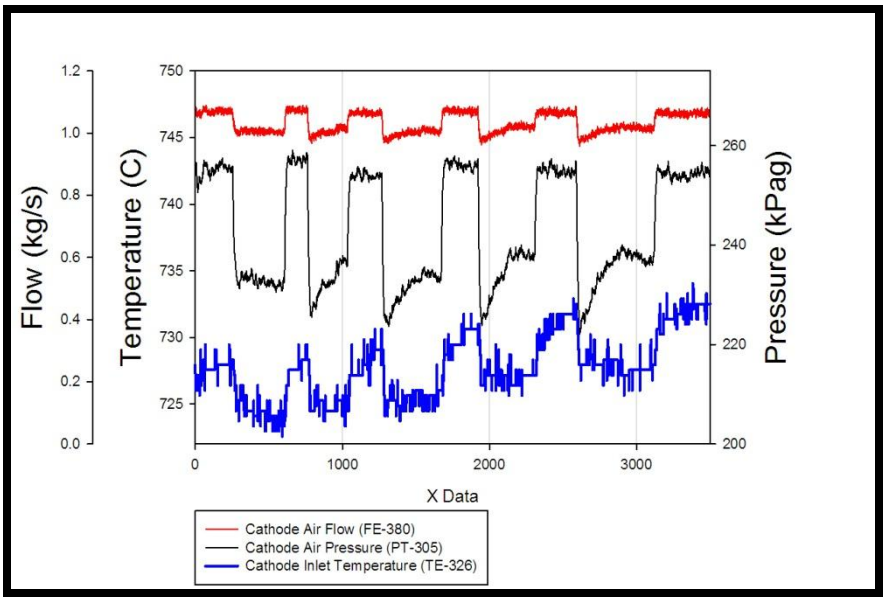

Figure 1.10: SOFC cathode inlet parameters during electrochemical start-up

Figures 1.8-1.10 illustrate the presence of a number of operational dynamics that are associated with electrochemical (phase II) SOFC/GT hybrid start-up. Preliminary studies associated with phase I start-up suggest that its accompanied design challenges are significantly understood and manageable [11], but phase II appears to be the portion of start-up with more dynamic considerations and necessary control strategies. Characterization and management of electrochemical start-up for SOFC/GT hybrid systems is essential for hybrid technological development and integration into our currently existing energy arena.

1.5: Dissertation Project – Impact of Cold Air Post Compressor By-Pass on Electrochemical Hybrid System Start-Up

As illustrated in Figure 1.6 and presented in chapter 3, the HyPer facility and SOFC/GT hybrid systems generally have a large number of process variables that directly impact SOFC and system performance. The system user or operator has control over four of those variables; bleed air, hot air and cold air by-pass valve position, and turbine load. All of these variables play a significant role in determining the systems' operating states, and the characterization of the impact of said variables during system start-up are

essential in the development of control strategies to mitigate potentially harmful transient phenomena and assure safe and reliable system operation.

Initially, the HyPer facility was designed to provide a significant level of characterization and analysis on the system level but was only capable of lumped, "black-box" analysis of a simulated SOFC stack. Though system level, balance of plant analysis is both valuable and necessary in the pursuit of system level characterization, a higher level of fidelity with regards to SOFC analysis is critical to technological development. To that end, the development of a model that could be integrated with the HyPer facility and operate in real time within the HyPer configuration was paramount for technological advancement. For that reason, this proposed dissertation project had two main tasks:

1.) Completion and verification of a robust, spatio-temporal, real-time operating, SOFC model

2.) System and component level characterization of electrochemical start-up

1.5.1: One-Dimensional Real-Time SOFC Model

The lumped, 0-D, fuel cell model presented by Smith et al. [20, 21] and integrated into the HyPer facility using HiLS, was the result of the first stage of development of such a system. It was capable of extracting real-time data from the operating HyPer facility and simulating an operating SOFC in "black box" manner. Though the development and inclusion of this model allowed for valuable investigation on the feasibility and operability of SOFC hybrids, design sensitivities that pose significant challenges to integrating systems of this nature call for higher fidelity characterization of an operating SOFC. The model that has been developed for this dissertation is capable of operating in a temperature range from ambient to over 1800K, thus affording the capability to characterize the SOFC in inert, on-design, and off-design operating regimes. It is capable of SOFC characterization in distributed manner, profiling key thermal and

electrochemical results along the length of the reactant channel as well as in the temporal space. The model has been tested and verified via comparisons with pre-published data [44] as well as the IEA SOFC modeling benchmark [45]. The 1-D real-time SOFC model is described in greater detail in Chapter 4.

1.5.2: Cold-Air By-Pass / Fuel Cell Load Step Size Parametric Analysis

Changes in SOFC operating conditions affect internal SOFC thermal transport, turbine speed, pressure ratio, and cathode airflow; and this occurs in coupled transient manner. The ability to analyze the impact of fuel cell (and thus thermal effluent) transients on significant operational process variables is essential to reliable system operability.

Given the level of complexity inherent in SOFC/GT hybrid systems coupled with the large number of process variables necessary to characterize system performance, a preliminary scoping study was conducted to investigate the impact of user-controlled process variables on system performance. For the purpose of practicality and stall mitigation, respectively, variance of the bleed air valve position and turbine load were not included in the scoping study, resulting in a parametric study of both hot air and cold air by-pass coupled with initial fuel cell load to scope the system performance impact. Results of the scoping study, that are presented in chapter 3, coupled with experiential knowledge of the system led to the decision to conduct a detailed parametric analysis of cold air by-pass and fuel cell load on system performance during electrochemical start-up.

1.6: Results Summary

The experimental plan for this dissertation work, presented in chapter 3, outlines an investigation that is designed to characterize the impact of:

1.) Cold Air (CA) by-pass valve position and initial FC load on system wide and SOFC stack operation
2.) Utilizing a syngas as compared to a humidified hydrogen SOFC fuel feed on system wide and SOFC stack operation

Specifically with regards to characteristic properties of the cathode inlet stream, results show that CA by-pass valve position had an impact on temperature, pressure and flow during electrochemical start-up. Increased CA by-pass valve position diverted more air flow on the back side of the compressor into the post combustion volume, thus resulting in decreased cathode air flow. With regards to dynamic response, increases in CA by-pass valve position resulted in larger normalized decreases in cathode inlet temperature and smaller normalized decreases in both cathode inlet pressure and flow. The impact of CA by-pass flow on temperature can be attributed to increased levels of cold air in the post combustion volume which results in decreases in turbine exhaust temperature and ultimately decreases the amount of heat that can be transferred to the cathode inlet stream as well as the variation in required SOFC subsystem thermal effluent for nominal speed operation.

The most identifiable impact of CA by-pass valve position on the system operation is the amount of thermal effluent required from the SOFC sub-system. As more CA is by-passed from the back side of the compressor to the post combustion volume, air flow through the SOFC subsystem decreases. Given the decreased air-flow, more thermal effluent is required from the SOFC subsystem to maintain nominal turbine speed. When load is applied to the SOFC stack, the relative change in thermal effluent from the system is less for larger amounts of CA by-pass, thus resulting in less significant changes in pressure and flow through out electrochemical start-up for both LBSC as well as OL.

Given the ability to control turbine speed, larger initial load sizes were employed for the LBSC investigation. Though the major concern with regards to SOFC operation is

failure induced by thermal transients, the significant pressure changes observed in the cathode inlet pressure during SOFC start-up with the smallest step size proved to be threatening to the cells mechanical durability. Though increasing CA by-pass valve position decreased the impact of these pressure changes, modulating CA by-pass did not prove to be sufficient in mitigating mechanical failure due to pressure change.

For both the OL and LBSC investigation, in addition to the concern of evolution of potentially harmful temperature gradients due to by-product heat generation, a significant decrease in inlet temperature resulted in a significant cooling effect that competed with the cell operational heating and contributed to the formation of peak temperature gradients in the upstream portions of the SOFC. The impact of CA by-pass on cathode air flow, did however contribute to the mitigation of temperature gradient formation. Decreases in CA by-pass flow, which results in both increased cathode airflow and a smaller decrease in cathode inlet temperature contributed favorably to decreasing spatial temperature gradients through-out electrochemical start-up.

Utilizing methane rich syngas fuel feed provided intra-stack cooling that illustrated the capability to assist with the mitigation of temperature gradients, but also has the ability to have some harmful effects. For sufficient load (i.e. 100A for the LBSC case), the temperature gradients were significantly decreased and managed due to the presence of the endothermic DIR in the SOFC stack after the application of load. For smaller loads (i.e. 30A for the OL case), the by-product heat generation was not sufficient enough to provide enough thermal energy to counteract the DIR and post load dT/dx profiles were significantly negative. For both the HH and syngas investigations, there was not an observed temperature gradient beyond the 12 K/cm mark identified by Nakajo et al. [12], that suggest that thermomechanical failure was not of significant concern.

1.7: Original Contribution

The original contribution of the work presented in this dissertation is as follows:

1.) Development of a real-time operating, robust, spatio-temporal SOFC model capable of simulating and characterizing fuel cell operation from ambient temperature, through the inert heating and/or cooling phase, electrochemical start-up and shut-down, and even off design conditions.
2.) A complete parametric analysis and coupled characterization of the impact of CA by-pass and initial FC load on electrochemical start-up of an SOFC/GT hybrid system
3.) A preliminary parametric analysis and coupled characterization of the impact of fuel feed composition and initial FC load on electrochemical start-up of an SOFC/GT hybrid system

CHAPTER 2

BACKGROUND & LITERATURE REVIEW

The research effort presented in this dissertation aims to characterize the dynamic behavior of a SOFC/GT hybrid system during electrochemical start-up using HiLS. SOFC/GT hybrid systems synergistically link the operational by-products of two different power generating systems, solid oxide fuel cells and gas turbines, to develop a coupled system that can significantly improve both operational efficiency and environmental impact.

Though the technology is promising, as stated in the introduction, the individual power generating components of hybrid systems have a number of operational and design sensitivities that make the component coupling and system operation quite challenging. Given those challenges, there is tremendous effort in the research, development and design of these systems.

This chapter of the dissertation presents background information and review of literature that is applicable to SOFC/GT hybrid system development with a particular emphasis on hybrid system and SOFC dynamic modeling. The chapter will begin with a review of SOFC/GT hybrid systems, highlighting some of the salient characteristics of both SOFCs and gas turbines that make the integration of these systems so challenging. The SOFC/GT hybrid system review will also present and discuss the Siemens-Westinghouse SOFC/GT hybrid system that was developed and operated by the University of California Irvine. In addition to successful developmental efforts, a discussion on the most current research efforts will be presented along with a discussion

on the applicability of using HiLS to investigate hybrid system development. The second, and final section of this chapter, will discuss some of the recent developments in the arena of SOFC modeling and the need and value of real time dynamic SOFC models for front end hybrid system development.

2.1: SOFC/GT Hybrid Systems

SOFC/GT hybrid system development aims to couple solid oxide fuel cells and gas turbines in a synergistic fashion for the purpose highly efficient, stationary power production. As explained in Chapter 1, solid oxide fuel cells are high temperature, electrochemical conversion devices that produce electricity from the oxidation of hydrogen. SOFCs are similar to batteries due to their electrochemically produced power, but much like an engine, they will operate continually as along as adequate fuel is supplied. The overall equation governing the electrochemical reaction for operating SOFCs is presented in equation 2.1.

$$H_2 + \frac{1}{2}O_2 \rightarrow H_2O + Electricity + Heat \tag{2.1}$$

As illustrated by the equation, hydrogen is the primary constituent in the fuel stream that contributes to electrochemical activity. Though operation of a hydrogen based fuel stream allows for zero emission operation, the ability to produce pure hydrogen, given current technology, can be a difficult arrangement. To that end, another valuable attribute of SOFCs is their fuel flexibility. Given their nickel containing anode as well as their high operating temperature, SOFCs promote both steam reformation and water gas shift inside the fuel channel. Both of these reactions produce hydrogen which supports SOFCs' ability to operate off of methane or syngas, which can be produced from the gasification of coal or other carbon containing organic compounds. Ultimately, SOFCs have a variety of fuels that can drive their operation which afford them the ability to

operate within our current fueling infrastructure or transition as necessary with changes in the power generation arena.

In an operating SOFC, approximately 50% of the chemical energy from hydrogen oxidation is converted to electrical energy and the other 50% manifests in the form of by-product heat. One of the major operational sensitivities is the impact of significant spatial temperature gradients and time rates of temperature change on SOFC mechanical durability [12]. The generation of heat from cell operation as well as the generation and/or sinking of heat from reactant stream chemistry, requires sound thermal management to ensure that regimes of potential mechanical failure are avoided.

The primary means of SOFC thermal management is cathode air flow. The oxidant is typically fed to the cell in excess to ensure electrochemically sufficient supply, but it is also supplied in excess to cool the cell and manage internal thermal dynamics. In SOFC/GT hybrid systems, the cathode air flow is compressor exhaust, which is heavily controlled or influenced by the speed of the turbine. The oxidant channels of the SOFC stack are the key component of the system where the synergistic exchange occurs. The turbine needs heat to operate, which is provided by the fuel cell, and the fuel cell requires air for cooling as well as electrochemical activity, which is provided by the compressor that is driven by the turbine. Given that this is the key area of power system coupling, it is also the system coupling that requires the most attention in the research and design phase.

In addition to the thermal sensitivities that must be considered with the coupling of compressor exhaust to cathode air flow is the pressure sensitivities of SOFCs as well. Though improved cell performance is observed at elevated pressures, pressurization has been shown to exacerbate uneven distribution of reactants, which can degrade stack performance [21]. It also makes the cell susceptible to significant changes in operating pressure that can contribute to mechanical failure as well [46]. Similar to cathode inlet flow, pressure is highly correlated to turbine speed which is highly coupled to fuel cell operation via system thermal effluent. With regards to fuel cell operation, SOFCs rarely

operate at or close to 100% fuel utilization. This is primarily due to the harmful effects of fuel depletion and starvation on SOFCs [6]. Consequently, for the sake of safety and reliability, the unutilized fuel must be oxidized before the SOFC exhaust stream is fed to the turbine. The combustion of this unutilized fuel is a significant source of heat for the hybrid system, but has the potential to add complexity when analyzing system transient response. Both by-product heat from cell operation and heat of combustion of the unutilized fuel are used to fire the gas turbine in SOFC/GT hybrids. Though the SOFC does provide heat to the working fluid, the entire "SOFC sub-system" is responsible for providing the thermal effluent to the system.

SOFCs present their challenges, with regards to thermal and pressure sensitivities in hybrid systems. Managing thermal gradients, temporal rates, and pressure changes during live dynamic operation to preserve the SOFC will be critical as this technology is developed and deployed. The design considerations on the turbine side are not as large in number, but as significant in importance. Paramount among these challenges is compressor surge and stall. Explained in Chapter 1, compressor surge and stall ultimately results in an instantaneous halt in turbine speed which causes a significant decrease in both cathode inlet mass flow and pressure. Given the sudden decrease/elimination of air flow to the cathode and the propagation of pressure waves throughout the system, compressor surge cannot only damage the turbine/compressor assembly, but also significantly threatens the mechanical durability of the SOFC as well. The precise cause of surge and stall, in SOFC/GT hybrid systems is being investigated, but experiential evidence shows that significant changes in system thermal effluent greatly contributes to the occurrence of surge and stall events; thus, system transients caused by changes in FC sub-system operation must be managed appropriately to protect both the turbine/compressor assembly as well as the SOFC from damage and failure.

All of the sensitivities and design challenges discussed significantly affect a major component of system operation, which is start-up. Given the thermal and pressure related

sensitivities of SOFCs, heating them to operating temperature from an ambient state, must be done in a slow and methodical fashion to preserve the mechanical integrity of the SOFC. Inert heating of SOFC stacks has taken up to 6-8 hours [11, 21, 47]. Conversely, gas turbines require a quick start-up, arriving at nominal speed within 2-3 minutes of initiated start-up. The integration of these two power systems with such disparate time scales poses a significant operational challenge, but particularly with regards to system start-up.

Though challenges exist with regards to system integration and reliable operation, the fact remains that the benefit from design and erecting of these types of systems can prove extremely beneficial in the energy arena. Most technological innovations in the energy arena are incremental in nature, resulting in minor increases in efficiency points. SOFC/GT hybrid technology harnesses the capability to increase power generation efficiency on the order of 15-20 percentage points [9], all the while having the ability to flexibly utilize various fuels and potentially operate in a zero emission state. Hybrid systems make use of the by-product heat from FC subsystem operation for firing gas turbines, and uses the pressure in the fluid from the compressor exhaust to maximize SOFC operation. Though challenging, synergistically melding these two power systems harnesses a tremendous capability for transformative change in the energy arena.

2.1.1: SOFC/GT Research and Development Efforts

Significant work has been, and is currently being, conducted in the research and development of SOFC/GT hybrid systems. Presented in this section will be a brief discussion on SOFC/GT hybrid systems that have been successfully constructed and operated, along with observations and insights from those research and design efforts.

2.1.1.1 Operated Hybrid Systems

The solid state energy conversion alliance (SECA), is a program funded and operated by the U.S. DOE to structure and support the development of SOFCs to accelerate their commercialization and introduction to the energy marketplace. There are three member groups in the alliance: industry teams, core technology development teams and federal government experts. The industry teams are primarily focused upon hardware development and market penetration. The technology development teams, primarily consisting of universities and national labs, are focused upon the addressing the research problems facing the industry teams. The federal government coordinates the program and, most importantly, encourages a broad national perspective of SOFC technology development, beyond company-specific interests [9].

To accelerate the development of SOFCs, SECA adopted four basic strategies:

(1) A "mass customization" approach to resolve the market entry dilemma — initial costs are too high to sell a large number of units, while high volume production is needed to bring the cost down
(2) Integration of government, industry, and scientific resources to leverage their respective skills by placing them in appropriate roles
(3) Utilization of a common research and development program available to all industrial teams to eliminate redundancy
(4) Intellectual property provisions that enable all industry participants to benefit from breakthroughs by the scientific participants, thereby enhancing technology transfer.

Accompanying these strategies are two main goals:

(1) Developing SOFCs for distributed generation applications like auxiliary power units, military power generation, and remote power generation.

(2) Secondly, SECA is a large part of the FutureGen program. SECA fuel cells are the building blocks of the FutureGen zero emissions power, which is the ultimate goal of the Clean Coal Power Initiative.

Under the umbrella of the SECA program, two efforts have been conducted to develop, construct and operate SOFC/GT Hybrid systems. The first by Siemens Westinghouse Power Corporation (SWPC) which was test in 2000, and one by General Electric (GE) which began testing in 2005. Rolls Royce corporation has also erected a facility as well [48].

2.1.1.1.1 Siemens Westinghouse Power Corporation 220kW Hybrid

Through the coordination of the SECA program, a 220kW tubular SOFC/GT hybrid was designed and manufactured by the Siemens Westinghouse Power Corporation and operated through the National Fuel Cell Research Center at the University of California – Irvine.

Figure 2.1: SWPC 220kW SOFC/GT Hybrid

Nearly 3200 hours of testing was conducted on the system, illustrated in Figure 2.1, between 2000 and 2003. During the testing the system produced 500 MWh of

electricity and operated at 53% thermal efficiency (LHV) [21]. This demonstration was the first in the world of a pressurized SOFC hybrid system. The stack was consisted of 1152 individual tubular SOFC cells operated at 3atm (absolute). The turbine used was an Ingersoll-Rand microturbine originally rated at 75kW.

2.1.1.2 Hybrid System Research and Literature Review

Given the fiscal risks and challenges, as well as the experimental limitations that are associated with SOFC/GT hybrid systems, few have been constructed for operational or testing purposes. Most research and investigation done in the field has relied upon either computational modeling or HiLS experimental efforts.

A number of modeling efforts have been sought to characterize SOFC/GT hybrid operation, with significant contributions being made by the Thermochemical Power Group from the University of Genoa, and the National Energy Research Laboratory in Morgantown, WV. A foundational study in this arena from Magistri et al. [49] presents a computational model of a hybrid system based on a personal (5kW) turbine and an SOFC stack. The work focused on a combination of design point and off design hybrid system performance characterization as well as presented a preliminary evaluation of energy costs. The design point analysis presented a full load operating condition with a cell temperature of 1238K, an air utilization factor of 0.3114 and a cell operational efficiency of 48%. This resulted in a hybrid system design point efficiency of 56.3% with a turbine inlet temperature of approximately 1173K. The author notes that the hybrid system design point operational efficiency is high, but advancements in SOFC technology can contribute to higher efficiency systems. Part power hybrid system analysis illustrated a decrease in system efficiency for a decrease in the amount of electrical power produced by the system. Operating at 55% full power resulted in hybrid system and SOFC stack efficiency decreases of 10 and 7 points, respectively, when using a fixed speed turbine. Similar trends were observed for systems using a variable speed turbine as well. For

variable speed turbines, an increase in SOFC efficiency and a decrease in plant efficiency were observed for decreased turbine rotational speed. This was due to the increase in effectiveness of the recuperator at lower air flow rates which resulted in a higher SOFC inlet temperature at part power. This work provided a substantive analysis of off design operation, accounted for component flexibility and accompanied the technical work with a preliminary financial analysis. The work was primarily foundation, as topics essential to system operation and design such as failure analysis, ambient condition impact, scalability, transient analysis, and internal component (i.e. SOFC) dynamics were not considered or presented. Magistri conducted another study, characterizing a larger scale (2 MW) SOFC/GT hybrid using Rolls Royce's IP-SOFC [39]. This study built upon the last by including a finite volume model for the SOFC to capture internal operating diagnostics (though the internal results were not presented) and an analysis of the impact of ambient conditions. The ambient conditions study illustrated that increases in ambient temperature increase the stream temperatures throughout the entire system and increase HS efficiency. The impact of ambient conditions on system operation is observed in this dissertation study as well. These two studies by Magistri are extremely foundational as they present the development and implementation of models to simulate and characterize system general system operation for on and off design conditions.

Additional studies investigating the impact of ambient conditions on hybrid system operation are presented by Roberts et al. [50] and Maclay et al. [46]. Roberts et al. [50] present an analysis of the impact of varying daily load profiles and ambient condition variation on FC/GT hybrid systems. The model used in the study characterized a 1.15 MW pressurized SOFC/GT hybrid designed around the Capstone C200 micro-turbine generator. Results illustrated that though respective increases and decreases resulted from increases in ambient temperature, controllers could be implemented to maintain a constant system power on a range of -5 °C to 35°C. The system also illustrated the capability to follow grid load demand with maximum demand occurring at mid-day.

Gas turbine power remained nearly constant throughout the transient response with SOFC power following the trend of the load demand closely. Though, this study investigated the impact of variations and load demand on system performance, uncontrolled impact of ambient condition variation on system performance was not presented. This data would be valuable in developing alternative control strategies and methodologies for maintaining required system power demand. A complementary study separating the system response while operating with a pre-designed controller would be both appropriate and valuable. Maclay et al.[46], studied the impact of daily pressure and temperature effects on turbomachinery stability in SOFC/GT hybrid systems. Similar to Roberts et al., this work primarily discussed the efficacy of a controller to control the impact of said ambient effects on system operation. Changes of 14K in ambient temperature resulted in turbine speeds ranging between 3475 RPM to 3745 RPM and turbine inlet temperatures ranging between 1004K and 1012K. Changes in ambient pressure from 99.3kPa to 103.3kPa result in less than 100 RPM change in turbine speed and a 1K change in turbine inlet temperature. Results of the work illustrated that the effects of diurnal temperature and pressure effects could be well controlled system wide, but similar to Roberts et al., a study independent of an implemented control algorithm to capture unfiltered system dynamics would be valuable for obtaining a baseline understand of system dynamics.

In continuing on the hybrid system (HS) development path, control and utilization of air management has been identified as an essential tool for reliable and safe SOFC/GT hybrid system operation. Traverso et al. present a work that analyzes and compares transient and steady-state performance characteristics of different types of turbo machinery for controlling air through a pressurized SOFC stack that is integrated into a hybrid system [41]. The three control mechanisms identified in the work were variable speed control, by-pass valve control and bleed valve control. The work presents the impact of using these mechanisms to control cathode air-flow on a number of system

operating parameters such as turbine power, surge margin, and recuperator exit temperature. The results exhibited that the variable speed microturbine was the best option for off design SOFC/GT operation due to its ability to control airflow as well as decreasing failure possibilities by minimizing system complexity. By-pass flow exhibited the ability to better maintain FC operating pressure during off-design operation, which is essential in ensuring reliability of the stack. And the impact of bleed valve control was minimal. The model that was used did have the ability to characterize the system operation in transient fashion, but no transient characterization was presented or discussed.

Tucker et al. presents a work [14] studying airflow management control for SOFC/GT hybrid applications. Using the HyPer facility, the work illustrates that the impact of CA (post compressor) bypass flow has a much more significant impact on flow throughout the system than bleed air by-pass. Furthermore, bleed air by-pass has been shown to directly decrease system efficiency without much benefit as well as increase required fuel. CA by-pass flow was able to divert 49% of cathode air flow with a significant impact to system efficiency (19.6% increase in required fuel over base case). Bleed air, though not very effective for controlling air flow, was effective for increasing shaft load and absorbing thermal transients with reduced by-pass flow. Its impact on efficiency was significant, requiring a 39% increase in fuel for a bleed air flow of 20.8% of the compressor inlet flow. It was also very effective in increasing surge margin. HA by-pass is an effective means of controlling cathode air flow as well.

Determination of the hybrid system operating envelope was investigated by Tucker et. al as well [15]. In this study, bleed air, hot air and cold air by-pass flow was varied, in addition to turbine load and SOFC load. It was determined that FC power output could be increased 30% or turned down 57% from its nominal load of 220A. Cathode airflow could be varied for a 17% increase to a 39% decrease from its nominal condition of 1.4 kg/s through a stack of 3225 cells. An overall system operating range of

228kW to 737 kW was demonstrated, representing a potential 69% turndown. This work was foundational for the HyPer facility and the SOFC/GT hybrid community, given its comprehensive parametric analysis of all four system state control variables and their impact upon the range of operability and achievable performance. Identifying the feasible bounds of operation for the HyPer facility as well as the development of a methodology for determining an operating envelope for SOFC/GT hybrids was tremendously beneficial for the advancement of the field.

Building upon the studies of system operation at steady state, transient characterization will be key in the development of control strategies for large scale distributed operation. Ferrari et al. [51] developed a transient model of the NETL HyPer facility and conducted a comparative study between experimental results and work presented by Shelton et al. [40]. The results and particularly the dynamic response of the models and the empirical results of the facility compare very well. The model presented by Ferrari was slightly more accurate than the one presented by Shelton et al., because experimental data was used to generate the turbo machinery maps for the conditions considered. The study presented by Shelton et al. describes the model while also characterizing turbine start-up. Agreement between the model and empirical results did not compare very well yet, the dynamic response did align with the actual system dynamic response. The lack of correlation is mainly contributed to the difference in the turbine map used for the model verses the one that applies to the HyPer facility. This work focuses solely on phase 1 gas turbine start-up and does not include an embedded SOFC model nor does it consider impacts on the SOFC during start-up.

Mueller et al. [47, 52] presented two investigations focused upon transient modeling and analysis of SOFC/GT hybrid systems. The initial work [52] investigated the use of control strategies on a small scale SOFC/GT system to improve the transient capability of system operation (i.e. speed of transient response to system perturbations). Particularly, the work investigated controlling system combustor temperature by

manipulating fuel cell current. The results illustrated the ability to obtain system efficiencies of 60% during steady state operation and efficiencies as high as 40% during transient response. This work was followed by a study presenting the design, simulation and control of a large scale, 100MW SOFC/GT hybrid system [47]. In similar fashion, the results of this work illustrated that efficiencies of 60% could be obtained during steady operation and presented a comprehensive set of recommendations that could be employed in the development of design strategies for maximizing system performance during transient operation.

Jiang et al. [38] presents a study that utilizes a computational model to develop control strategies for start-up and part-power operation. This investigation focused primarily on SOFC operation and dynamics as opposed to the gas turbine. The model used was however of the lumped parameter type and provided minimal insight on the internal dynamics experienced by the SOFC.

The HyPer facility was one of the first of its kind to utilize HiLS to characterize an SOFC while operating in hybridized manner with a gas turbine. The concept was developed and implemented by Smith [21] and then used to characterize the impact of FC transients on system operation and vice versa. Liese et. al [19] presents the initial, 0-D, lumped parameter model that was used in the HyPer facility along with preliminary results which demonstrate its operability as it was coupled with the HyPer facility. Smith et al. [20] used the model coupled with the HyPer facility to investigate the impact of load transients on system operation. Load increases and decreases of 15A between 292A and 307A on the SOFC stack were conducted. Changes in FC load impacted the amount of thermal effluent that was provided to the system from the SOFC subsystem and ultimately resulted in rapid changes to turbine inlet temperature and thus turbine speed. Pressures and flows in the system will eventually follow suit with turbine speed transients. As stated by Smith, although little change in system energy input and output was realized during the current demand transients, significant short term responses were

observed that indicate challenges for hybrid system control. Though true on a system level, the lumped nature of this model did not allow for it to fully capture the internal SOFC dynamics which, given the operating state of the system, can be significant and potentially threatening to system reliability.

Tucker et al. conducted a study using the HyPer facility to determine the impact of system transients on SOFC operation [17]. Step changes in HA by-pass valve position while the system was operating in OL (variable turbine speed) resulted in a decrease in cathode air-flow, a decrease in turbine speed, and consequently had an impact on the SOFC. Results illustrate that the first 100s to 200s of the transient response to a step increase in HA by-pass valve position resulted in an SOFC dynamic response that was significantly different than when the SOFC simulator was not activated. The change in airflow impacted electrochemical activity in the FC and chemical activity in the post combustor thus affecting the thermal effluent from the SOFC sub-system in transient manner and operational dynamics from the entire system. Though this investigation was very beneficial in characterizing the impact of SOFC operation on system dynamics when cathode air flow changes, significant insight on the impact on the SOFC could not be obtained given the level of fidelity of the model.

2.2: SOFC Modeling Efforts

The first key contribution of this dissertation work is the development of a 1-D, real time operating SOFC model capable of operating in-the-loop with a gas turbine to simulate SOFC-GT hybrid system operation. This section presents some pre-existing work in the area of SOFC modeling by dissecting the field into subsections of steady state, dynamic, and real time modeling efforts. Discussion of prior modeling art with brief comparisons with the model developed for this presentation and presented in Chapter 4 are presented.

2.2.1 Steady State Models

A number of steady state, SOFC modeling efforts have been conducted to characterize cell performance [44, 53-56], thermal response [28, 29], and transport phenomena [6, 25, 57, 58] respectively. Campanari and Iora [27, 59] conducted two studies in which they implemented and refined two steady state models for both a tubular and planar cell geometry. The tubular work [27] presents a steady state model that has been calibrated using available empirical data for two separate tubular SOFC modules operating under pressurized conditions. The work also presents a sensitivity analysis on the impact of activation energies and pre exponential factors on cell performance and operation, given the wide range of values found in the literature. The work illustrates the importance of operational parameter calibration with empirical data to accurately characterize electrochemical losses and cell performance. The planar SOFC work presented by Campanari and Iora [59] compares a coarse grid and a fine grid, finite volume SOFC models. The study showed that the fine grid model did offer more detail on the internal operation of an SOFC but that there was a point of diminishing returns depending upon your operating regime. In addition to the comparison, a parametric analysis was done to investigate the impact of different heat losses, air ratios, and inlet temperature assumptions upon cell operation. This analysis corroborated the importance of minimizing peripheral heat losses and optimizing air flow to minimize significant thermal gradients in the SOFC. The sensitivity studies presented by Campanari and Iora were foundational in characterizing the importance of properly identifying material properties and levels of discretization in modeling efforts. Other steady state modeling efforts have placed particular focus on different components of SOFC design such as the impact of the presence of DIR [53, 60] and integrated planar solid oxide fuel cells [54].

The DIR focus in SOFC modeling has played a significant role in the development of models that characterize SOFC operation for gasification FC systems [44, 55]. The quasi 2-D model presented by Li et al. [44] is verified against the IEA

SOFC modeling benchmark and also presents a sensitivity analysis that was conducted to calibrate the model to characterize state of the art SOFC operation. This was done by identifying the appropriate activation energies for the anode and the cathode. Simulation results characterizing the model operation using both humidified hydrogen (HH) and syngas fuel feeds and operating in both a co-flow and counter flow arrangement are presented in distributed manner. In complimentary fashion, the work presented by Hernandez-Pacheco et al. [55] identified though simulation that variations in syngas fuel feed compositions have a very significant impact on SOFC operation and performance; and fuel feed composition and type can be used as a control mechanism to mitigate potentially harmful operational effects.

Given the significant thermal sensitivities that apply to SOFCs the utilization of modeling efforts to investigate the impact of various operating states and conditions on the thermal state of the cell have been conducted [28, 29]. Chyou developed 1-D and 2-D models that were used to characterize the thermal condition of the cell while operating at a steady condition [28, 43]. The work was primarily a proof of concept and showed validity, as illustrated via strong agreement with the experimental results from the literature. Sudaprasert developed a three-dimensional model that investigates the impact of isothermal and adiabatic wall boundary condition assumptions on stack thermal conditions [29]. The work illustrated that isothermal stack wall boundary conditions allowed for lower operational and maximum temperatures given the transfer of heat to the atmosphere, but resulted in significant maximum interior temperature. The adiabatic boundary elevated average cell operational temperature and produced maximum values near the fuel and air outlets. Though beneficial, this work lacked a three-dimensional characterization of the electrochemical performance which plays a significant role in understanding cell operation, and given the coupled nature between electrochemistry and cell thermal conditions. Mitigation strategies for addressing significant temperature gradients could be developed as well.

Mass transport and its impact on cell performance has been addressed in the literature. Chan et al. presents work investigating the micro pore structure of the SOFC [58]. The model used in the investigation characterizes the complex relationship between electron, ion and gas molecule transport and chemical reaction at the triple phase boundary. The work determines the impact of anode particle and pore size on SOFC electrochemical polarization losses and general operation. Yakabe et al. [56] investigate the impact of CO-CO_2 binary fuel feed and a methane reformed syngas mixture on cell operation as well as the impact of electro-oxidation of CO. Results showed a minimal impact on concentration polarization between the HH and CO-CO_2 fuel feeds and good agreement with the results found in the literature. Nelson et al. [6] and Cayan et al. [57] look specifically at the impact of mass transport on SOFC performance. Cayan et al. [57] present a correction factor that can be applied to Fick's law in SOFC models to account for inaccuracies at higher levels of current draw. This is very beneficial when computational burden affects mass transport calculations and thus was applied in the model used for this dissertation effort [57]. Nelson and Haynes investigate the impact of rib contact area on mass and electron transport employing a 2-D analytical mass transfer model [6]. This work identifies what has been coined a "fuel depletion current density" which is the current density at which fuel is not necessarily fully consumed, but it exist in an amount that is not sufficient enough to ensure that it will be present at the TPB in adequate amount. This in-depth analysis illustrates the flaws in the button cell approximation and presents performance metrics and correction factors that can be employed to better represent cell mass transfer.

2.2.2 Dynamic Models

A number of works have been published regarding SOFC dynamic and transient modeling, most of which focus upon the areas of standard operational performance [35, 61-63], SOFC start-up [18, 43, 64, 65], or applications for integrated systems [19, 36, 66,

67]. Achenbach's three-dimensional transient planar SOFC stack model [30] laid a framework for computationally characterizing the operation of SOFCs. The model simulates thermal and electrochemical operation, accounting for reactant stream chemistry and anode recycle, and allowing for simulations of various flow types. Published in 1994, it remains a popular reference.

With regards to dynamic characterization of standard operating performance, Aguiar, et al. [61], presents a follow up to a previously discussed article [53]. In the work, simulations of a planar SOFC being subjected to various load changes were presented. Particular focus was placed on max temperature control of the SOFC via a PID air flow controller that used outlet fuel stream temperature as its control variable. Though the work exhibited the ability to control maximum SOFC temperature, an analysis of internal temperature gradients and thermal transport as well as spatio-temporal data of electrochemical parameters were not presented. Additionally, most of the tubular SOFC work that was reviewed [33, 35, 53] focused upon transient response to load changes, but neither internal dynamics nor the impact of balance of plant or system feedback are presented or discussed.

Start-up work primarily focuses upon thermal effects when load is applied to the SOFC. The only reviewed investigation that presents a spatial temperature gradient analysis is presented by Damm and Federov [68], and conversely it does not account for electrochemical activity but only inert heating or cooling of the SOFC during start-up and shut-down. Damm and Federov present a reduced order transient model to characterize inert heat-up and cool-down for SOFCs. To minimize thermal shock and creep of SOFC, the model was used to identify regimes of heightened spatial temperature gradients, temporal derivitives and minimized heating time. The analysis illustrated that by increasing the velocity of the air stream and lowering the Peclet number, an optimal design point was achieved. The results of this work presented effective strategies for SOFC phase I, inert start-up heating.

Chyou, et al. [43] conducted a study to investigate the impact of electrochemical start-up, employing stepwise load applications. The main premise of the work was to develop and identify an effective means of "loading" the fuel cell in stepwise manner while minimizing thermal impact to the SOFC and decreasing start-up time. Parameters such as cell temperature variation and ramp rate were the characterizing parameters of interest for the transient analysis. The optimized case resulted in a maximum temperature ramp rate of approximately 4.4 K/min and a total response time of approximately 40min. The development and implementation of a start-up strategy of this nature is beneficial for the SOFC arena, particularly with regards to the work that is presented in this dissertation.

Salogni et al. [36] present the development and validation of a non-linear dynamic lumped parameters model of a SOFC stack suitable for integration into models of complex power plants. Coupling an SOFC module into an integrated/hybrid modeling framework allows for system dynamic feedback on SOFC operation to be captured and realized. As with most modeling efforts, the work presented is completely computational and, though the SOFC operation that can be characterized does account for system feedback, it does not hone the accuracy of an actual hardware facility.

Leucht et al. [66] present the modeling and simulation framework for a SOFC model for hybrid system applications. The work investigates control approaches such as air and fuel flow management, power management and POx air control. Preliminary seed results illustrate the impact of dynamic load variation experiments on cell operation. One major drawback about this model relates to its SOFC characterization. Its electrochemical modeling approach is not fundamental, but rather purely empirical, given that a look-up table is used to determine electrochemical parameters. Though this may increase the level of accuracy for the model for a particular SOFC, it does not afford the flexibility to conduct sensitivity analyses or to observe the impact of various material or component selections on SOFC operation and performance.

2.2.3 Real-Time Models

Very few real-time models have been developed and disclosed in the literature. Real-time capability is both valuable and necessary for HiLS applications, which provide the inherent value of coupling the flexibility of modeling and the accuracy of actual hardware. Liese et al. [19] presented a real-time model. The model was of the lumped parameter type and was coupled with the HyPer facility to characterize SOFC operation while operating in-the-loop with a gas turbine in the HyPer facility. The next iteration of that model, presented by Hughes et al., was 1-D and allowed for spatio-temporal characterization of the SOFC while operating in the loop [18]. The model has been used to characterize load change using both HH as well as a syngas fuel feed. Inert heating characterization capabilities have been exhibited. The model presented by Hughes et al. is the one that is used in this dissertation work.

2.3 Summary

The background and literature review chapter presents and discusses a plethora of work in the SOFC/GT hybrid arena. The concept design of the systems have illustrated tremendous ability to impact the energy arena and thus a number of government and independent research efforts are underway to develop SOFC technology along with its hybridization with gas turbines. The Solid State Energy Conversion Alliance (SECA), operated by the U.S. Department of Energy (U.S. DOE), has been in support of this effort for quite some time with successes such as the construction of the HyPer facility to empirically address the system integration challenges associated with hybrid systems.

The literature review presented a wide array of research efforts in the SOFC modeling and SOFC/GT hybrid system research areas. The majority of the hybrid system studies were conducted using empirical models and focused heavily on characterization of the system in various operating states and the development of strategies to improve system performance. SOFC modeling literature presented was either heavily foundational

with respect to modeling development for SOFCs or segmented their focus to either thermal dynamics or electrochemical dynamics, and did not address the important coupling component between the two. Some of the dynamic SOFC models did investigate SOFC start-up, but did not account for system/ BOP feedback nor were they coupled in hybrid manner.

Very few real time models, aside from the one presented in this work, have been identified in literature. Initially of the lumped type, the model presented in Chapter 4 has been upgraded and developed into a 1-D, SOFC model that is used to characterize the SOFC in spatio-temporal fashion. Aside from the work done at the HyPer facility and presented by Tucker et al. [69], the utilization of real-time SOFC models for hardware-based simulation of hybrid systems have not been conducted. The coupling of a 1-D, real time SOFC model with a hardware facility for the purposes of characterizing electrochemical start-up of a hybrid system was not found in literature and represents the novelty and accomplishment of this work.

CHAPTER 3

EXPERIMENTAL METHODOLOGY

Recent technological advancement and research efforts have demonstrated the capability to utilize hardware-in-the-loop simulation for the research and development of solid oxide fuel cell/ gas turbine hybrid systems [14, 20, 21]. The project presented by this dissertation work focuses on utilizing HiLS methodology for investigating the electrochemical start-up phase of a SOFC/GT hybrid system. The work presented involves empirical investigations conducted using the HyPer facility, a HiLS SOFC/GT hybrid system simulation facility established by the U.S. Department of Energy's National Energy Technology Laboratory in Morgantown, WV.

Presented in this chapter is a detailed description of the HyPer facility and the experimental plan used to investigate the impact of electrochemical start-up on component-level and system-wide performance. First, a detailed description of the HyPer facility hardware and its operational and control components are presented. Next, the original experimental hypothesis for the dissertation project, followed by the results of a scoping study used to finalize the project's focus, will be discussed and developed. Finally, the experimental plan that was conducted to investigate the impact of electrochemical start-up on system performance is presented.

3.1: Facility Description

The HyPer facility, presented in Figure 3.1, is a pilot scale, SOFC/GT hybrid power plant simulator located at the U.S. DOE NETL in Morgantown, WV. The HyPer facility is composed of a 120 kW gas turbine compressor assembly, a 1-D distributed, real time operating, fuel cell model, an air plenum and associated piping to represent a SOFC stack, and all associated balance of plant hardware components. In addition to all of the

operational components, pressure, temperature, flow and speed sensors are strategically located throughout the system for the purpose of monitoring and controlling system operation and analyzing system performance.

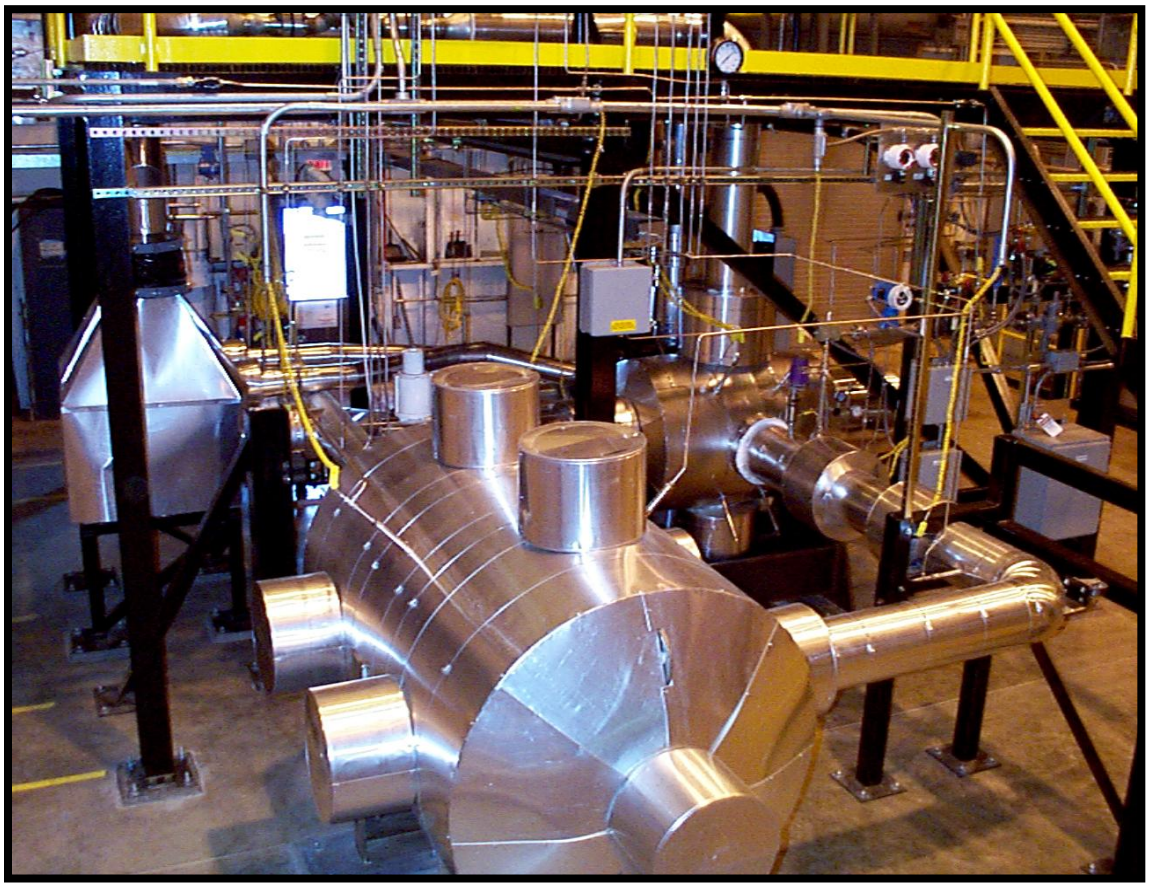

Figure 3.1: Photo of the HyPer facility at the U.S.DOE NETL in Morgantown, WV

The 1-D distributed fuel cell model was constructed on a Matlab-Simulink™ platform and integrated into the HyPer facility using dSpace™ controldesk software. The dSpace™ software has the ability to be coupled with Matlab-Simulink™ models and allows the user to change system inputs and observe transient changes in system operating parameters as desired. The model is built to operate in real time and, through the dSpace™ platform, can extract live inputs from the operating HyPer system and simulate and characterize fuel cell operation in real time. The model has the capability to produce current density, cathode oxidant stream temperature, solid fuel cell temperature

and polarization profiles that have both spatial and temporal resolution. The model used will be described in greater detail in Chapter 4.

3.1.1: System Hardware

The development of HiLS systems requires the inclusion of three main components for a complete facility capable of system analysis: hardware, instrumentation, and software. The hardware component of this HiLS facility is the physical plant that is located at the NETL facility. A simplified flow diagram of the HyPer facility is presented in Figure 3.2.

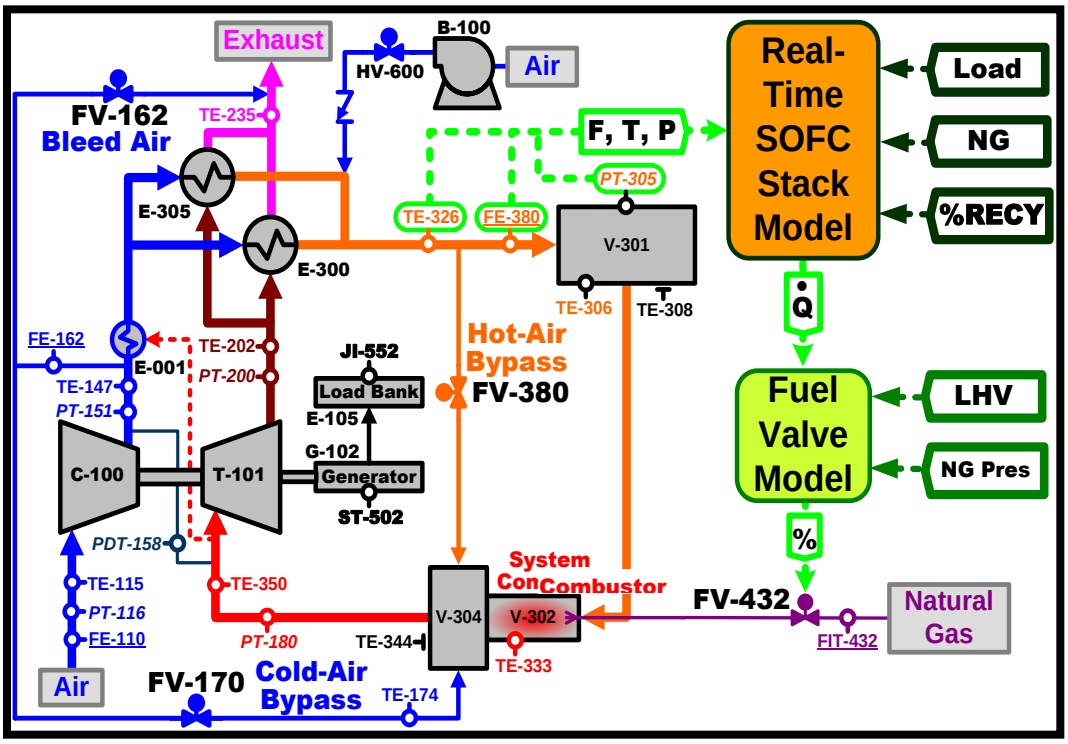

Figure 3.2: Simplified flow diagram for the HyPer simulation facility

The use of physical hardware provides a high level of accuracy in capturing the non-linear behavior and dynamics of the system. In addition, the coupling of hardware and software allows more flexibility and robustness within the simulation since potentially computationally burdensome phenomena, such as flow dynamics, are already accounted for by the hardware. Section 3.1.1 provides a description of the hardware

components of the facility adopted from previous NETL HyPer publications [14, 16, 17, 21].

3.1.1.1. Gas Turbine/Auxiliary Power Unit (C-100, T-101, G-102)

A 120kW Garrett Series 85 auxiliary power unit is used as the turbine-compressor assembly for the HyPer facility. The APU makes use of a single shaft and consists of a direct coupled turbine, with a nominal operating speed of 40,500 RPM (T-101), a dual-stage radial compressor (C-100) and a synchronous, gear driven generator (G-102) used to produce electrical power. The electrical generator operates in synchronous fashion at 400 Hz and is loaded by an isolated resistor bank (E-105). System operators determine the generator load, via electrical resistance, and it can be varied through a range of 0-75kW. The compressor is designed to deliver 2 kg/s of flow at an approximate pressure ratio of 4 and a discharge temperature of 475K for an inlet at an ambient temperature of approximately 298K.

The unit was originally designed for aviation applications, and thus required jet fuel. The modification included removing the internal combustor from the APU and inserting modification (E-001). The new design allows the turbine to run only on heat provided by the fuel cell subsystem simulator combustor (V-302).

3.1.1.2. Heat Exchangers (E-300 and E-305)

The facility uses two counterflow, primary surface heat exchangers for preheating the inlet air to the pressure vessel (V-301), which is used to simulate the cathode air volume and associated manifolding; and this is done via heat exchange with the turbine exhaust. The two recuperators are connected in parallel to ensure that adequate heat is exchanged to the V-301 inlet stream, which represents the cathode inlet, under maximum flow conditions (2 kg/s). The maximum operating temperature on the exhaust and pressure sides are 910K and 780K, respectively. Limitations on the exhaust side are due

to turbine exhaust restrictions. The volumes of the pressure and exhaust sides of the recuperators are 110L and 260L, respectively. The heat exchangers have a nominal effectiveness of 89%

3.1.1.3. Pressure Vessels (V-301 and V-304)

The pressure vessels are used to provide a physical representation of the fuel cell air manifold and cathode volume (V-301) and the post combustion volume (V-304) of a representative fuel cell sub-system. The vessels were designed to accommodate simulating various selections of fuel cell stack design and rating. The air plenum (V-301) and associated piping has a volume of 2000L, and the post combustion volume (V-304) has a volume of 600L.

3.1.1.4. By-Pass Valves

System pressure drop is one of the critical parameters used to characterize the system performance. Minimization of losses throughout the system contributes to more efficient operation. Given the importance of minimization of system pressure drop with regards to maximizing system efficiency, no valving was placed in the main pressure loop connecting the compressor exhaust to the turbine inlet [21]. This strategy provides a mechanism for reducing system pressure drop, but it must be accompanied by an effective means of cathodic flow control for thermal management of the solid oxide fuel cell. For the purpose of addressing this need, three by-pass valves are used: cold air (routes compressor exhaust into the post combustion volume), hot air (by-passes air from the exhaust of the heat exchangers to the post combustion volume) and bleed air (by-passes compressor exhaust to the atmosphere). The locations of these valves are indicated in Figure 3.2. A study characterizing the impact of the by-pass valves on cathodic airflow and system performance was conducted and published by Tucker et. al. [17]. Their individual characteristics and general impact on system performance are presented.

3.1.1.4.1. Cold Air By-Pass (FV-170)

The flow path of compressor discharge permitted by the use of cold air by-pass is presented in Figure 3.3. As illustrated, the cold air by-pass valve allows the compressor exhaust to flow directly to the post combustion volume, bypassing the heat exchangers, air plenum and combustor.

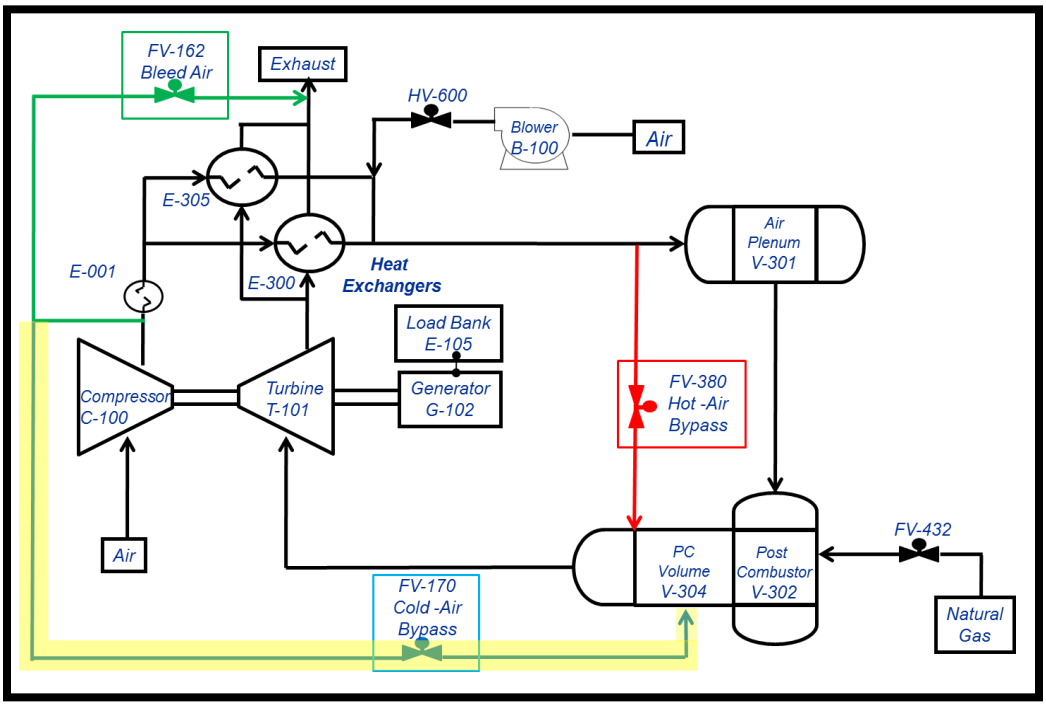

Figure 3.3: Cold air by-pass flow path

The cold-air by-pass valve is effective in modulating the cathode air flow rate, and increasing the valve's opening results in a decrease in cathode inlet temperature. It is also very effective at mitigating compressor surge since increasing CA by-pass increases air flow through the compressor which moves the operating state away from the stall line, and is a key component in the stall recovery mechanism that has been developed and integrated in the HyPer system control panel. FV-170 is a Fisher V150 Vee-Ball control. The valve is air actuated and has a 15.4 cm inside diameter. At its 100% open position, FV-170 can divert 68% of the compressor's discharge flow.

3.1.1.4.2. Hot Air By-Pass (FV-380)

Hot air by-pass is used to divert airflow from the exit of the heat exchanger to the post-combustor volume, thus by-passing the fuel cell simulator air plenum, piping and combustion volume. The flow path is illustrated in Figure 3.4. Use of hot air by-pass provides a mechanism for controlling and modulating cathode air flow while minimizing the impact on associated balance of plant. The impact of hot air bypass on air pre-heat exchange and turbine inlet temperature is smaller, thus resulting in it having a minimal impact on cathode inlet temperature. Prior work [14] has also shown that it has a minimal impact on surge and stall phenomena as well.

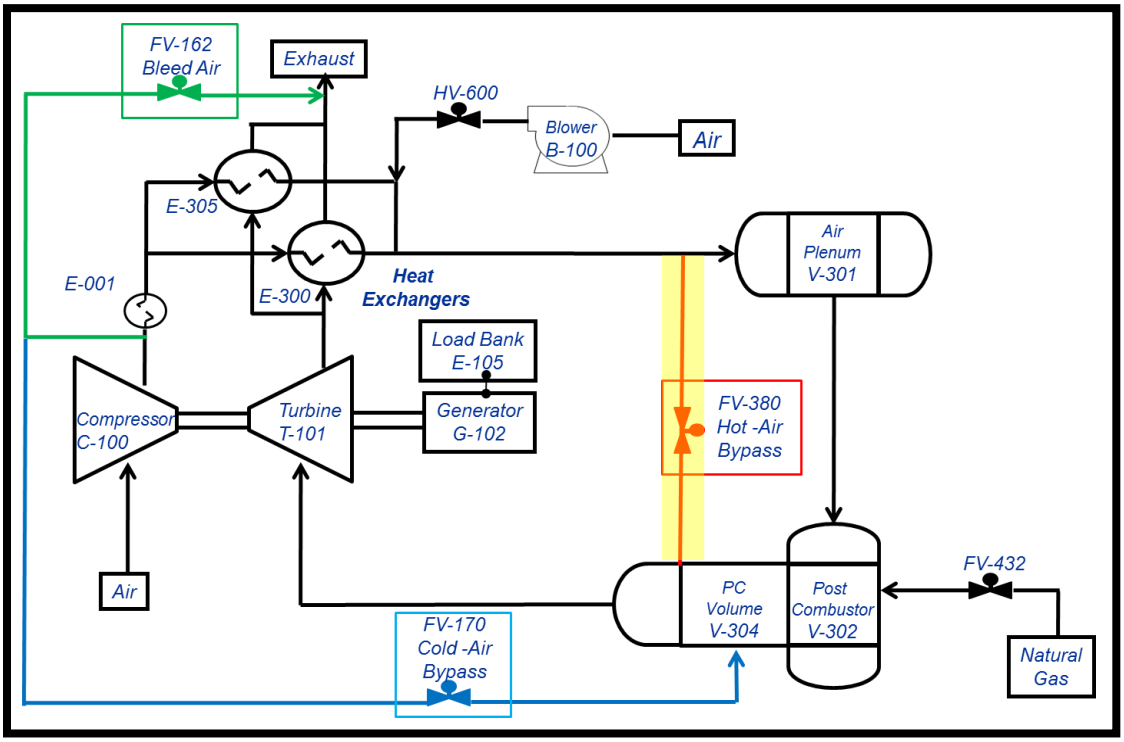

Figure 3.4: Hot air by-pass flow path

FV-380 is an air actuated, 15.4 cm inside diameter Valteck MaxFlo 3 eccentric rotary plug control valve. The valve is designed for pressurized operation at temperatures in excess of 673 K and has a full range slew rate of approximately 2 seconds. A 100% open condition results in a diversion of 54% of compressor discharge flow.

3.1.1.4.3. Bleed Air By-Pass (FV-162)

FV-162 is used to divert compressor discharge directly to the system exhaust, as illustrated in Figure 3.5. Bleeding air to the exhaust provides an effective means of increasing mass flow through the compressor since it diverts air directly to the atmosphere, without increasing the pressure ratio, which can increase stall margin, but it directly results in a decrease in system efficiency, since the air that is bled is not being used to generate any power. Given the deleterious impact on system efficiency, bleed air is typically only used as a means for mitigating surge and stall.

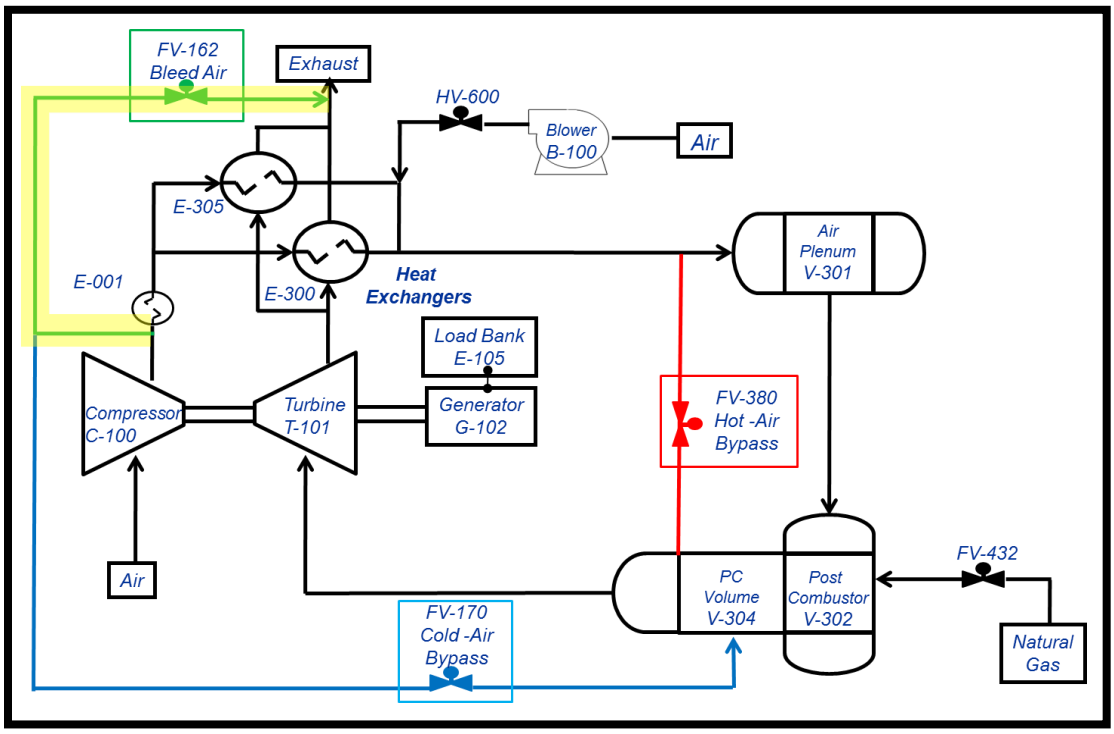

Figure 3.5: Bleed air flow path

The bleed air valve is a Valtek ShearStream segment ball control valve. FV-162 is air actuated and has a 15.4 cm inside diameter and has a full range slew rate of about 1.5 s. The maximum valve position is 15% open which results in approximately an 8% diversion of compressor discharge flow. This upper limit on bleed air is primarily influenced by its impact on turbine exhaust temperature and system limitations.

3.1.1.5. Fuel Cell Simulator/Post Combustor (V-302)

The thermal effluent from the simulated fuel cell subsystem is physically represented by the combustion of natural gas in the system post combustor, also referred to as the fuel cell simulator. When operating in the HiLS configuration with the SOFC subsystem model, fuel fed to the natural gas diffusion flame burner (V-302) is controlled by way of the percent open position of the natural gas fuel valve (FV-432). The 22 L combustor is constructed in a 19.4 cm inner diameter, schedule 80 Incaloy 800AT pipe welded directly to the inlet nozzle of the post combustion volume. The combustor is air cooled and is designed specifically for natural gas fuel and for the airflow rates expected from the air plenum.

3.1.1.6. Fuel Valve (FV-432)

The fuel flow to the fuel cell simulator post combustor is the key control mechanism used to simulate the thermal characteristics of the effluent produced by the fuel cell subsystem. The flow of natural gas is controlled by a high-speed electromechanical valve that is manufactured by the Woodward Governor Company and designated as the Woodward Swift Gas Metering System. It is designed to give accurate and reliable fuel flow metering for turbine engines up to 2MW. When operating in HiLs configuration, the fuel valve is controlled by a reverse fuel valve model through the Woodward AtlasPC Control System, which is capable of operating with time steps as small as 5ms. The fuel valve consists of a sonic flow metering section which provides choked flow conditions to mitigate the impact of downstream pressure on flow rate. Valve design allows it to maintain choked flow for pressure ratios as large as 0.85, although typical pressure ratios across the fuel valve in the HyPer facility are usually near 0.5. The valve has a slew rate of 150ms within the transitional range of 10% to 90% open.

3.1.2: Sensors & Instrumentation

The HyPer facility was developed as an investigative tool for the design and development of SOFC/GT hybrid systems. To that end, process flow sensors and instruments are strategically positioned throughout the system for the purpose of system control and data acquisition for experimental investigation. As illustrated in Figure 3.2, pressure, temperature, and flow are extracted from various locations of interest along the main flow path and through by-pass flow paths as well, which affords operators the ability to extract data for experimentation and design purposes. Given the focus of this dissertation project, the data provided from a select set of sensors are of particular interest and, for the sake of brevity, are the ones presented below. A more comprehensive set of instrumentation and sensor descriptions are provided by Smith [21].

3.1.2.1. Turbine Rotational Speed (ST-502)

Optical sensor (ST-502) is used to measure the rotational speed of the turbine in RPM. The sensor picks up laser light reflected from a rotating target on the end of the generator shaft and transmits the pulse train to the frequency input of the Atlas control system. The optical sensor provides a 1,200 Hz signal at the nominal 40,500 RPM. The uncertainty of the optical sensor is 0.12%. The dynamic range of the turbine speed is between 1,000 and 50,000 RPM.

3.1.2.2. Compressor Inlet Flow (FE-110)

FE-110 is an annubar flow meter which provides a mechanical average of difference between stagnation and static pressure in the inlet pipe to determine flow into the compressor. The inlet pipe is 30cm inner diameter and FE-110 is located 3.1m from the pipe inlet and 2.4m from the compressor inlet, thus allowing for fully developed flow at the point of measurement. FE-110 uncertainty is 0.99%

3.1.2.3. Compressor Bleed By-Pass Flow (FE-162)

FE-162 is an annubar flow meter similar to that used in a similar manner to FE-110. It is located in a 15cm inner diameter pipe routed to the system exhaust manifold and stack as illustrated in Figure 3.2. FE-162 has an uncertainty of 1.5%.

3.1.2.4. Turbine Inlet and Outlet Conditions

Turbine inlet conditions are measured using PT-180 for pressure and TE-350 for temperature. The uncertainty for these sensors was found to be 0.29% and 0.18%, respectively. The turbine outlet conditions are measured using PT-200 for pressure and TE-202 for temperature. The uncertainty for these sensors was found to be 0.29% and 0.12%, respectively. Turbine exhaust gas temperature is tightly managed and a control strategy to keep TE-202 measurements in an acceptable regime.

3.1.2.5. Fuel Cell Simulator Inputs (PT-305, TE-326, FE-380)

The process flow parameters at the inlet of the air plenum, which represents the stack's manifold and cathodic combined oxidant volume are live, real-time inputs to the fuel cell subsystem model, and they are of particular interest in the presently reported investigation of SOFC electrochemical start-up. The sensors used to acquire this data for input to the SOFC model are described below.

3.1.2.5.1. Cathode Inlet Pressure (PT-305)

The pressure is measured inside the air plenum (V-301) using PT-305. PT 305 has an uncertainty of 0.27%.

3.1.2.5.2. Cathode Inlet Temperature (TE-326)

The temperature of the mixed streams exiting the recuperators which are operating in parallel is measured using thermocouple TE-326. The temperature is acquired just upstream of the hot air by-pass valve, FV-380, and has an uncertainty of 0.01% in the temperature regime up to 670K [17].

3.1.2.5.3. Cathode Inlet Flow (FE-380)

The primary air flow through the fuel cell simulator is measured at the entrance of V-301 using an annubar flow meter (FE-380) that is similar to FE-110. It is positioned inside a 15cm inner diameter pipe which is routed through V-301, V-302 and V-304. FE-380 has an uncertainty of 0.70%.

3.1.3: Control Modules

Efficient and reliable operations and controls are essential to safe and consistent operation of any power generating facility. The control system developed for the HyPer facility consists of three control modules and a main control panel used for start-up operation and emergency procedures. The main control panel, referred to as the QUADLOG, is illustrated below in Figure 3.6. The main control panel includes controls and process indicators for system purge and combustion ignition, which are the two essential sub-processes for system start-up. There are also safety operation interlocks and buttons for emergency mitigation procedures.

The two buttons on the control panel used for emergency mitigation are the stall recovery button (blue button, top right corner of panel) and the emergency stop button (bottom right hand corner). The stall recovery button is used to eliminate the occurrence of a surge and/or stall event when the operator receives audible indication from the system that the threat of such an event is imminent. When the stall recovery button is depressed, the cold-air bypass instantly moves to 55% open stem position, resulting in increased mass flow through the compressor and a translation in the operating regime from the stall line to a safer operating condition. A depression of the emergency stop button results in an immediate shut-down of the facility. This can have a deleterious effect on the turbine/compressor assembly and the associated balance of plant; it is only to be used in matters of extreme emergency.

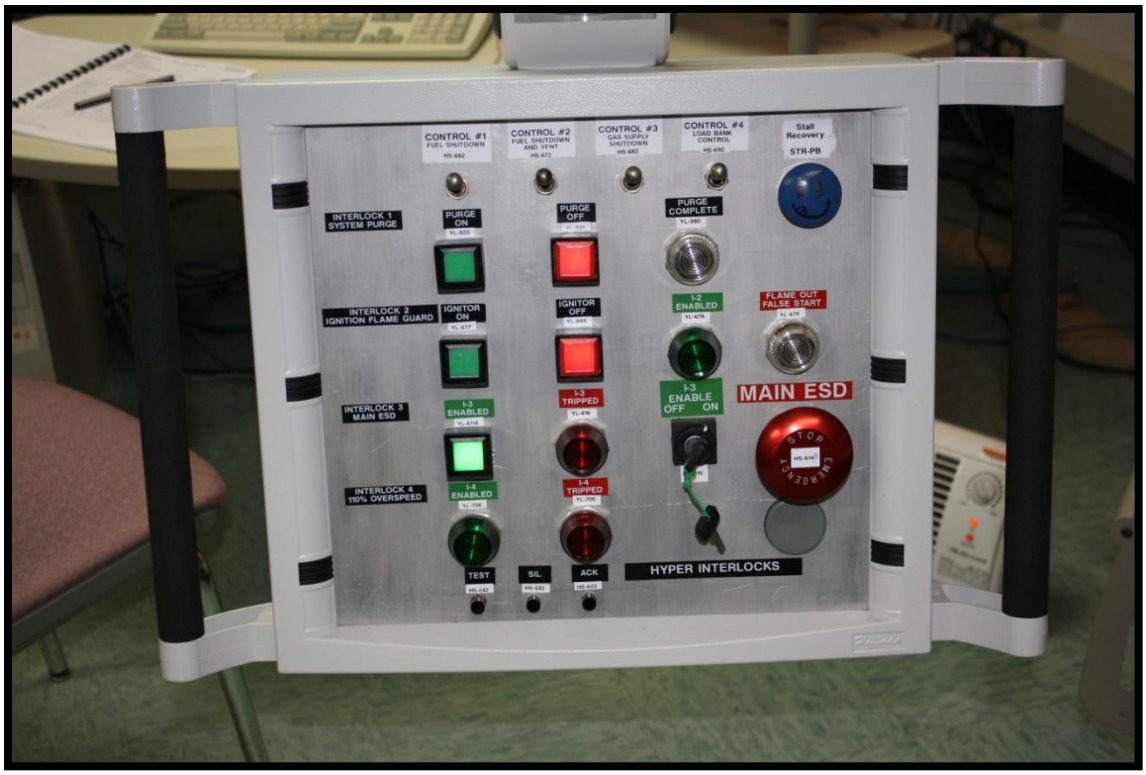

Figure 3.6: HyPer facility main control panel

The three control modules that have been designed for use with the HyPer Facility are the Woodward AtlasPC, the APACS and the dSpace. The Woodward AtlasPC houses all of the system control algorithms for reliable system operation. The main responsibilities of the Atlas controller are the by-pass valve, fuel valve and turbine speed control. It is also responsible for high speed data acquisition in as small as 5ms time steps. The APACS module is the main observational and operational system of the HyPer facility. In addition to controlling the load bank, bleed air valve, and system blower, most of the essential process variables are observed in real time from the APACS computer. In addition to displaying the process variables, it also records them every 400ms. The APACS module is also the main safety system, housing all interlocks and controlling the opening of all safety valves. The dSpace module is primarily responsible for the software component of the HiLS. The fuel cell model is housed and operated through the dSpace computer. The system is also capable of high speed system data acquisition with time

steps as small as 80ms. Detailed descriptions of the three modules are presented in this section.

3.1.3.1. Woodward AtlasPC

The AtlasPC is manufactured by the Woodward Governor Company and is designed primarily to serve as a basic fuel controller for the HyPer facility. The AtlasPC, presented in Figure 3.7, is built around a modest 266MHz Pentium CPU with 64MB RAM. The Atlas PC operating system is the real-time VxWorks OS which is essential to system functionality. VxWorks ensures the real-time, high speed, 5ms update time of the controller outputs.

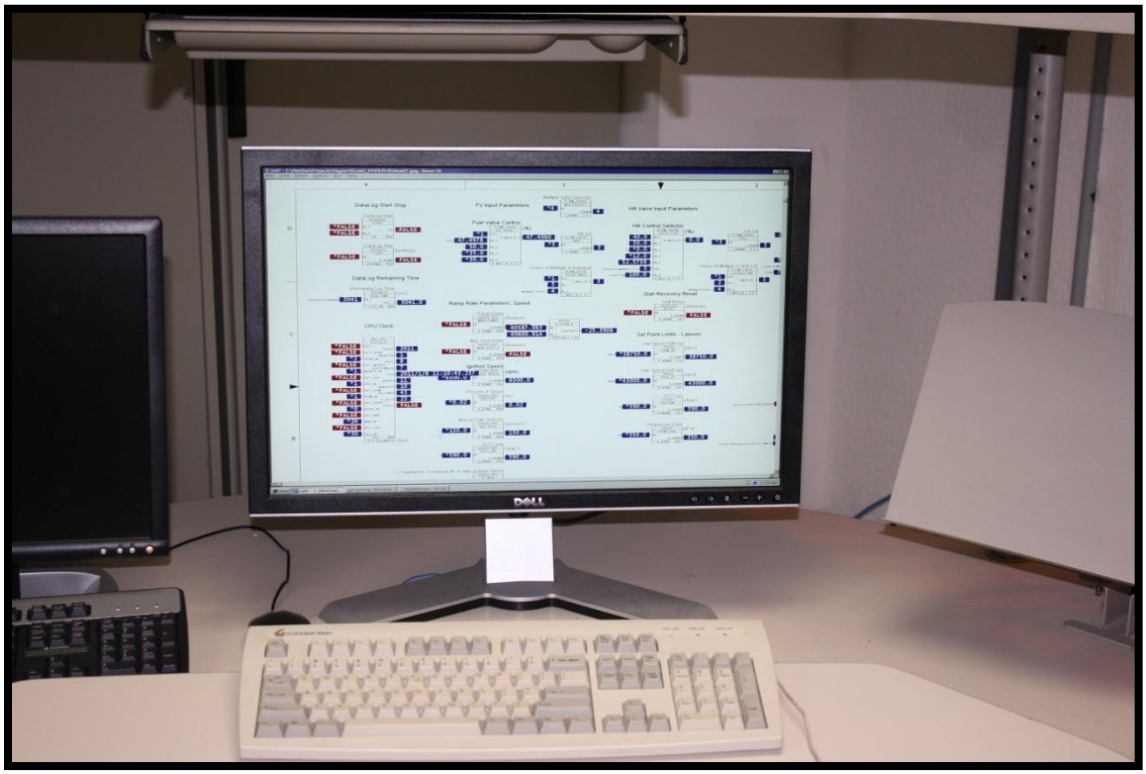

Figure 3.7: AtlasPC control system computer

Explicitly illustrated in Figure 3.7 is Woodward's Graphical Application Program (GAP). The GAP is a graphical coding program that uses functional blocks and paths to develop control algorithms. It also serves as a graphical user interface (GUI) for users and operators to communicate with the control system. The GAP has the capability of

coupling with real-time compiled Matlab/Simulink models which provides the ability for flexibility and robustness with programing controls. Specifically, as it applies to the HyPer facility, it affords the necessary capability and flexibility for integration of the fuel cell model with HyPer hardware.

The Atlas is also capable of high speed data acquisition. The data log feature has variable sample rates but it can acquire data in as small as 5ms time steps. It stores the data in on-board memory in log file format, which is compatible with most text reading and spreadsheet reading programs.

3.1.3.2. APACS

The APACS platform, which was manufactured by Siemens Moore Process Automation, is the main process controller and data acquisition platform for the HyPer facility. The APACS user interface mechanism is presented in Figure 3.8.

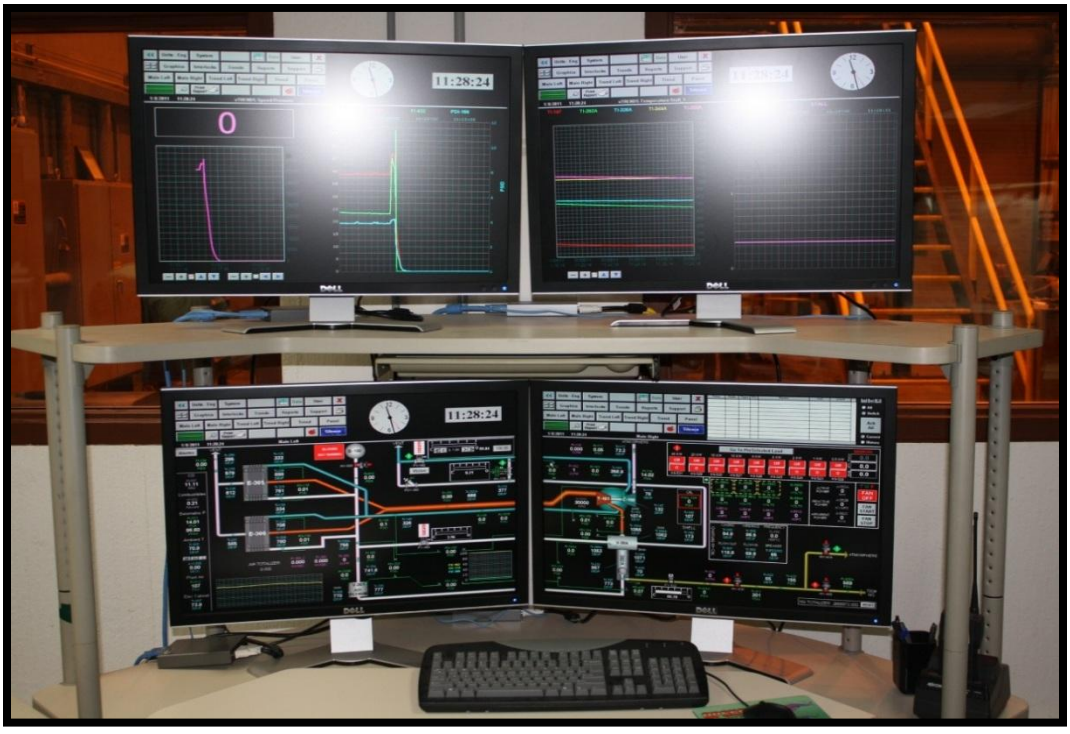

Figure 3.8: APACS control system interface

For the HyPer facility, the APACS control module handles the majority of process controls and operator commands. Specifically, the operators can control blower operation, valve position, fuel safety valves, and the generator's resistance load bank. The APACS system also houses all of the operational interlock strategies and displays the operating parameters of the system in real time, on the bottom screens, and select parameters with respect to time, on the top monitors.

All of the control and operational systems used in the HyPer facility are capable of data acquisition, and the APACS is responsible for the majority of the operating data capture. Given that the APACS is responsible for the acquisition of 82 process variables, APACS acquires data in 400ms time steps.

3.1.3.3. dSpace – Fuel Cell Model Control

The fuel cell subsystem model used in the HyPer facility was developed in the Matlab/Simulink™ platform, compiled in real-time workshop and is operated through the dSpace control desk software program. The dSpace control desk software is designed for managing and implementing real-time HiLS experiments with Simulink models. The model has two sets of inputs; one is user-defined and is prescribed by the operator, and the other is operationally dependent upon and extracted from the operating HyPer facility. The user-defined inputs are managed and delivered to the system via the dSpace control system presented in Figure 3.9.

The fuel cell model operator can control certain fuel cell input parameters such as current demand and anode fuel flow. Other operating inputs, such as cathode inlet temperature, pressure, and flow rate, are system dependent and provided to the dSpace control module via a connection with system sensors and instrumentation. The values of those operationally dependent variables are extracted in real time and displayed through the dSpace control module interface.

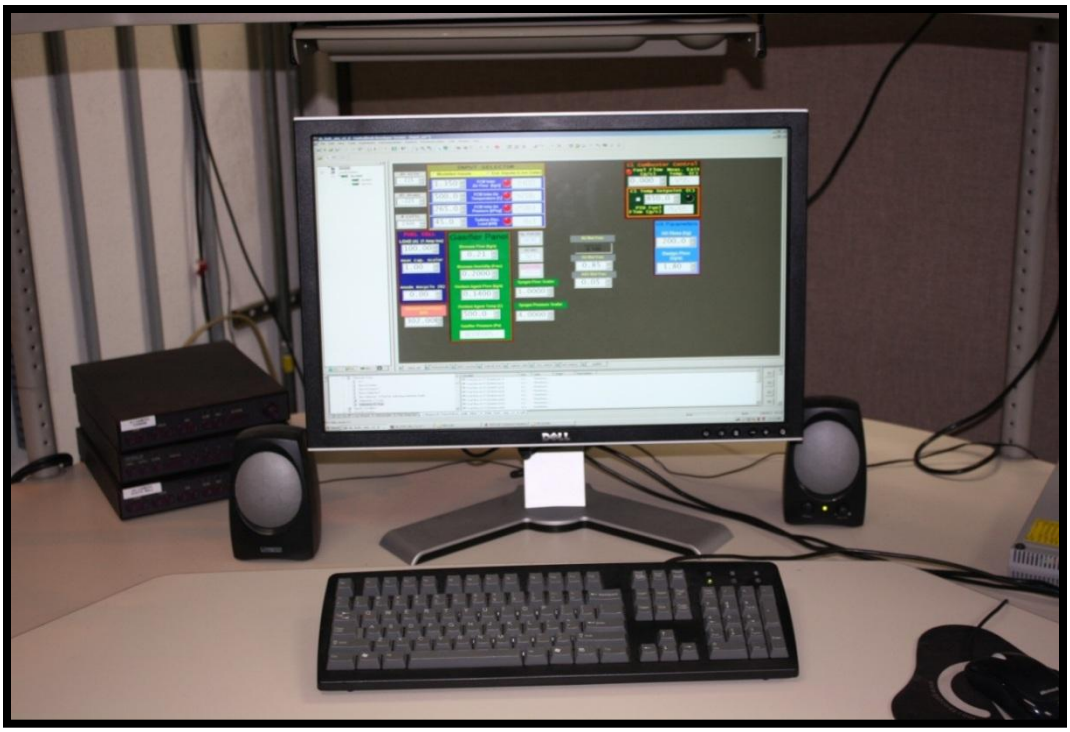

Figure 3.9: dSpace fuel cell model control interface

3.2: HiLs Integration

Hardware-in-the-loop simulation (HiLS) is a methodology that couples both hardware and software for the sake of flexible computational-empirical investigation. As illustrated in Figure 3.10, HiLS combines the accuracy that is associated with strict empirical investigation and the flexibility of numerical modeling and simulation to test dynamic behavior in an accurate and reliable fashion, all the while mitigating excessive hardware risk.

The Hyper facility utilizes HiLS to investigate the impact of hybridizing solid oxide fuel cells and gas turbines for stationary, large-scale power production. The software component in the HyPer's HiLS configuration is a fuel cell subsystem model that characterizes SOFC operation while operating in the hybrid arrangement. Real-operating measures of pressure (PT-305), temperature (TE-326) and flow (FE-380) of the inlet cathode air stream are fed to the fuel cell model from sensors and instrumentation embedded in the HyPer facility, and, correspodingly, a heat output from the fuel cell

subsystem is calculated. The heat output, or thermal effluent, is then provided via a reverse fuel valve model, which controls the amount of fuel that is fed to the system combustor that is responsible for providing the heat which drives turbine operation. The hardware component of HyPer is the turbine-compressor assembly and the remaining balance of plant components illustrated in Figure 3.2.

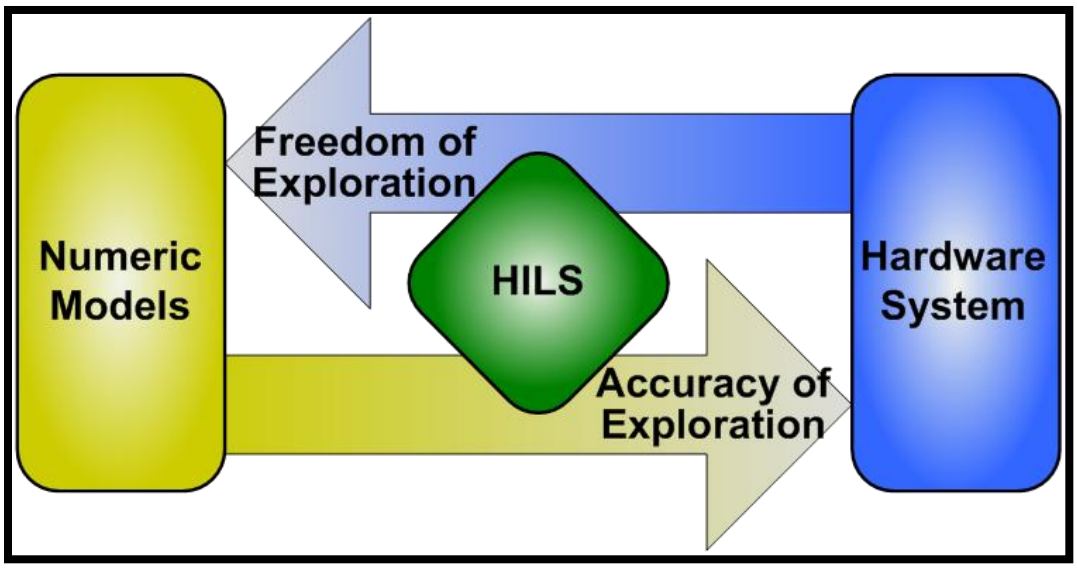

Figure 3.10: HiLS operational schematic [21]

An essential component to the development of this HiLS test facility is a real-time operating SOFC subsystem model. The model is responsible for not only characterizing the operating of an SOFC in a hybrid arrangement, but ultimately the total heat that is released from the subsystem (including the SOFC as well as the post combustion of unutilized fuel). This approach transfers only one parameter back to the operating hardware facility, but previous studies substantiate the appropriateness and applicability of this approach in the HyPer system [21]. The dynamics associated with changes in turbine speed, which are initiated by changes in thermal effluent from the fuel cell subsystem, are dominant with regards to hybrid performance. The internal construction of the robust 1-D, real time fuel cell model that is used in the HyPer facility is described in detail in Chapter 4; the operator interface, however, is presented below in section 3.2.1.

3.2.1: SOFC Model Graphical User Interface

The 1-D SOFC subsystem model GUI was built, and is operated, through the dSpace controldesk software program. As designed, there are three main operating screens of particular interest to the operator: main input screen, operational parameter screen, and profile capture screen. The main input screen is presented in Figure 3.11

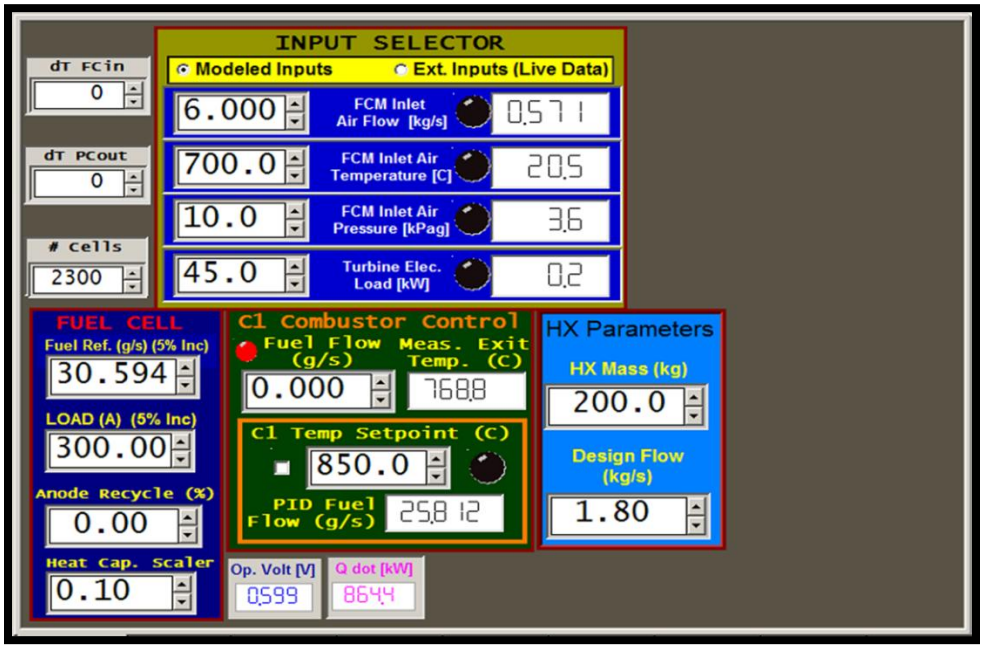

Figure 3.11: dSpace main input screen

The user inputs as illustrated from the figure are as follows: anode fuel flow, current demand, anode recycle %, heat capacity scalar, number of cells, ΔT at the SOFC inlet, ΔT ant the post combustor outlet.

The user-prescribed input parameters can be changed while the model is not running, or while operating, in the loop in real time. The operator is also required to determine whether the system prescribed inputs (cathode inlet parameters) will be user prescribed or extracted live. This feature allows the operator to run the model in off-line manner as well as in the loop. The operator also has control over cathode inlet preheat via a pre-combustor. The pre-combustor component of the model is equipped with a controller and can operate off of a prescribed fuel flow or calculate the necessary fuel

flow for a desired output temperature. For the purpose of convenience, operational voltage and SOFC subsystem thermal effluent are also displayed on the main input screen. The operational parameter screen is presented in Figure 3.12.

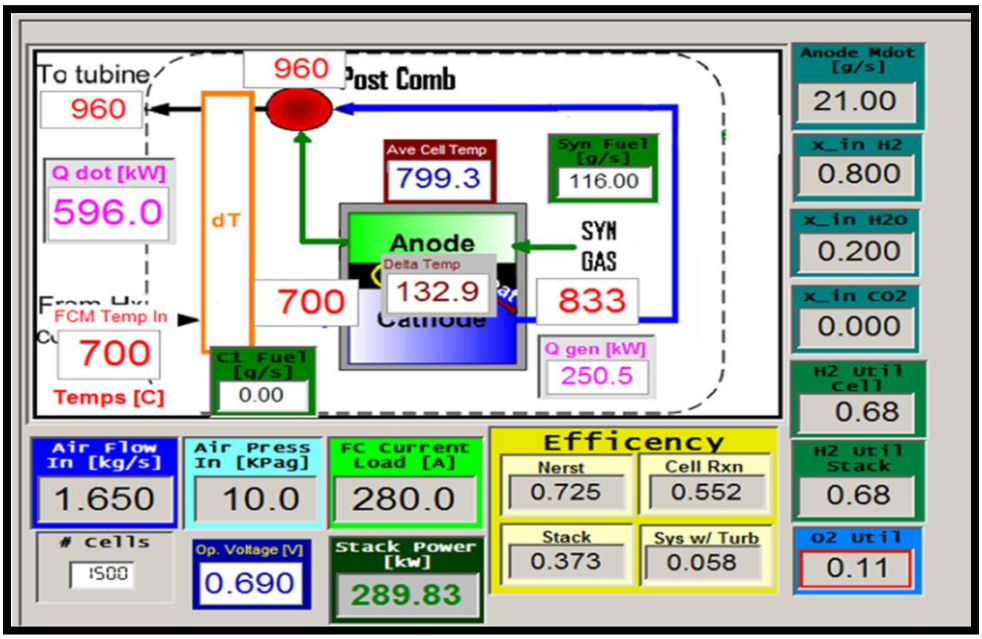

Figure 3.12: dSpace operational parameter screen

The operational parameter screen provides all of the essential system operational outputs. As illustrated, user-prescribed input parameters such as fuel flow and current demand are translated to this screen, and operational parameters such as efficiency, stack power, operational voltage, inlet and outlet fuel composition, and fuel and oxygen utilization are displayed as well. The main part of the display includes a temperature process flow diagram which includes the system inlet temperature, SOFC inlet and outlet temperatures, post combustor inlet and outlet temperatures and ΔT across the fuel cell. The operational parameter screen also displays the overall "Qdot" (i.e., subsystem thermal effluent) as well as the SOFC "Qgen" (i.e., cell stack heat generation) values as well. The dSpace profile capture screen is presented in Figure 3.13

One of the most valuable attributes of the SOFC model integrated into the HyPer Facility is its ability to provide 1-D distributed characterization, in real time. The dSpace

profile capture screen, illustrated in Figure 3.13, displays the SOFC operational parameters of interest on a spatially distributed basis and in real time manner. The profiles update to reflect the dynamic response to system transients throughout any system perturbation. The parameters presented in this screen shot are all electrochemical in nature, including the local current density, Nernst potential and polarization losses. Other distributed parameters of interest such as fuel stream compositions, internal heat generation, and solid and oxidant stream temperatures can be displayed.

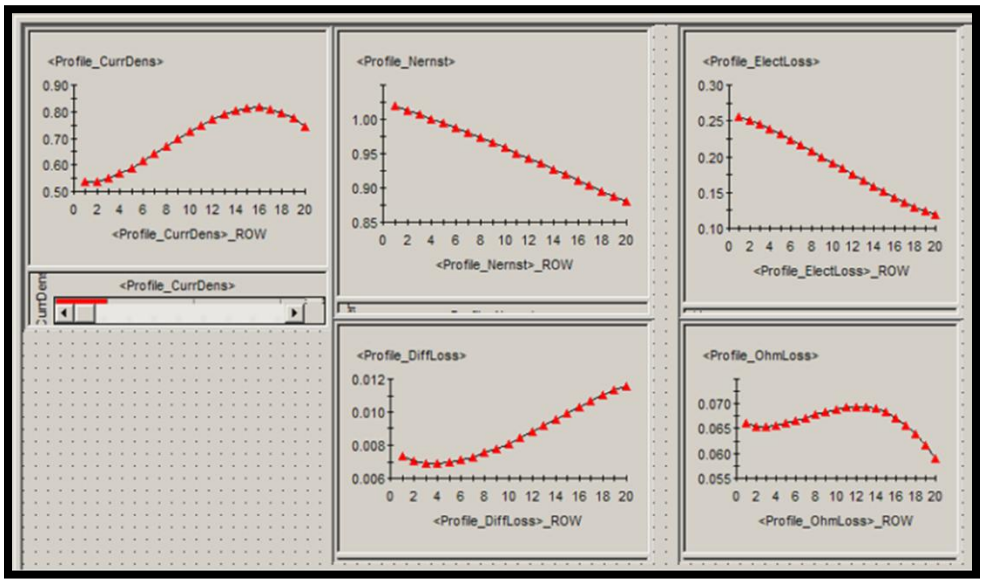

Figure 3.13: dSpace profile capture screen

3.3: Scoping Study

The operating envelope of the HyPer facility is determined by the state of four operator-controlled system inputs: bleed air, hot air, cold air by-pass valve positions, and turbine load. The nature of the electrochemical start-up study supports the need for initial fuel cell load to be a parameter of study for the parametric analysis. The impact on the dynamic system response of the previously listed operator controlled inputs were determined through a scoping study and its results will determine what other control variables will be included in the investigation.

As previously discussed in Section 3.1.1, compressor bleed has a significantly negative impact on system efficiency [14] and is primarily used as a means to increase stall margin to ensure safe and reliable system operation. Though compressor bleed will have some effect on system operation, given its primary use as a safety mitigation mechanism, it was not included as a control parameter for the scoping study.

Turbine load, which is representative of the electrical energy that may be requested by the grid, or some other device, is primarily used in the HyPer facility as a means to control turbine speed. The HyPer facility control system has two algorithms that are used to keep the rotational speed of the turbine in a tolerable regime; one is fuel valve speed control, which controls the amount of fuel which is fed to the combustor, and the other is load based speed control (LBSC), which controls the amount of load that is placed on the turbine. Given that the fuel feed to the SOFC will be constant through the experiments, and the fuel cell will be in control of the system fuel valve (FV-432), LBSC is the only turbine control methodology that can be used for this investigation. LBSC requires a minimum amount of load (50kW for this investigation) that must initially be placed on the turbine and thus that *initial* turbine load will be fixed and will not be varied for the investigation presented in this dissertation.

The elimination of compressor bleed and turbine load as control parameters for investigation only allows for hot air and cold air by-pass valve position to be considered. Past empirical studies show that safe operating regimes for hot air and cold air by-pass valve positions range between 0%-40% and 30%-70% open, respectively. Considering the base conditions that are presented in Table 3.1, an experimental plan for the scoping study to determine the impact of the variation of hot air and cold air by-pass valve positions was devised.

Table 3.1: HyPer facility base conditions

Parameter	Value
Bleed Air	10%
Hot Air	10%
Cold Air	40%
Turbine Load	50kW

The premise of the scoping study is to investigate the impact of cold air and hot air by-pass valve positions on the dynamic response of the system. Since the hot air by-pass valve position is at the lower end of its safe operating regime for the base case, valve positions of 20% and 30% open were investigated for hot air by-pass. For the cold air by-pass, positions of 30% open and 50% open were tested. The scoping was designed to mimic the planned parametric study of the electrochemical start-up investigation; accordingly, for the sake of alignment, test were conducted in both the OL and LBSC configurations, and differing amounts of load were placed on the fuel cell model for each experiment. The test matrix illustrating the experimental test matrix for the scoping study is outlined in Table 3.2.

Table 3.2: Scoping study test matrix[1]

		CA - 40%		HA - 10%	
		HA - 20%	HA - 30%	CA - 30%	CA 50%
LBSC	150A				
	100A				
	50A				
OL	50A				
	40A				
	30A				

[1] All scoping study experiments were conducted with a humidified hydrogen fuel feed simulated.
[2] Represents the step change in temperature applied to the FC inlet stream to account for necessary heat exchange
[3] The value was resolved using a contact (area-specific) resistance of 8 mΩ-cm2 for the sake of this investigation based upon inspection of empirically resolved profiles as presented by ThyssenKrupp in Material Data Sheet No. 4060.

The experimental plan for the scoping study is as follows:

1. Start the facility
2. Ensure base conditions for compressor bleed and turbine load are set (i.e., 10% open for compressor bleed and 50kW for turbine load)
3. Adjust hot air and cold air by-pass valves to the positions denoted by the test matrix
4. Allow all hardware components to reach thermal equilibrium (i.e. steady state)
5. Activate fuel cell (FC) model and transition into on-line mode
    - On-line mode means that the fuel cell model is acquiring cathode inlet pressure, temperature, and air flow from the operating HyPer facility and simulating SOFC performance based upon those parameters.
6. Place the FC model in fuel valve control
    - Once the FC model is in fuel valve control, the thermal effluent that is calculated by the fuel cell model is correlated to a fuel valve position so that the calculated physical heat from the fuel cell sub-system can be simulated by the appropriate combustion of natural gas in the HyPer facility. At this point, the fuel cell model is operating "in-the-loop" with the HyPer facility.
7. Once all operators are ready, place load on the FC model, as indicated by the experimental test matrix.
8. After 15 min for LBSC or 10 min for OL experiments, remove the load from the FC model. Given the significant thermal impact that shedding turbine load has on the system, the 15 min timeframe was employed for the LBSC experiment to allow more time for the system to arrive at steady state.

In addition to determining the impact of cold air and hot air valve positions on system dynamic response, another essential purpose behind conducting the scoping study was to determine reasonable initial FC loads that could be tolerated by the turbine. During the testing, complete load shedding of turbine load (from 50kW to 0kW) was observed for initial FC loads of 150A for the LBSC configuration. This is due to the large decrease in thermal effluent that results from an application of 150A, subsequently requiring a large amount of turbine load to be removed to maintain a nominal operating speed of 40,500 RPM. For the OL tests, turbine speeds close to the lower end of the ±5% operating regime were observed for initial FC loads of 50A. This significant decrease in turbine speed, similarly to the load shedding observed for the LBSC test, is due to the large decrease in thermal effluent that accompanies an application of 50A of load. Given the saturation of the load based speed controller (i.e. complete load shedding) for the 150A LBSC scoping test, and the harmful underspeed scenario observed for the 50A OL scoping test, those two experiments were removed from the final experimental plan. Given the similar trends for the lower initial FC loads and the uncertain accuracy and validity of the results from the 150A LBSC and 50A OL cases for reasons explained above, only the results from the 100A and 40A cases for the LBSC and OL scenarios are presented and analyzed in the following section.

3.3.1: Scoping Study Results

As previously stated, the HyPer facility has numerous amounts of process variables that can ultimately be affected by any dynamic or transient event. The electrochemical start-up investigation is focused upon characterizing system dynamic response to a transient event caused, or initiated, by the SOFC (i.e. placing initial load on the FC); thus, although the investigation is system-wide, there is a particular focus on the impact of SOFC operation.

The system parameters of particular interest to fuel cell operation are air plenum (V-301) inlet pressure (PT-305), temperature (TE-326) and flow (FE-380), which are the parameters that are fed directly into the fuel cell model to characterize SOFC operation while operating in-the-loop. As explained in Chapter 1, SOFCs have thermal and pressure sensitivities that pose significant threats to cell mechanical reliability and cell operation. Given these sensitivities, and the experimental focus on SOFC operation, pressure and temperature data for the 100A LBSC and 40 A OL test are presented and analyzed for the scoping study.

3.3.1.1 Air Plenum Inlet Pressure Investigation

Figure 3.14 presents the change in cathode inlet pressure for the hot air valve position variance for the LBSC experiment. The load is placed on the FC model at t=0s and as illustrated by the figure, before the load is placed on the FC, the air plenum (cathode) inlet pressure is approximately 350kPaa. Given the fact that HA bypass does not divert flow through or around any pressure drop component prior to it being fed into the air plenum, there is minimal to no impact of hot air by-pass valve position on the magnitude of the pressure observed.

Once the load is placed on the fuel cell, fuel energy is being virtually converted to both electrical energy and thermal energy; thus, the thermal effluent to the system decreases (i.e. since the fuel heating value is no longer exclusively converted to thermal energy) causing a decrease in turbine speed, which results in a decrease in cathode inlet pressure. Once the turbine speed decreases, the LBSC algorithm sheds load from the turbine, causing the turbine speed to increase and resulting in an increasing inlet pressure to the cathode. This system dynamic response results in minimum cathode inlet pressure existing within the first 20 seconds succeeding the transient event. As the turbine speed and cathode inlet pressure recover after the LBSC controller takes effect, the resulting pressure, as illustrated by Figure 3.14, approaches its initial value and the variance

between the values for the different experiments is minimal. The difference to note, between the results of the two experiments, is the minimal pressure observed during the transient response. For the hot air by-pass valve, 20% open case, the pressure decreases by approximately 25 kPa, whereas it only decreases by 20 kPa for the 30% case. This preliminarily suggests that an increase in hot air by-pass valve position will decrease the change in cathode inlet pressure during electrochemical start-up, which ultimately has a positive effect given the impact of pressure change on SOFC mechanical durability.

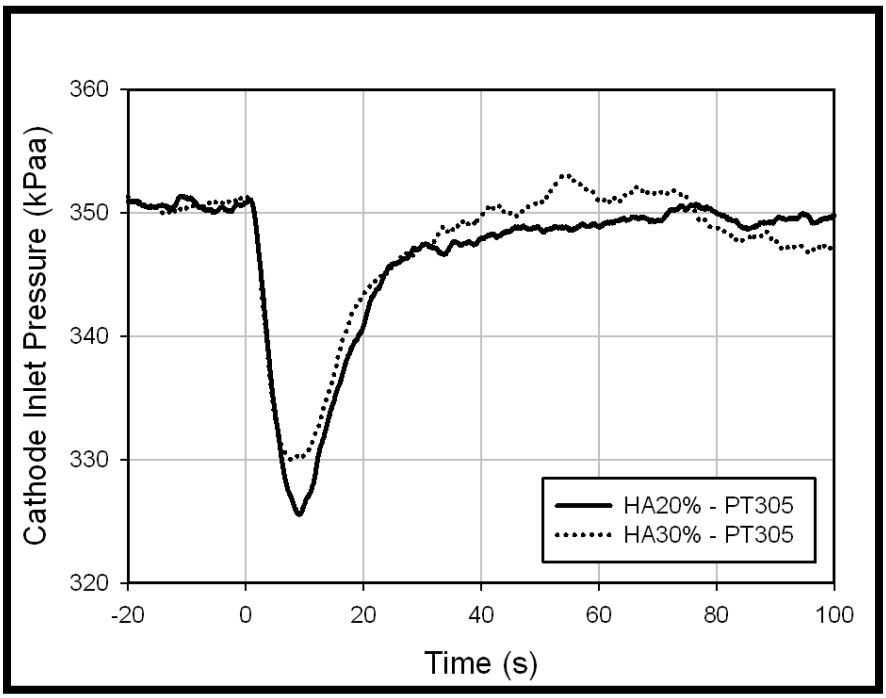

Figure 3.14: Cathode inlet pressure for hot air by-pass variance experiment - LBSC

The decrease in turbine speed due to the increase in fuel cell load reduced the amount of heat provided by the SOFC subsystem and thus resulted in a decreased plenum inlet temperature. The transient impact on air plenum temperature is illustrated in Figure 3.15. As illustrated, the air plenum inlet temperature is higher both initially and throughout the transient for the 30% hot air valve case in comparison to the 20% hot air valve case. Since the tests were conducted on different days, and HA by-pass valve position has minimal impact on air plenum inlet temperature, the significant (10K) difference in temperature can be attributed to changes in ambient conditions. The

increased bypass flow allows for decreased enthalpy changes in the turbine inlet stream and thus a decreased impact on turbine inlet temperature and consequently cathode inlet pressure throughout the transient.

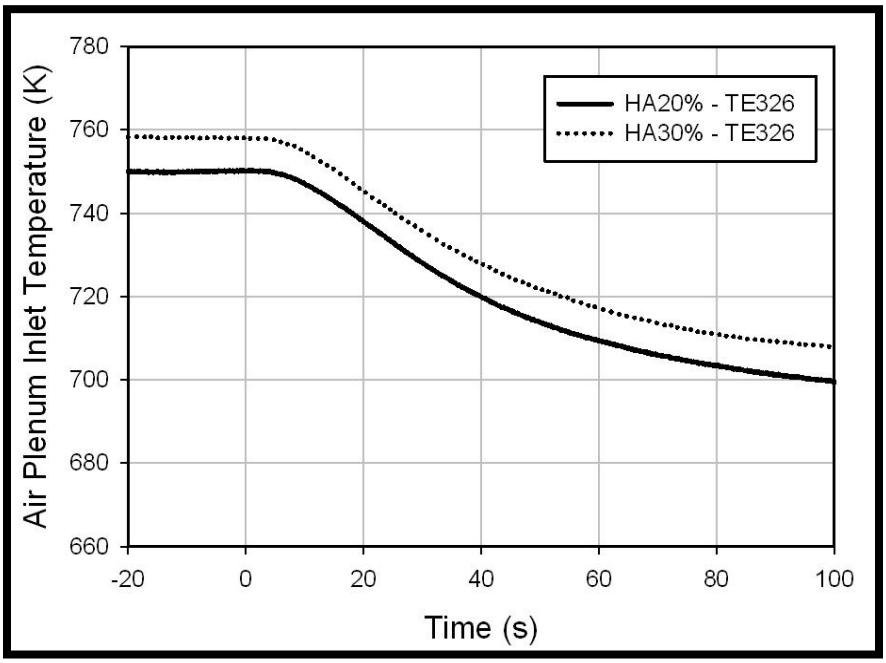

Figure 3.15: Air plenum inlet temperature for hot air by-pass variance experiment – LBSC

The impact of cold air by-pass valve position is illustrated in Figure 3.16. Unlike hot air, cold air by-pass has an impact on the inlet pressure prior to and throughout the transient event. Prior to the load change, an increase of 10 kPa is observed for the 30% cold air by-pass case relative to the 50% by-pass case. The increase in cold air by-pass decreases the amount of "resistance" seen by the compressor exhaust which results in a decrease in compressor discharge pressure and decreased inlet pressure to the air plenum [17]. Once load is placed on the FC at t=0s, the cathode inlet pressures for both cold air by-pass cases significantly decrease, along with turbine speed, until a minimum is reached and then begin to recover to their original nominal value. To determine the impact of cold air by-pass position on system dynamic response, the cathode inlet pressure was normalized by its initial steady state value for both the hot air and cold air variance experiments and presented in Figure 3.17.

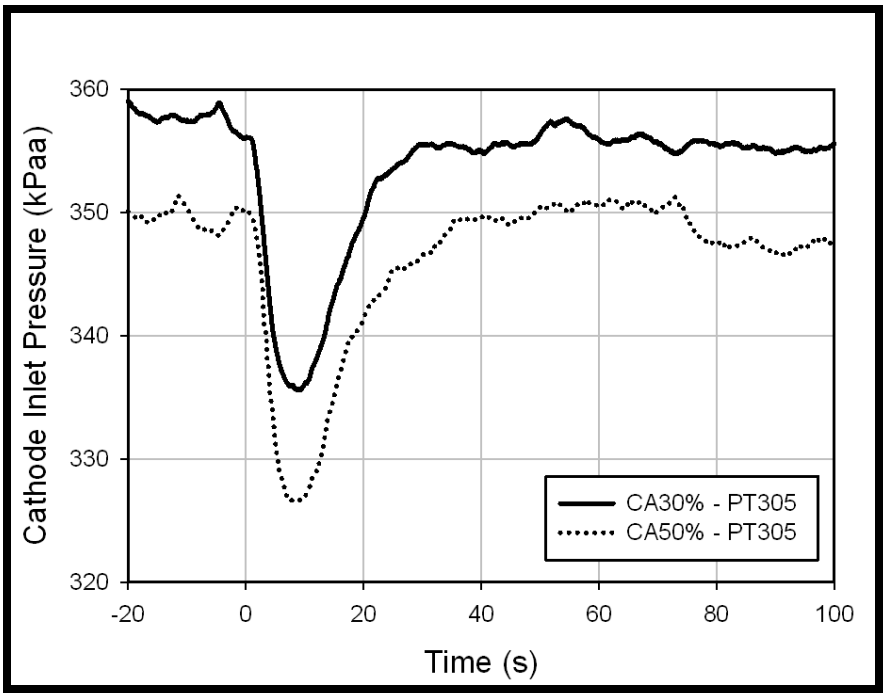

Figure 3.16: Cathode inlet pressure for cold air by-pass variance experiment – LBSC

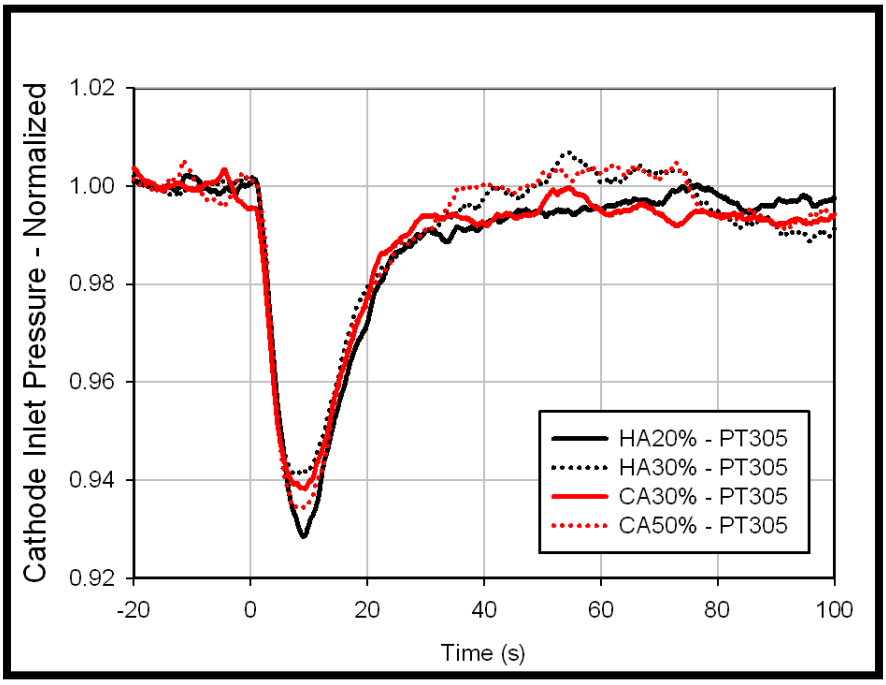

Figure 3.17: Normalized cathode inlet pressure for cold air and hot air by-pass variance experiment – LBSC

For the hot air variance experiment, the minimum cathode inlet temperature is 94.1% of its initial value for the 30% case and decreases to 92.9% of the initial value for the 20% case. With regards to the cold air by-pass variance experiments, the minimum pressure for the 30% cold air by-pass case is approximately 94.1% of its initial value and it decreases to 93.6% for the 50% cold air by-pass case. These results illustrate that modulating cold air by-pass impacts the overall magnitude of the cathode inlet pressure throughout system operation which can ultimately impact overall cell performance; in addition, modulating hot-air by-pass has a more notable impact on the dynamic response of cathode inlet pressure resulting in more significant decreases during system transient response for decreased hot air by-pass position.

The impact of by-pass valve variance on the air plenum inlet temperature is presented, in normalized fashion, in Figure 3.18. Though not illustrated in the figure, the *actual* air plenum inlet temperature, prior to the increase in FC load, for the cold air variance experiment is approximately 772 K, both for the 30% and 50% open cold air by-pass cases. The decrease in turbine exhaust temperature on the hot side of the heat exchanger supersedes the effect of decreasing flow on the cold side of the heat exchanger which results in a decreased inlet temperature to the air plenum.

The dynamic response of the air plenum inlet temperature is best illustrated through Figure 3.18. Though air plenum inlet temperature is increased for increased hot air by-pass valve position, throughout the entire transient, as illustrated in Figure 3.15, there is no difference in the dynamic response of the temperature through the first 100 seconds of the transient as illustrated in Figure 3.18. Conversely, the cold air by-pass flow, which in coupled fashion decreases turbine inlet temperature, and decreases pressure and mass flow to the air plenum, has no impact on the initial air plenum inlet temperature prior to the load change, but it does, however, impact the dynamic response to the increase in FC load. Approximately 100s after load is placed on the FC, TE-326 was 93.9% of its original value for a cold air by-pass valve position of 50%, whereas it

was approximately 94.7% of its original value when the cold air by-pass valve was set to 30% open. This result is primarily a result of the impact of system dynamics through the post compressor heat exchangers. The increased cold air by-pass allows for decreased mass flow through the plenum and provides more air with lower enthalpy to the turbine inlet stream which decreases turbine exhaust temperature and thus has a more significant cooling effect on air plenum inlet stream.

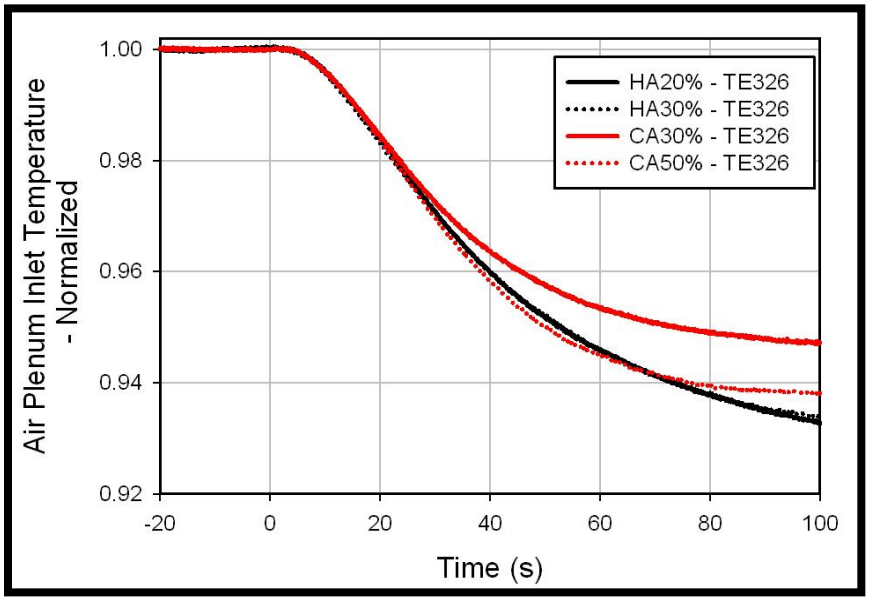

Figure 3.18: Normalized air plenum inlet temperature for cold air and hot air by-pass variance experiment – LBSC

The impact of hot air and cold air by-pass valve position on air plenum inlet pressure and temperature, for the 40A FC load OL scenario, are presented in Figures 3.19 and 3.20, respectively.

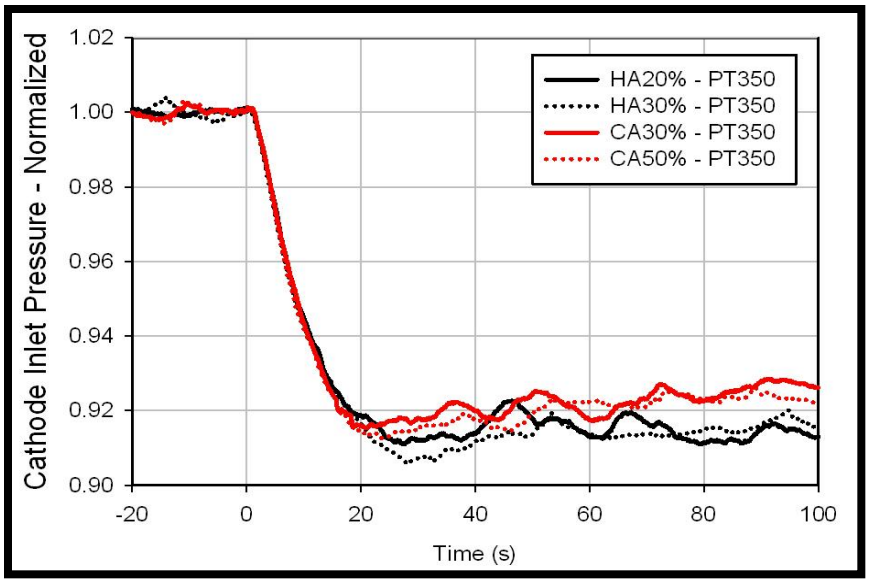

Figure 3.19: Normalized cathode inlet pressure for cold air and hot air by-pass variance experiment - OL

As illustrated in Figure 3.19, the impact on PT-305 is negligible. Air plenum inlet pressure is heavily correlated to turbine speed and the trends presented in the figure strongly correlate with the decrease in turbine speed to a new steady state value after load is placed on the FC. Figure 3.20 presents the normalized dynamic response of TE-326 to the increase in FC load.

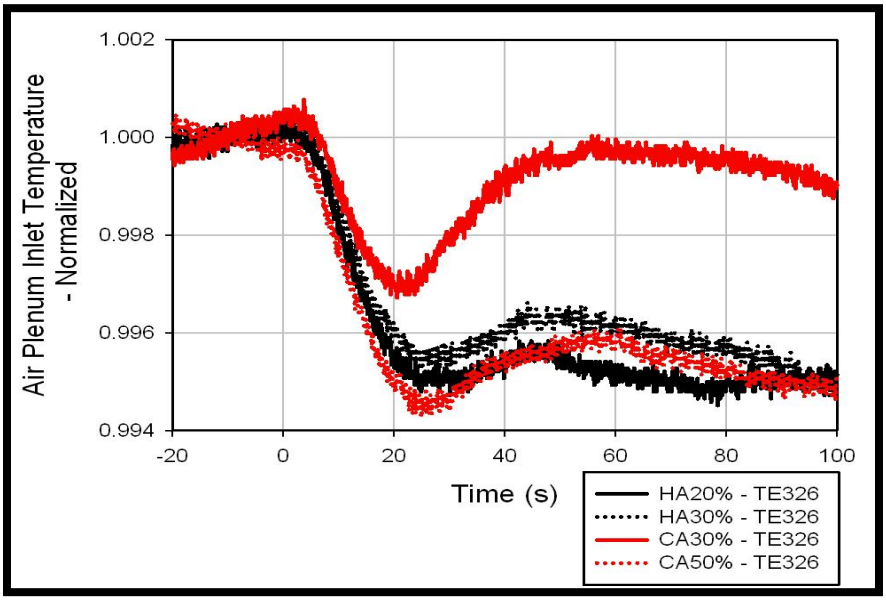

Figure 3.20: Normalized air plenum inlet temperature for cold air and hot air by-pass variance experiment – OL

Similar trends observed for the LBSC case are observed for TE326 in the open loop scenario. As illustrated, hot air by-pass has a minimal effect on the dynamic response of air plenum inlet temperature but decreases in cold air by-pass result in notable increase in the magnitude of TE-326 throughout the transient response. Though the trends are similar to the LBSC scenario, the profile of the dynamic response is noticeably different. For the OL scenario, a sharp decrease in TE-326 is observed once the load is applied to the fuel cell. Since physical heat is being removed from the system, and there is no change in turbine load to compensate for the change in physical heat, it is expected that the decrease in available thermal energy would quickly transfer to the working fluid. After approximately 20 seconds after the load is placed on the FC, the impact on heat exchanger dynamics start to effect the air plenum inlet temperature and a sharp increase is observed. Eventually TE-326 reaches a maxima, and subsequently appears to approach some steady value. The dynamic response, appears to be more significant for the 50% cold air by-pass case than for the 30% case, but ultimately the results show that the cause and effect of this transient dynamic behavior must be studied further.

The scoping study results that were presented illustrated the impact of cold air and hot air by-pass valve positions on the dynamic behavior of the pressure and temperature of the air stream that is fed into fuel cell simulation system of the HyPer facility. The results show that hot air by-pass has a more significant impact on dynamic behavior with regards to pressure transients but cold air by-pass has a more significant impact on the dynamic behavior of plenum inlet temperature. Though the cold air by-pass did not have as significant of an impact as hot air by-pass on the dynamic behavior of PT-305, modulating cold air by-pass did result in completely different operating pressures and some impact on the dynamic behavior or pressure was observed. Given the significant effect of cold air on TE-326 dynamic behavior coupled with apparent effects on both the absolute operating pressure as well as pressure dynamics, the focus of the dissertation

work will be on characterizing the impact of cold air by-pass and initial fuel cell load during electrochemical start-up.

3.4: Experimental Plan

Given the presented results of the scoping study, and the apparent impact of cold air by-pass on dynamic response and system performance, the focus of the experimental investigation for this dissertation project is the impact of cold air by-pass valve position and load step size on dynamic operation during electrochemical start-up. The test matrix that was used to carry out the experimental plan is presented in Table 3.3.

Table 3.3: Experimental plan test matrix

		CA = 35%	CA = 40%	CA=40% Syngas	CA= 60%
LBSC	50A				
	75A				
	100A				
	125A				
OL	10A				
	20A				
	30A				
	40A				

In alignment with the scoping study, investigations in both the OL and LBSC configurations were conducted. To conduct a comparative analysis a base cold air valve position of 40% was selected. A 40% base case affords investigating reasonable operating states at cold air valve positions above and below the base condition, and it represents an empirically resolved valve position that maximizes system efficiency and minimizes surge and stall risk. It is important to note that the relationship between CA by-pass and cathode inlet flow are nonlinear as illustrated by work conducted by Tucker et al. [14].The relative impact of 60% CA by-pass on cathode inlet flow as compared to 35% vary significantly with 35% CA by-pass yielding a 1% increase in cathode inlet flow

from the base case and 60% yielding nearly a 15% decrease from the base case. For the structured experimentation, three experiments will be conducted to ensure reproducibility of the given results. Statistical analysis is provided in Section 3.4. The condition for the base case that will be used for the comparative studies are presented in Table 3.4.

Table 3.4: Experimental base case parameters

Parameter	Value
Bleed air	10%
Hot Air	10%
Cold Air	40%
Turbine Load	50kW
Initial FC Load	100A (LBSC) 30A (OL)
Number of Cells	2300
dT in[2]	225K

As presented, the HyPer system base parameters are the same as they were for the scoping study investigation. The initial FC loads of 100A and 30A for LBSC and OL, respectively, are significantly large enough to observe internal dynamics and transient response while affording the opportunity to compare load current values that are both greater and less than these base cases.

The "dT in" metric represents the step increase in temperature that is imposed to the cathode inlet stream by the SOFC subsystem model. Given the operational temperatures of the components used in the HyPer facility, the maximum plenum inlet temperature is approximately 850K which is not adequate for electrochemical activity. Typically, some sort of balance of plant component would be utilized that would provide some form of heat exchange via waste heat or pre-combustion to elevate the temperature to an adequate level. For this investigation, the main premise of the electrochemical start-up investigation is to both quantitatively and qualitatively assess the dynamic system

[2] Represents the step change in temperature applied to the FC inlet stream to account for necessary heat exchange

response during electrochemical start-up, and solely capture the impact of turbine dynamics on SOFC operation. Ultimately, the data acquired and the analyzed will provide system designers both necessary and sufficient information for the component selection and design to maximize the reliability and efficiency of SOFC/GT hybrids. For that purpose, the impact of necessary balance-of-plant components, such as pre-heat combustors and heat exchangers, that would typically be included in the fuel cell subsystem design, were not modeled in this investigation. To account for the necessary heat exchange, a virtual "delta temp" was imposed on the fuel cell inlet stream. This virtual heat exchange accounts for the heat input yet preserves the natural dynamic response of the fuel cell subsystem inlet temperature to turbine transients alone. This preservation in the capture of complete dynamic response of all process variables will directly contribute to the design of balance of plant components that maximize reliability during start-up and efficiency in operation. Though an entire SOFC subsystem, including all balance of plant components, is not modeled, this approach provides a datum that will be used to assess the impact of adding other system components in the completion of hybrid system design.

3.5 Statistical Analysis / Reproducibility

To ensure that the acquired results were valid, each experiment was conducted successively 3 times. Though randomization of order would have been ideal, previous work [39] as well as facility experience exhibits that ambient conditions can have a significant impact on system operation. To address the impact of variability of ambient conditions, the 3 replicates were conducted in succession. This section presents the experimental results for turbine load and cathode inlet pressure and temperature and accompanying error analysis for the LBSC and OL bases cases. The statistical analysis assumes a normal distribution and all of the error bars presented on the plots in this

section represent a 99% confidence interval about the sample mean which is presented on each plot as well.

3.5.1 Load Based Speed Control

The turbine speed, cathode inlet pressure and flow results from electrochemical start-up experiments with 40% CA by-pass and 100A of initial load are presented in Figures 3.21-3.23, respectively. As illustrated, there is very good agreement between all three runs and all of the data points. The maximum standard deviations and relative errors for all three parameters is presented in Table 3.5.

Table 3.5: LBSC error analysis statistical parameters

Parameter	Max Standard Deviation	Relative Error
Turbine Speed (RPM)	206.232	0.53%
Cathode Inlet Pressure (kPaa)	4.627	1.36%
Cathode Inlet Temperature (K)	3.979	0.59%

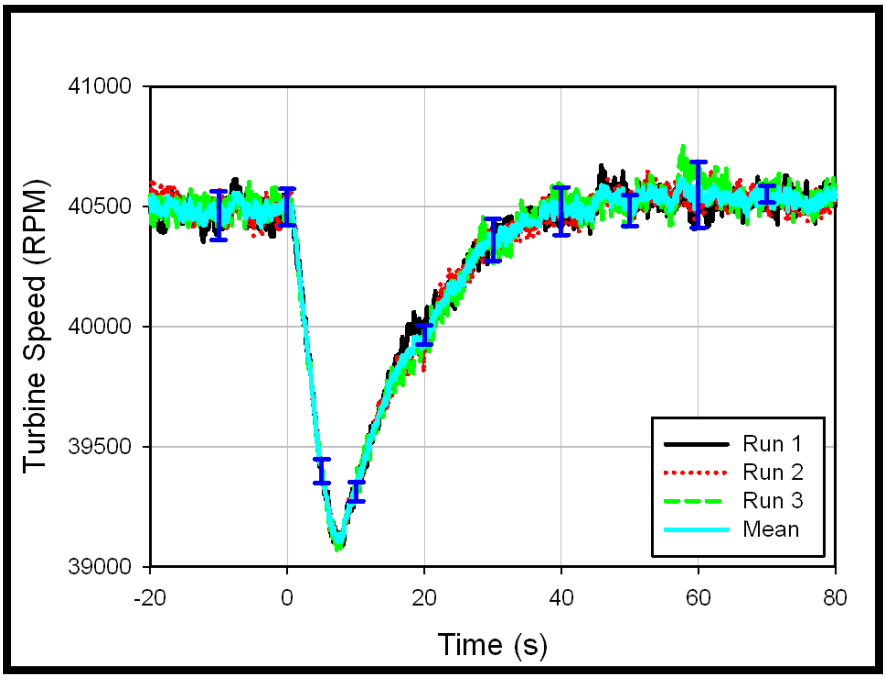

Figure 3.21: Turbine speed replicate comparison – 100A initial FC load - LBSC

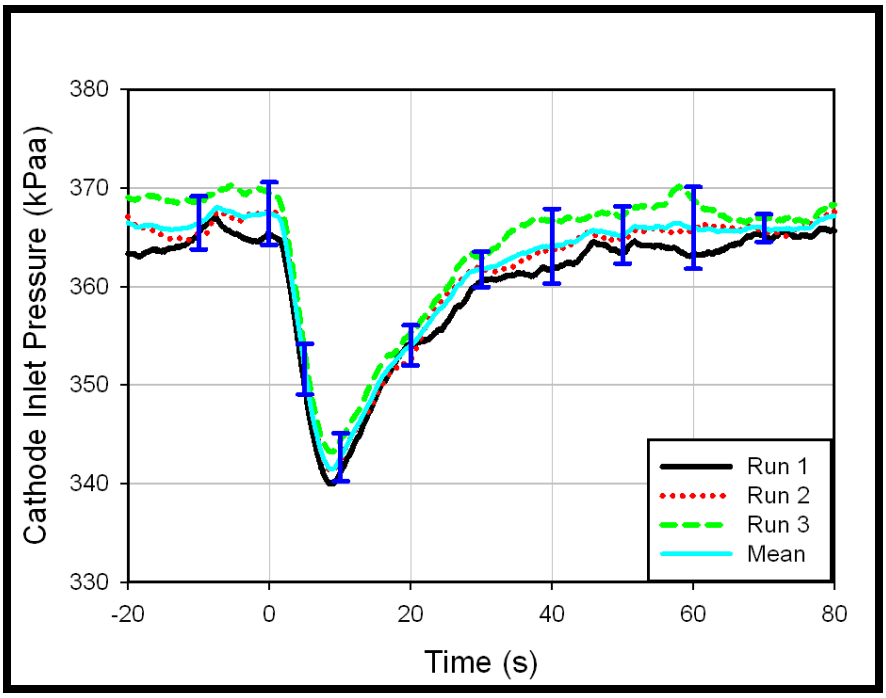

Figure 3.22: Cathode inlet temperature replicate comparison – 100A initial FC load - LBSC

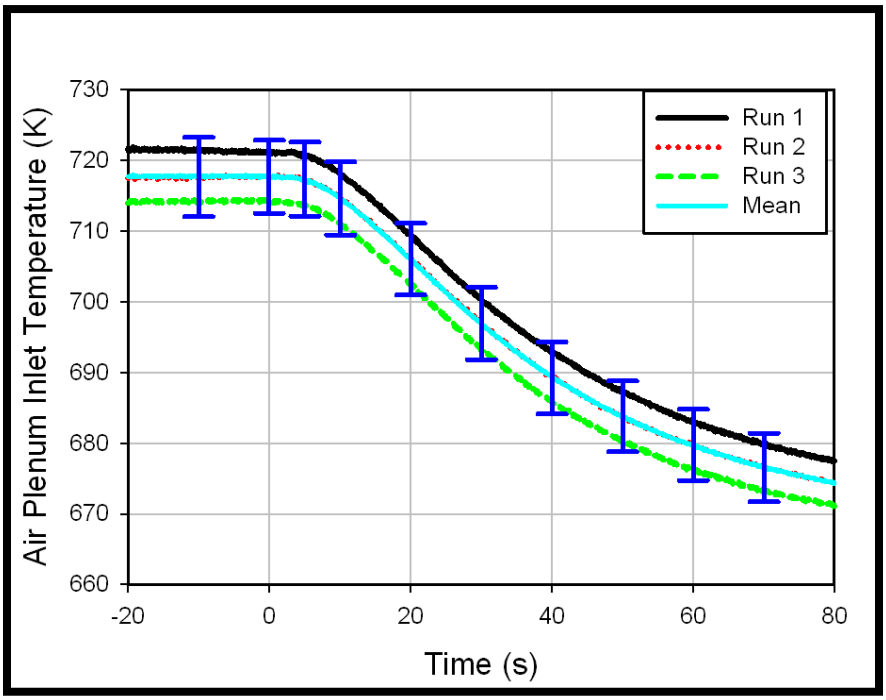

Figure 3.23: Air plenum inlet temperature replicate comparison – 100A initial FC load – LBSC

3.5.2 Open Loop

The open loop turbine speed, cathode inlet pressure and flow results from electrochemical start-up experiments with 40% CA by-pass and 30A of initial load are presented in Figures 3.24-3.26, respectively. As illustrated, there is very good agreement between all three runs and all of the data points. The maximum standard deviations and relative errors for all three parameters are presented in Table 3.5.

Table 3.6: OL error analysis statistical parameters

Parameter	Max Standard Deviation	Relative Error
Turbine Speed (RPM)	492.192	1.26%
Cathode Inlet Pressure (kPaa)	7.087	2.08%
Cathode Inlet Temperature (K)	1.421	0.21%

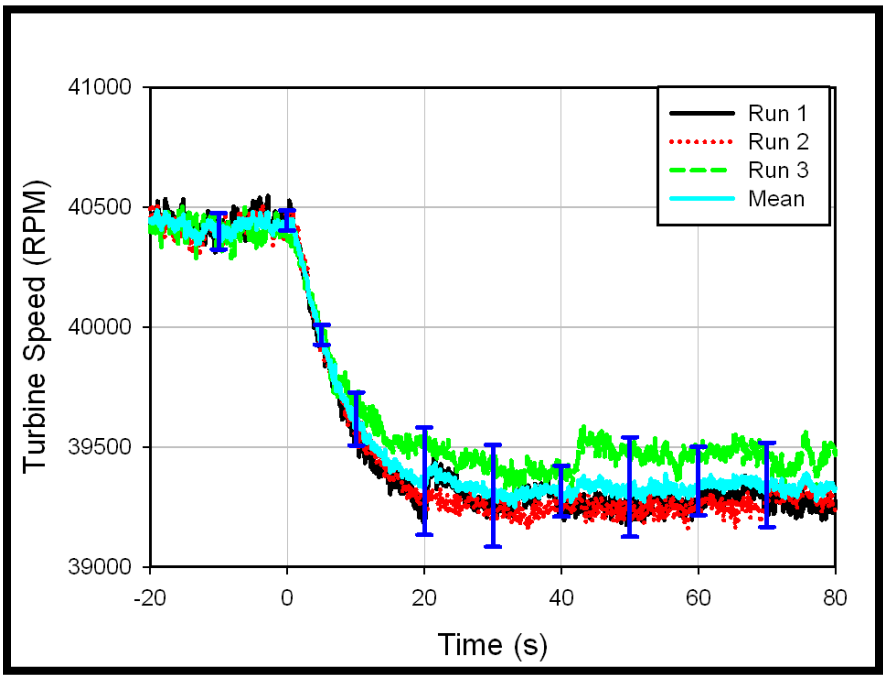

Figure 3.24: Turbine speed replicate comparison – 30A initial FC load - OL

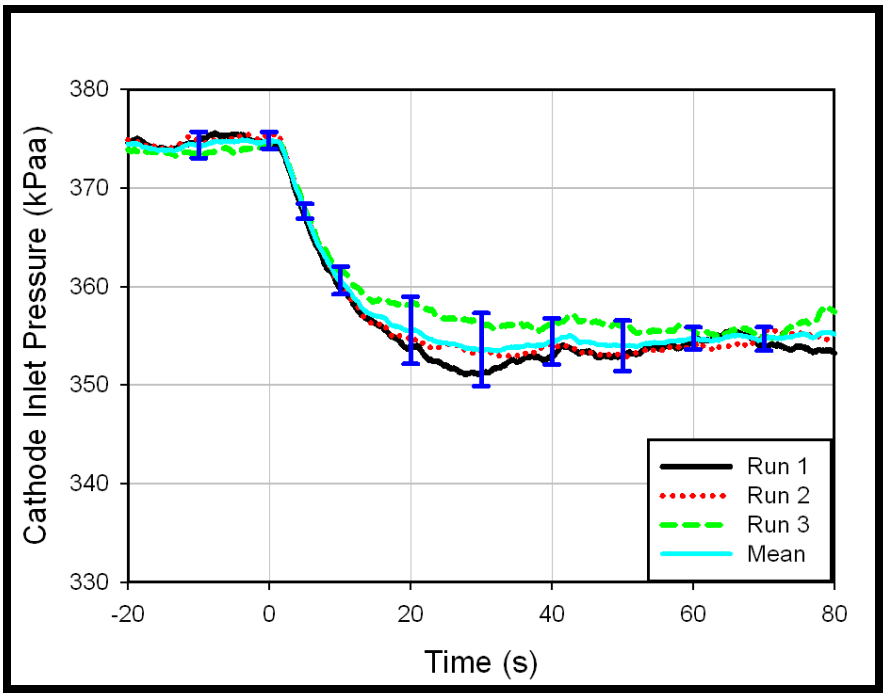

Figure 3.25: Cathode inlet pressure replicate comparison – 30A initial FC load - OL

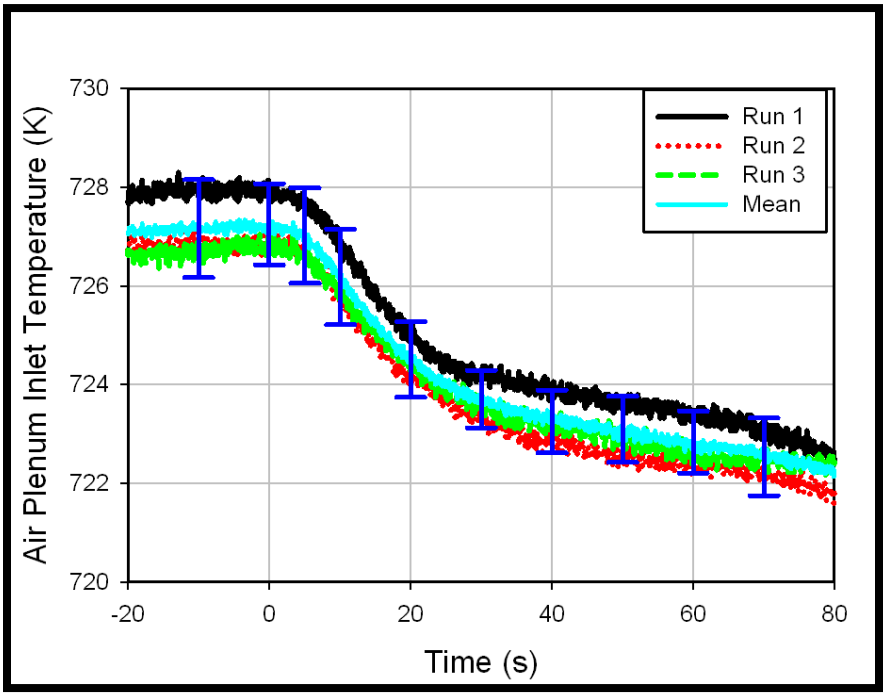

Figure 3.26: Air plenum inlet temperature replicate comparison – 30A initial FC load – OL

3.6 Turbine Replacement

At the conclusion of the 40% CA experiments, the original auxiliary underwent a mechanical failure which resulted in a necessary replacement of the turbine/compressor assembly to complete the experimental plan. Hereafter, the results of a calibration study, comparing the dynamic output of air plenum inlet temperature between the HyPer facility that used the new turbine relative to the old turbine, are presented. The remaining cathode inlet parameters (i.e. pressure and flow) compared very well between the new and old turbines and are not presented in this section. Figure 3.27 and 3.28 present the cathode inlet temperature for the new and old turbines in normalized and absolute manner, respectively, for the 100A initial FC load, 40% CA by-pass LBSC experiments.

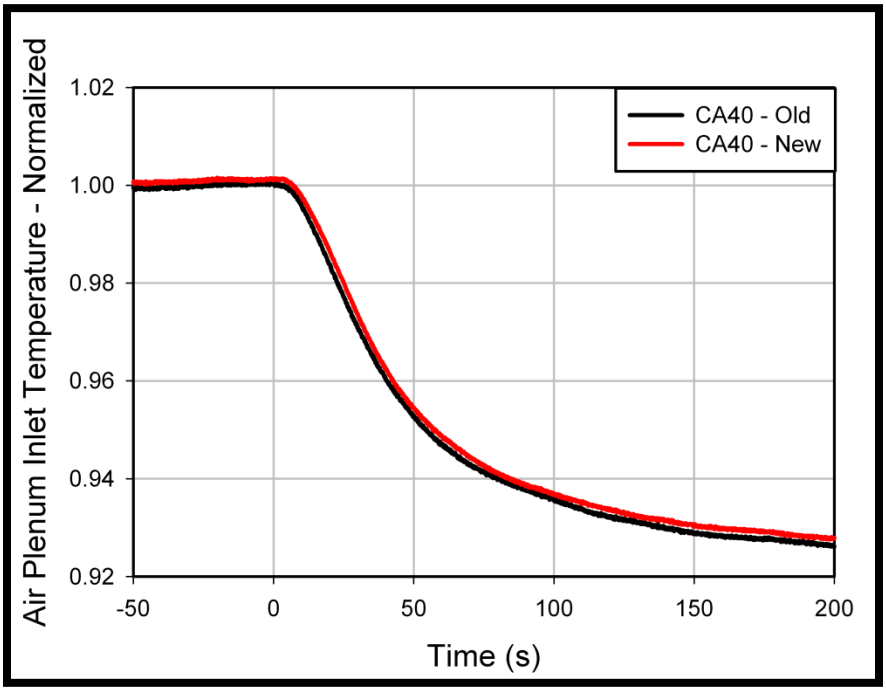

Figure 3.27: Normalized air plenum inlet temperature 100A initial FC load, 40% CA by-pass base case – LBSC calibration study

As illustrated by Figure 3.27, the dynamic response of the cathode inlet temperature compares very well between the new and old turbines with very similar (nearly identical) trajectories observed for both the new and old turbines. The absolute response shown in Fig. 3.28, however, illustrates a deviation of approximately 60K in the

absolute value of the temperature of the air stream entering the air plenum. The temperature profiles have nearly the same dynamic response, and the approximate 60K increase in temperature is present throughout the entire transient response.

The normalized and absolute air plenum temperature profiles for the 30A initial FC load, 40% CA by-pass OL base case comparative studies are presented in Figures 3.29 and 3.30, respectively. Unlike the LBSC case, Figure 3.29 presents a noticeable change in dynamic response of the air plenum inlet temperature between the new and old turbines. Both the new and old turbines illustrate a decrease in normalized air plenum inlet temperature within the first 30s of the transient start-up response.

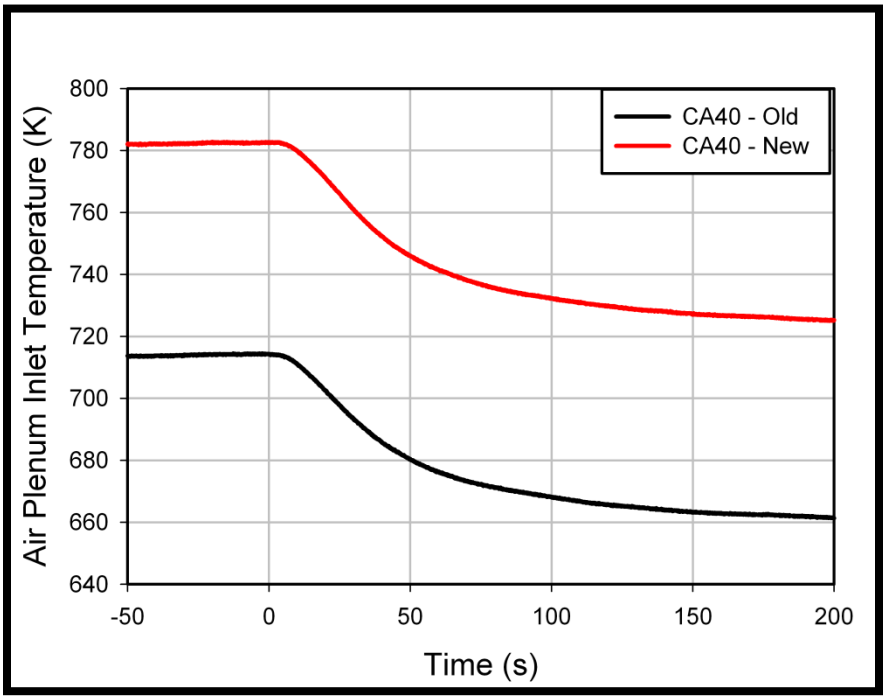

Figure 3.28: Absolute air plenum inlet temperature 100A initial FC load, 40% CA by-pass base case – LBSC calibration study

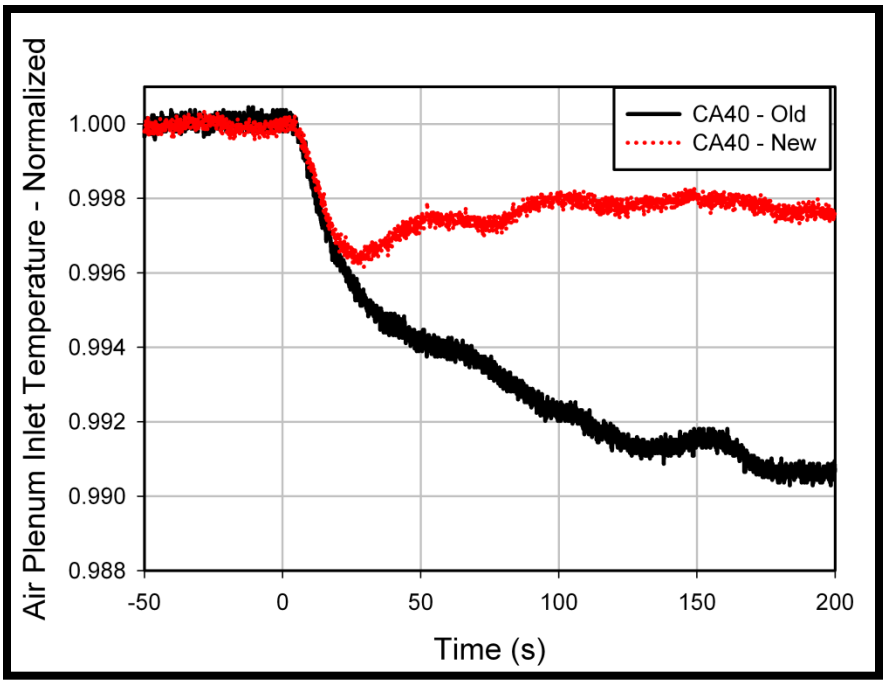

Figure 3.29: Normalized air plenum inlet temperature 30A initial FC load, 40% CA by-pass base case – LBSC calibration study

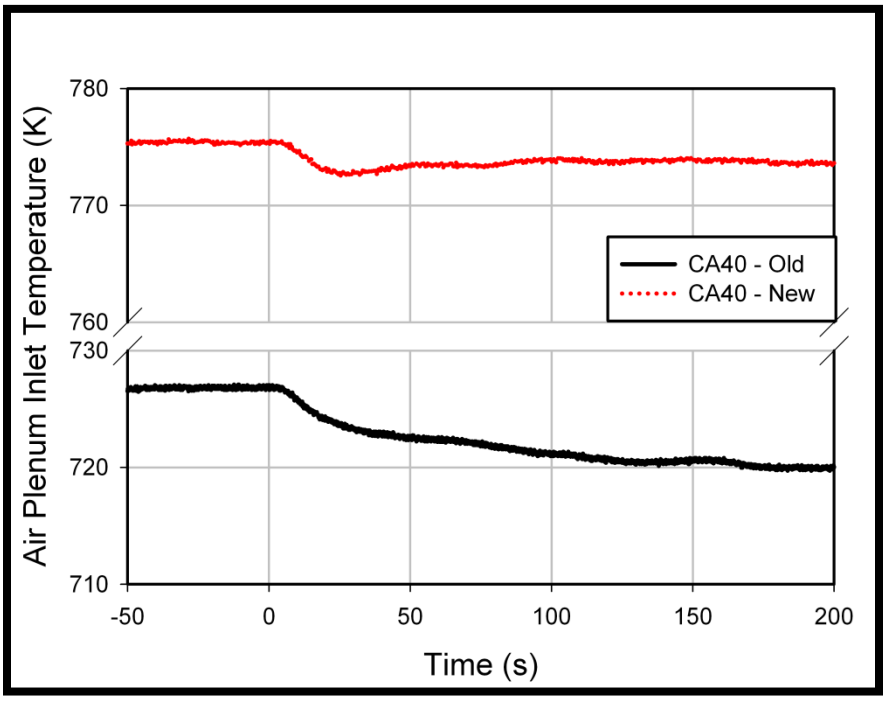

Figure 3.30: Absolute air plenum inlet temperature 100A initial FC load, 40% CA by-pass base case – LBSC calibration study

After approximately the 30 second mark the air plenum inlet temperature for the old turbine continues to monotonically decrease to a steady state value nearly 1% less than its pre-load steady value. The new turbine reaches a minimum that is nearly 0.04% less than its pre-load steady state value and ultimately arrives at a new steady value that is approximately 0.02% less than the pre-load value. The normalized comparison not only illustrates that the relative magnitudes of the air plenum inlet temperature have changed but dynamic response is notably different as well with distinctly different profiles illustrated for the new and old turbine. Though the dynamic response is different for the OL configuration as compared to LBSC, the difference in air plenum inlet temperature of approximately 60K that was present for the LBSC system configuration is nearly present for the open loop configuration as well, as presented in Figure 3.30.

Currently, the reason for the observed differences in the thermal behavior between the two turbines utilized for this study is unknown. Given that the old turbine was completely rebuilt, it is expected that the performance would experience some change but a detailed investigation to determine the mechanical differences between the two units and the impact of those differences on the performance of the system would need to be investigated. Ultimately, this work is focused upon capturing the general system response to electrochemical light-off and providing qualitative conclusions that drive recommendations for future development that is supported by quantitative data. Though slight variations are observed in the thermal performance, the capability to characterized the system in comprehensive manner during electrochemical start-up remains viable and will be presented in the remainder of this work.

CHAPTER 4

ONE-DIMENSIONAL, REAL TIME SOFC MODEL

4.1 1-D Model Description

A robust, distributed, one-dimensional fuel cell model was developed for integration into the HyPer facility at NETL in Morgantown, WV. This model and corresponding simulation are designed to operate in real time, and to be integrated into an operating SOFC/GT hybrid arrangement using HiLS [18]. Previously, NETL developed a lumped real-time, fuel cell model that was successfully coupled with the hybrid arrangement using HiLS [19-21]. The higher fidelity 1-D model provides the user the ability to observe and capture the local, internal tranport phenomena of an operating fuel cell with variable levels of spatial resolution in a transient manner. The model output of particular interest for integration into the HyPer facility is the thermal effluent from the fuel cell system. This value is comprised of the by-product heat generation from the operating fuel cell and the heat released due to combustion of unutilized fuel exiting the fuel cell. This chapter outlines the design of the design of the one-dimensional fuel cell model that has been integrated into the HyPer facility and exhibits its capabilities though presentation of data from experiments in which fuel cell load demand is both increased and decreased in stepwise fashion

4.1.1 Model Overview

The 1-D, distributed, real-time operating fuel cell model that was built in Matlab-Simulink™ was integrated into the HyPer facility though dSpace™ control desk. The software simulates a co-flow, anode-supported SOFC operating within a SOFC/GT hybrid arrangement.

The SOFC model characterizes a representative cell on a distributed basis with respect to space in the direction of fuel and oxidant flow (i.e. down the direction of the flow channel) and employs a coupled finite difference/ finite volume approach. The finite difference methodology is applied to the resolution of the solid and oxidant stream thermal profiles, and the finite volume approach is used for the electrochemical characterization. Similar to the cell geometry, the level of discretization in the flow direction is variable but sensitivity studies supported employing 20 "nodes"/"volumes" (i.e. points of calculation) along the length of the SOFC. The discretization scheme is illustrated in abbreviated fashion (only 9 "nodes") in Figure 4.1.

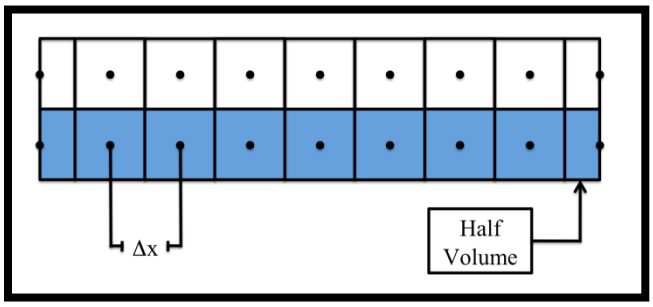

Figure 4.1: 1-D SOFC model discretization

In the schematic presented in Figure 4.1, the two levels of nodes/volumes illustrated represent the oxidant stream and SOFC "solid" (which is actually taken to be the integrated average of SOFC balance materials including the PEN, interconnects and fuel stream), respectively [68]. As illustrated, the discretization scheme is the same for both regions. This allows the thermal communication between the two to be readily modeled. Also notice that nodes have been explicitly placed at the entrance and exit of the SOFC. This approach, though valid, results in the presence of "half-volumes" at the entrance and exit of the numerically discretized cell.

The model was developed to resolve temperature profiles of both the solid SOFC material as well as the oxidant stream. Note that given the anticipation of lower mass flow rates and higher inlet temperatures, the fuel stream's participation in heat transfer was approximated to be minor in comparison to the oxidant stream.

The cell geometry of the simulated SOFC can be varied by the operator and is established in the model via user prescribed inputs. The required geometric parameters include:

- Total cell length, width and height
- Oxidant channel height and width
- Anode, cathode and electrolyte thickness
- Number of channels

The two constraints on the cell geometry include:

1.) The same interconnect "half" is used on both the anode and cathode sides

2.) The fluid channels are rectangular

It is important to note, however, that the impact of non-rectangular flow channels and non-symmetrical interconnects on cell performance is a potential area of investigation and study for SOFC technological development.

In addition to the cells' geometric parameters, the necessary operational inputs are as follows:

- Cathode inlet parameters:
    - Temperature, pressure and mass flow rate
- Number of cells
- Current demand
- Fuel flow
- Fuel composition

While operating "in the loop", all of the operational inputs listed are prescribed by the model operator, with the exception of the cathode inlet parameters. During HiLS operation, the cathode inlet parameters will be provided to the model, in real-time manner, from sensors embedded in the HyPer system hardware illustrated in Figure 3.2, along with a prescribed temperature rise associated with a virtual heat exchange just

upstream of the SOFC stack. While the model is operating in offline manner, those parameters would be prescribed by the user. Once the model is given the required inputs, it characterizes overall cell operation and performance. Scalar outputs such as, but not limited to, fuel utilization, oxygen utilization, operating voltage, stack power, cell ΔT and stack Q_{gen} are calculated. Fuel cell subsystem thermal effluent, which is the key parameter that is used to control the FV-432 fuel valve and simulate thermal transients from the fuel cell subsystem, is calculated as well.

Given the combination of real-time operation and 1-D distributed characterization, internal profiles of various SOFC operating parameters can be acquired on a spatio-temporal basis. A comprehensive list of those parameters is provided below.

- SOFC temperature
- Oxidant temperature
- Local current density
- Nernst potential
- Electrochemical losses
- Activation, Diffusion, Ohmic
- Fuel species partial pressures
- By-product heat generation

4.1.2 Operational Parameters and Assumptions

The following set of assumptions was employed when constructing the presented model.

- Fuel is comprised of any combination of H_2, CH_4, CO, CO_2, H_2O, N_2 for the purposes of representing a number of desired syn-gas mixtures
- Air is presumed to be 79% N_2 and 21% O_2
- Each local control volume has unform properties (temperature, pressure, species concentration)
- Interconnects have negligible impact on bulk material ohmic loss due to high electrical conductivity
- Water gas shift reaction is presumed to occur at equilibria
- Direct internal reformation of methane occurs at the fuel-anode surface
- Hydrogen is the only electrochemically active constituent in the fuel channel, given the expected dominance of shift reaction with respect to CO consumption
- Due to a large Peclet number conduction heat transfer in the gas stream is negligible.
- In situ radiation heat transfer is considered negligible due to the slender unit cells

The operational parameters used for the model is presented in Table 4.1

Table 4.1: Model constants and parameters

Diffusion Polarization [44, 57]	
Pore diameter, d_{pore} (anode and cathode)	$1x10^{-6}$ m
Porosity, ε (anode and cathode)	0.5
Tortuosity, τ (anode and cathode)	3
Activation Polarization [44]	
Pre-exponential factors	
Anode, γ_{an}	$5.5x10^{8}$ A/m^2
Cathode, γ_{ca}	$7x10^{8}$ A/m^2
Activation Energies	
Anode, E_{an}	50 kJ/mol
Cathode, E_{ca}	100 kJ/mol
Transfer coefficient, α	0.5
Ohmic Polarization [44, 45]	
Temp. dependent resistivities, ρ	
Anode	$\left[\frac{95\times10^{6}}{T_{PEN}}\exp\left(-\frac{1150}{T_{PEN}}\right)\right]^{-1}\Omega-m$
Cathode	$\left[\frac{42\times10^{6}}{T_{PEN}}\exp\left(-\frac{1200}{T_{PEN}}\right)\right]^{-1}\Omega-m$
Electrolyte	$\left[3.34\times10^{4}\exp\left(-\frac{10.300}{T_{PEN}}\right)\right]^{-1}\Omega-m$
Direct Internal Reformation [30]	
Pre-exponential factor, γ_{sr}	4274 mol/s-m^2-bar
α Coefficient	1
β Coefficient	0
Activation Energies, E_{an}	82,000 J/mol
Diffusion Coefficient Correction [57]	
C	$4.88x10^{-4}$
N	2
i_{ref}	1 A/m^2
Diffusion Volumes [70]	
H_2	6.12
H_2O	13.1
O_2	16.3
N_2	18.5

4.1.3 Geometry

For the case studies presented in this paper, the operation of a co-flow SOFC with a 20 cm x 20 cm electroactive area is simulated. Figures 4.2 and 4.3 illustrate the cross-sectional geometry of a unit cell and PEN respectively.

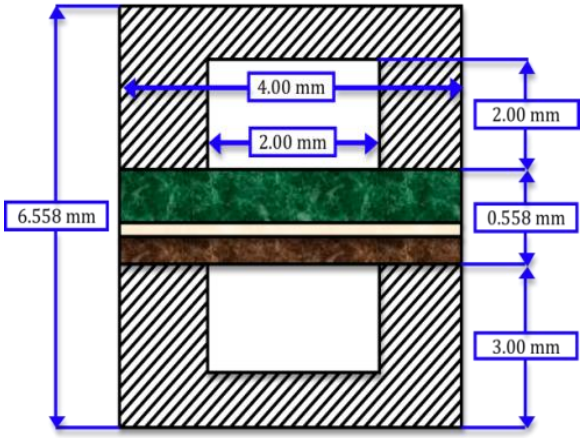

Figure 4.2: SOFC unit cell interconnect geometry (not to scale)

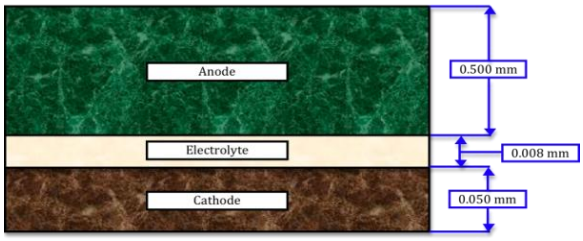

Figure 4.3: SOFC unit cell PEN geometry (not to scale)

4.1.4 Electrochemical Model

4.1.4.1 Operating Voltage Calculation

The operating cell voltage is calculated by accounting for electrochemical losses and subtracting them from the local Nernst potentials. The relation used to determine operating cell voltage is presented in Equation 4.1. The methodology used to resolve the respective electrochemical terms are presented in subsequent subsections. The Nernst potential is the maximum possible voltage that can be obtained and is a function of

temperature and partial pressures of the electrochemically active species. V_{Nernst} is derived from Gibbs free energy drop and is calculated using Equation 4.2 [19].

$$V_{cell} = V_{Nernst} - \eta_{dif} - \eta_{act} - \eta_{ohm} \tag{4.1}$$

$$V_{Nernst} = -\frac{\Delta G^{o}_{H_2O}}{2F} + \frac{R_u T}{2F} \ln\left(\frac{p_{H_2} p_{O_2}^{\frac{1}{2}}}{p_{H_2O}} \right) \tag{4.2}$$

4.1.4.2 Diffusion Polarization

The electrochemical reactions in operating fuel cells take place at the electrode-electrolyte-reactant stream interface, also known as the triple phase boundary (TPB). Due to diffusive effects through the anode and cathode, reactant concentrations at the reaction sites will differ from their bulk concentrations in the fuel and oxidant streams. The difference in concentration (or partial pressure) between the reactant stream and (TPBs) due to these diffusive effects manifests as a loss in voltage. This diffusion polarization, referenced in Equation 4.1, is quantitatively presented in Equation 4.3 [71].

$$\eta_{dif} = \frac{R_u T}{2F} \left(\ln\left(\frac{x_{H_2,bulk}}{x_{H_2,TPB}} \frac{x_{H_2O,TPB}}{x_{H_2,Obulk}} \right) + \frac{1}{2} \ln\left(\frac{x_{O_2,bulk}}{x_{O_2,TPB}} \right) \right) \tag{4.3}$$

The reactant mole fractions at the TPB (x_{TPB}) are resolved using Equations 4.4-4.6 [19, 44].

$$x_{H_2,TPB} = x_{H_2,bulk} - \frac{R_u T}{2F} \frac{i \delta_{an}}{p_{an} D_{an,eff}} \tag{4.4}$$

$$x_{H_2O,TPB} = x_{H_2O,bulk} + \frac{R_u T}{2F} \frac{i \delta_{an}}{p_{an} D_{an,eff}} \tag{4.5}$$

$$x_{O_2,TPB} = 1 + \left(x_{O_2,bulk} - 1 \right) \exp\left(\frac{R_u T}{4F} \frac{i \delta_{ca}}{p_{ca} D_{ca,eff}} \right) \tag{4.6}$$

For the sake of computational burden and as justified by applicable work in the SOFC field [53, 56, 71], the assumption of hydrogen as the only electrochemically active specie supports the assumption of equimolar counter diffusion of H_2O and H_2 on the anode side. Attempts to include multi-component diffusion were not included into the real-time model due to computational burden and its potential threat to real-time operation.

The model resolves ordinary binary diffusion coefficients using the Fuller-Schettler-Giddings method presented in Equation 4.7 [70].

$$D_{12} = \frac{0.00143T^{1.75}}{pM_{12}^{1/2}\left[\left(\sum v\right)_1^{1/3} + \left(\sum v\right)_2^{1/3}\right]} \tag{4.7}$$

The effective molecular weight, M_{12}, that is used to resolve the ordinary diffusion coefficient, is presented in Equation 4.8.

$$M_{12} = 2\left[\left(\frac{1}{M_1}\right) + \left(\frac{1}{M_2}\right)\right]^{-1} \tag{4.8}$$

The effective diffusivity coefficient presented in Equation 4.7 accounts for only ordinary (binary) diffusion. The Knudsen diffusivity of each species is resolved using Equation 4.9; and the effective diffusion coefficient for each species, which accounts for both ordinary and Knudsen diffusion, is presented in Equation 4.10. The characteristic pore diameter used is presented in Table 4.1 [44, 57].

$$D_{K1} = 48.5 d_{pore}\left(\frac{T_{PEN}}{M_1}\right)^{1/2} \tag{4.9}$$

$$D_{1,eff} = \frac{\varepsilon}{\tau}\left(\frac{1}{D_{12}} + \frac{1}{D_{1K}}\right)^{-1} \tag{4.10}$$

The electrode-specific diffusivities for anode and cathode are presented in Equations 4.11 and 4.12, respectively. [44, 53]

$$D_{an,eff} = \left(\frac{p_{H_2O}}{p_{an}} \right) D_{H_2,eff} + \left(\frac{p_{H_2}}{p_{an}} \right) D_{H_2O,eff} \tag{4.11}$$

$$D_{ca,eff} = D_{O_2,eff} \tag{4.12}$$

A correction factor which is used to account for the error associated with using Fick's law to characterize diffusion during SOFC operation is included in the resolution of the diffusion coefficient [57]. The empirically resolved correction factor accounts for the impact of current draw on diffusion through the porous electrodes and is presented in Equation 4.13. The effective diffusivity is calculated in Equation 4.10.

$$D_i^{eff^*} = D_i^{eff} \left(1 + sign(v_i) c \frac{i}{i_{ref}} \right)^n \tag{4.13}$$

For equation 4.13, the v_i term is the stoichiometric coefficient of the species of interest and i is the current density. The constants i_{ref}, c and n are empirically resolved and presented in Table 4.1.

4.1.4.3 Activation Polarization

The activation polarization represents the electrochemical loss associated with overcoming the activation energy for electrochemical activity at each electrode. The development of the activation polarization is derived from the Butler-Volmer expression, which is presented in Equation 4.14.

$$i = i_o \left(\exp\left(\frac{\alpha n F \eta_{act}}{R_u T_{PEN}} \right) - \exp\left(\frac{-(1-\alpha) n F \eta_{act}}{R_u T_{PEN}} \right) \right) \tag{4.14}$$

In Equation 4.14, n represents the number of electrons transferred, which is taken to be 1 (in terms of individual electron transferred) rather than 2 (number of electrons transferred per oxygen ion) as clarified by Hernandez-Pacheco et al. [44, 55] and α

represents the transfer coefficient or the symmetry factor which is commonly taken to be 0.5 [19, 72].

The governing Butler-Volmer expression is implicit with respect to activation polarization as illustrated in Equation 4.14. Given that current density is a fuel cell model input and activation polarization is explicitly required to resolve the SOFC operating voltage, implicitly resolving activation polarization using this equation poses a significant computational burden. Accordingly, an approach toward developing an explicitly defined mathematical approximation for the activation polarization is warranted. The approach reported by Noren and Hoffman is used in this model and presented in Equation 4.15 [44, 72].

$$\eta_{act} = \left(\frac{R_u T_{PEN}}{\alpha n F} \right) \sinh^{-1} \left(\frac{i}{2 i_o} \right) \tag{4.15}$$

Each electrode individually contributes to the activation polarization for the entire cell; thus, Equation 4.15 must be applied to both the anode and cathode. Expressions for the exchange current density of the anode and cathode, respectively, are required and adopted from Li [44, 55, 59] as presented in Equations 4.16 and 4.17.

$$i_{o,an} = \gamma_{an} \left(\frac{p_{H_2}}{p_{amb}} \right) \left(\frac{p_{H_2O}}{p_{amb}} \right) \exp \left(- \frac{E_{act,an}}{R_u T_{PEN}} \right) \tag{4.16}$$

$$i_{o,ca} = \gamma_{ca} \left(\frac{p_{O_2}}{p_{amb}} \right)^{0.25} \exp \left(- \frac{E_{act,ca}}{R_u T_{PEN}} \right) \tag{4.17}$$

Parameter values for the activation polarization are presented in Table 4.1 [19, 54].

4.1.4.4 Ohmic Polarization

Ohmic loss accounts for the voltage loss due to the internal electrical resistance of the fuel cell. The model specifically accounts for electrical resistance due to the PEN assembly as well as the oxide scale contact resistance that forms during operation [71,

73]. The overall electrical resistance of the PEN is a function of the temperature dependent resistivities as well as the geometry of the PEN components (i.e. thickness and cross-sectional area). Overall resistance of the PEN is a summation of the resistances of each component and is presented in Equation 4.18. The resistance of the interconnects was presumed small relative to the PEN and oxide scale values, and thus was neglected.

$$R_{PEN} = \sum_{k=an,ca,ele} \left[\frac{\rho_k \delta_k}{A_k} \right] \tag{4.18}$$

The calculation of the ohmic losses is based upon Ohm's Law as presented in Equation 4.19.

$$\eta_{ohm} = iA_{eff} \left[R_{PEN} + R_{oxide} \right] \tag{4.19}$$

The R_{oxide} value was determined empirically by ThyssenKrupp and is provided by Material Data Sheet No. 4060 [73].[3]

4.1.4.5 Species Concentration Calculation

One of the key advantages of using SOFCs as stationary power producing devices is their fuel flexibility. SOFCs have the ability to operate off of synthesis gas mixtures containing methane and carbon monoxide due to the anode's catalysis of the steam reformation reaction, presented in Equation 4.20 and the promotion of the water gas shift reaction, presented in Equation 4.21, given the elevated SOFC operating temperature.

$$CH_4 + H_2O \rightarrow 3H_2 + CO \tag{4.20}$$

$$CO + H_2O \rightarrow H_2 + CO_2 \tag{4.21}$$

As illustrated, hydrogen is a product of both steam reformation and water gas shift and is presumed to be the electrochemically active fuel (i.e., carbon monoxide is presumed to "shift" with comparatively negligible electrochemical activity).

[3] The value was resolved using a contact (area-specific) resistance of 8 mΩ-cm2 for the sake of this investigation based upon inspection of empirically resolved profiles as presented by ThyssenKrupp in Material Data Sheet No. 4060.

The characterization of the steam reformation reaction is based upon a chemical kinetic approach taken from literature and presented in Equation 4.22 with associated parameters presented in Table 4.1 [30, 44, 59].

$$r_{sr} = \gamma_{sr} p_{CH_4}^{\alpha} p_{H_2O}^{\beta} \exp\left(-\frac{E_{act,sr}}{R_u T_{PEN}}\right) A_{rx} \tag{4.22}$$

The water gas shift reaction is presumed to occur at equilibrium and its equilibrium constant has also been empirically resolved and is presented in Equation 4.23 [27, 44].

$$K_{p,shift} = \frac{p_{H_2} p_{CO_2}}{p_{H_2O} p_{CO}} = \frac{x_{H_2} x_{CO_2}}{x_{H_2O} x_{CO}} = \exp\left(\frac{4276}{T} - 3.961\right) \tag{4.23}$$

4.1.5 Thermal Model

The thermal component of the model resolves the temperature profile for both the oxidant stream and the balance of the fuel cell assembly inclusive of both solid material and the fuel stream via an implicit/explicit finite difference methodology, which employs the use of a tri-diagonal matrix algorithm. As designed, the model accounts for conductive heat in the solid material, convective heat transfer between the oxidant and the SOFC; and heat generated due to chemical kinetics as well as cell operation. Encapsulated in the thermal model is also a temperature-dependent, thermophysical properties sub-routine which includes the empirically resolved thermophysical properties of SS441 which were resolved at NETL-Albany [18, 74, 75]. The model includes correlations that characterize the thermal behavior of SS441 over an exhaustive range of temperatures which transcend standard SOFC operation (300K-1800K).

The robust range of temperatures included in the model affords the capability to characterize a broad range of operating conditions including inert heating, electrochemical start-up or “light off”, standard on-design conditions, and off-design operation.

4.1.5.1 SS441 Thermophysical Properties

Stainless steel 441 (SS441) is a ferritic stainless steel alloy that is currently being investigated and developed for use in SOFC interconnects. NETL is currently conducting in-house research for the development and integration of SS441 in the SOFC technological space as a novel and useful interconnect material and its properties have been included for use in this model. The research efforts at NETL-Albany included an extensive investigation on a number of different properties, but for the construction of this model the properties of particular interest are thermal conductivity and specific heat capacity.

The temperature dependent specific heat capacity and thermal conductivity are presented for SS441 on a temperature range of 300K – 1500K in Figure 4.4.

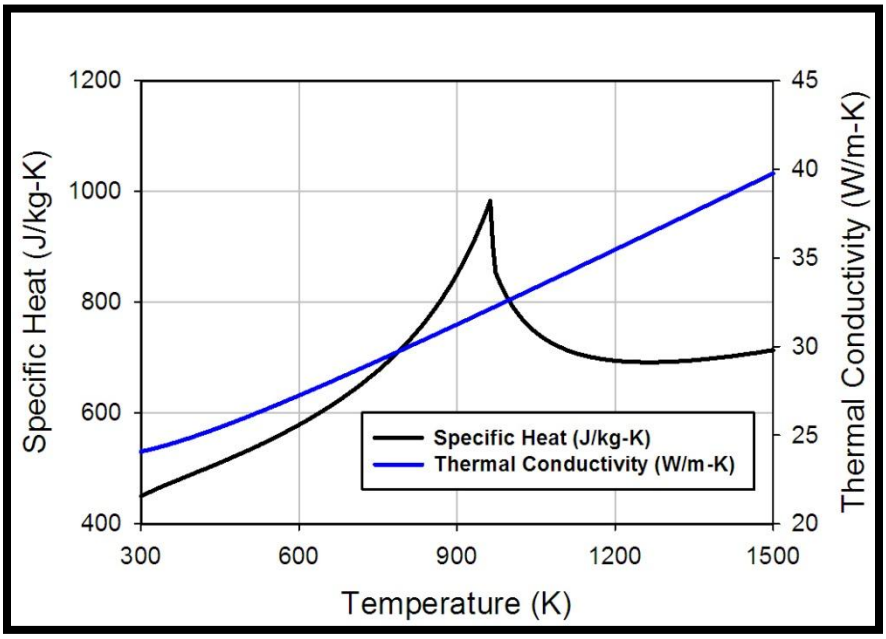

Figure 4.4: SS441 temperature dependent thermophysical properties - low temp

As illustrated, the thermal conductivity is essentially linear over the presented temperature range. The specific heat shows a behavior similar to exponential growth between ambient temperature and about 960K but after a peak value of ~1000 J/kg-K is reached, an abrupt change in form is observed for the SS441 specific heat. This observed

discontinuity is due to the change in SS441 from a ferromagnetic material to a paramagnetic material at approximately 960K. The selected thermophysical properties over a higher temperature regime (1500K – 1800K) are presented in Figure 4.5.

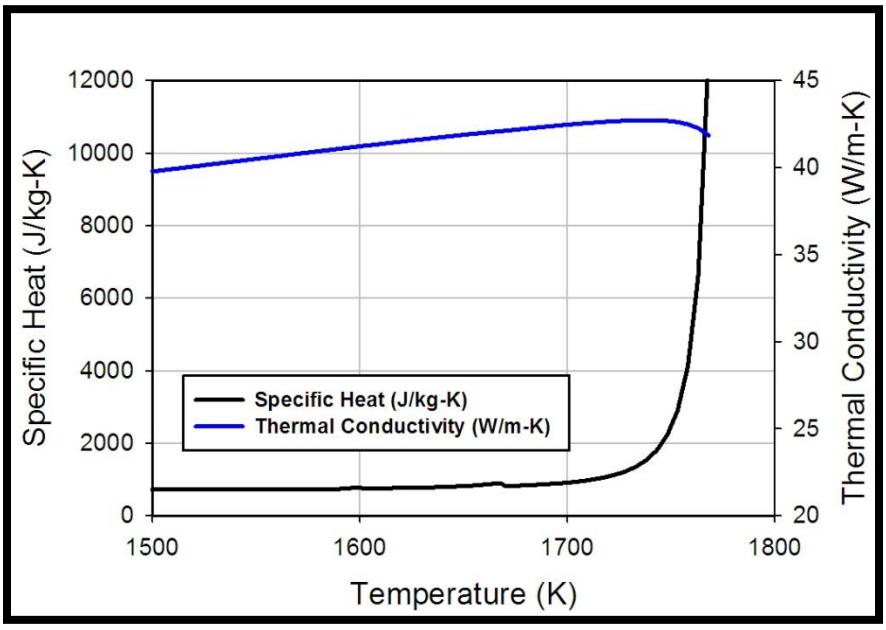

Figure 4.5: SS441 temperature dependent thermophysical properties - high temp

Similar to the lower temperature regime, the thermal conductivity shows consistently linear behavior, with a slight decrease above 1750K; the specific heat, however, shows a seemingly uniform value until about 1750K, at which point, exponential growth is observed. This steep exponential growth is due to paramagnetic behavior of the material at higher temperatures.

Given the consistently uniform behavior observed by SS441 thermal conductivity, a third order polynomial, with an R-squared value greater than 0.99, was able to be developed and integrated into the model to characterize thermal transport through the solid material, which is presented below in equation 4.24.

$$21.6909 + 0.0055 \times T_{PEN} + 7.4806e^{-6} \times T_{PEN}^{2} - 2.0972e^{-9} \times T_{PEN}^{3} \qquad (4.24)$$

Given the dynamic temperature dependent behavior of the specific heat, as exhibited through Figures 4.5 and 4.6, three curve fit expressions were required on three various temperature intervals to obtain a tolerable amount of accuracy (R-squared >0.99).

Expressions, as a function of temperature for the specific heat on the following intervals: a.) 300K – 963.15K, b.) 963.15K – 1603.15K and c.) 1603.15K – 1800K are presented respectively in equations 4.25 – 4.27 below.

$$131.0124 + 1.7433 \times T_{PEN} - 0.0029 \times T_{PEN}^2 + 2.0937e^{-6} \times T_{PEN}^3 \tag{4.25}$$

$$576.1938 + 288e^{6} \exp(-0.0145 \times T_{PEN}) + 0.0911 \times T_{PEN} \tag{4.26}$$

$$902.9201 + 5.1902e^{-93}\left(\frac{\exp(0.1243 T_{PEN}) - 1}{0.1243}\right) \tag{4.27}$$

4.1.5.2 Temperature Profile Resolution

The temperature profiles of the cathode airflow stream, as well as the solid oxide fuel cell assembly, are calculated using a finite difference approach presented in Equation 4.28.

$$\begin{aligned} &\beta\left[\frac{kA_c}{(\Delta x)^2}\left(T_{i+1}^{n+1} - 2T_i^{n+1} + T_{i-1}^{n+1}\right) + hA_g\left(T_\infty - T_i^{n+1}\right)\right] \\ &+ (1-\beta)\left[\frac{kA_c}{(\Delta x)^2}\left(T_{i+1}^{n} - 2T_i^{n} + T_{i-1}^{n}\right) + hA_g\left(T_\infty - T_i^{n}\right)\right] \\ &+ q'''A_c(\Delta x) = \rho C_p(\Delta x)\left[\frac{T_i^{n+1} - T_i^{n}}{(\Delta t)}\right] \end{aligned} \tag{4.28}$$

For the sake of computational stability and accuracy a "beta" value of 0.74 (i.e., fractional weighting of implicit formulation) was employed.

The subscript and superscript indices represent the spatial and temporal domains, respectively. A_c represents the cross-sectional area for conduction heat transfer, from volume to volume along the axis of current density variation. The Δx term represents the spatial distance between the nodes, and the Δt term represents the time step for each iteration. For the purpose of this analysis, the cathode air stream was prescribed with a

composition of 79% N_2 and 21% O_2. Its temperature-dependent heat capacity expression was developed using NASA/Chemkin Polynomials [76]. Due to expectations of sufficiently high Peclet numbers, gas phase conduction was neglected in the air stream and the conductive elements of Equation 4.28 were not included in this temperature field's evolution. The thermal response in the stack is dominated by interconnect material properties. Expressions for the temperature dependent thermophysical properties of SS441 were provided by a SigmaPlot™ curve fit. The heat generation (*q'''*) term from the operating fuel cell is provided in Equation 4.29.

$$q''' = HG_{cell} + HG_{WGS} + HG_{SR} \tag{4.29}$$

$$HG_{cell} = i\left(\frac{-\Delta H_{H_2OFormation}}{2F} - V\right) \tag{4.30}$$

$$HG_{WGS} = -\Delta n_{CO}\Delta H_{WGS} \tag{4.31}$$

$$HG_{SR} = -\Delta n_{CH_4}\Delta H_{SR} \tag{4.32}$$

The HG_{cell} term from Equation 4.30 represents the by-product heat generation from the cell due to the electrochemical reaction that results in the formation of water. The HG_{WGS} and HG_{SR} terms from Equations 4.31 and 4.32 represent the heat generated from the water gas shift and steam reformation reactions, respectively.

4.2 1-D Model Verification

The underlying purpose behind the HyPer project is the development of a mechanism to design SOFC/GT hybrid systems for power generation. Currently, there exists minimal empirical data for validation studies, yet model verification is essential to substantiate utilization for this investigative study. Thus, comparisons with an IEA benchmark [45] and previously published model [44] are presented. The conditions for the IEA comparisons are presented in Table 4.2.

Table 4.2: IEA benchmark parameters

Geometry	
Anode Thickness	0.05 mm
Cathode Thickness	0.05 mm
Electrolyte Thickness	0.15 mm
Interconnect Thickness	2.50 mm
Rib Width	2.42 mm
Cell Length	100 mm
Cell Width	100 mm
Operating Conditions	
System Pressure	1 bar
Inlet Temperature	1173 K
Air Ratio	7
Fuel Utilization	85%
Mean Current Density	3000 A/m^2

The IEA provides benchmarking data for both a humidified hydrogen mixture (90% H_2, 10% H_2O) as well as a methane rich syn-gas mixture (26.26% CH_4, 17.1% H_2, 2.94% CO, 4.36% CO_2, 49.34% H_2O). The comparison results from the humidified hydrogen simulation are presented in Table 4.3. As presented the results compare very well with the IEA benchmark data and all parameters fall within, or close to, the bounds presented in the report.

Table 4.3: IEA benchmark comparison - humidified hydrogen

Parameter	**Benchmark**	**1-D Model**
Voltage (V)	0.702-0.722	0.7159
Max Current Density	0.373-0.396	0.3935
Max PEN Temp (°C)	1049-1098	1048
Outlet Air Temp (°C)	1048-1067	1047

The comparison results from the methane rich syn-gas mixture case are presented in Table 4.4.

Table 4.4: IEA benchmark comparison – syngas

Parameter	Benchmark	1-D Model
Voltage (V)	0.633-0.649	0.6105
Max Current Density	0.304-0.367	0.3477
Max PEN Temp (°C)	1021-1034	1029
Outlet Air Temp (°C)	1016-1026	1028

Though the voltage does fall below the minimum bound presented, the performance parameters are generally comparable to the benchmark data for the syn-gas mixture simulation. The deviation between the conservative operating voltage calculated by the presented model and the IEA benchmark are presumably due to more detailed activation and diffusion polarization calculations than those presented in the IEA benchmarking report.

To further verify the results of the model, comparisons with a steady state, finite volume, SOFC model for coal-based IGFC system analysis, published by Li et al. [44], was made. In this work, Li presents the results of a sensitivity analysis conducted to assess the impact of anode and cathode side activation energies. The analysis reported that activation energy values of 50 kJ/mol and 100 kJ/mol on the anode and cathode sides, respectively, best represented state of the art SOFC performance, and those parameters are used in the model and presented in Table 4.1. The results of the comparisons for the (co-flow) humidified hydrogen case are presented in Table 4.5. For the sake of comparison, similar geometric parameters as those presented by Li et al. [44] are incorporated. The distributed electrochemical parameters are exhibited in Figure 4.6.

Table 4.5: NFCRC Comparison – humidified hydrogen (co-flow)

Parameter	NFCRC	1-D Model
Voltage (V)	0.8	0.81
Average Current Density	0.52	0.52
Maximum Current Density	0.65	0.727
Average Power Density	0.42	0.42
Peak PEN Temp (°C)	859	851
Air Outlet Temp (°C)	856	849

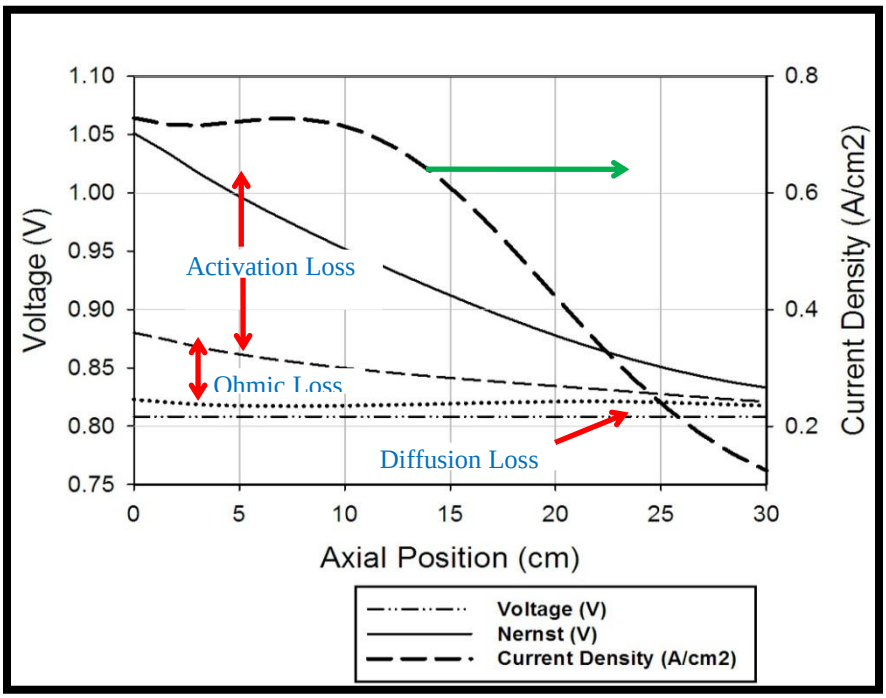

Figure 4.6: Electrochemical profiles for comparison with the NFCRC data : humidified hydrogen (co-flow)

As presented, the results between the two models compare well. The most significant point of deviation is the maximum current density, which varies by approximately 0.08 A/cm^2.

The electrochemical profiles compare very well with those presented in Li et al. [44] as well, with the exception of the current density. There is a more significant

decrease in local current density from entrance to exit in the 1-D model presented in this paper. This difference may be primarily attributed to more detailed diffusivity calculations that result in an elevated current density at the inlet and a lower minimum at the fuel channel outlet.

The NFCRC comparison results from the (co-flow) syn-gas simulation are presented in Table 4.6 and Figure 4.7.

Table 4.6: NFCRC Comparison – syngas (co-flow)

Parameter	NFCRC	1-D Model
Voltage (V)	0.8	0.8153
Average Current Density	0.3	0.3
Maximum Current Density	0.35	0.381
Average Power Density	0.24	0.25
Peak PEN Temp (°C)	790	793
Air Outlet Temp (°C)	789	792

The table and the figure exhibit good agreement with the NFCRC model for the syn-gas simulation. Similar to the humidified hydrogen simulation, the maximum local current density is higher for the 1-D model presented than for the NFCRC model.

Figure 4.7 presents the electrochemical profiles for the syn-gas simulation. As illustrated, the local current density maximum translates downstream for the syn-gas case relative to the humidified hydrogen case, which is expected, given the upstream production (via direct internal reformation) of hydrogen for electrochemical activity. A point of distinction between the present and NFCRC results is the location of maximum local current density. Figure 4.7 shows a maximum local current density approximately half way down the length of the fuel channel whereas the NFCRC model predicts its location to be approximately two-thirds of the channel length. The difference in cell performance is attributed to differences in electrochemical loss calculations. The models still compare well.

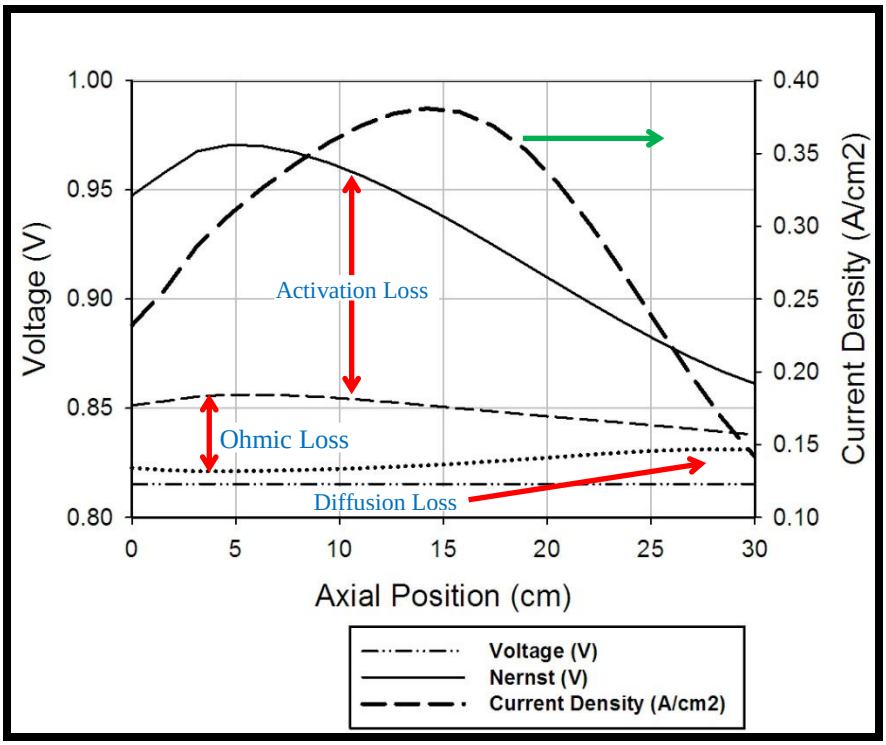

Figure 4.7: Electrochemical profiles for comparison with the NFCRC data : syn gas (co-flow)

4.3 Case Study I: Inert Heating

In addition to real-time operation allowing hardware-in-the-loop simulation (HiLS) capabilities, one of the key and novel components of the presented SOFC model is its ability to thermally characterize cell operation across a broad range of operating conditions. The expanded database of thermophysical properties allows for SOFC operation across an extensive range of conditions, including inert heating. The inert heating characterization capabilities of the SOFC model are presented through a case study, during which the SOFC is heated during gas turbine start-up.

The experiment conducted simulated the inert heating of a SOFC stack, comprised of 2300 cells, during a cold turbine start-up (i.e. all of the system's hardware components were initially at ambient temperature) of the HyPer facility. The heat necessary to start the system is provided from the combustion of natural gas in the system combustor (V-302), which is illustrated in Figure 3.2. The start-up control strategy ramps

the turbine speed at a rate of 2% until a nominal turbine speed of 40,500 RPM is reached. During the system start-up all of the by-pass valves were closed and no load was placed on the turbine. The resulting SOFC inlet parameters during the heat up are presented in Figure 4.8.

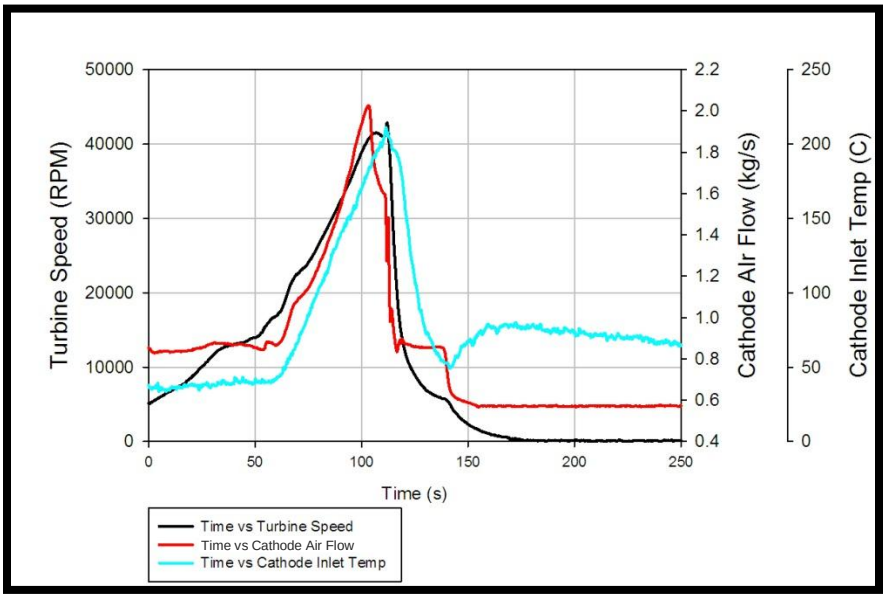

Figure 4.8: SOFC inlet parameters and turbine speed during inert heating start-up

As illustrated in Figure 4.8, air flow and temperature of the stream that is fed into the SOFC are uniform for the first 60 seconds of the simulation, at which point ignition occurs and turbine speed, cathode inlet temperature and air flow increase and reach a maximum value at approximately 100 seconds into the simulation. Typically, turbine start-up involves a transition in turbine rotational speed from an initial rest state to its nominal operating speed. The experimental data presented is extracted from a HyPer start-up that resulted in a stall event. Surge and stall is a phenomena which causes a halt in turbine rotation thus resulting in a sudden decrease in both air flow and inlet air temperature to the fuel cell as illustrated in the plot [14, 15]. Characterization of inert heating during gas turbine start-up has significant value and merit with regards to system reliability and design of control strategies. The data presented, however, illustrates the thermal impact of failure events on SOFCs when operating in a hybridized fashion.

Specifically, stall events illustrate the presence of both inert heating (before the stall event) and cooling (after the stall event) and the impact of that transition on internal thermal transport. Additionally, in the presently reported simulation there are initially large temporal derivatives of temperature toward the leading edge of the fuel cells. This could cause thermomechanical failure (via "thermal shock") of actual cells; hence, the robust investigation afforded by the HiLS is further manifested, and alternative design routes may be pursued. The SOFC spatio-temporal temperature profile plot is presented in Figure 4.9

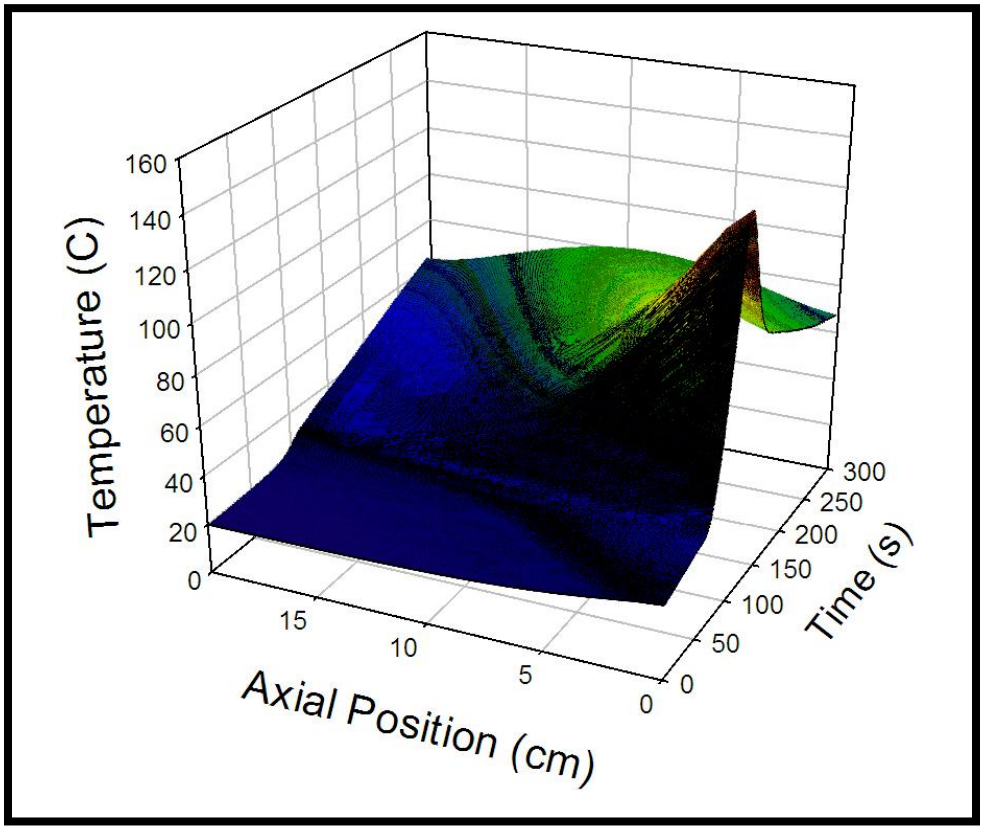

Figure 4.9: SOFC solid temperature profile during start-up simulation

The SOFC and oxidant stream spatio-temporal temperature profile plots, presented in Figures 4.9 and 4.10 respectively. The SOFC spatio-temporal plot, presented in Figure 4.9, illustrates uniform spatial profiles throughout the first 60 seconds of the simulation. At approximately 65 seconds, an increase in the SOFC solid profile is observed. This is due to the heat that is being convected from the inlet air stream to the

SOFC stack. Enhanced heating in the upstream portion relative to the downstream portion of the cell is observed. A maximum temperature of approximately 145°C exists at the SOFC inlet after approximately 110 seconds of simulation. The quick heat-up observed can be attributed to a relatively small time constant of 114.64s assuming an average air flow of 1.4 kg/s. The equation for the time constant is presented below in Equation 4.33.

$$\tau = \frac{m_{cell} C_{p_{cell}}}{\dot{m} C_{p_{air}}} \tag{4.33}$$

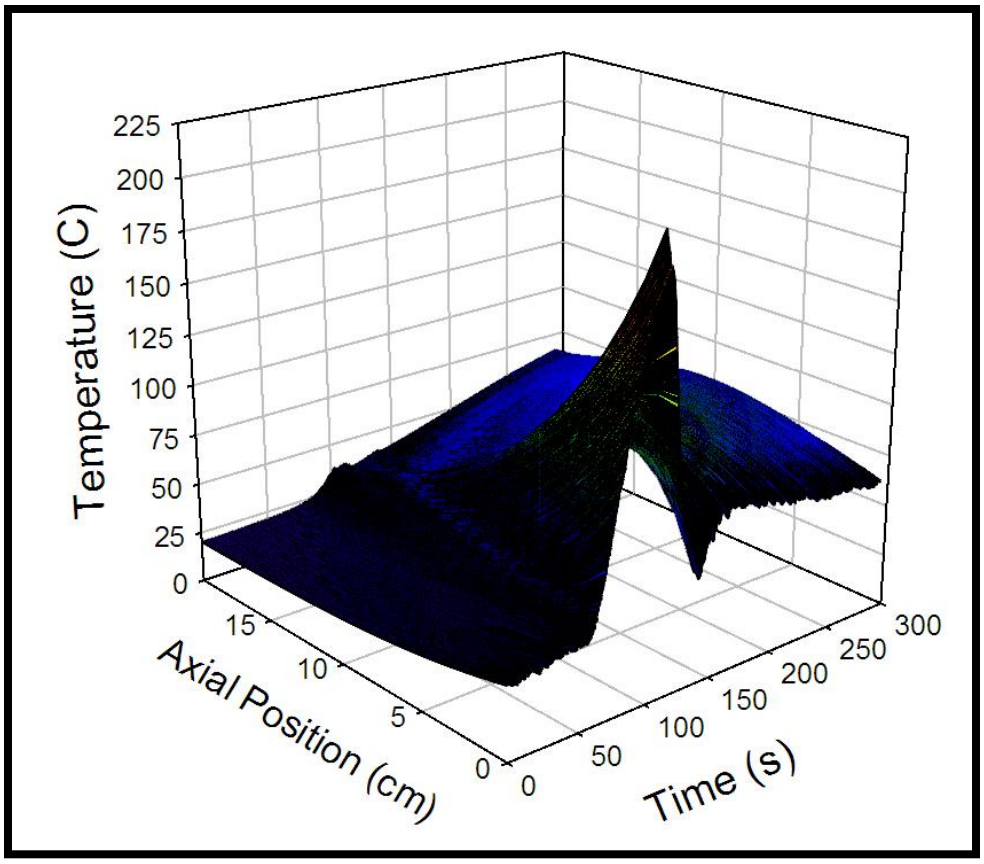

Figure 4.10: SOFC oxidant stream temperature profile during start-up simulation

The temperature profile, with respect to time, at the SOFC inlet will mirror the temperature profile in Figure 4.8 and exhibit similar trends to that of the SOFC solid temperature profile. The observed decrease in the direction of the flow is due to the heat

transfer from the oxidant stream to the SOFC solid. After the stall event occurs, the inlet air temperature approaches its final baseline value of approximately 60°C and the solid temperature at the SOFC inlet is approximately 75°C, which corresponds to a reversal of the direction of heat transfer from the SOFC to the oxidant stream. This effect can be observed in Figure 4.10. As illustrated, the oxidant stream temperature increased through the upstream portion of the fuel cell. Prior to the stall, the amount of heat transferred to the downstream portion of the cell was much less than the upstream portion, thus resulting in lower downstream cell temperatures. This variation in cell temperature caused yet another reversal, wherein heat transfer occurred from the oxidant stream to the SOFC in the downstream half of cell even after stall as is illustrated in Figure 4.10.

The rapid transient stimulus on the fuel cell during start-up coupled with a stall event results in significant thermal dynamics in the SOFC. These dynamics are best illustrated through the assessment of spatial temperature gradients (dT/dx) and temporal derivatives (dT/dt) in the cell during *attempted* start-up.

The impact of start-up on SOFC thermal dynamics is illustrated through the temporal spatial gradient profile shown in Figure 4.11. The most significant thermal gradients (overall maximum magnitude of 12 K/cm) occur near the inlet of the fuel cell, approximately 100s into the simulation across segment 3. According to Nakajo et al. [12], the maximum dT/dx magnitude of 12 K/cm resides in the neighborhood of significant probability for themomechanical failure. The occurrence of the most extreme spatial gradients coincides with the maximum inlet temperature into the fuel cell stack. The magnitude of the spatial gradients diminishes in the direction of the flow, with values near zero existing near the SOFC exit. The impact of the cooling of the oxidant stream, after the stall event, is exhibited by the positive dT/dx values at the cell inlet, between times of 150 and 300 seconds.

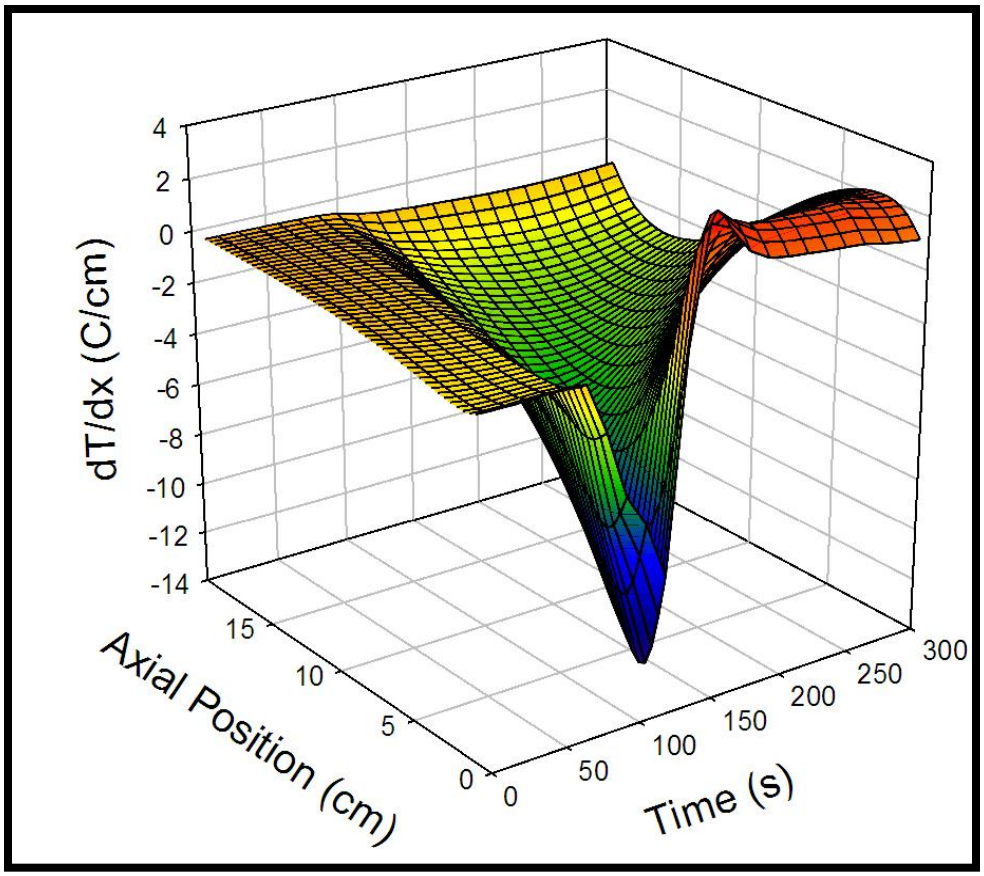

Figure 4.11: SOFC solid temperature profile during start-up simulation

Figure 4.12 presents the dT/dt profiles for the SOFC solid at the SOFC inlet and exit and select interior locations approximately a quarter and halfway down the length of the cell. The dT/dt values become positive throughout the entire SOFC, approximately sixty seconds into the simulation. This is a direct result of thermal energy being added to the HyPer facility and an increase in SOFC oxidant inlet temperature, which serves as the thermal stimulus for the SOFC solid material. The dT/dt values generally decrease with increasing node position (axial position) due to reduced heat from the oxidant stream to the SOFC downstream of the inlet to the cell. The stall event and corresponding decrease in inlet air temperature result in a significant decrease in dT/dt values, with the most significant decrease occurring at the inlet.

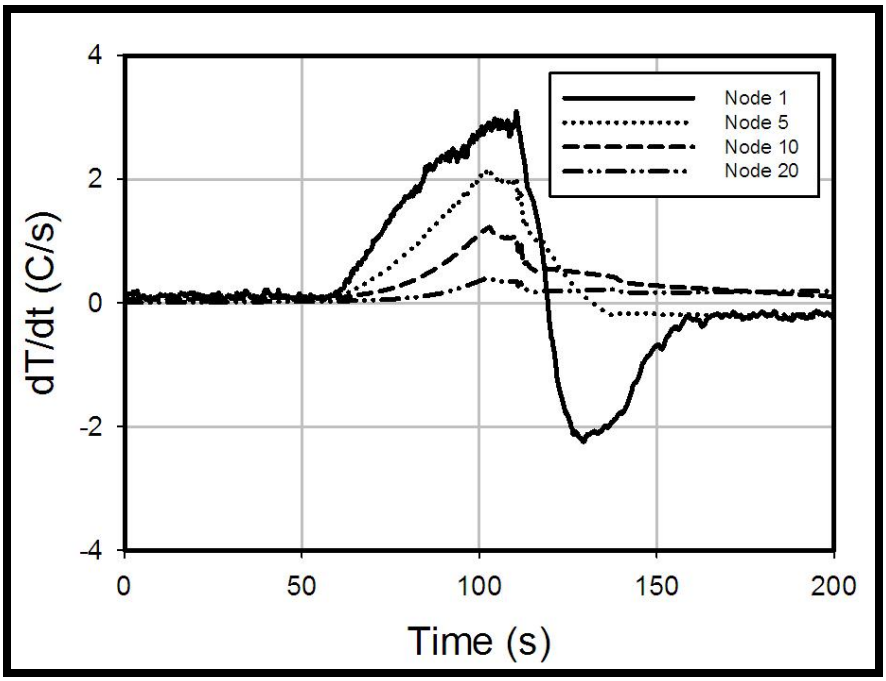

Figure 4.12: Temporal derivatives of SOFC solid temperature for nodes 1, 5, 10, 20

4.4 Case Study II: Open Loop Load Change

For the purpose of testing and presenting the capabilities of the model, while at electrochemically active operating conditions, an experiment simulating a 10% load increase from 200A to 220A was conducted in an open loop configuration (no turbine speed control mechanism). The operational parameters of the experiment for the system and the fuel cell model are presented in Table 4.7.

As presented in Figure 4.13 all five of the constituents in the given inlet stream are present. A monotonic decrease in methane concentration is observed along the length of the fuel channel, along with a maximum in hydrogen content. This maximum in hydrogen is a trade-off between the electrochemical consumption of hydrogen and fuel stream chemistry.

CO and CO_2 show a monotonic increase along the cell length, which supports the significant impacts of the occurrence of both direct internal reformation and water gas shift. This is also supported by the decrease in consumption of water along the length of the fuel cell as the methane concentration decreases. The moderate to significant decrease

in water concentration in the upstream portion of the cell can be mainly attributed to the presence of the steam reformation. The increase in H_2O concentration downstream can be attributed to a decrease in consumption of water due to the near complete consumption of methane and an increase in water production due to heightened electrochemical activity.

Table 4.7: System and fuel cell model parameters for the load change experiment

System Parameters	
Bleed Air Bypass	86%
Hot Air Bypass	0%
Cold Air Bypass	30%
Turbine Load	50 kW
Fuel Cell Model Parameters	
Initial Load	200 A
Initial Voltage	0.810 V
Final Load	220 A
Final Voltage	0.785 V
Fuel Flow	123.00 g/s
Number of Cells	2300

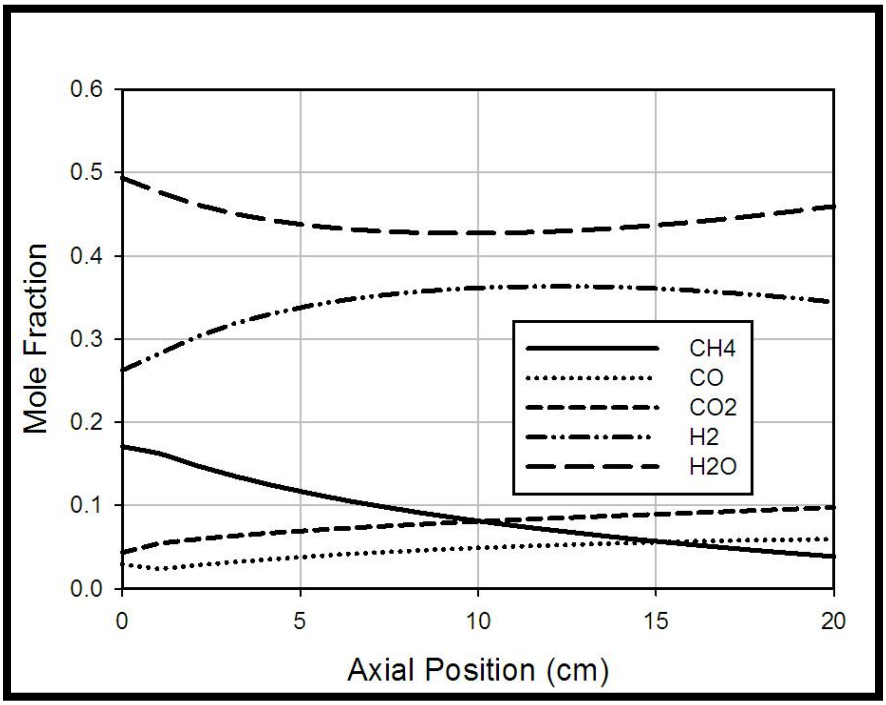

Figure 4.13: Steady state fuel composition profiles before load change (220A)

Figure 4.14 presents the current density, electrochemical losses, and operating voltage profiles for the SOFC prior to the load change being imposed. The most dominant of the electrochemical losses, activation loss, exhibits a mild interior maximum, which occurs due to competing effects between increasing local current density and temperature, approximately 25% down the fuel channel. The local current density profile exhibits a general increase along the length of the fuel cell to a maximum value of approximately 0.575 A/cm^2 near the channel exit. The current density profile supports the significant impact of temperature on electrochemical activity. The cell voltage is uniform along the entire SOFC, based upon the expected Dirichlet boundary condition of equipotential electrodes, and approximately equal to 0.8 V.

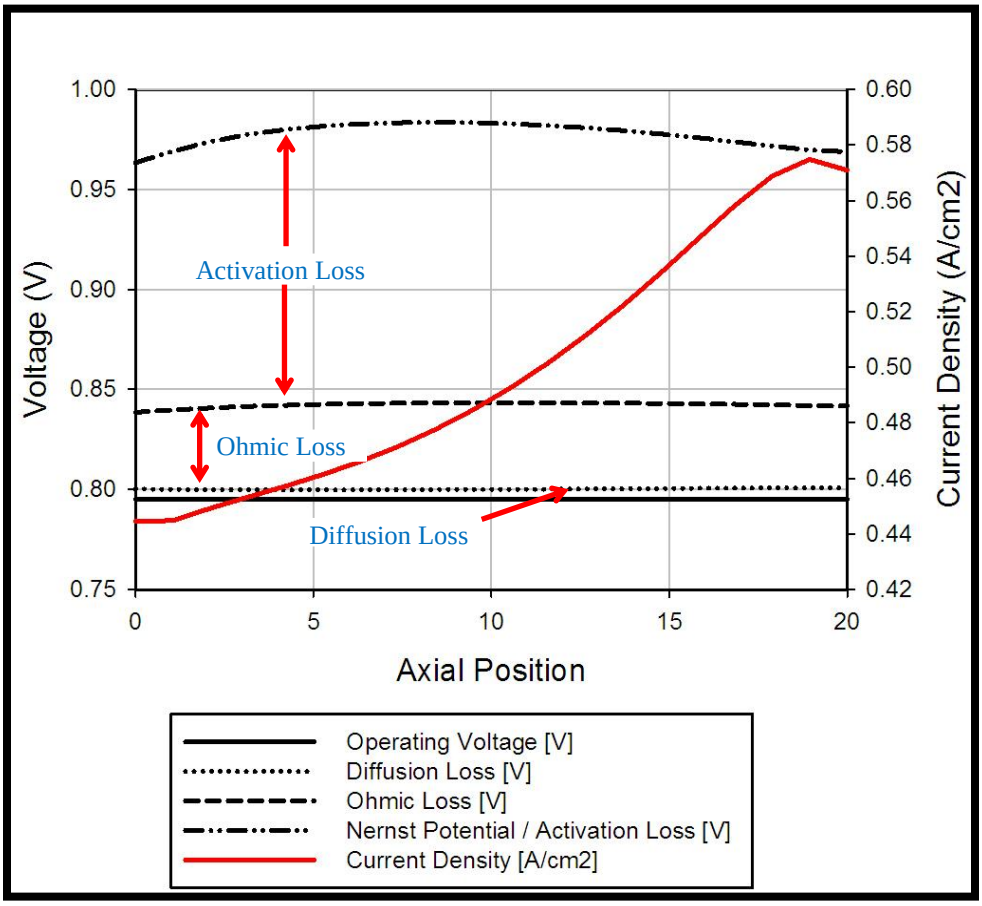

Figure 4.14: Steady state fuel composition profiles before load change (220A)

The data in Figures 4.14 presents steady state SOFC operation while operating "in-the-loop", prior to the 10% increase in current demand (200A – 220A) being imposed on the stack. The inlet parameters to the fuel cell model prior to the step increase in load (at time 0) are presented in Table 4.7. After the step increase in load, the fuel utilization increased from 43.6% to 46.3%. There is not a corresponding 10% increase in fuel utilization; because the load increase changes cell operating temperature and local current density distribution. These changes in operating conditions cause corresponding variations in fuel stream chemistry (e.g., internal reformation), and these variations affect the functionality of fuel utilization upon load current. The increases in current demand and fuel utilization result in an increased conversion of chemical energy to electrical energy from the SOFC and consequently a decreased thermal effluent from the fuel cell subsystem. The increases in current demand and fuel utilization result in an increased conversion of chemical energy to electrical energy from the SOFC and consequently a decreased thermal effluent from the fuel cell subsystem. The impact of the load change on the system thermal effluent, and consequently turbine speed is presented in Figure 4.15.

Figure 4.15 presents the thermal effluent from the SOFC sub-system as well as the turbine speed throughout the load change transient. The increase in current demand results in a decrease in thermal energy from the SOFC sub-system. The system thermal effluent, or "Q_{dot}", decreases from approximate 1480 kW, to a minimum value of approximately 1410 kW after the increase in load is imposed on the fuel cell at time zero. Beyond the initial (downward) spike in thermal effluent, a thermal recovery occurs. The hybrid system simulation entails a constant extensive heating value of fuel being supplied to the stack. This heating value supply manifests as power from the stack, sensible heating of the stack and thermal effluent to the bottoming turbine (the latter of which is shown in Fig. 4.15). Temporal changes to these three energies-in-transit are constrained

to sum to zero, again because their total equals the constant fuel extensive heating value. Accordingly, the recovery in thermal effluent shown after the spike in Fig. 4.15 corresponds to the difference between decreases in stack sensible heating (as steady state is approached) and increases in stack power (as cell temperature and efficiency rise).

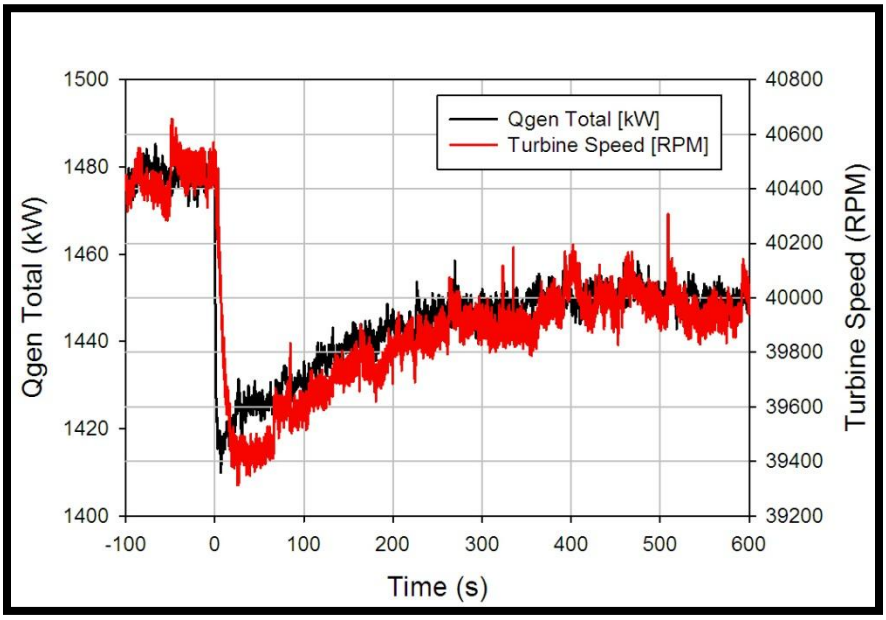

Figure 4.15: SOFC subsystem thermal effluent and turbine speed during load change

Figure 4.16 presents the cathode inlet parameters during the load change transient. As illustrated, both the flow and the pressure of the oxidant stream leaving the heat exchanger and entering the SOFC cathode significantly decrease once the fuel cell load increases.

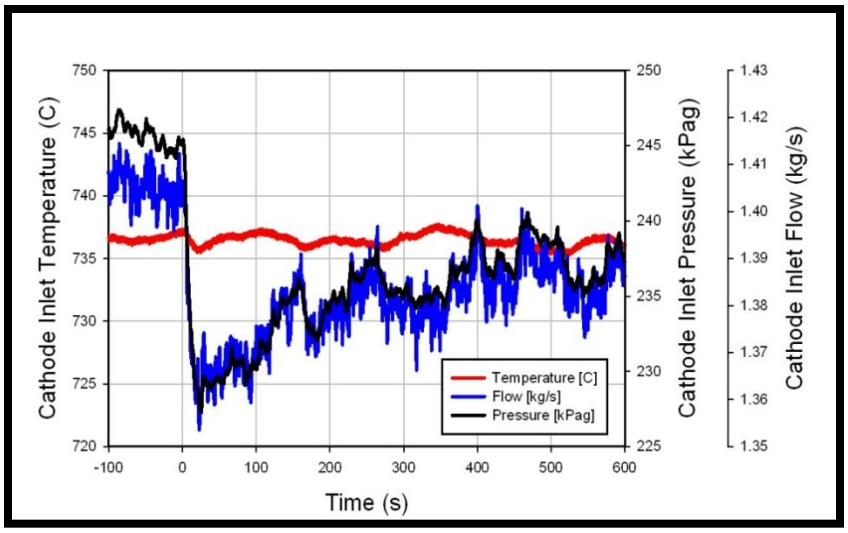

Figure 4.16: SOFC cathode inlet parameters during load change

The inlet pressure and flow decrease from approximately 246 kPag to a minimum of 227 kPag and from approximately 1.41 kg/s to a minimum 1.35 kg/s, respectively, resulting in a maximum pressure drop of 19 kPa and a maximum decrease in mass flowrate of 0.06 kg/s.

The inlet pressure and flow equilibrate to approximately 237 kPag and 1.39 kg/s, respectively. Interestingly, Figure 4.16 illustrates no significant change in the cathode inlet temperature. This is due to competing effects of the streams passing through the pre-cathode heat exchange system. The competing effects of decreased turbine exhaust temperature with decreased compressor mass flow results in an essentially stable fuel cell subsystem inlet temperature (for this simulated episode). Changes in the thermal effluent from the fuel cell subsystem have an impact on almost all of the system parameters produced, but the ones of particular interest as it pertains to the performance of the real-time SOFC model are the cathode inlet parameters presented in Figure 4.16. Pressure (PT-305), temperature (TE-326) and mass flow (FE-380) into the air plenum (V-301) of the HyPer Facility, which again is the apparatus that is used to represent the cathode air volume, are fed directly into the fuel cell model in real time. These parameters are used to simulate SOFC performance, which ultimately determines the necessary amount of

thermal effluent that needs to be fed to the system to represent that from an operating SOFC subsystem. In addition to controlling the amount of fuel, and thus, thermal energy fed to the facility, the real-time, SOFC model, is able to characterize the fuel cell performance in the spatio-temporal regime. The impact of system transients on performance parameters, such as solid and oxidant stream temperatures, spatial and temporal temperature gradients, current density, polarization losses and species concentrations can be observed and analyzed with respect to both space and time. The solid and oxidant spatio-temporal temperature profiles are presented in Figures 4.17 and 4.18, respectively.

Figure 4.17 presents the temperature profile of the SOFC solid material throughout the transient response of the induced load change. As illustrated in the figure, there exist local minima in the spatial temperature profiles approximately 25% downstream from the SOFC inlet prior to the step increase in load. The overall maximum temperature occurs at the outlet of the SOFC. The apparent change in concavity in the temperature profile is again due to the presence of the significantly endothermic steam reformation reaction near the fuel cell entrance, which has a significant cooling effect, thus creating a local minimum in solid temperature. Once the change in load is induced at time "0", an overall increase in the solid SOFC profile is observed. This is due to a combination of increased by-product heat generation within the simulated stack leading to sensible heating of the cells and a propagated decrease in compressor airflow given reduced "firing" of the turbine. The change in local temperature, after the transient event, appears to be more significant at the exit of the reactant channels as opposed to the inlet. This can be attributed to the stability of the inlet air temperature throughout the load change, diffusion of more heat downstream due to an increase in by-product heat generated, a lower mass flow rate through the cathode which results in decreased cell cooling, and an enhanced upstream cooling effect due to the occurrence of steam

reformation. The coupled spatio-temporal oxidant stream temperature profile is presented in Figure 4.18.

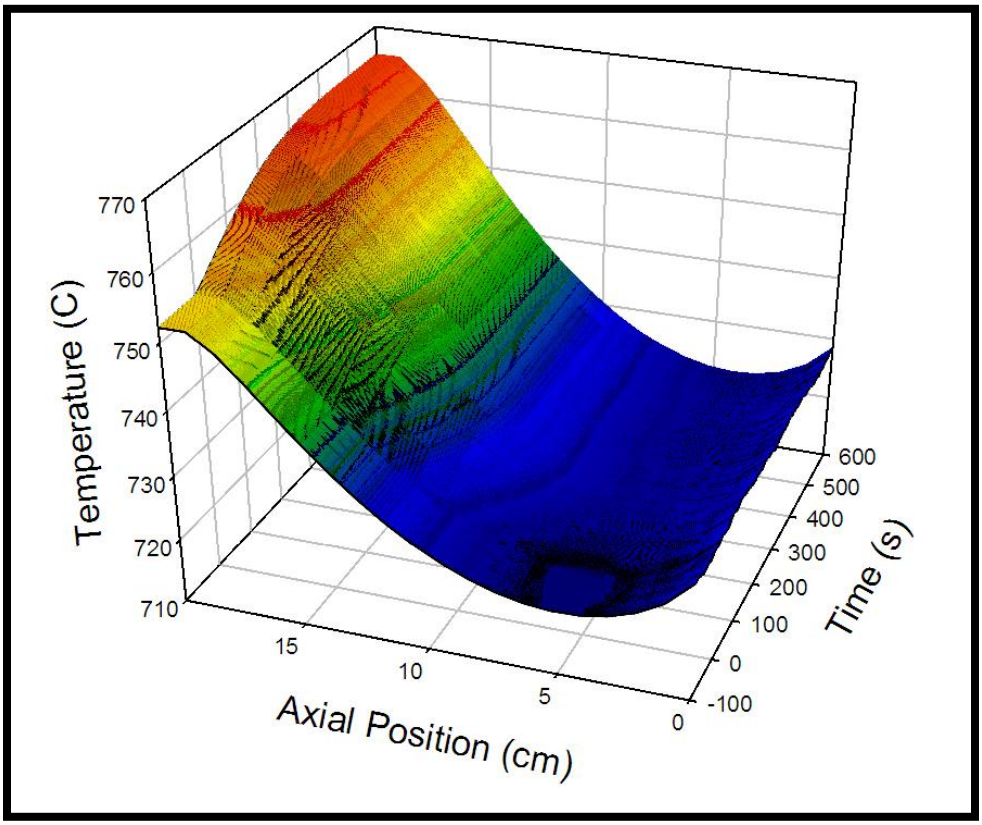

Figure 4.17: SOFC solid spatio-temporal temperature plot during load change

Figure 4.18 presents the temperature profile of the oxidant stream with respect to time. As expected the profile has the same general trend as that of the solid material. An overall increase in the temperature is seen from the point of the load increase at time 0 with an apparent new steady state profile existing after 10 min from the transient event. The only means of thermal communication between the oxidant stream and the solid material is convective heat transfer, thus, the observed changes in the temperature profile are directly induced by the change in temperature of the solid material and the oxidant flow rate (oxidant inlet temperature does not change), hence the similarities in the general temperature profiles.

Resolving the temperature profiles of both the solid and the oxidant stream affords the ability to analyze thermal transport dynamics in the fuel cell, more

specifically, analysis of spatial gradients and temporal derivatives. Given the brittle and mechanically sensitive nature of SOFC materials, management of thermal transport is an area of particular interest in the SOFC research. Spatio-temporal plots of the spatial gradient and temporal derivative of temperature in the SOFC are presented in Figures 4.19 and 4.20, respectively.

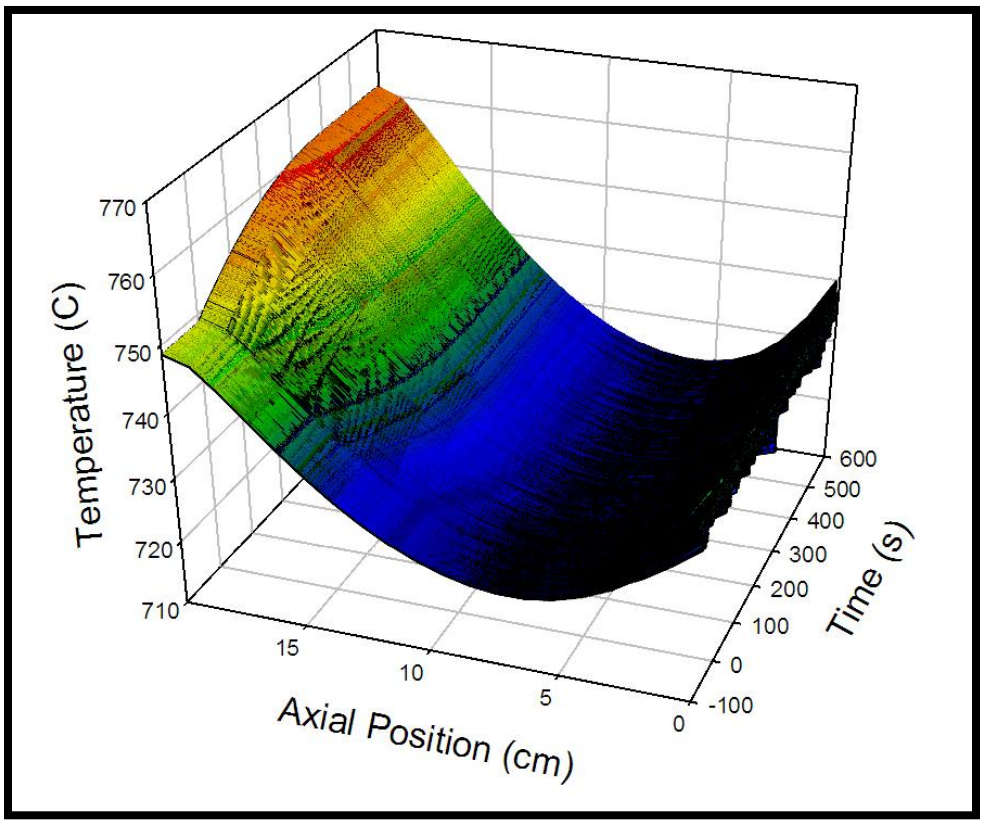

Figure 4.18: SOFC oxidant stream spatio-temporal temperature plot during load change

The spatial temperature gradient throughout the load change simulation is presented in Figure 4.19. The spatial profiles before and after the load change appear to have very similar trends, though a noticeable increase in magnitude is observed after the load perturbation. The dT/dx values at the channel entrance are negative. This is due to the decrease in temperature from the occurrence of the highly endothermic steam reformation reaction, producing a local minimum in the solid temperature profile approximately 25% downstream from the channel entrance. The presence of the local

solid temperature minimum aligns with a dT/dx value of zero observed approximately 25% downstream from the entrance as well. As presented, the dT/dx values increase in the downstream direction resulting in a maximum spatial gradient approximately 75% downstream from the channel entrance.

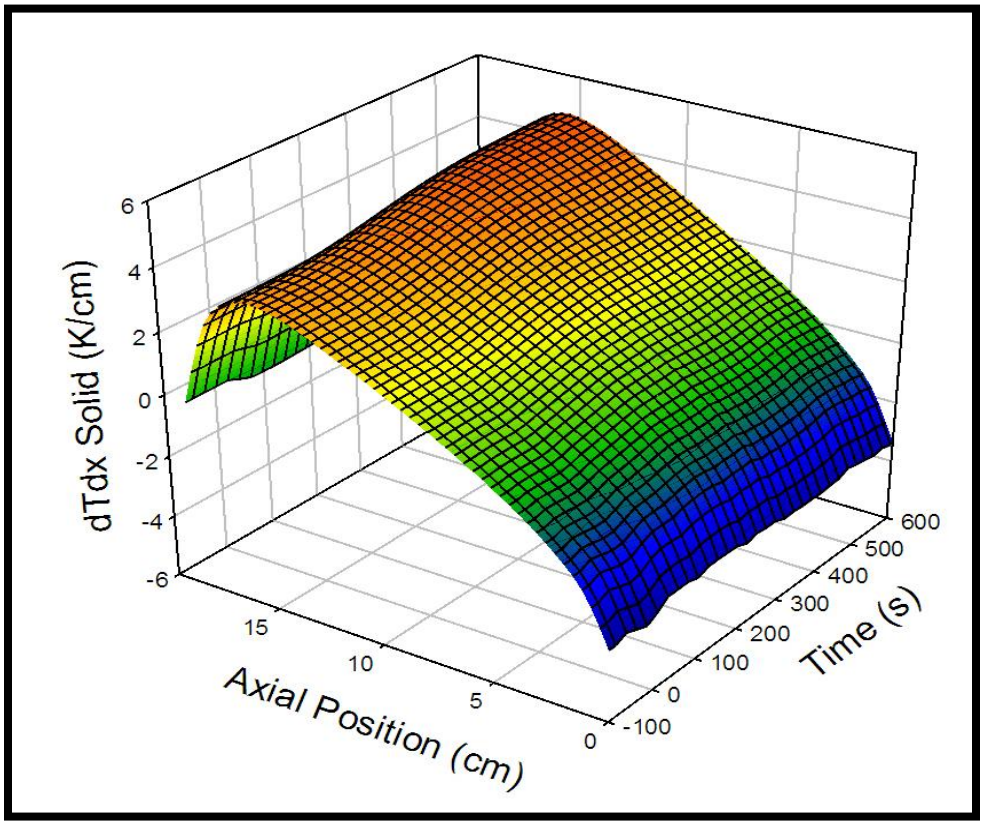

Figure 4.19: SOFC spatial temperature gradients plot surrounding load change

Once the maximum spatial gradient value is reached, there is a significant decrease in the dT/dx profile. This trend is due to the adiabatic boundary condition at the exit which results in the temperature profile leveling and the presence of the overall maximum temperature existing at the channel outlet. The maximum gradient magnitude that is associated with endothermic steam reformation (at the inlet) is 3.7 K/cm. The largest temperature gradient is approximately 4.7 K/cm and approximately 75% downstream, which are generally safe in comparison to limiting values presented by Nakajo et al. [12].

The time rate of change of the temperature of the solid material is presented in Figure 4.20. The spikes in dT/dt values observed at the inlet are primarily due to the boundary condition of the oxidant stream (i.e., oxidant temperature at the inlet is prescribed to be equal to the temperature of the inlet air) and its impact on SOFC solid calculations. Specifically, the observed variance in dT/dt near the cell inlet is due to signaled noise at the interface between the facility imbedded thermocouple and the fuel cell model.

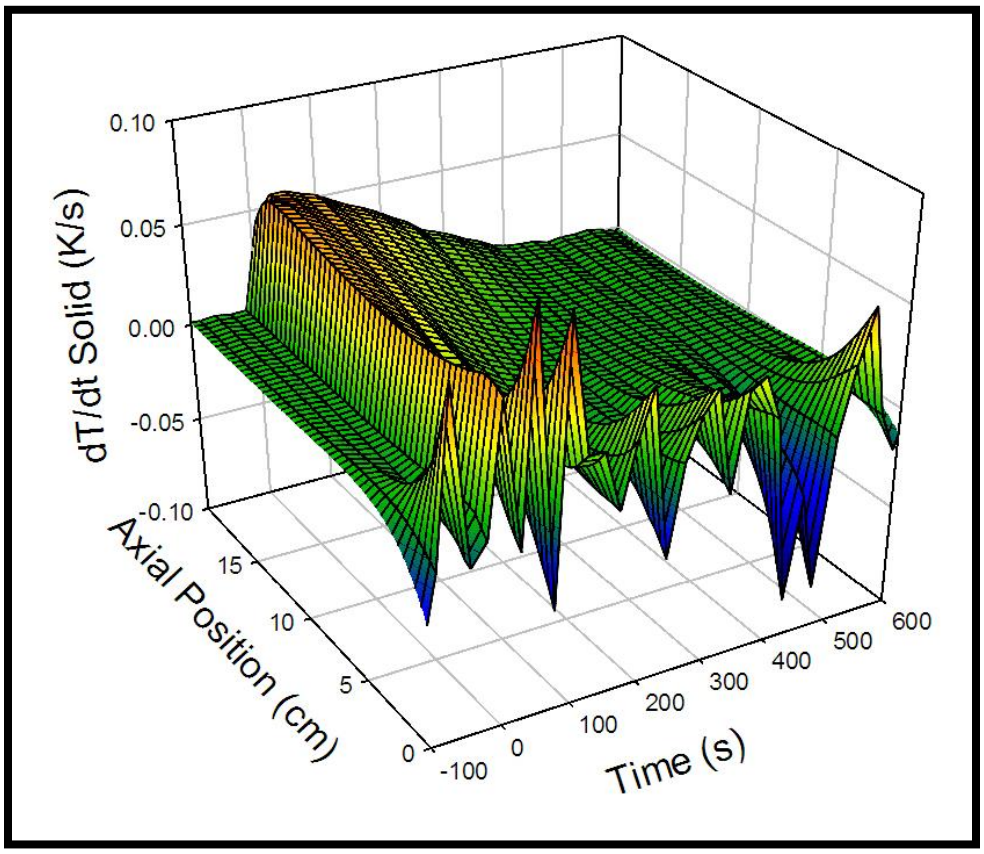

Figure 4.20: SOFC solid temporal temperature derivatives spatio-temporal plot surrounding load change

The figure illustrates a dT/dt value of approximately zero prior to the load change, indicative of an initial steady state, at which point it increases to an overall maximum value. This exhibits the cells' thermal response to changes in current demand and the increase in operational by-product heat. Once the increase in load is imposed, the temporal temperature derivative quickly approaches its maximum value then gradually

approaches zero, which represents a transition towards a new steady state and steady operating conditions. It is important to note, however, that the return to that steady state dT/dt value of zero is more gradual in the downstream portion of the cell than it is in the upstream portion. In the upstream portion of the cell, the balancing effect between the by-product heat generation and the cooling from steam reformation results in a quicker return to steady state temperature. The decreased activity of internal reformation downstream, due to the upstream consumption of methane, results in a significant temperature increase due to by-product heat generation and the majority of the cooling that is provided is via oxidant flow, thus resulting in a slower, more gradual return to a steady temperature. The spatio-temporal SOFC temperature plot, in Figure 4.18, illustrates the more "sluggish" downstream thermal response relative to the upstream response. The load change produced a maximum dT/dt value of less than 0.06 K/s. This temperature change would result in less than 4 degrees per minute.

In addition to thermal characterization and analysis, electrochemical parameters are calculated on a distributed basis with respect to time. Two of the key operational, electrochemical performance metrics of interest are local current density and operational voltage. The current density spatio-temporal profile throughout the load change is presented in Figure 4.21. The Nernst potential profile with accompanying electrochemical loss profiles, which comprise the operational voltage as presented in Equation 4.1, are presented in Figure 4.24 and Figures 4.26-4.28.

The local current density profile throughout the load change, with respect to time, is presented in Figure 4.21. The initial local current density values range from a maximum at the exit of approximately 0.57 A/cm^2 and a minimum at the inlet of approximately 0.45 A/cm^2. Once the new steady state profile is achieved, the maximum and minimum values range approximately between 0.66 A/cm^2 and 0.47 A/cm^2. There is a much more noticeable difference in the increase of local current density at the outlet as opposed to the inlet. These results can be directly contributed to the coupling of

electrochemical activity (i.e. current density) and operating temperature. Given the more significant increase in local temperature at the outlet as opposed to the inlet, during the load change, as illustrated in Figure 4.17, the greater increase in local current density at the outlet relative to the inlet is expected and presented in the figure. A direct comparison of these profiles is presented below in Figure 4.22.

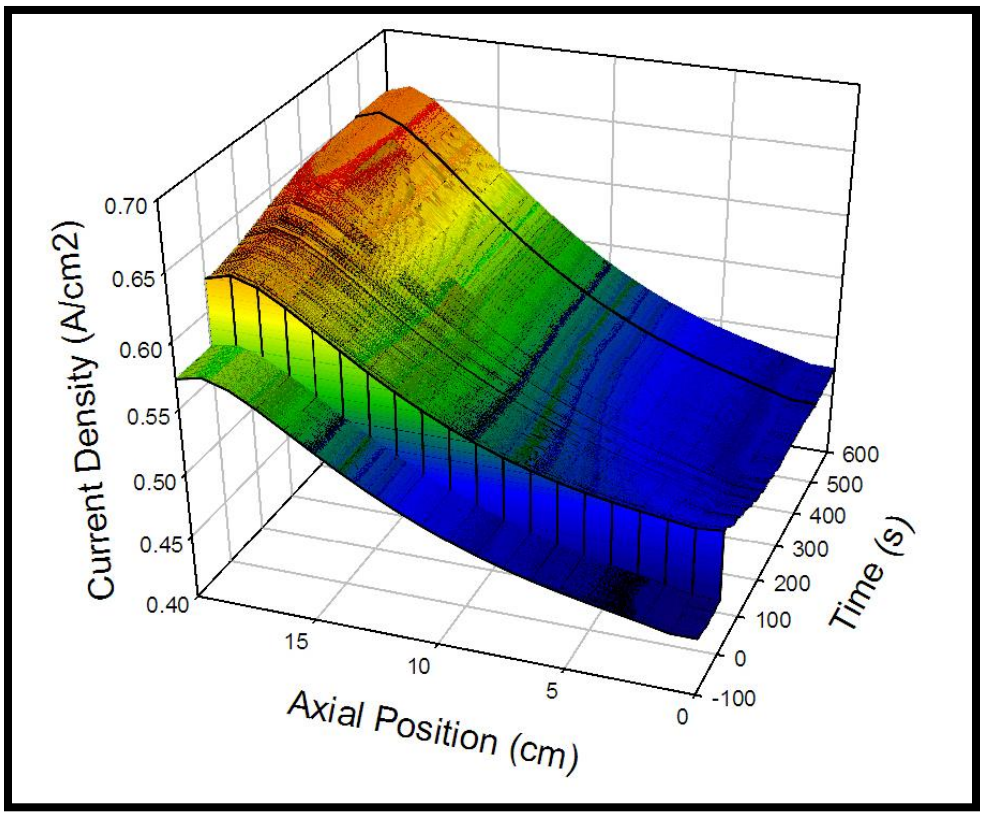

Figure 4.21: SOFC current density spatio-temporal plot before and after load change

The pre and post load change steady state local current density profiles are presented in Figure 4.22. The variation in the difference in the local values at the inlet versus the outlet are illustrated here as well. These results can be directly contributed to coupling of electrochemical activity (i.e. current density) and operating temperature. Electrochemical activity tends to occur more readily at higher temperatures; thus, heightened local current density values are going to exist at locations of higher local operating temperature. Given the more significant increase in local temperature at the

outlet as opposed to the inlet during the load change, as illustrated in Figure 4.15, the greater increase in local current density at the outlet as opposed to the inlet is expected. The increase in current density also results in increased hydrogen consumption, which effects current density distribution as well, but given the relatively moderate fuel utilization for this study, the current density distribution is primarily influenced by cell temperature distribution.

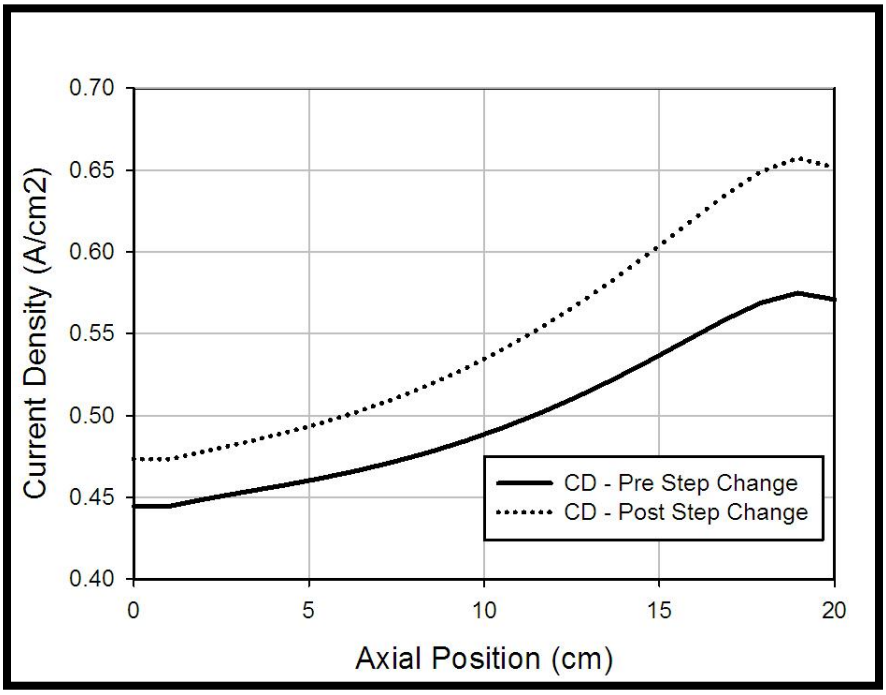

Figure 4.22: Steady state local current density profiles before and after load change

The local solid (and oxidant stream) temperature profiles, before and after the load change, are presented in Figure 4.23 to further support this coupling effect. As illustrated in the figure, the temperature of both the oxidant and solid material decrease in the upstream portion of the cell as the thermal condition is heavily dominated by the highly endothermic steam reformation, followed by a gradual increase with a maximum value observed at the exit due to by-product heat generation from cell activity. At the inlet of the SOFC, the oxidant stream is actually heating the SOFC since the cell has been "cooled" by the DIR. Further downstream, the oxidant and solid temperature profiles exhibit a crossover effect with results in an elevated SOFC temperature as compared to

the oxidant stream. This further illustrates the transition from the dominance of DIR to by-product heat in downstream portions of the cell. As load is applied, cells produce more by-product heat thus resulting in a shift upstream for local minima of solid and oxidant stream profiles as well as the profile crossover. The maximum temperatures for the solid and oxidant streams also increased in magnitude due to the increase in FC load.

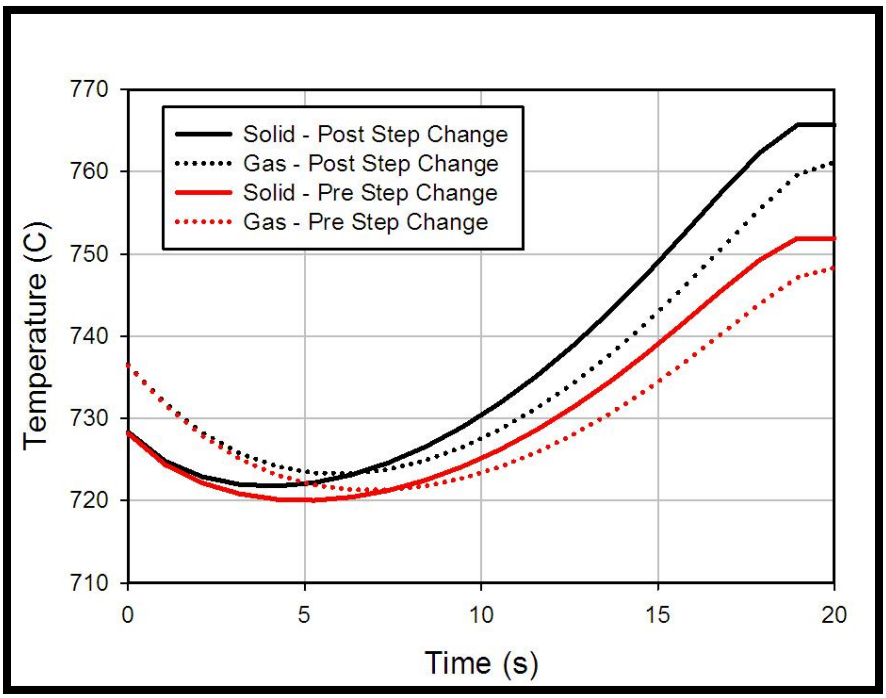

Figure 4.23: Steady state solid and oxidant stream profiles before and after the step change

At time 0, the 10% increase in current demand results in a step increase in the current density profile as illustrated in Figure 4.21. There exists a transition from the profile that is observed immediately following the step change in current demand to the steady state profile that is observed at the end of the transient response (i.e. 600s) and presented in Figure 4.22. The spatio-temporal SOFC solid temperature plot presented in Figure 4.17 presents the same behavior for the thermal response as well. This further illustrates and supports the coupling between the temperature and the local current density. Once the change in load is imposed, the temperature profile begins to gradually increase and approach the new steady state condition. A more significant thermal

transition period for the downstream portion of the cell, as opposed to the upstream portion of the cell is observed, similar to the current density transition as well.

As presented in Equation 4.1, the operating voltage of the operating SOFC stack is obtained by calculating the theoretical maximum voltage, known as the Nernst potential, and subtracting from it the diffusion, activation and ohmic electrochemical losses. The spatio-temporal profile of the Nernst potential, is presented in Figure 4.24.

Equation 4.2 quantitatively illustrates the dependency of Nernst potential on both temperature and species concentrations. Given that dependency as well as the variance of both quantities along the length of the fuel cell, a variance in Nernst potential is expected and presented in the figure.

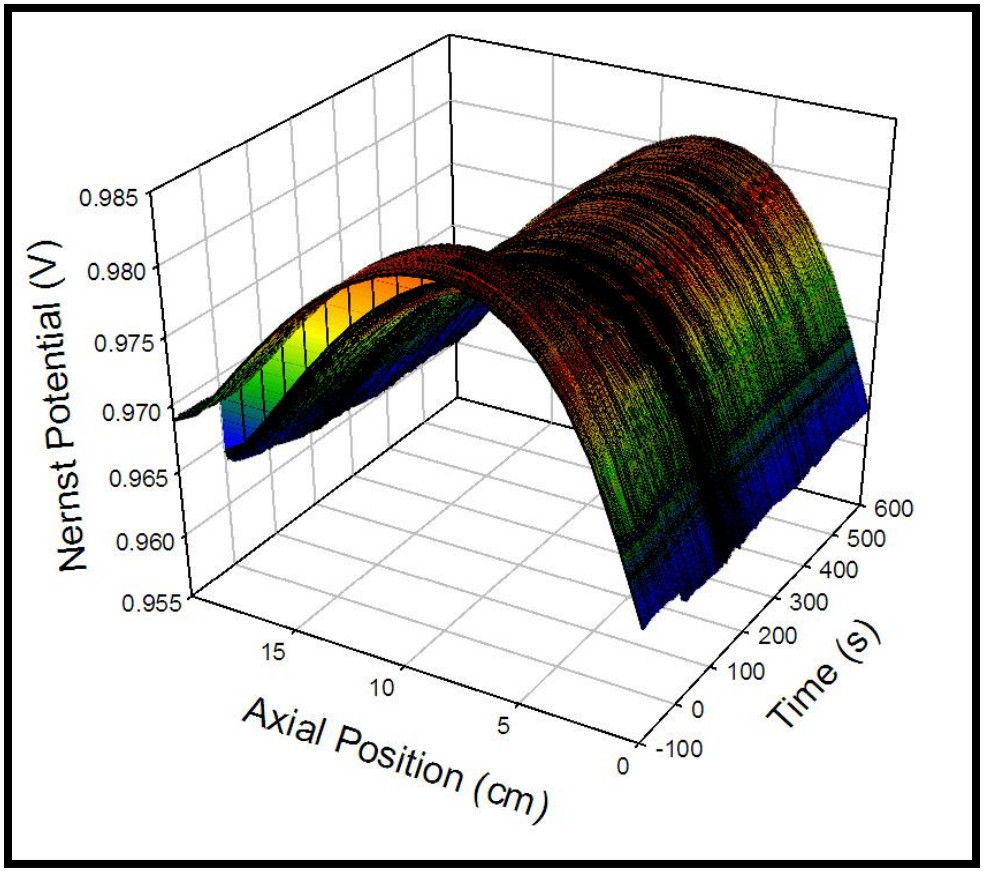

Figure 4.24: SOFC Nernst potential spatio-temporal plot before and after load change

A seemingly quadratic profile of the Nernst potential is observed before and after the step increase in load. This observed general profile is opposite in concavity to the temperature profile which manifests some of the Nernst potential's negative correlation with temperature. A local maximum is observed approximately 30% downstream from the fuel channel inlet, which aligns closely with the region of minimum temperature and higher hydrogen concentration due to direct internal reformation, which supports the preceding temperature trend. Downstream from the local maxima, increasing temperature and the decreasing hydrogen concentration, contribute a gradual decrease through the remaining portion of the cell.

The hydrogen concentration profile, presented in Figure 4.25 has a similar profile to that of the Nernst potential presented in Figure 4.24. The downward concaved quadratic shape of the hydrogen concentration plot exhibits its direct relationship with the Nernst potential. As illustrated, the Nernst potential and the hydrogen concentration do not follow the same exact trend since the Nernst potential is dependent upon temperature as well.

The step increase in load which caused an increase in electrochemical losses and SOFC temperature, thus causing a decrease in Nernst potential, directly contributes to the decreased operating voltage. As the system continues to thermally respond, a gradual decrease in downstream Nernst potential due to increasing temperature, and increase in upstream Nernst potential due primarily to increasing H_2 fuel stream chemistry yield (from an elevated cell temperature) is observed.

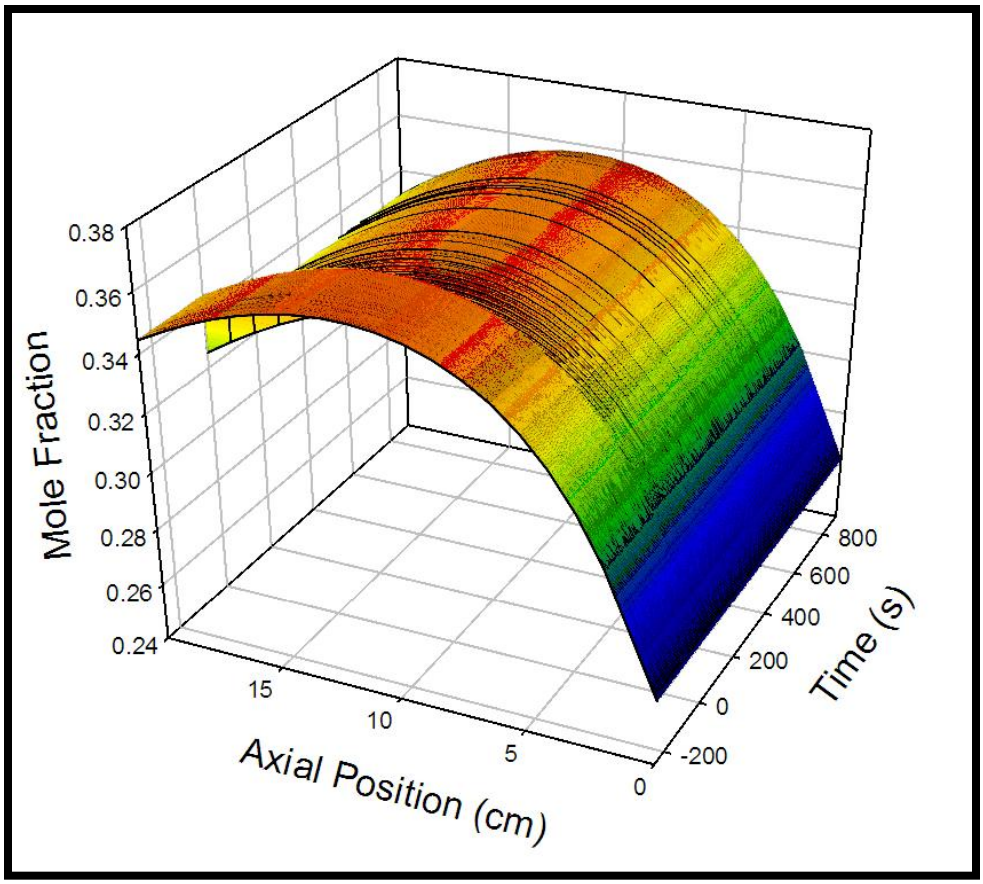

Figure 4.25: Spatio-temporal hydrogen concentration profile before and after load change

The electrochemical loss due to diffusion through the porous PEN electrodes, is presented in Figure 4.26. As exhibited by Equations 4.3-4.6, diffusion polarization (or diffusion loss) is dependent upon both local temperature and current density. Given that the model parameters have been selected to simulate SOFCs with very thin electrodes, the diffusion polarization term is expected to be the least significant, and such is the case when compared to the activation and ohmic loss terms presented in Figures 4.27 and 4.28 respectively.

The combined effects of current density, temperature distribution and fuel stream chemistry, all contribute to the diffusion loss profile observed in Figure 4.26. The maximum value is observed at the cell exit, which in addition to the maximum temperature, also coincides with the maximum local current density. A local minimum is

observed approximately 25% downstream from the inlet, which aligns closely with the local minimum temperature and maximum Nernst potential. The step increase in current demand results in a step increase in diffusion polarization as expected, and as with the other electrochemical parameters, the effect of the thermal transition to steady state temperature is observed as the diffusion polarization profile increases.

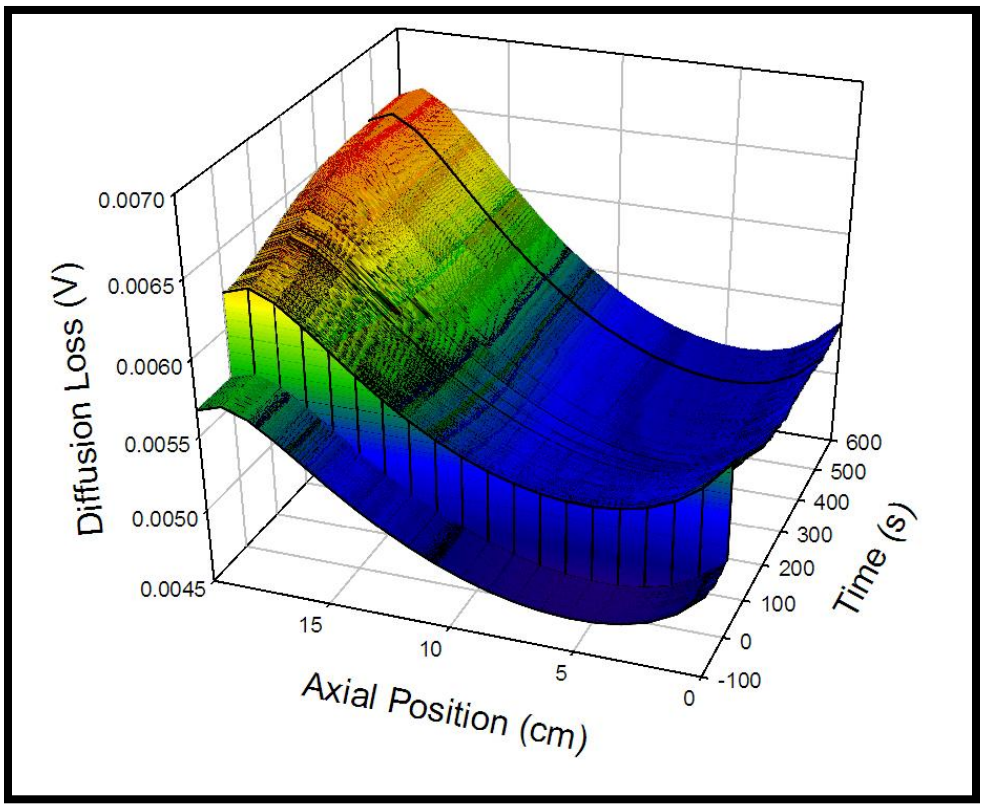

Figure 4.26: SOFC diffusion loss spatio-temporal plot before and after load change

It is apparent from Figure 4.25 that the effect of H_2 concentration on diffusion polarization is more significant than temperature. Generally, polarization terms decrease with increasing temperature but the significant variance in concentration along the fuel channel appears to have a more dominant effect than temperature. Figure 4.27 presents the activation loss spatio-temporal profile through the system transient response to the load change.

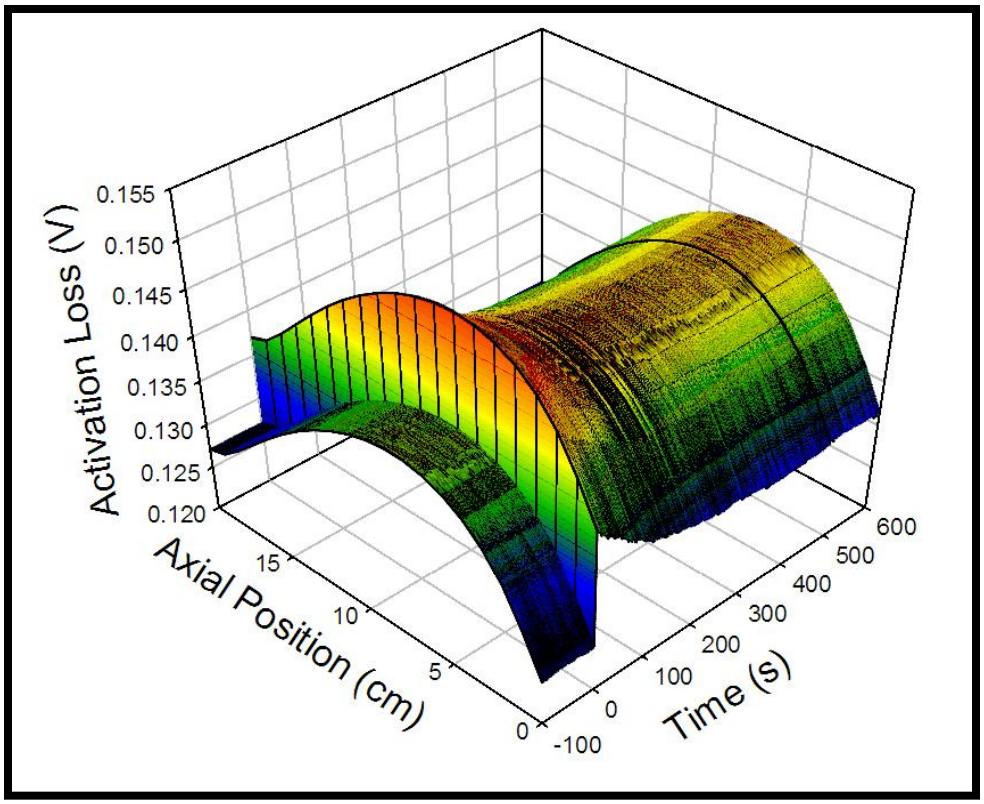

Figure 4.27: SOFC activation loss spatio-temporal plot before and after load change

The activation loss represents the decrease in voltage that results from the necessary activation energy for electrochemical activity at each electrode. Given the state-of the art design that this model is attempting to simulate, activation loss is the most dominant of the three electrochemical loss terms. The effect of temperature on activation polarization is evident from the profile presented in the figure. As illustrated, η_{act} decreases with increasing temperature. The maximum activation loss value occurs approximately 30% downstream from the fuel channel inlet which aligns well with the region of minimum temperature. Similarly to other electrochemical profiles, a step increase in activation polarization occurs at time 0, which is the temporal point at which the step increase in load is imposed. The gradual decrease in the overall profile from t=0 is also observed, which directly corresponds to the thermal transition period to steady state. The ohmic polarization, which represents the electrochemical loss due to electrical resistance, is presented in Figure 4.28.

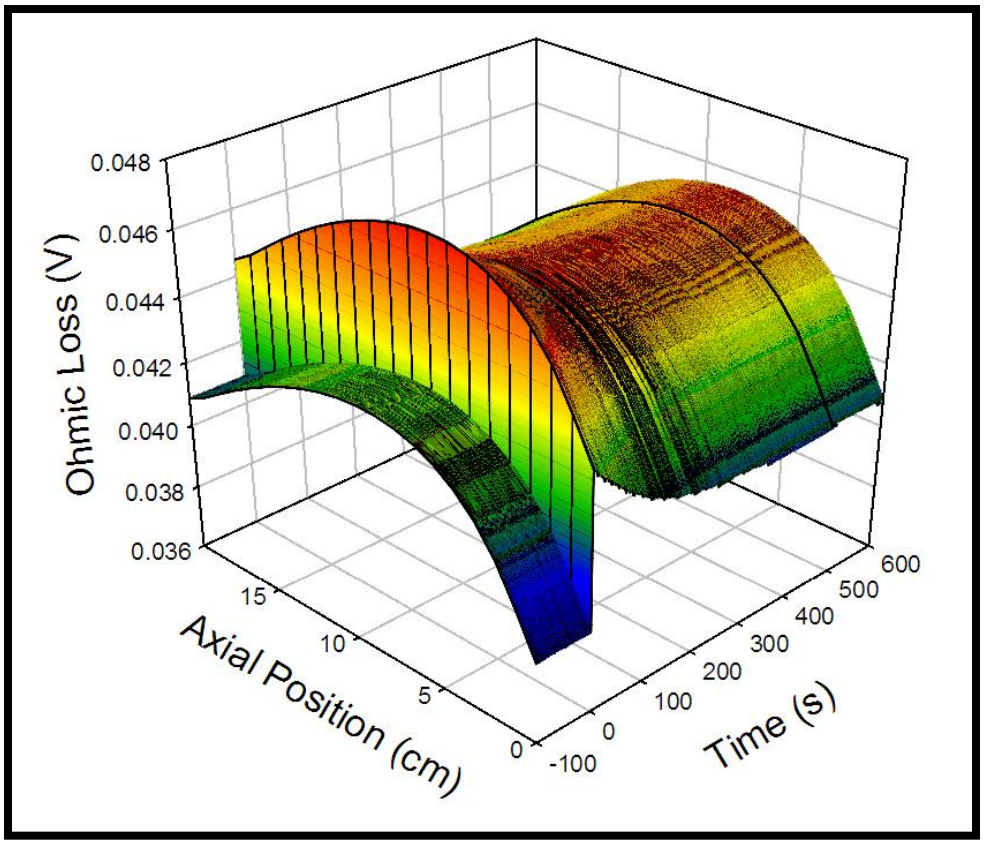

Figure 4.28: SOFC ohmic loss spatio-temporal plot during load change

Ohmic loss is also favorably influenced (i.e., decreases) by increased temperature, but is unfavorably influenced (increases) by increased current density. Since regions of elevated temperature tend to correspond with regions of elevated current density, the dependence of ohmic polarization on both temperature and current density has competing effects and results in local maxima that are shifted downstream from the location of the local temperature minima. A step increase in the ohmic polarization profile occurs at time 0, along with the step change in current. The decrease in ohmic loss due to gradually increasing temperature throughout the transient response to steady state is also observed.

CHAPTER 5

COLD AIR POST COMPRESSOR BY-PASS INVESTIGATION – LBSC

The primary focus of this dissertation work is to characterize the impact of CA post compressor by-pass flow on the dynamic response of an SOFC/GT hybrid system during electrochemical start-up. Chapter 3 outlined the experimental plan employed to characterize the system transient response, which includes varying both initial FC load and CA by-pass valve position in parametric manner. Initial FC load is varied on a range of 50A – 125A in equal 25A increments for CA by-pass valve positions of 35%, 40% and 60% open. Results and analyses from the CA post compressor by-pass investigation for a direct fired, recuperated SOFC/GT hybrid system employing a load based speed control (LBSC) algorithm are presented in this chapter for a humidified hydrogen fuel feed. In prefacing manner, it is important to note that due to turbine failure, the CA by-pass 60% experiments were conducted using a new turbine/ compressor assembly.

5.1 Base Case – Initial FC Load: 100A, CA By-Pass Valve: 40%

For the purpose of investigating and analyzing the impact of initial FC load and CA by-pass on system dynamic response, a base case of 100A of initial FC load and a 40% open CA by-pass valve position were selected. Given the development of turbine start-up and stall mitigation strategies with the HyPer facility, 40% cold-air by-pass has been selected as a base CA by-pass position given its well-known and safe operating regime with regards to stall margin and its ability to provide sufficient flow to the virtual SOFC. The 100A initial FC load provides a baseline load that is sufficiently large enough to demonstrate significant system and SOFC dynamics while simultaneously residing within the range of initial FC load values so that comparisons can be made for both larger and smaller initial load step sizes.

Figure 5.1 illustrates the system process flow parameters that serve as inputs to the real time SOFC model, described in detail in Chapter 4. As outlined in the experimental plan, the system was allowed to come to steady state prior to the experiment and the steady state values of the FC model input parameters are illustrated between times -100s and 0s in Figure 5.1. As illustrated, the pressure of the oxidant stream entering the virtual SOFC stack was approximately 366kPaa, the temperature was approximately 939K and inlet air flow was approximately 1.41kg/s. For all of the data presented in this chapter, t=0s signifies the time at which the indicated initial FC load is placed on the virtual SOFC stack. As Figure 5.1 illustrates, the decrease in physical heat provided by the FC subsystem, resulting from the stepwise increase in FC load from 0A to 100A, causes a decrease in all of the system process parameters that serve as inputs to the FC model.

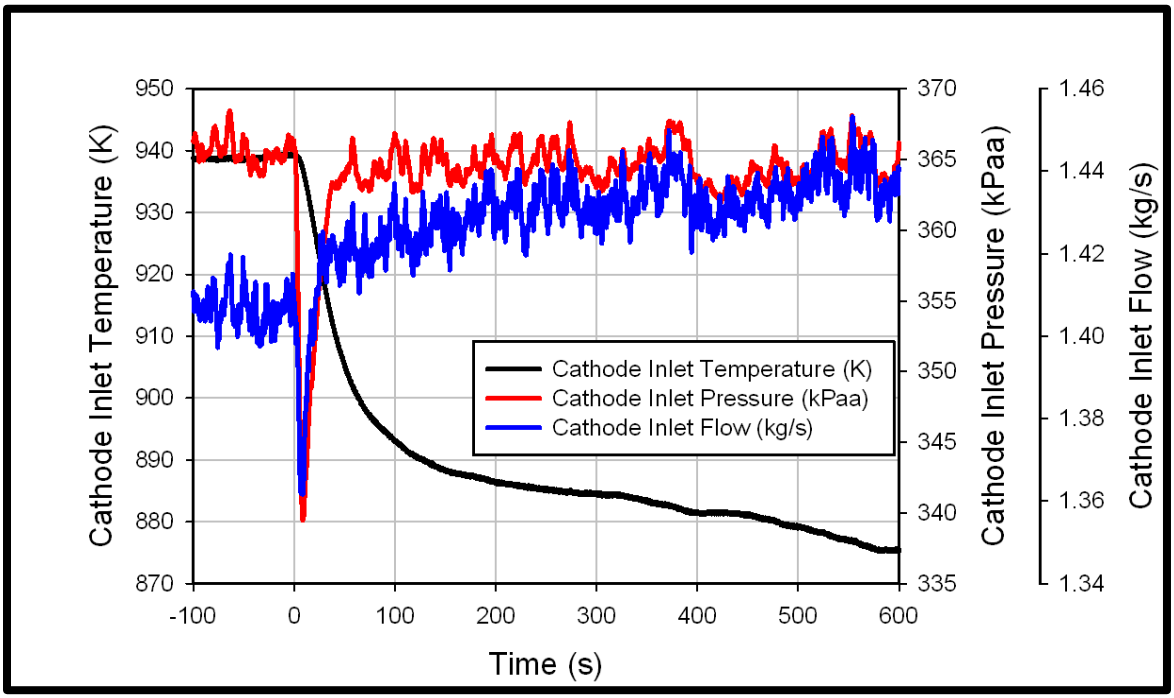

Figure 5.1: FC inlet parameters - 100A FC load, 40% CA by-pass: LBSC base case

The decrease in physical heat or Q_{dot} from the FC subsystem results in a sharp decrease in turbine speed, which causes the decrease in cathode inlet pressure and flow that is observed in Figure 5.1. Inlet pressure decreases by approximately 26kPa to

340kPaa and the inlet flow reaches a minimum value of approximately 1.36 kg/s. Once load is placed on the virtual SOFC at t=0s and turbine speed begins to decrease, the LBSC algorithm begins to shed electric load from the turbine (initially 50kW) in attempts to maintain the nominal turbine speed of 40,500 RPM for the new amount of heat that is actually being provided to the system. Through the transient start-up response, while operating in LBSC, the turbine speed will initially decrease to some minimum value and eventually increase in response to load shedding initiated by the LBSC algorithm. This results in an increase in turbine speed which causes an increase in both pressure and flow to the SOFC cathode. The "steady" values of both pressure and flow observed after the turbine speed transient appear to decrease and increase, respectively. As turbine load is removed from the shaft after current is drawn from the fuel cell, both the turbine inlet and exhaust temperatures decrease which results in a subsequent decrease in cathode inlet temperature due to a decrease in heat available for heat transfer to the compressor exhaust. This decrease in cathode inlet temperature causes a decrease in compressor back pressure which ultimately increases mass flow through the compressor and thus the entire system.

The FC inlet temperature decreases rapidly when the initial load is placed on the FC, as illustrated in Figure 5.1. The initially rapid decrease displayed by the FC inlet temperature gradually subsides as the turbine speed returns to its nominal operational speed 40,500 RPM value after the LBSC has taken effect and sheds the appropriate amount of load. The impact of this transient response of the FC inlet temperature is observed by the solid FC material, for which a spatio-temporal profile is presented in Figure 5.2. As the figure illustrates, the inlet temperature of the SOFC has a very similar profile, with respect to time, as that of the FC inlet gas temperature presented in Figure 5.1.

As indicated previously, the load is placed on the SOFC at t=0s. Prior to load being placed on the cell, the SOFC was at a uniform temperature of approximately 937K

which is adequate for electrochemical activity. Once load is placed on the cell, the SOFC becomes electrochemically active and starts to produce both current and by-product heat from cell operation. At time t=0s, the temperatures within the SOFC increase due to the by-product heat generation, and the formation of a non-uniform temperature distribution with a local temperature maxima at the outlet of the SOFC is observed approximately 300s after the load is placed on the virtual SOFC. After the local temperature maximum is observed, the cooling effect of the decreased inlet temperature and increased mass flow is observed along the SOFC. The temperature profile formed is one of gradual increase from inlet to exit, with a solid FC temperature of approximately 879K at the FC inlet and 950K at the FC exit, respectively. It is evident, from the temperature profile illustrated by Figure 5.1, that the system has yet to reach a steady condition; yet the solid temperature profile of the SOFC shows that after approximately 300s, the internal dynamics of SOFC operation due to start-up have subsided and the SOFC stack is primarily responding to thermal transients caused by other system parameters (i.e. FC inlet flow parameters).

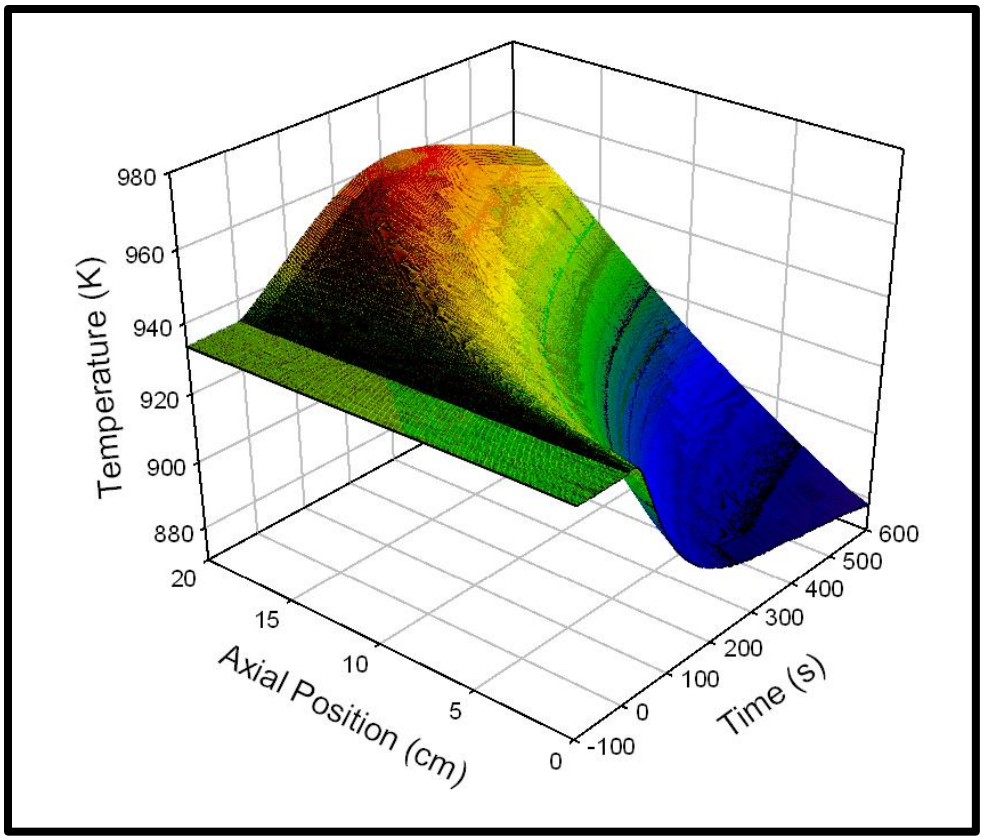

Figure 5.2: Spatio-temporal solid temperature plot - 100A FC load, 40% CA by-pass: LBSC base case

The impact of the generation of by-product heat that is observed in Figure 5.2, coupled with the impact of decreasing inlet temperature observed in Figure 5.1, initiates internal thermal dynamics during electrochemical start-up. The competing effects of the generation of thermal energy due to cell operation and the presence of a peak temperature of over 960K near the FC exit, and the cooling of the FC inlet temperature stream, results in the formation of a peak spatial temperature gradient in the upstream portion of the FC. As illustrated in Figure 5.3, the peak of 6.20K/cm is approximately 1cm downstream from the FC inlet and approximately 135s after the initial load is placed on the FC.

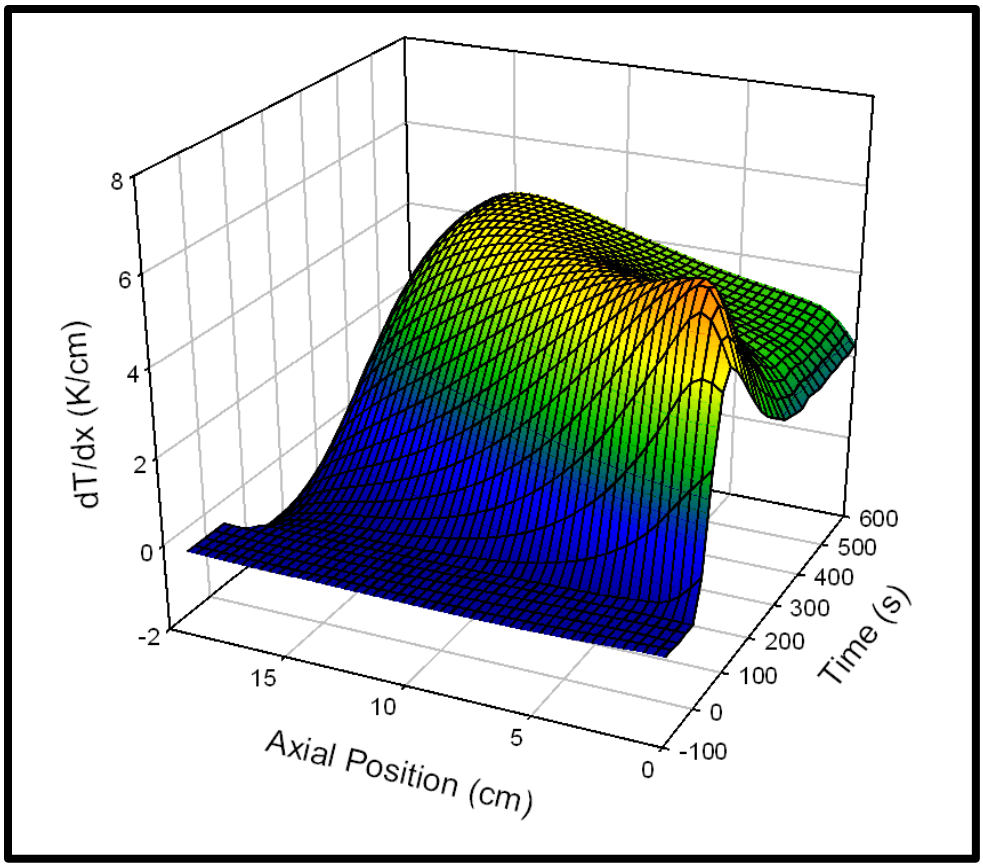

Figure 5.3: Spatio-temporal spatial temperature gradient plot - 100A FC load, 40% CA by-pass: LBSC base case

Figure 5.3 illustrates the spatial temperature gradient in the SOFC during electrochemical start-up in spatio-temporal manner. As presented in the figure, the spatial temperature gradient is approximately 0K/cm prior to placing the initial FC load on the FC. At t=0s, there is a minor decrease in spatial gradient, which can be attributed to the increase in SOFC temperature downstream due to by-product heat generation and the imposed adiabatic boundary condition at the exit of the FC. As the start-up response continues, a gradual increase in dT/dx values along the length of the FC are observed. Larger values are present at the inlet of the FC relative to the exit, given the competing effects of thermal energy generation and FC inlet stream cooling effects; as well as boundary conditions. After the formation of the maximum spatial gradient, approximately 135s into the transient response, a decrease in the spatial gradient near the inlet decreases

to an apparent steady value for the remainder of the transient response. The spatial dT/dx profile does not appear to significantly change with time throughout the final 250-300 seconds of the experiment. As similarly concluded from the temperature profile analysis, the SOFC's dynamic response to the application of load appears to dissipate and the internal transients observed appear to be primarily due to the dynamic response of the SOFC's subsystem parameters.

As presented in the real-time 1-D model description in Chapter 4, the electrochemical activity of the cell is heavily influenced by the temperature profile and internal thermal transport of the SOFC. To illustrate the dynamic impact on electrochemical activity, the transient response of local current density spatial profile throughout the start-up period is presented in Figure 5.4. At the initial time of load application, the local current density is highest at the inlet of the SOFC and monotonically decreases along the length of the FC. Given the uniform temperature profile prior to electrochemical start-up, the distribution of current is primarily influenced by the concentration of reactants, with the maximum concentration of hydrogen present at the inlet of the SOFC. Once by-product heat is generated and the cooling effect of the increased mass flow and decreased inlet temperature is observed, the current density profile begins to transition, ultimately resulting in a maximum current density near the exit of the FC and a minimum current density at the FC inlet.

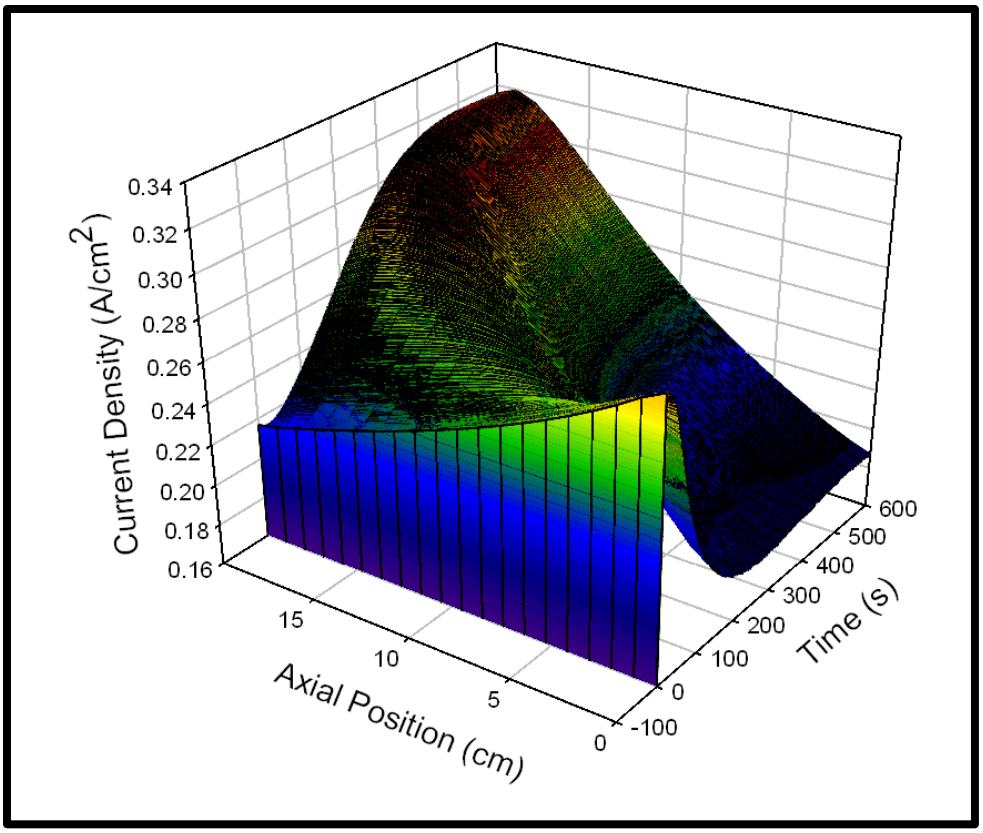

Figure 5.4: Spatio-temporal current density plot - 100A FC load, 40% CA by-pass: LBSC base case

Once load is placed on the FC and the local current density maximum shifts from inlet to exit, the spatio-temporal current density plot has a very similar profile to that of the spatio-temporal temperature plot that is presented in Figure 5.2. This further supports the significant impact of SOFC temperature on the cell electrochemical activity. The impact of the current density distribution on reactant concentration is presented in Figure 5.5.

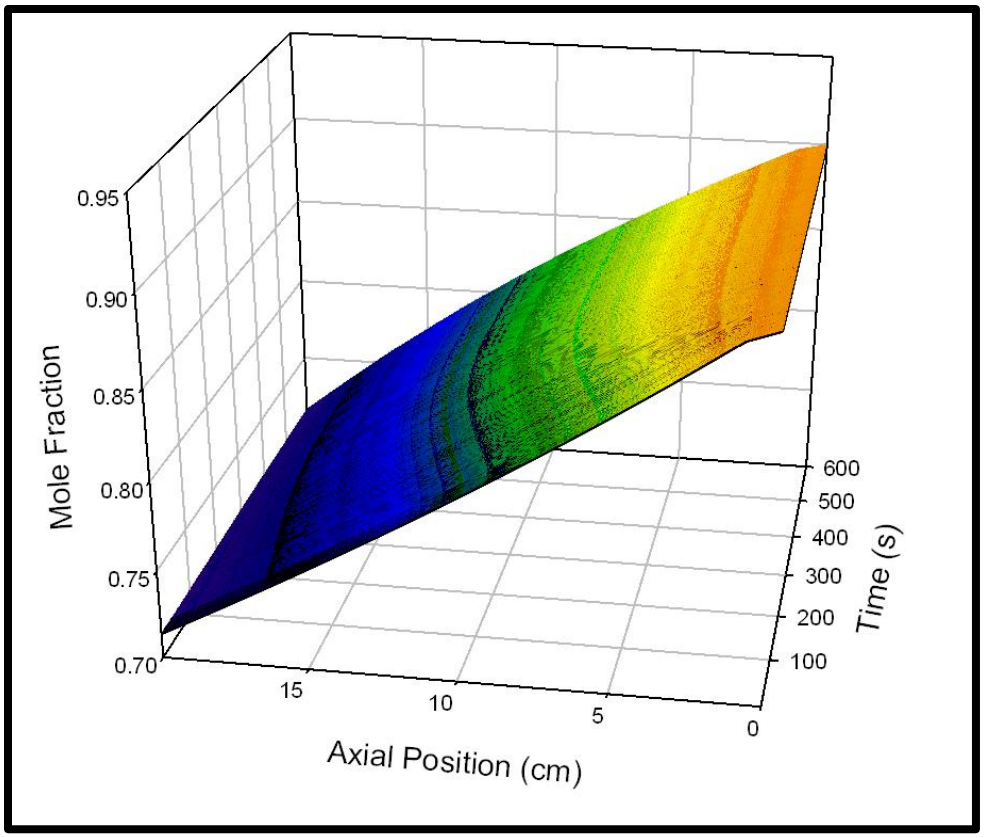

Figure 5.5: Spatio-temporal hydrogen concentration plot – 100A FC load, 40% CA by-pass: LBSC base case (humidified hydrogen fuel feed)

Figure 5.5 illustrates the local hydrogen concentration throughout the start-up period. A virtually simulated fuel flow of 22.6 g/s of H_2 was fed to the SOFC to maintain a FC subsystem thermal effluent of approximately 1400kW prior to the experiment. Given these conditions, the 100A load only utilizes approximately 21.2% of the fuel, which results in a hydrogen mole fraction of approximately 0.71 at the exit of the FC throughout the electrochemical start-up. A low fuel utilization of this nature mitigates the chance for internal local current density maxima and results in a generally monotonic, nearly linear decrease in H_2 concentration along the length of the cell. Figure 5.5 does illustrate a slight to moderate change in contour of the surface plot within the first 300 seconds of the start-up period, which can be attributed to the impact of current density redistribution, illustrated in Figure 5.4, on H_2 consumption.

5.2 System Performance

The structured nature of the HyPer facility allows for the experimental data to be naturally partitioned into two components: system performance data, characterizing the performance and the process parameters of the facility, exclusive of the SOFC; and SOFC performance data, which characterized the operation and performance of the SOFC stack while operating in the hybrid arrangement. This section presents data characterizing the impact of CA by-pass valve position and initial FC load on system process parameters. Given their direct impact on SOFC performance and operation, turbine speed, FC inlet temperature (which includes TE-326 + dTin, which represents an increase in FC inlet temperature due to some heat exchange mechanism), pressure (PT-305) and flow (FE-380) will be presented in addition to the transient response of FC subsystem heat generation and system wide pressure drop.

The CA by-pass valve is located on the back side of the compressor and diverts a portion of the cathode exhaust into the system combustor downstream of the virtual FC (air plenum) and upstream of the turbine. Increasing CA by-pass percent open valve position diverts more air to the combustion volume; thus decreasing the amount of compressed air that passes through the heat exchangers and into the virtual SOFC. Figure 5.6 illustrates this effect by presenting the airflow into the cathode of the virtual SOFC for CA by-pass valve positions of 35%, 40% and 60% open for the 100A initial FC load application. The impact of CA by-pass valve position cathode inlet flow is explained in further detail by Tucker et al. [14].

Prior to the application of load, the air flow into the virtual cathode (i.e., air plenum) was approximately 1.43kg/s, 1.4kg/s and 1.2kg/s for the respective by-pass valve positions of 35%, 40% and 60% open, respectively. This variation in cathode inlet flow demonstrates the capability to control airflow to the cathode, using CA by-pass. Given the fact that cathode air flow is the primary means of SOFC thermal management, the ability to control cathode air flow using CA by-pass will be an essential mechanism

for control algorithm designers to maintain safe operating conditions for the SOFC with regards to thermal transport.

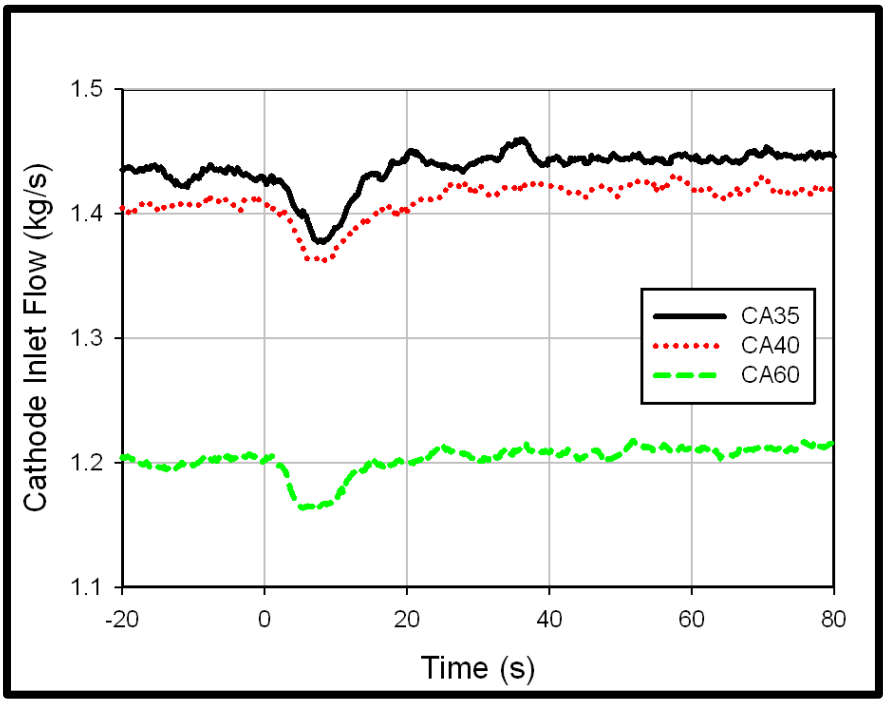

Figure 5.6: FC inlet flow vs. time – CA by-pass comparison, 100A FC load: LBSC

As illustrated in Figure 5.6, once load is applied to the virtual SOFCs at t=0s, a decrease in cathode inlet flow is observed. A minimum flow is quickly reached followed by a quick return to a steady flow rate approximately 60s after the load is applied. This dynamic response can be directly tied to the decrease in turbine speed due to the removal of physical heat from the system that results from FC load application, and the successive increase in turbine speed that results from the LBSC controller shedding load from the turbine in response to the decrease in heat generated by the FC subsystem; thus allowing its speed to return back to its nominal value of 40,500 RPM. To better illustrate the dynamic impact of CA by-pass on cathode inlet flow dynamic response, the cathode flow rates are presented in normalized fashion throughout the first 80 seconds of the electrochemical start-up in Figure 5.7[4].

[4] All normalized parameters are normalized by the mean value of their steady state, pre-load application profiles

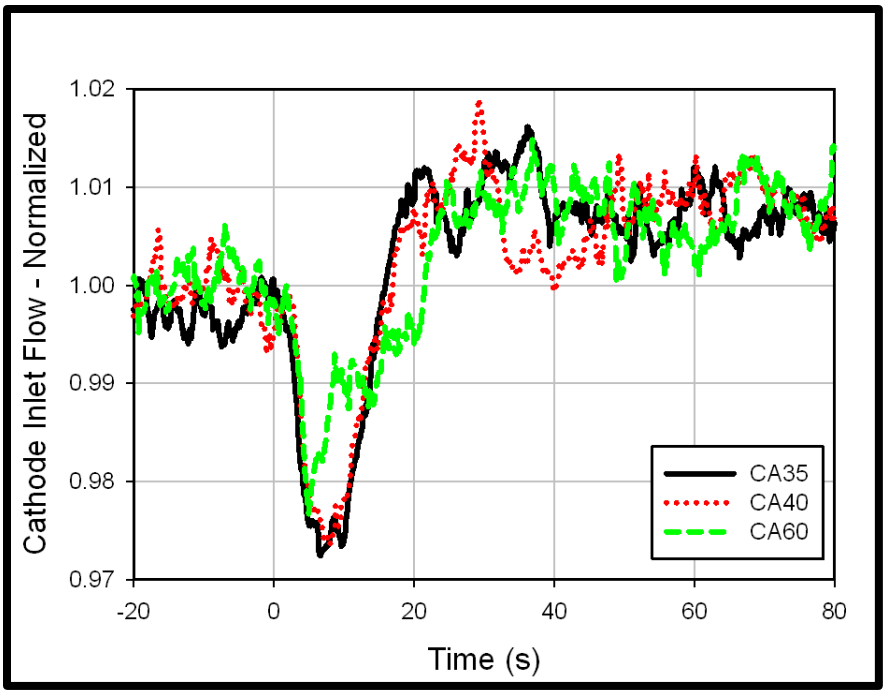

Figure 5.7: Normalized FC inlet flow vs. time – CA by-pass comparison, 100A FC load: LBSC

The 35% and 40% CA by-pass valve position cases have a decrease in mass flow to a minimum value of approximately 97.3% of its initial pre-load steady value, whereas the minimum value for the CA by-pass valve position of 60% is approximately 97.6% of its initial pre-load steady value, as presented in Figure 5.7. It is important to note here that the replacement of the turbine compressor assembly that occurred prior to the 60% CA by-pass experiments could contribute to the difference in normalized turbine response for the 60% CA case, but calibration studies comparing the dynamic response of the overhauled turbine illustrate very strong agreement in dynamic response between the old and new turbine compressor assemblies, particularly with respect to cathode inlet flow. After the load is applied and the minimum cathode inlet flow is achieved, an increase in turbine mass flow to approximately 1% above the initial steady state value is observed for all three CA by-pass valve position cases, which is very close to the 0.99% uncertainty value presented for FE-110 presented in chapter 3. As explained in conjunction with Figure 5.1, this increase in mass flow can be attributed to the decrease

in physical heat from the system, which decreases the temperature of the working fluid entering the turbine. That, in turn, decreases the temperature of the fluid on the back side of the compressor, which decreases compressor back pressure and increases system airflow. The decrease in turbine load imposed by the LBSC algorithm increases the mass flow through the system. which moves the operating state further away from the stall line.

In complementary fashion, Figure 5.8 presents the normalized cathode inlet flow for the four initial FC loads of interest: 50A, 75A, 100A, and 125A respectively. The larger the initial FC load, the greater the amount of heat that is removed from the system, thus resulting in a more significant change in turbine speed and consequently mass flow. The figure also illustrates that the impact of the load increase on minimum cathode inlet flow diminishes at higher loads, further illustrated by the very small variation between the minimum cathode inlet flow values for the 100A and 125A experiments. This was due to the decreased effectiveness of the LBSC controller as an approach to saturation was observed at larger initial FC loads.

The load step size, and thus the amount of heat removed from the system, has an impact on the steady cathode inlet flow after the step increase in load. As illustrated in Figure 5.8, the steady flow after the load change for both the 100A and 125A experiments has a sharper initial trajectory to its steady value than the 50A and 75A cases. This again can be attributed to the amount of heat that is being removed from the system and the responsiveness of the turbine speed after the load has been shed for the larger step increases in load.

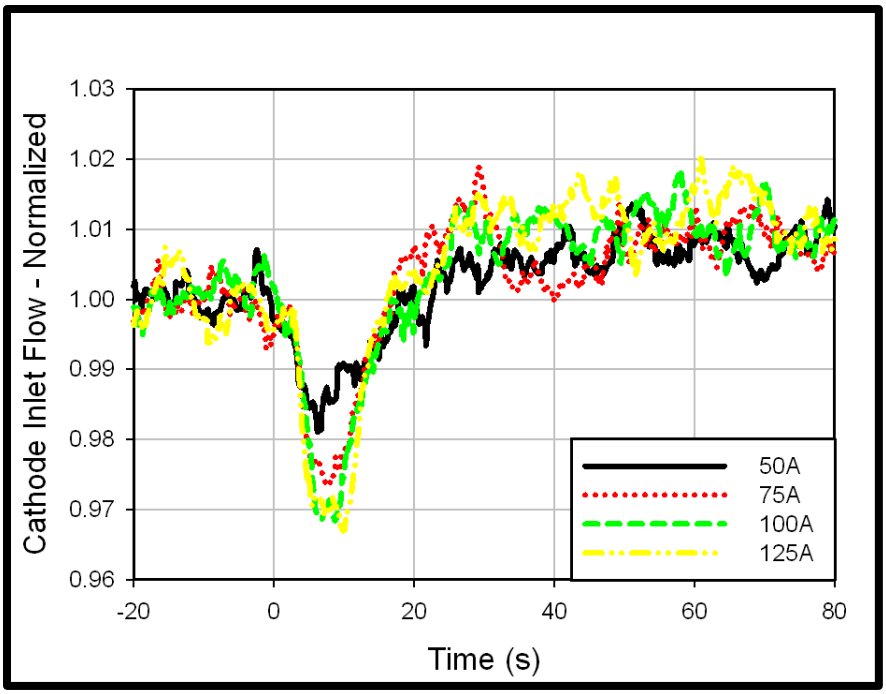

Figure 5.8: Normalized FC inlet flow vs. time – initial FC load comparison, 40% CA by-pass: LBSC

The cathode inlet flow is heavily correlated to the turbine speed. The impact of CA by-pass valve position and initial FC load on turbine speed are presented in Figures 5.9 and 5.10, respectively.

The minimum turbine speed for the 35% and 40% CA by-pass valve positions are very similar and less than for the 60% case. The increase in by-passed cold air decreases the turbine inlet temperature by bypassing more cold air to the system combustor and decreases the amount of flow though the FC, as illustrated in Figure 5.6. This in turn, makes the impact of FC load changes less significant with regards to the amount of energy entrained in the working fluid entering the turbine; thus decreasing the impact of FC load changes on turbine speed. Though noticeable, the approximately 0.3% difference normalized turbine speed between the minimum value observed for the 60% CA case as compared to the 35% and 40% CA cases will have a very minimal effect on the overall turbine operation. It is important to note that though the dynamic operation of the new turbine that was used for the 60% CA experiments compares well with that of the old

turbine used for the 35% and 40% CA experiments, the replacement does produce a level of experimental uncertainty that does not allow the establishment of definitive conclusions with regards to relative operation for 60% CA by-pass. A supplemental analysis investigating system operation for 35% and 40% CA by-pass using the new turbine would be necessary to justify explicit, conclusive statements and will be discussed in the future works section in Chapter 8. Given the decrease in turbine inlet temperature at higher flow rates, more fuel must be fed to the FC subsystem to maintain a pre-load steady state turbine speed of 40,500 RPM and an initial turbine load of 50kW. The fuel flow rates of humidified hydrogen to the 2300-cell SOFC stack for the 35%, 40%, and 60% open position CA by-pass experiments were 22.3g/s, 22.6g/s, and 25.3g/s, respectively.

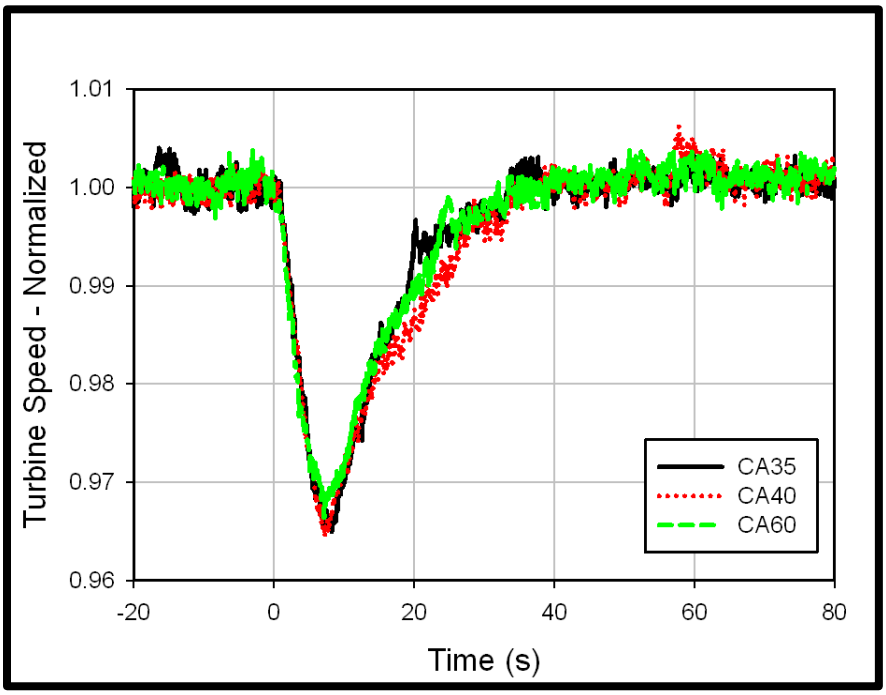

Figure 5.9: Normalized turbine speed vs. time – CA by-pass comparison, 100A FC load: LBSC

The impact of initial FC load on turbine speed is illustrated in Figure 5.10. As previously stated for the CA by-pass valve position comparison, the initial FC load comparison plot for turbine speed is very similar to that for cathode inlet mass flow

illustrated in Figure 5.8. Increases in load result in more significant decreases in minimum turbine speed after the initial FC load is applied. Similarly to the cathode inlet flow case, the minimum turbine speed for the 100A and 125A experiments are very similar. This is partially due to a decreased effectiveness in LBSC controller response for higher initial FC loads and the approach to saturation (i.e. complete load shedding) for both the 100A and 125A case. The impact of saturation can be further supported by the later time occurrence of the minimum turbine speed for the 125A case and the similar return trajectory to nominal turbine speed for both of the higher initial FC load scenarios.

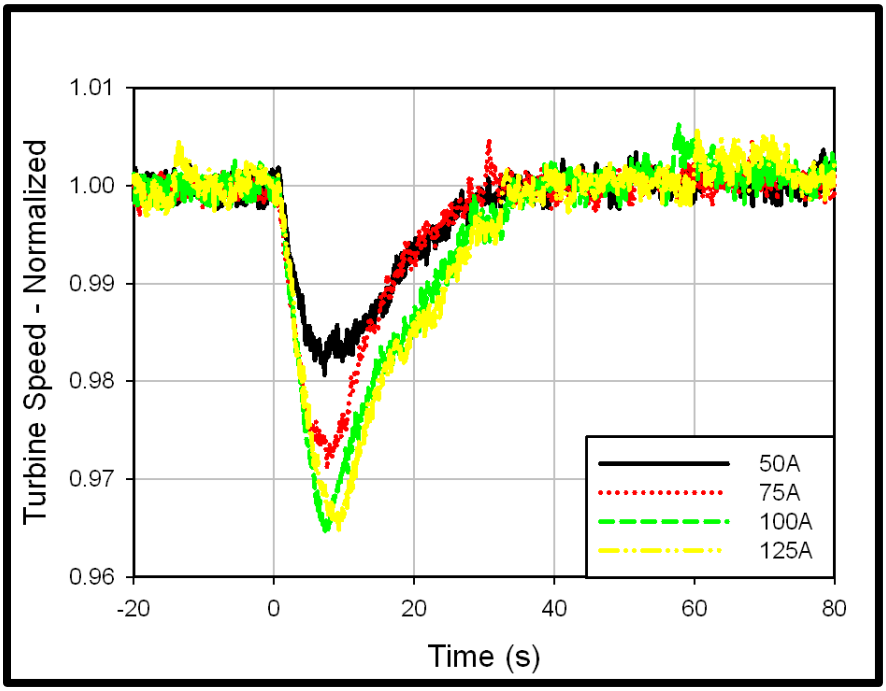

Figure 5.10: Normalized turbine speed vs. time – initial FC load, 40% CA by-pass: LBSC

It is important to note for these cases that for the higher initial load scenarios (initial FC load = 100A & 125A), the minimum turbine speed is approximately 3.5% less than the nominal turbine speed which is close to the ±5% turbine speed range for safe turbine operation. Given the fact that both of the higher initial FC loads nearly saturated the controller (i.e. turbine load of 0kW after the FC load was applied), it is justifiable to forecast that while employing the currently utilized LBSC algorithm, significantly

increasing initial FC load beyond the 125A upper experimental limit could result in a greater than 5% underspeed scenario, which would most likely initiate a surge and stall event. If system control designers are able to design a tool that would allow for significant initial FC load applications of greater than 125A, a more robust LBSC algorithm would have to be employed to ensure that the 5% underspeed threshold is not surpassed.

The changes in turbine speed discussed are directly caused by decreases in heat generated by the virtual SOFC subsystem, and the impact of CA valve position on heat generated by the SOFC subsystem is illustrated in Figure 5.11.

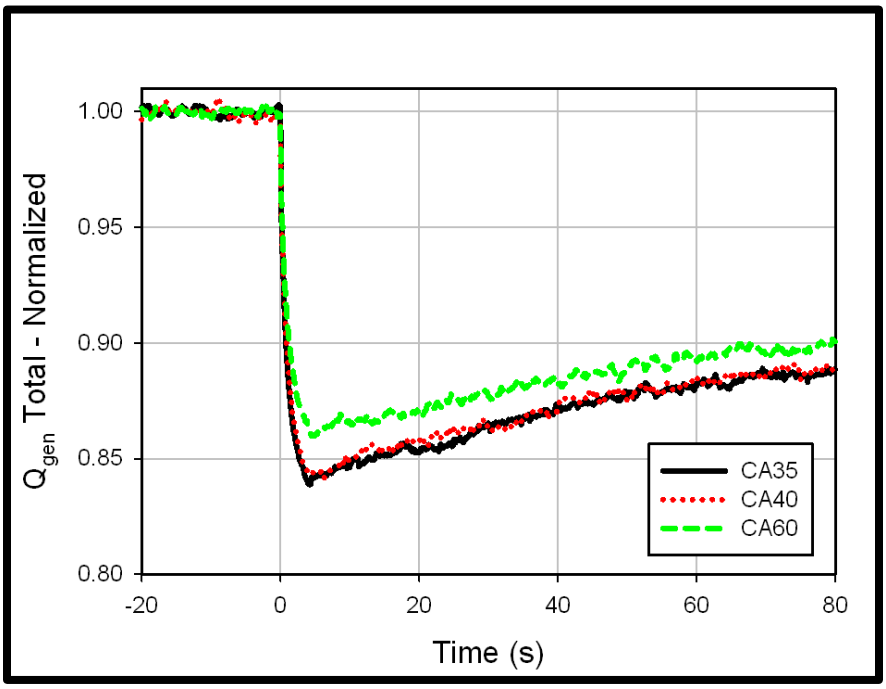

Figure 5.11: FC subsystem heat generated vs. time – CA by-pass comparison, 100A FC load: LBSC, 100A initial load

Figure 5.11 presents a less significant decrease in total heat generated from the FC subsystem for the CA by-pass 60% open case than for the 35% and 40% experiments. This can be primarily attributed to the increased fuel flow for the CA 60% open case. As previously stated, the fuel flow for the CA 60% case is significantly higher than for the 35% and 40% scenarios. This is due to the decrease in amount of flow to the virtual FC,

which results in a decreased turbine inlet temperature; this must be compensated for by increasing the amount of fuel to the FC subsystem. Given that the amount of load is fixed, this results in more unutilized fuel available for post combustion and a larger minimum and steady value of total heat released from the FC subsystem after the load has been applied. The steady state, pre-load heat generated from the subsystem was approximately 1400kW for the 35% and 40% CA by-pass cases and nearly 1600kW for the 60% case. Again, note that the 60% CA by-pass experiments were conducted using a new turbine. It is important to indicate, however, that the results of the comparative calibration studies illustrated that for a CA by-pass valve position of 40% open and an initial FC load of 100A, the initial fuel valve (FV-432) position increased from 48.13% open to 49.47% open, which indicates that more fuel is necessary to maintain a nominal speed and 50kW of turbine load with the new turbine. Though the fuel valve position for the base case is increased for the new turbine, the normalized impact remains the same, with approximately a 15% decrease in fuel valve position resulting from load application for both the new and old turbine, which is similarly illustrated in Figure 5.11. This supports the conclusion that though the amount of fuel that is provided pre-load has increased for the new turbine, the decreased impact of the 100A initial FC load on heat generated to the system for electrochemical start-up with 60% CA by-pass is justified. The impact of initial FC load step size on heat generated by the FC subsystem is presented in normalized fashion in Figure 5.12.

As expected, increases in load result in an increased impact on both minimum heat generated from the system during the transient response, as well as steady value achieved throughout the transient event. As illustrated, the impact of the 25A load increase from successive experiments appears to be equal, with an approximately 5% decrease in minimum subsystem heat generated for all successive increases in load and approximately a 3.5% decrease in heat generated 80 seconds after the load application for all successive increases in load.

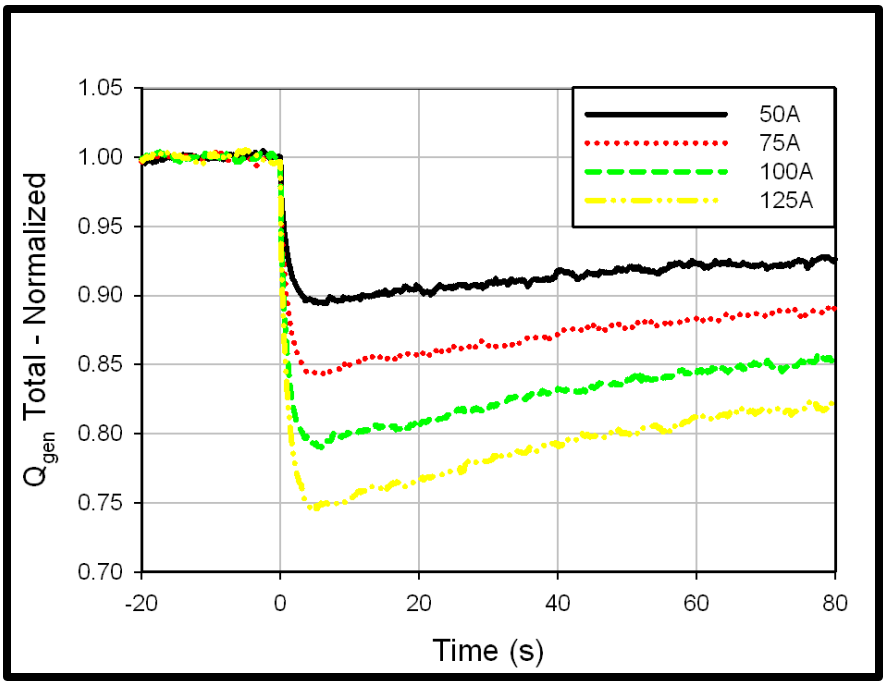

Figure 5.12: FC subsystem heat generated vs. time – initial FC load comparison, 40% CA by-pass: LBSC

Since larger applications of FC load resulted in more significant decreases in FC subsystem heat generated, it is feasibly projected that the minimum turbine speed value observed would be noticeably lower for an initial FC load of 125A as compared to the 100A case. The similarities observed in the minimum turbine speeds for these two cases, and the disparities between their time of occurrence, further supports the effect that greater load increases has on the LBSC algorithm efficacy.

The amount of fuel fed to the combustion volume directly impacts the amount of heat that is provided to the system, and thus impacts the temperature of the oxidant stream entering the virtual FC. The dynamic response of 100A of initial load on inlet temperature is illustrated in normalized fashion in Figure 5.13.

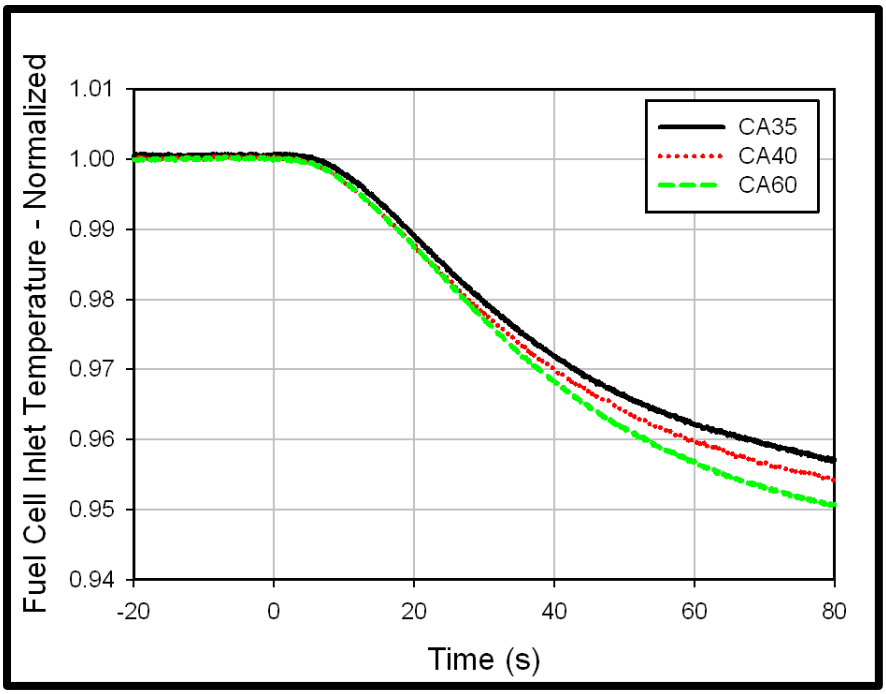

Figure 5.13: FC inlet temperature vs. time – CA by-pass comparison, 100A FC load: LBSC

As illustrated by the figure, an increase in CA bypass position results in a larger decrease in FC inlet temperature. Eighty seconds after start up, the FC inlet temperature decreases to approximately 95.8% of its initial value for the 35% CA case, 95.5% for the 40% CA case and 95.0% for the 60% CA case. Though a noticeable trend of decreased FC inlet temperature for increased CA by-pass is observed across the range of CA by-pass values, the final temperatures only vary across a 1% range when compared to their original steady state values. Though relatively insignificant, this 1% range can represent as large as a 10K range in temperature as a function of valve position. Furthermore, the temperature variation ranges beyond one standard deviation at the 80 second mark, as presented by the statistical analysis in Chapter 3, and the deviation continues to vary throughout the electrochemical start-up transient response, thus illustrating the statistical significance of the results. The 10K temperature range can have a slight to moderate impact on cell operation, but furthermore provides control system designers another control mechanism to maintain the operating state of the system during electrochemical

start-up transient response. In addition to its impact on dynamic response as illustrated by Figure 5.13, CA by-pass valve position also impacts the absolute FC inlet temperature. Pre-load FC inlet temperatures were approximately 960K, 940K, and 980K, respectively. The decrease in pre-load initial FC inlet temperatures with increased CA by-pass position is expected given that increased CA by-pass flow results in a decreased turbine exit temperature, which decreases the amount of heat exchange from turbine exhaust to the inlet into the virtual FC, which consequently decreases the inlet FC temperature. The increase in absolute FC inlet temperature for the 60% CA by-pass can be solely attributed to the new turbine.

The comparative calibration studies showed that the FC inlet temperature was significantly increased (approximately 50K) for the new turbine relative to the old turbine. The impact of CA by-pass position on FC inlet temperature also illustrates the need to include components in FC sub-system design that provide the appropriate amount of heat, ensuring that the FC is at an adequate enough temperature to safely operate in an electrochemically active state. Depending upon the heat exchange mechanism (i.e., pre combustion), increases in CA by-pass may result in greater amounts of fuel to preheat the FC inlet stream, thus deleteriously impacting system efficiency. Ultimately, the impact of CA by-pass on FC inlet temperature demonstrates the need for trade studies and trade-off analysis during the comprehensive SOFC subsystem and operational control strategies design phase.

The impact of initial FC load on FC inlet temperature is illustrated in Figure 5.14. The increase in initial FC load increases the amount of fuel that is removed from the system, therefore resulting in more significant decreases in FC inlet temperature. One thing to note about the LBSC configuration is that it resulted in longer timeframes for arrival at steady state. Even after the initial 80 seconds of electrochemical start-up, the FC inlet temperature continues to decrease well beyond the 600 seconds of experimental inspection. This phenomenon illustrates the significant impact that changes in turbine

load have on thermal energy and transport throughout the system. Accordingly, although the initial dynamic impact of FC initial load on FC inlet temperature is of particular interest for this study of electrochemical start-up, investigating and quantifying the impact of changes in turbine load on system-wide thermal transport will be critical in reliably operating and implementing SOFC/GT hybrid systems.

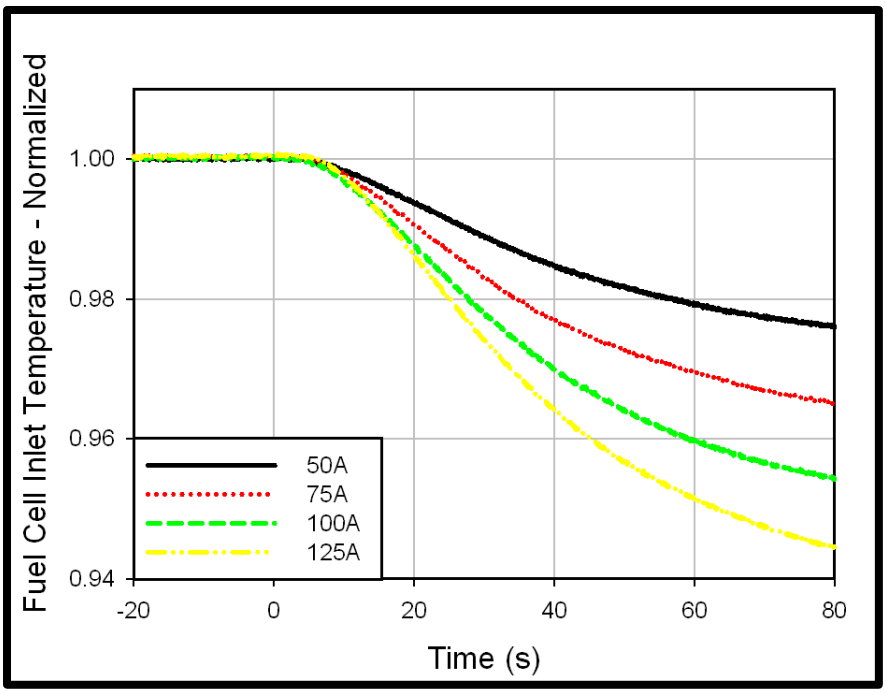

Figure 5.14: FC inlet temperature vs. time – initial FC load comparison, 40% CA by-pass: LBSC

Given the thermal sensitivities of SOFCs, appropriately managing inlet FC temperature dynamics will be essential in preserving the mechanical and operational integrity of the SOFC. In addition to thermal sensitivities, given SOFC's brittle nature, they can also be negatively affected by significant changes in pressure. As previously illustrated, the changes in turbine speed initiated by the application of FC load cause quick and significant decreases in cathode inlet flow. In addition, those turbine speed changes result in notable decreases in cathode inlet pressure.

The normalized impact of CA by-pass valve position and initial FC load on cathode inlet pressure is illustrated in Figure 5.15. The impact of initial FC load on

minimum cathode inlet pressure appears to decrease with increasing valve position, with the most significant decrease occurring between the 35% and 40% CA by-pass cases. Similarly to the FC inlet temperature case, approximately a 1% range of pressures was observed which can represent an absolute range of approximately 4kpa (40 millibars), which is significant given that it represents 40% of the allowable range of pressure change for the SOFC cathode air stream. Removal of heat from the system decreased turbine speed and consequently the amount of compressor work. This in turn decreases the compressor ratio and decreases the exit pressure from the compressor. As illustrated by the compressor map, increased compressor mass flow that results from increased CA by-pass results in a decreased pressure ratio, and thus a decreased compressor exit pressure. The decrease in pressure ratio is maintained throughout the transient response to electrochemical start-up for increased CA valve positions and a less significant impact on cathode inlet pressure is observed. It is important to note that the minimum cathode inlet pressure observed for the CA 35% case is lower than that observed for the 40% and 60% cases. Though this trend is expected since the increased mass flow that results from increased CA by-pass results in increased flow through pressure drop components, the approximately 0.5% difference is not greater than a standard deviation as calculated from the replicate studies and thus cannot be deemed statistically significant. Ultimately the impact of CA by-pass valve position on the dynamic response of the cathode inlet pressure is insignificant and can be decoupled from attempts to control and maintain tolerable cathode inlet pressure values during electrochemical start-up.

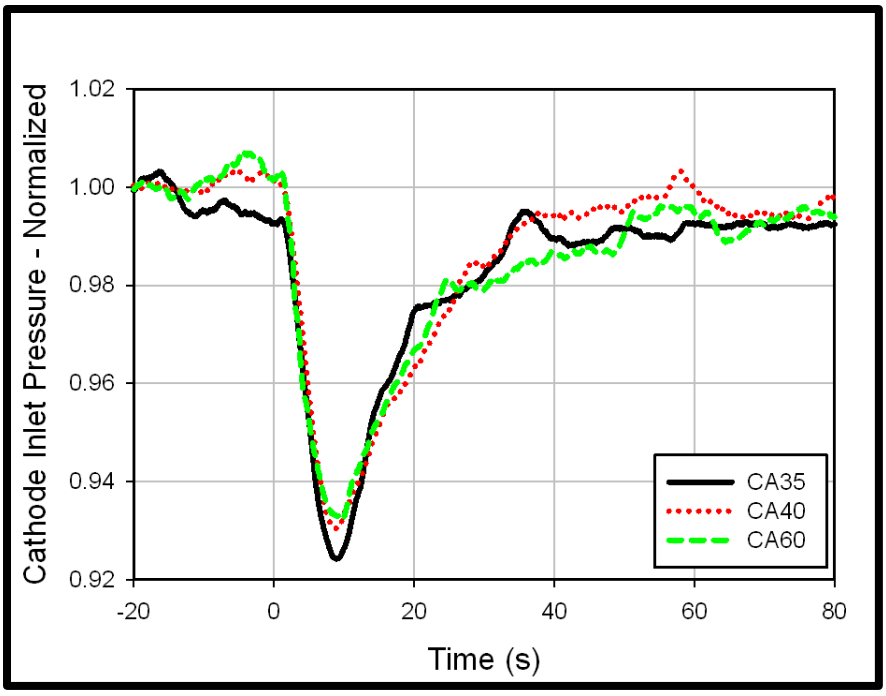

Figure 5.15: Normalized FC inlet pressure vs. time – CA by-pass comparison, 100A FC load: LBSC

The inlet cathode inlet pressures for the 35%, 40% and 60% CA by-pass cases are approximately 360kpaa, 369kpaa and 360kpaa respectively. Again, it is important to note that, although the transient response of the turbine/compressor assembly remained generally consistent between the new and old turbine, the values of absolute operating parameters did vary and the decreased value of cathode inlet pressure for the 60% CA case as opposed to the 40% CA case can be attributed to the changing of turbines. For the three cases illustrated in Figure 5.15, the minimum cathode inlet pressure ranged between 92.5% and 93% of the initial value, which resulted in changes in cathode inlet pressure of approximately 25 – 30kpa. This is significantly outside the range of the tolerable 10kpa pressure change that is amenable for SOFC reliability [13]. This is another operational challenge that must be directly addressed in the design of control strategies for these SOFC/GT hybrid systems.

Figure 5.16 illustrates the impact of initial FC load on cathode inlet pressure. As expected, the trends follow very closely with the other process flow variables and a more

significant decrease at higher loads is observed. The impact of turbine speed on cathode inlet pressure appears to be evident at higher loads also, given the later occurrence of the minimum pressure for the 125A initial FC load relative to the 100A case, as well as the similar return trajectories to the post-load application steady cathode inlet pressure.

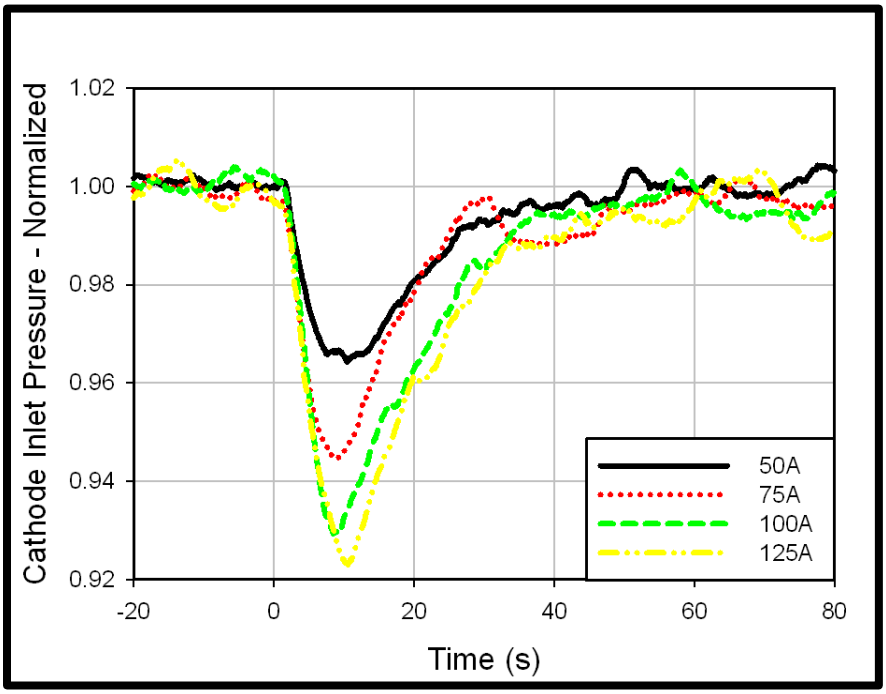

Figure 5.16: Normalized FC inlet pressure vs. time – initial FC load comparison, 40% CA by-pass: LBSC

5.3 SOFC Performance

This section presents results characterizing the impact of electrochemical start-up on SOFC performance and operation. In this section, operational parameters such as stack power, cell-level operating voltage and cell-level polarization losses are presented and analyzed. Similarly to the system performance analysis, comparisons are made with respect to both CA by-pass valve position as well as initial FC load during electrochemical start-up.

One of the key SOFC performance parameters of interest for SOFC/GT hybrid systems is stack power. Hybrid system design and development initiatives typically establish desired power production targets, and many of the paper studies developed

broach greater than 50% of total system power production being from the SOFC stack component of the system [1]. Though power production and efficiency ratings are not of the utmost importance when investigating system start-up, the underlying purpose of this study is to provide data and analysis that facilitate control strategies for transitioning hybrid systems to steady and continuous operation. Characterization of stack power trajectories through the start-up period will be pivotal in minimizing the amount of time it takes to get to steady operation and maximizing the efficiency once the final operational state has been achieved.

In addition to stack power, tracking stack operating voltage is essential in determining the operating envelope of SOFC/GT hybrid systems as well. With regards to an SOFC stack's operational regime for a given fuel utilization, there exists a current at which concentration (diffusion) polarization terms begin to have a dominating effect, the cell voltage quickly approaches zero and the cell is no longer operational [7, 8]. The chance of reaching the point of limiting current is very unlikely for electrochemical start-up; however, tracking cell voltage through the start-up period will be extremely beneficial in both avoiding this dangerous regime during start-up and providing operational strategies for steady state attainment.

Figure 5.17 presents stack power and voltage throughout the first 600s of electrochemical start-up for a 100A initial FC load for all three CA by-pass valve positions of interest. The stack power, which is a product of the current density, operational voltage, and number of cells in the stack, is thus heavily influenced by the operational voltages (given that the other two parameters are fixed). In complementary fashion, cell electrochemical activity and thus cell voltage, is heavily influenced by cell operational temperature. The average cell temperatures prior to the application of load for the CA 35%, 40% and 60% cases were 957.5K, 933.6K and 976.85K, respectively. (**Note**: The misalignment of the CA 60% case with the general trend of decreasing cell temperature with increasing CA by-pass is due to the turbine replacement and the

variance in inlet temperature to the virtual SOFC). The impact of average cell temperature on electrochemical performance can be illustrated in Figure 5.17. Once load is placed on the cell, operational voltage decreases in stepwise manner from the Nernst potential to its respective value depicted in Figure 5.17. The initial cell voltage at t=0s was approximately 0.91V, 0.88V, and 0.936V for the CA 35%, 40% and 60% cases respectively.

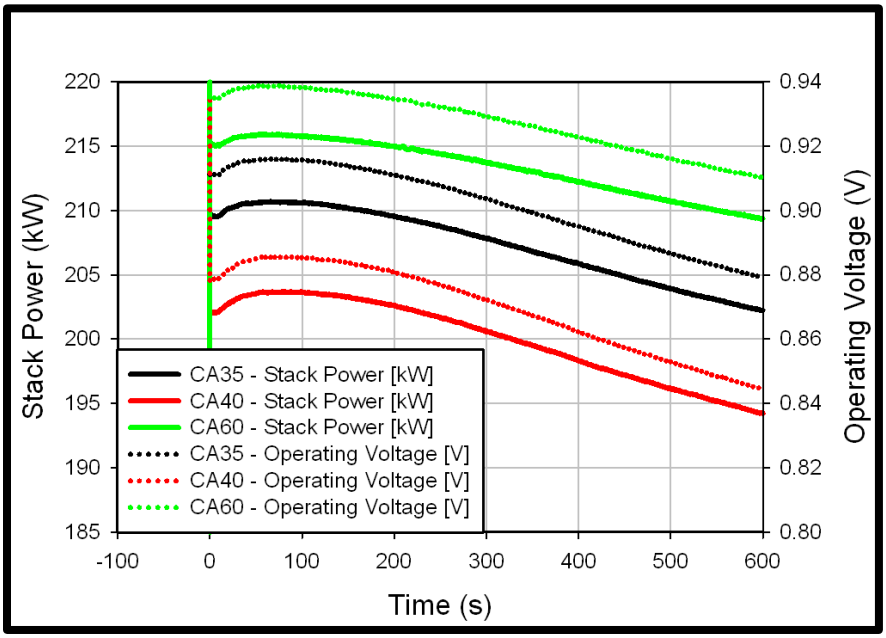

Figure 5.17: Stack power and operating voltage vs. time – CA by-pass comparison, 100A FC load: LBSC

The impact of the dynamic response is interesting to note as well. The peak voltage occurs approximately 50s after the initial load application for all three cases. This is due to the increase in cell operating temperature due to by-produce heat generation and the delayed effect of convective cell cooling. Once the combined cooling effect of slightly increased cathode inlet mass flow, illustrated in Figure 5.7, and decreased cathode inlet temperature, illustrated in Figure 5.13, takes effect, the operating voltage begins to decrease and steadily declines throughout the 600s plotted in Figure 5.17. As illustrated, the voltage decreases approximately .03V, .04V and.03V for the CA 35%, 40% and 60% cases, respectively. This can also be attributed to the impact of system

operation on cell operating temperature. The average cell temperature for the given CA by-pass cases of interest were 933.86K, 913K, and 953.5K respectively, 600s after the initial FC load was applied. Since all of these values result in an increase in average cell temperature of approximately 20K for each case, the dynamic response illustrates that electrochemical behavior (i.e., voltage) is not linearly dependent upon temperature.

It is also important to note that the mass flow rate is significantly lower for the 60% CA by-pass case than it is for the 35% and 40% CA by-pass case, as illustrated in Figure 5.6. This decreased inlet mass flow results in higher oxygen utilization values, and thus causes more variations in distributed cell temperature, which can potentially affect both current density distribution and overall cell voltage. This will be further explored in the following section. The impact of initial FC load on stack power and operational voltage are presented in Figures 5.18 and 5.19, respectively.

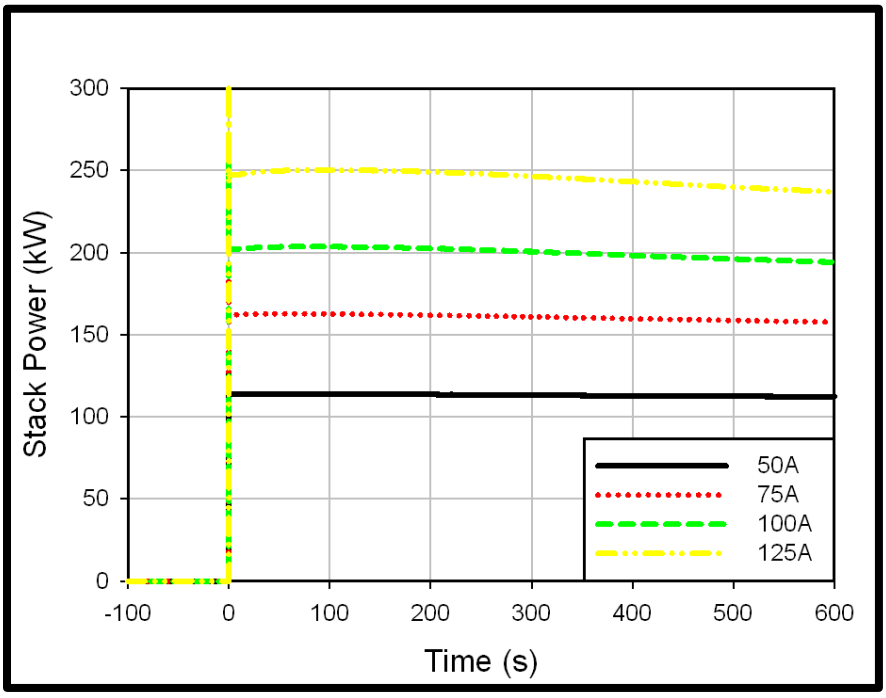

Figure 5.18: Stack power vs. time – initial FC load comparison, 40% CA by-pass: LBSC

Figure 5.18 illustrates the impact of initial FC load on SOFC stack power for the CA 40% case throughout the first 600s after the load has been applied. As illustrated in

the figure, the initial stack power prior to load application is 0; once load is applied, the stack power ranges between 100kW and 250kW for the fuel cell stack load range of 50A to 125A . More significant deviations in stack power throughout the start-up transient response are observed at higher loads. The stack power profiles appear to be nearly uniform for the 50A and 75A initial FC loads, but the significant amount of heat that occurred in the 100A and 125A cases resulted in extended system (and SOFC) thermal response. There were more noticeable variations in stack power after the initial FC load application. For the 125A case, a decrease in initial stack power of 10kW is observed at the 600s mark. The dynamic response of initial FC load on stack power can be directly correlated to system operational voltage, which is presented in Figure 5.19.

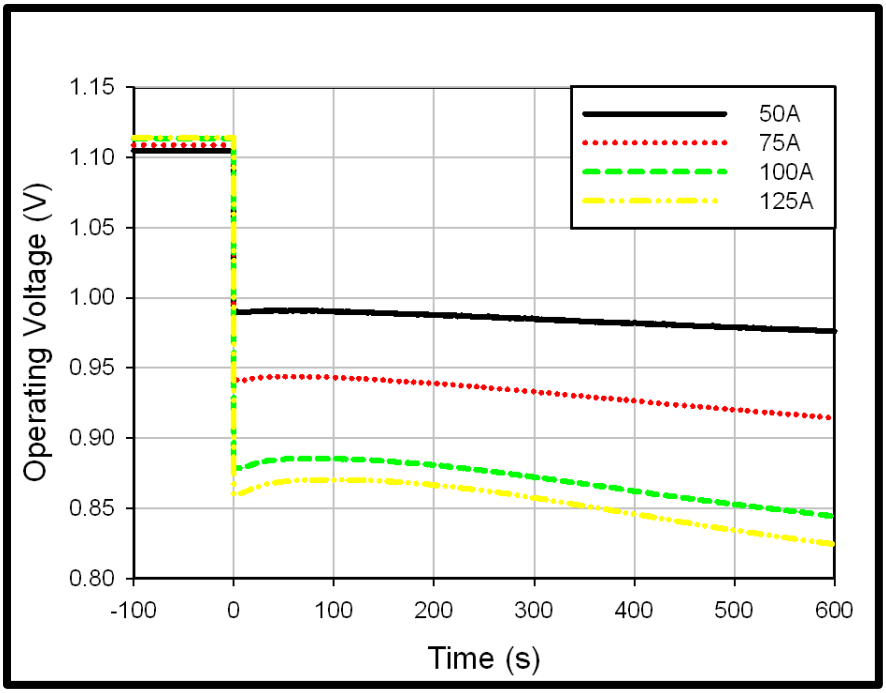

Figure 5.19: Operational Voltage vs. time – initial FC load comparison, 40% CA by-pass: LBSC

SOFCs display a significant decrease in system operating voltage with increasing load and then a small increase in voltage drop on the V-i curve occurs at higher loads, on which the relationship between current and voltage is essentially linear. This is illustrated by decreased impact on operational voltage that is observed for the successive 25A load

applications in Figure 5.19. As illustrated, the application of 50A, 75A and 100A result in voltage decreases of approximately 0.1V, 0.16V, and 0.22V respectively. An initial load of 125A results in a decrease from the initial Nernst potential of approximately 0.24V, which is only 0.02V greater than the 100A case; thus, load steps of this magnitude are presumed to place the stack in the linear regime of the V-i curve where increases in load have a less significant impact on initial operational voltage. There appears to be a greater impact on the secondary dynamic response of operating voltage to the initial load application, as loading increases. The decrease in operating voltage from its initial value at the point of load application to its value 600s after electrochemical start-up is more significant for higher applications of FC load. Changes in operational voltage from initial loading values to values 600s after the load application range from 0.015V for the 50A experiment to 0.04V for the 125A experiment. This variation in operational voltage is due primarily to the thermal transient response of the system. It is important to note that the dynamic response between the 100A initial FC load case and the 125A initial FC load case is very similar. It is apparent that the operating voltage is influenced by cell operating temperature dynamics, and in coupled manner there is an impact of the operating cell's location on the polarization curve. As presented in Equations 4.1 and 4.2 in Chapter 4, the operating voltage is determined by calculating the maximum possible voltage (i.e. Nernst potential) and subtracting from it the electrochemical losses due to cell operation. Prior to load application, which signifies the electrochemical start-up of the system, the "operational" voltage of the cell is its maximum potential voltage, or its Nernst potential. Once load is placed on the cell, current is drawn, and the operational voltage decreases to an "actual" value that accounts for losses due to cell operation. The remainder of this section outlines the impact of CA by-pass valve and initial load on activation, diffusion and ohmic electrochemical losses. Figures 5.20 and 5.21 illustrate the impact of CA by-pass and initial FC load on activation polarization for the SOFC cell stack, respectively.

As presented in Figure 5.20, increases in CA by-pass valve position from 35% to 40% result in an increased average activation loss for the SOFC stack. This is due primarily to decreased operational cell temperature for increased CA by-pass valve position. SOFCs operate more efficiently at higher operational temperatures, which results in a general decrease in activation polarization.

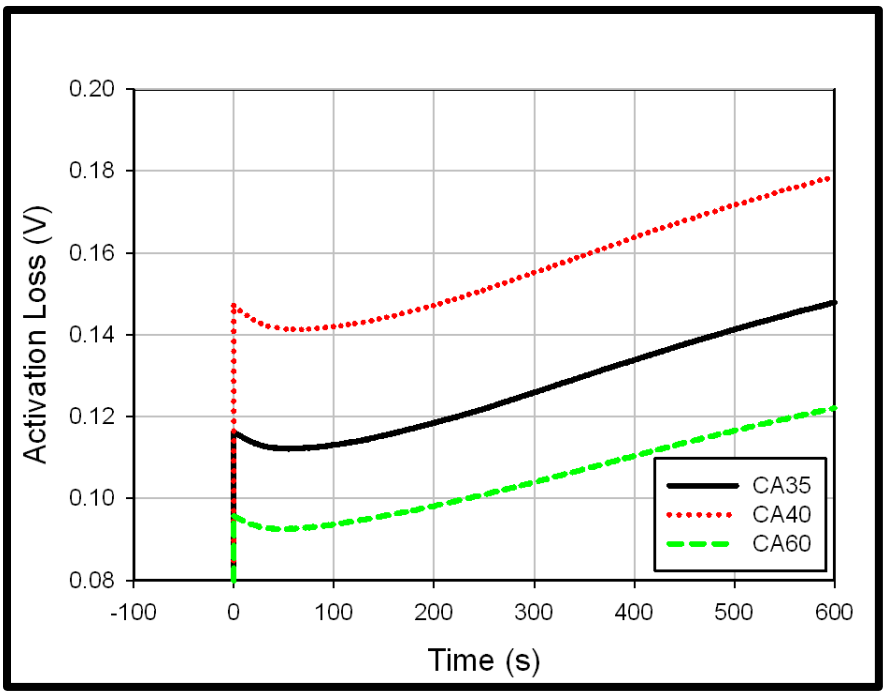

Figure 5.20: Average activation loss vs. time – CA by-pass comparison, 100A FC load: LBSC[5]

The CA 60% case goes against the general trend of increasing CA by-pass, resulting in decreased activation polarization due to an elevated SOFC operating temperature obtained in conjunction with the new turbine. The dynamic behavior throughout the transient response of electrochemical start-up appears to be very similar for all of the by-pass valve positions. From inspection, all of the profiles follow a very similar trajectory throughout the first 600s of the start-up transient response, with the CA 35% and 40% cases presenting increases of approximately 0.032V by the 600s mark after the load had been placed on the SOFC. The 60% CA by-pass case only presented an

[5] Electrochemical losses reported are an arithmetic average of all local values calculated

increase of 0.02634V, but given the governing equations for activation polarization presented in Equations 4.15-4.17 in Chapter 4, at higher temperatures, the activation polarization is less affected by changes in exchange current density, thus resulting in a lower magnitude of increase by the 600s after start-up. Furthermore, decreased airflow for increased CA by-pass results in less rapid cooling and consequently a slower increase in polarization losses. The impact of FC load on activation loss is illustrated in Figure 5.21.

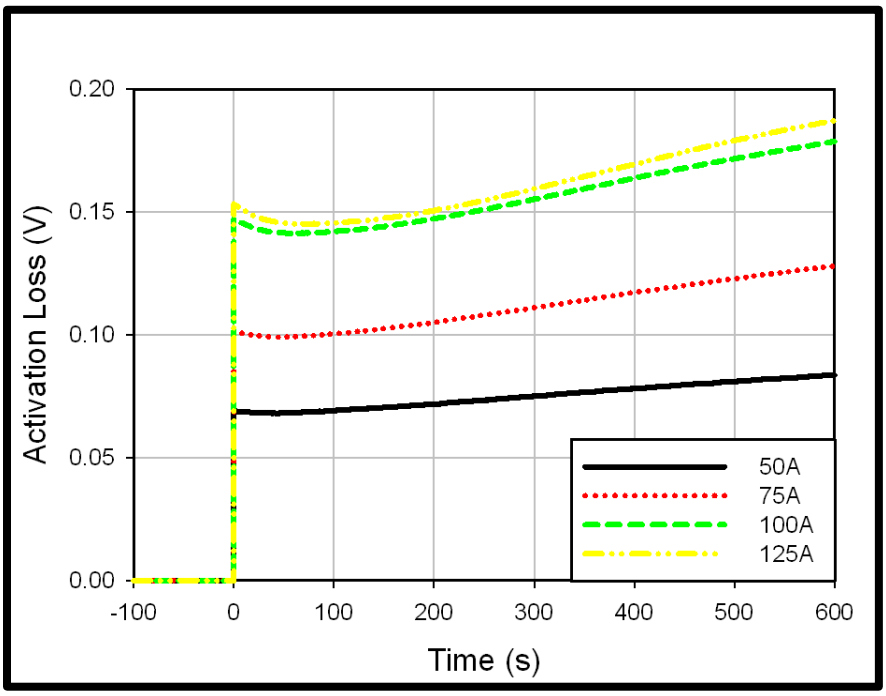

Figure 5.21: Average activation loss vs. time – initial FC load comparison, 40% CA by-pass: LBSC[5]

Increases in initial FC load result in increases in magnitude of the activation loss profile. This illustrates that there is an impact on the dynamic response of activation loss with respect to initial FC load. The increase in activation loss from its initial post load activation value to its value at t=600s is 0.0146V, 0.0267V, 0.0316V and 0.0338V for the initial FC load applications of 50A, 75A, 100A and 125A, respectively. This illustrates the increase in dynamic effect of FC load application at higher loads. This dynamic response can be attributed to thermal transport resulting from the increased removal of

heat from the system and increased SOFC thermal dynamics due to by-product heat generation and increased FC cooling at higher loads.

The transition to the ohmic polarization dominant portion of the power curve is again evident given the variation between the 100A and 125A scenario. As illustrated, the variation in activation loss is minimal between the 100A and 125A case, and the operating voltage broaches a less significant impact of current draw on operating voltage between those load application values as well; thus supporting that the operational regime has transitioned from the portion of the power curve where activation polarization dominates to the linear portion where ohmic loss is the dominant polarization term. Figure 5.22 presents the impact of CA by-pass valve position on the diffusion polarization for the SOFC stack for the 100A initial FC load case.

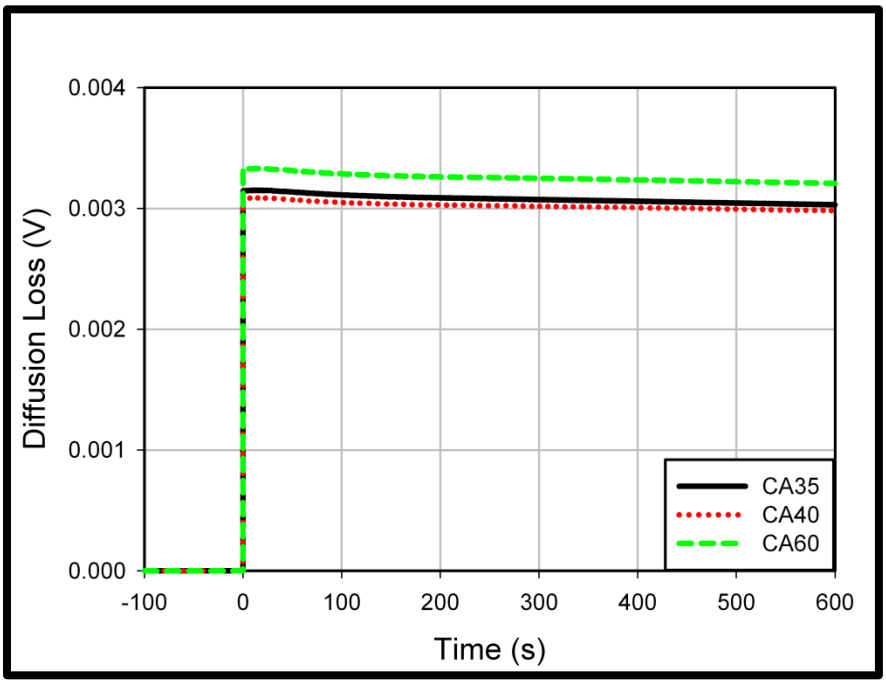

Figure 5.22: Average diffusion loss vs. time – CA by-pass comparison, 100A FC load: LBSC[5]

Diffusion loss characterizes the decrease in cell potential due to concentration losses from diffusion of electrochemically species through the SOFC electrodes. Given

the state of the art design that is characterized with this model, employing thin electrodes, the diffusion polarization terms are the least dominant of the three.

Figure 5.23 illustrates the impact of initial FC load on the diffusion polarization for the CA 40% scenario. Increases in current draw increase the magnitude of diffusion loss profiles. The dynamic behavior of the diffusion loss profiles later in the transient response is less significant than in the activation loss profile. This shows that the diffusion polarization is not as effected by thermal transport as significantly as activation polarization, which was presented previously; rather the re-distribution of the current density profile is the leading driver in the relatively modest dynamic response that is observed for the diffusion loss. Since the re-distribution of the current density profile occurs more radically at higher loads and more notable dynamic behavior is observed for higher loads, the rationale seems further supported.

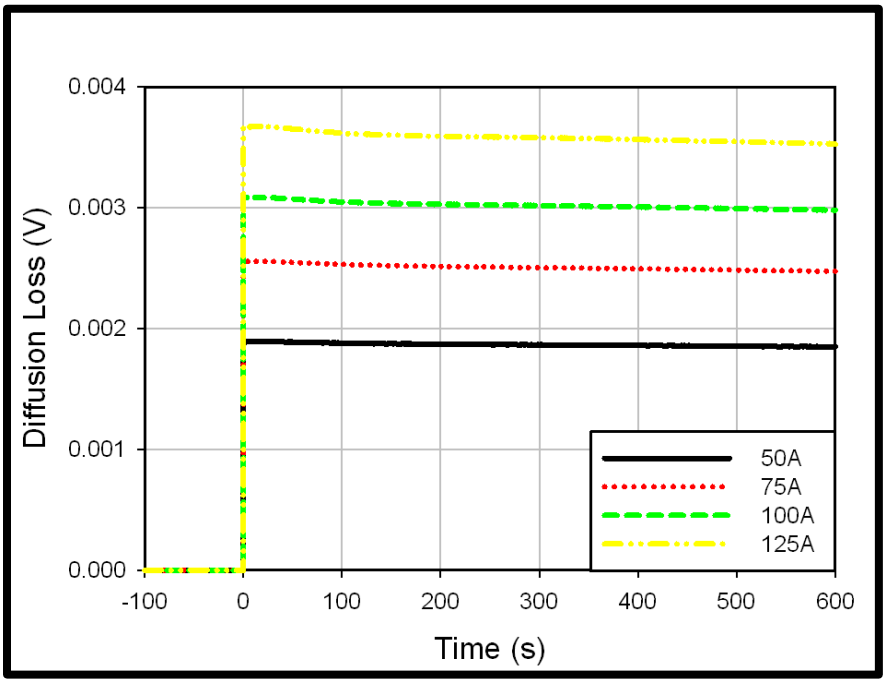

Figure 5.23: Average diffusion loss vs. time – initial FC load comparison, 40% CA by-pass: LBSC[5]

The variation of the impact of load increase is relatively constant across the entire range of load steps (50A – 125A), seemingly supporting that this investigation is far

away from the regime where the diffusion loss becomes dominant and cell voltage approaches its operational minimum.

The final electrochemical loss to consider is ohmic loss. This is loss in voltage due to electrical resistance. Similarly to activation loss, the ohmic loss is inversely influenced by cell operational temperature. The impact of increased operational temperature, resulting in a decrease in ohmic loss, is illustrated in Figure 5.24.

As illustrated, the higher operating temperature for the CA 35% case results in decreased ohmic polarization throughout the entire start-up transient response relative to the 40% case. The elevated operational temperature for the CA 60% case, given the thermal characteristics of the new turbine, results in its profile having the lowest magnitude of all three cases.

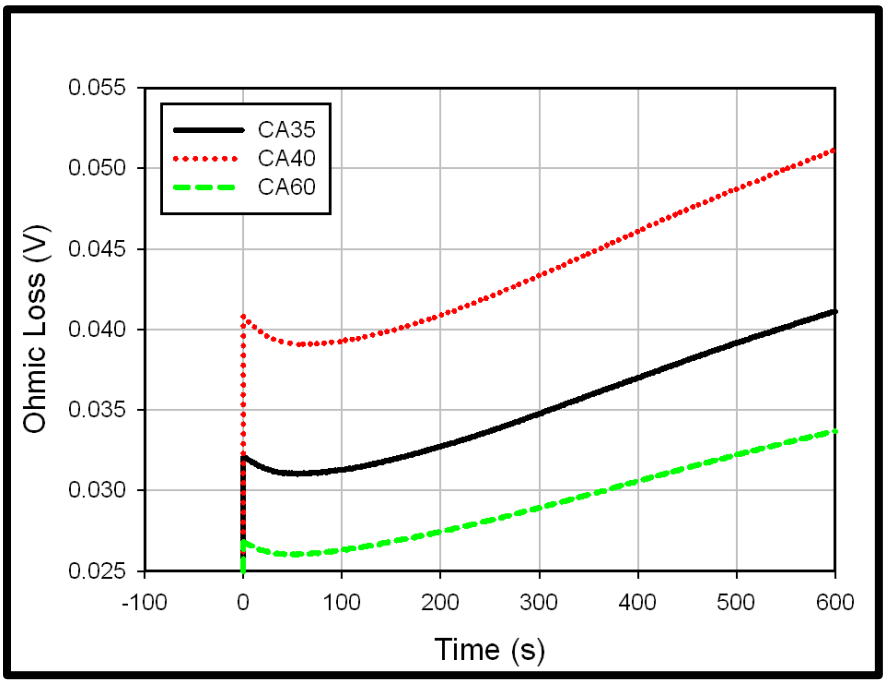

Figure 5.24: Average ohmic loss vs. time – CA by-pass comparison, 100A FC load: LBSC[5]

From inspection of Figure 5.24, there appears to be some impact on the dynamic response of ohmic loss. The decrease from the initial post FC load value seems to be more significant for decreased temperatures (i.e. CA 35% case vs. CA 60% case), as well

as the increase from the initial value to the ohmic loss at t=600s. The ohmic loss increased by 0.0090V, 0.0104V and 0.0069 respectively for the three CA by-pass valve positions of interest. This impact on dynamic response can be attributed to the impact of the variation of cathode inlet mass flow rate and temperature on SOFC thermal transport and response, as well as the impact of SOFC operating temperature on electrochemical dynamics. In alignment with the activation loss analysis, this illustrates the general trend of more efficient electrochemical operation at higher operational temperatures and a nonlinear relationship between temperature and polarization loss behavior. The impact of initial FC load on ohmic loss for the CA 40% case is presented in Figure 5.25.

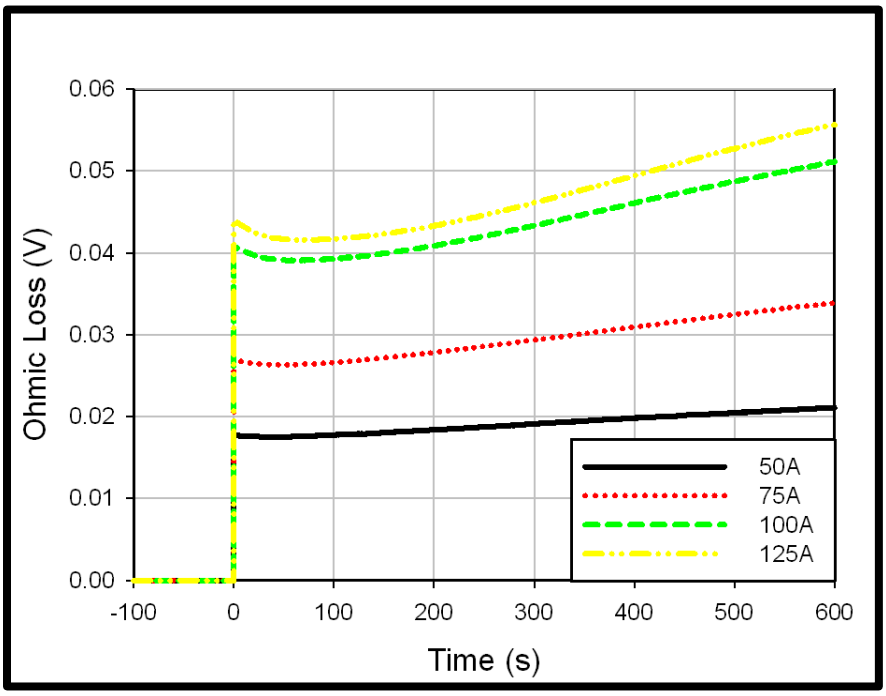

Figure 5.25: Average ohmic loss vs. time – initial FC load comparison, 40% CA by-pass: LBSC[5]

From inspection of figure 5.25, it is apparent that the magnitude of initial FC load for electrochemical start-up has an impact on the dynamic behavior of ohmic loss throughout the start-up transient response. The increase in ohmic loss from the point of application to t=600s after start-up is 0.0033V, 0.0071V, 0.0104V and 0.0116V for the successive load changes respectively. Increases in load increase both the magnitude of

ohmic loss at the initiation of the start-up phase as well as the amount of increase seen during the transient response. The former of these observations can be directly associated to the higher magnitude of current draw, which will naturally result in the production of more electrochemical losses; the latter can be attributed to the thermal dynamics of increased removal of heat from the system and the SOFCs' electrochemical response to the thermal transport.

As initial FC load increases, a decrease in the impact of load on ohmic loss is observed between the 100A and 125A case. A similar trend was observed for the activation loss, which is presented in Figure 5.21 for higher initial FC loads, but the relative impact still seems to be less apparent for the activation loss case in comparison to the ohmic loss case. The initial post FC load activation loss increased by 4.12% from the 100A to the 125A experiments, as compared to 7.88% increase for ohmic loss. This further supports that the application of these higher loads moves the SOFC stack into an operational regime where ohmic losses have a dominate impact on cell performance and the relationship between current density and voltage is linear.

5.4 Distributed Comparison

Section 5.3 presented key operational parameters of the SOFC stack, in singular manner, to characterize FC operation during electrochemical start-up with respect to both CA by-pass valve position as well as initial FC load. One of the key characteristics of the 1-D, real-time SOFC model is its ability to provide internal operating diagnostics in transient, real-time manner on a distributed basis. In this section, the impact of key dependencies such as solid SOFC temperature, current density, by-product heat generation and spatial temperature gradient will be presented and analyzed in distributed manner.

Figures 5.26 and 5.27 present the solid SOFC temperature for 100A initial FC load while varying CA by-pass valve positions, and 40% CA by-pass with varying initial

FC load, respectively. As illustrated in Figure 5.26, the FC is at a uniform temperature prior to placing any load on the cell at t=0s. The pre-load cell temperatures are different for the different CA by-pass valve positions, considering the effect they have on the inlet temperature to the virtual SOFC, with CA 60% having the highest pre-load temperature given the thermal dynamics of the new turbine compressor assembly. The pre-load solid temperatures are different for the three by-pass valve position cases, but the dynamic behavior appears to be consistent, regardless of CA by-pass setting.

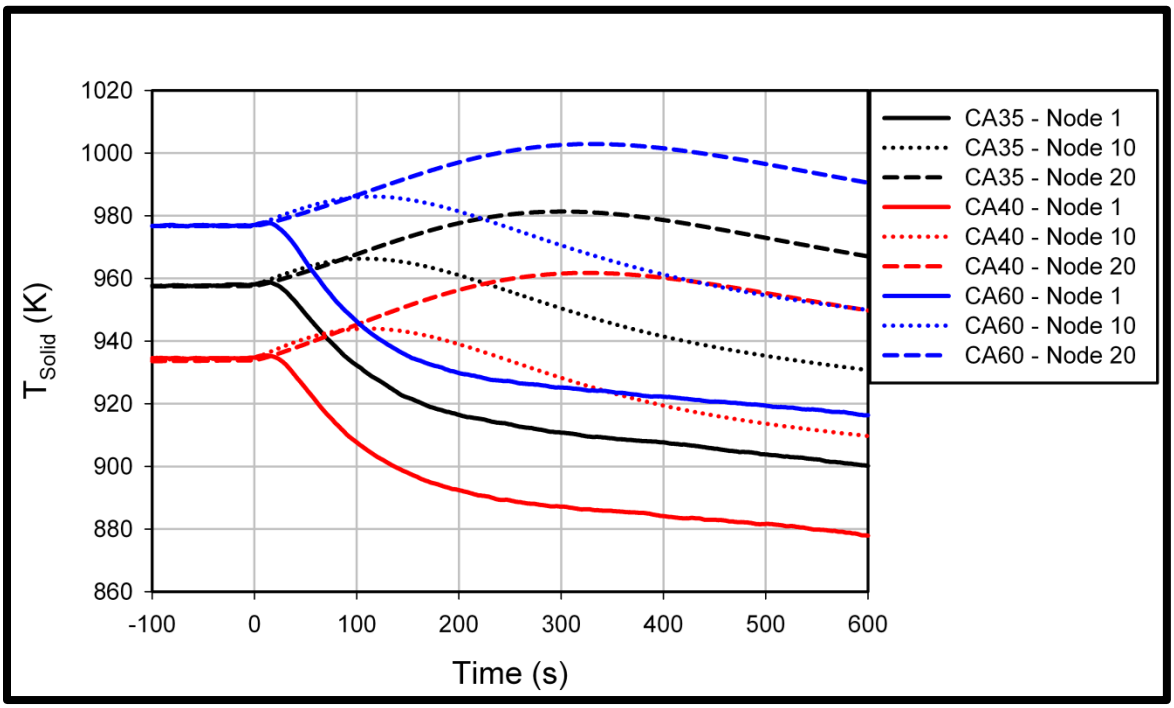

Figure 5.26: Local solid temperatures along the entire SOFC length – CA by-pass comparison, 100A FC load: LBSC

The deviations in the dynamic behavior of the solid temperature are most radically evident in the upstream portion of the SOFC. The temperature at the inlet of the SOFC is heavily influenced by the SOFC inlet temperature, which generally decreases with increasing CA by-pass flow, during transient response of electrochemical start-up. The general trends are very similar, with temperatures in the upstream portion of the cell decreasing very quickly due to the cooling effect from the decreasing temperature of the

inlet stream, and temperatures in the downstream portion increasing initially after load application due to by-product heat generation and associated heat transfer.

Some deviations in temperature profile can be observed downstream as well. As illustrated in Figure 5.26, the node at the exit of the FC reaches its maximum value at approximately 325s after the load application. This maximum value occurs slightly earlier for the 35% CA by-pass case and slightly later for the 60% CA by-pass case. The decreased mass flow with increased CA by-pass effects the cooling in the SOFC resulting in quicker or more sluggish thermal transport. The decreased air-flow results in an increase in O_2 utilization that is illustrated in Table 5.1

Table 5.1: O_2 fuel utilization values for electrochemical start up: LBSC

		50A	75A	100A	125A
CA 35%	t=0s	2.86%	4.26%	5.68%	7.15%
	Post-Load	2.84%	4.20%	5.64%	7.01%
CA 40%	t=0s	2.99%	4.42%	5.85%	7.31%
	Post-Load	2.94%	4.35%	5.76%	7.20%
CA 60%	t=0s	3.41%	5.16%	6.82%	8.52%
	Post-Load	3.38%	5.07%	6.65%	8.32%

Table 5.1 presents the oxygen utilization values for all three of the CA by-pass valve positions and all four initial FC loads investigated for the LBSC experiments. The O_2 utilization at t=0 represents the oxygen utilization at the time of load application, when the oxidant stream mass flow is equal to its pre-load, steady state value. The post-load value represents the O_2 utilization that is calculated approximately 600s after the load has been applied, at which point the mass flow has reached its new "steady" value. As illustrated by the values in the table, a decrease in O_2 utilization (increase in cathode inlet flow) after the load is applied, is observed for each case investigated. This is due to

the increase in mass flow through the compressor that results from the shedding of load from the turbine. Beyond the effect of the load application to oxygen utilization values, it is important to note that the values observed are generally small (<10%). This is primarily due to the low levels of current draw that are used for this experiment. These low O_2 utilization values, however, are advantageous for managing thermal transport in the SOFC and result in relatively rapid thermal transients and manageable and generally safe temperature gradients [12].

Once the maximum temperature at the exit of the FC is reached, a gradual increase in cell temperature from inlet to exit is observed for all three CA by-pass valve position cases. With the cooling effect of the decreased temperature of the inlet stream, the temperature along the entire length of the SOFC gradually decreases throughout the transient response.

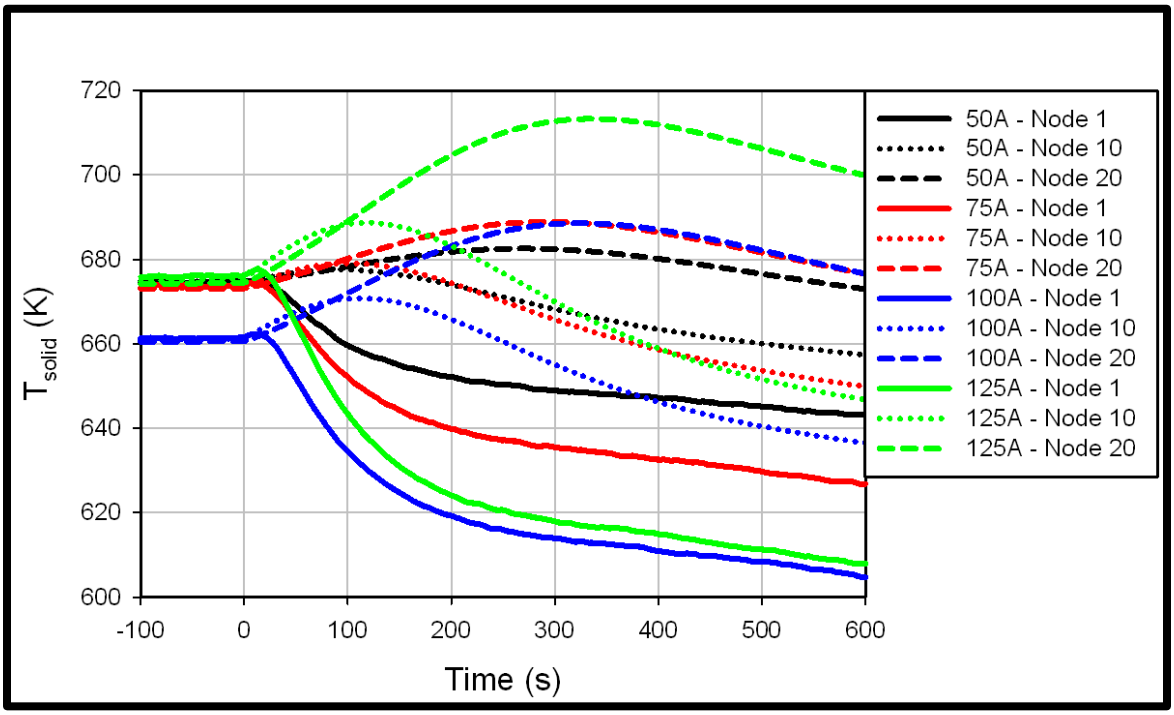

Figure 5.27: Local solid temperatures along the entire SOFC length – initial FC load comparison, 40% CA by-pass: LBSC

The local SOFC temperatures for a CA by-pass setting of 40% and varying initial FC loads is presented in Figure 5.27. It is important to note that the variation between the

initial SOFC temperatures prior to the application of load for the 100A case, as compared to the other three initial loads, can be attributed to variations in ambient conditions [39, 46].

With regards to internal thermal transport in the SOFC, application of load has two effects. First, it causes the formation of by-product heat generation due to cell operation in the SOFC; second, it removes some of the fuel energy from the system that would have been passed on to the working fluid as thermal energy, thus resulting in lower FC inlet temperatures and cooling of the SOFC stack. Increases in FC load thus result in a combination of increased by-product heat and increased FC inlet cooling which impact overall FC thermal transport. As illustrated in Figure 5.27, increases in initial FC load result in increases in temperature in the downstream portion of the FC, decreases in temperature in the upstream portion of the SOFC and an increase in the amount of time it takes for the entire cell to transition to the cooling phase. Transition to the cooling phase (the phase where no local FC temperature is increasing) occurs when the temperature at the FC exit has reached its maximum value. For increases in FC load, the solid temperature at the exit of the FC reaches its maximum at later time periods; as examples, maxima are reached at approximately 275s for the 50A case and 340s for the 125A case. At this point of transition, a gradual increase in local cell temperature is observed with respect to the direction of the flow, and all of the local temperatures gradually decrease with time.

The temperature rise from entrance to exit of the cell is also larger for larger initial FC loads. The deviation from node 1 to node 20 of the FC for a 50A load application is approximately 30K at t=600s as compared to approximately 90K across the FC for the 125A case. Greater by-product heat generation and decreased FC inlet temperature results in a more significant temperature rise across the FC.

CA by-pass valve position impacts initial steady state temperature of the SOFC and the amount of time it takes the cell to transition to its cooling phase. The transition

occurs at approximately 299.36 seconds, 324.72 seconds and 330.4 seconds for the 35%, 40%, and 60% CA by-pass experiments, respectively. The initial FC load increases the amount of time it takes the cell to transition to its cooling phase, as well as cell axial temperature rise once the cell has transitioned to the cooling phase. Transient behavior of the internal temperature profiles also suggests that the impact of by-product heat has a more significant impact in the downstream portion of the cell, as the system moves towards a new steady state.

The SOFC temperature directly impacts electrochemical activity, and thus the local current density distribution. The effects of CA by-pass valve position and initial FC load on the current density distribution are presented in Figures 5.28 and 5.29 respectively.

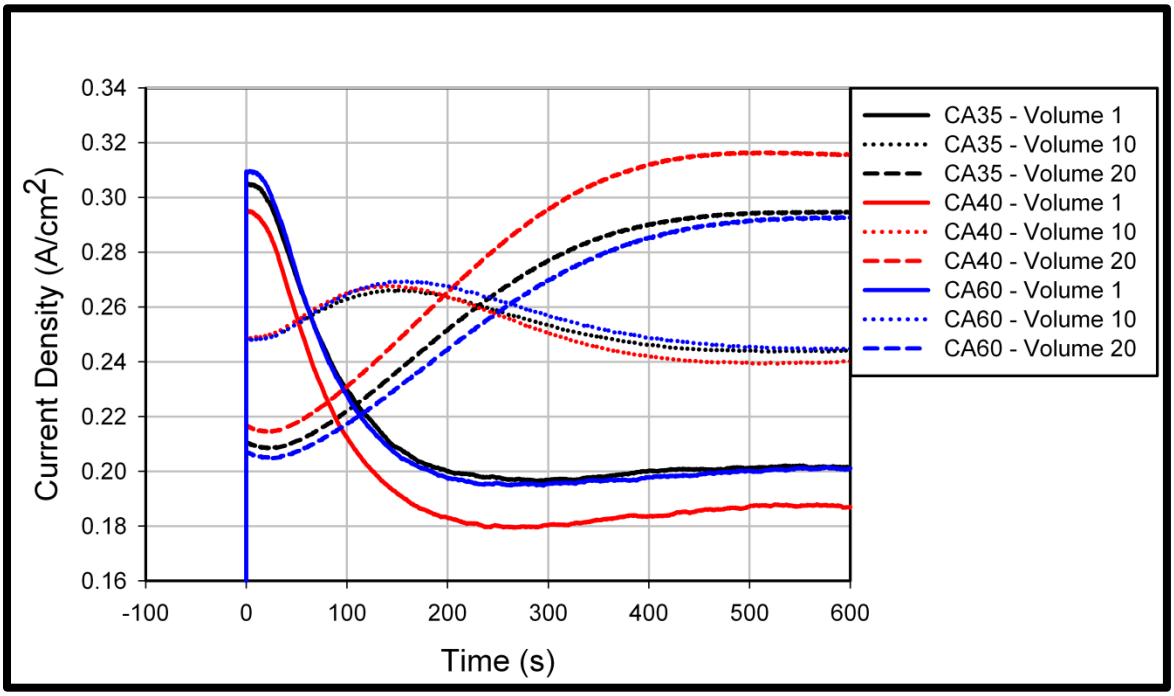

Figure 5.28: Local current density along the entire SOFC length – CA by-pass comparison, 100A FC load: LBSC

The elevated cell operating temperatures support elevated electrochemical activities, and given minimal restrictions on fuel and the relatively low fuel utilization

values during start-up, higher current densities occur at the cell entrance, which consequently must result in lower current densities at the cell exit.

The dynamic response of the local current densities is very similar for all three CA by-pass cases. Once the SOFC begins to operate, by-product heat generation and reduced inlet air temperatures cause an elevated temperature at the exit of the FC, as illustrated in Figure 5.26. The elevated downstream temperature and decreased upstream temperature result in a more significant variation in local current density profile with respect to axial location in the SOFC. The formation of an internal temperature distribution, which demonstrates an increasing trend from inlet to exit of the SOFC, is the primary driver causing the shift of the local current density maximum from inlet to exit and for the local minimum from exit to inlet. This is illustrated by the crossing of the local current density profiles at volumes 1 and 20, respectively, in Figure 5.28. A slight decrease in local current density is observed at the exit of the FC for all three CA by-pass cases. At the point of load application, the local current density is elevated in the upstream portion as compared to the downstream portion of the cell due to reactant availability. This results in a slightly increased temperature rise at the inlet as compared to the exit and correspondingly increased by-product heat in the upstream portion of the cell immediately after the application of load. As the cell equilibrates both thermally and electrochemically, the downstream temperature increases primarily due to generation of heat (with lessened impact of inlet air cooling) as well as a subsequent redistribution in local current density. The combination of these transient effects result in local minima and maxima with respect to time within the first 50s of electrochemical start-up at localized portions along the SOFC, as illustrated by the slight increases and decreases in local current density in the upstream and downstream portions of the cell, respectively. The coupled effects of thermal and electrochemical dynamic response result in the formation of other local and absolute extrema along the SOFC throughout the 600s following the application of load as well.

The 40% CA by-pass case has the most variation in its spatial current density profile at the 600s mark after the initial FC load application, with the 35% and 60% cases both presenting very similar profiles. Given that the general form of the temperature profiles are not significantly different for any of the three cases, the greater variation in current density along the length of the cell in the 40% CA bypass case can be attributed to the lower average operating temperature relative to the other CA bypass cases. With the SOFC temperature at the inlet of the FC nearly 100K less than the desired electrochemical light-off temperature after 600s, the ability for significant electrochemical activity at the inlet is greatly diminished, thus requiring an elevated current density downstream where the temperatures are more suitable for higher levels of current draw. Reactant availability typically contributes to current density distribution as well, but given the low to moderate fuel utilization values for these simulations (≈20%), reactant variation along the cell was minimal (as illustrated in Figure 5.5) and current density distribution was primarily influenced by temperature distribution. The similarity in the current density profiles for the 35% and 60% CA by-pass cases can be attributed to the elevated average operating temperatures. The preceding rationale provides an explanation of the trend, but a more in depth quantitative analysis will have to be conducted to conclusively identify all of the contributing factors.

The impact of initial load on current density distribution is illustrated in Figure 5.29. It presents the local current densities with respect to time for volumes 1, 10 and 20 of the virtual SOFC for electrochemical start-up with 40% of CA by-pass. The profiles for all four initial FC loads of interest illustrate the same general trend, with increases in load resulting in increased local current densities along the entire SOFC throughout the start-up transient response. Increases in load also result in increased variation in current density profile along the axial length of the FC.

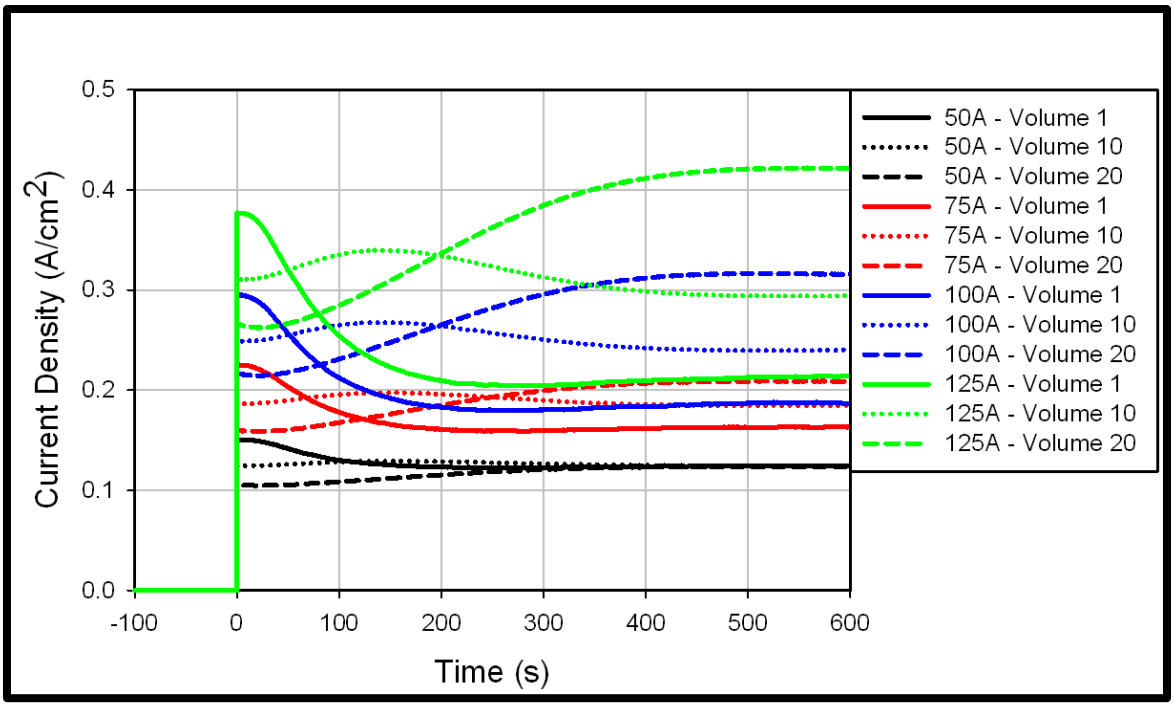

Figure 5.29: Local current density along the entire SOFC length – initial FC load comparison, 40% CA by-pass: LBSC

Elevated current draw results in more by-product heat generation and cooling from a decreased temperature inlet stream, creating more significant variations in FC axial temperature distribution, and consequently more significant variations in local current density distributions. Since fuel flow is remaining constant for these experiments, elevated fuel utilizations at higher loads also contribute to the variations in local current density profiles as well. For 50A of initial load, there is a minimal difference in the current density at the entrance and exit of the FC, whereas for the 125A case, the local current density at the entrance and exit varies by greater than 0.2A/cm^2. Similarly to Figure 5.28, the opposite trajectories of the leading and trailing edge current densities can be attributed to the transition to a new thermal profile with a maximum temperature at the exit and minimum at the inlet, thus resulting in the formation of a more electrochemically favorable condition downstream. Ultimately, current densities increase from inlet to exit of the fuel cell at the conclusion of electrochemical start-up. Equation 4.30 in Chapter 4 is used to calculate by-product heat generation for an operating cell. As presented in the

equation, the by-product heat is dependent upon current draw and operating cell voltage. The dependency of the heat generation on current density explains the similar trends observed in Figure 5.30, which illustrates the by-product heat generation in the SOFC during 100A electrochemical start-up for the three CA by-pass cases of interest in distributed manner. Figure 5.28 presents local current density for the same experiments in the same fashion. Given the highly coupled nature between by-product heat generation and current density, the similarities between the two trends can be attributed to that coupling and current density's thermal dependence as explained in conjunction with Figure 5.28. Though similar, the trends are not identical and that can be attributed to the impact of operational voltage on the production of by-product heat and the increase in cell operational efficiency (i.e. decrease in by-product heat generation) at increased operational temperatures.

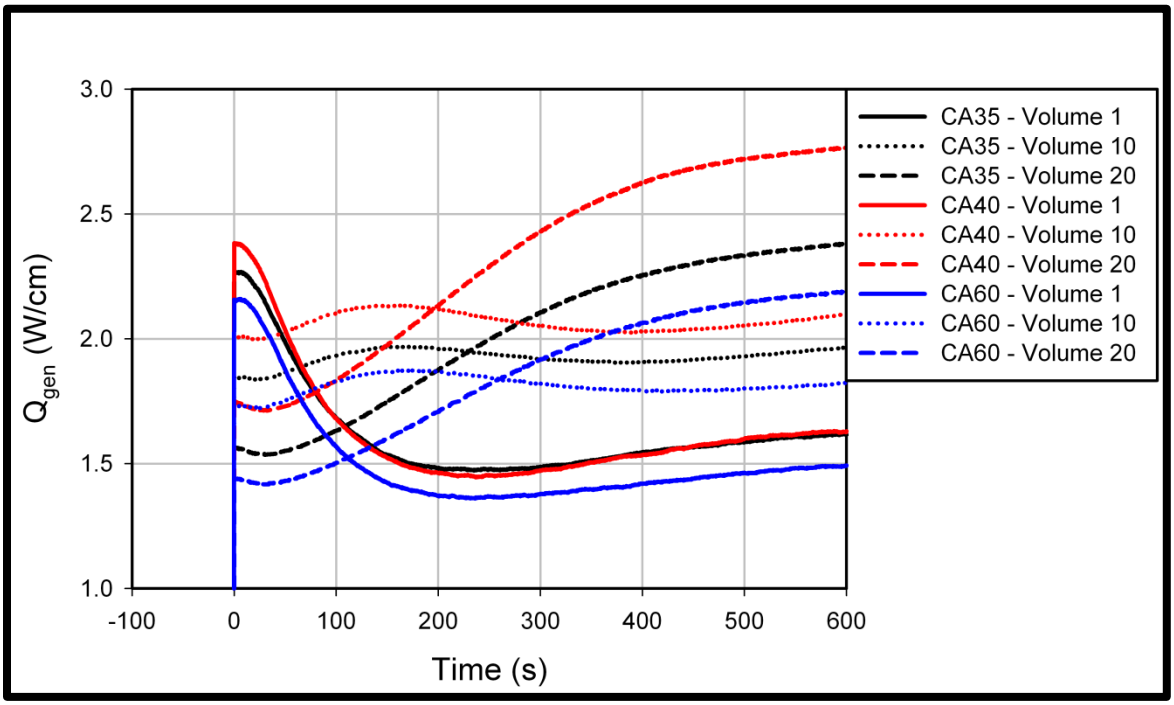

Figure 5.30: Local heat generation along the entire SOFC length – CA by-pass comparison, 100A FC load: LBSC

As discussed in Section 5.3 and illustrated in Figure 5.17, the operational voltage is lowest for the 40% CA by-pass case and largest for the 60% CA by-pass case due to

the impact of average operating temperature for the given experiments. The impact of operating voltage on by-product heat generation is evident since the by-product is largest for 40% CA by-pass, followed by 35% CA by-pass and 60% CA by-pass consecutively; and it is further illustrated by the gradual increase in by-product heat throughout the transient response, aligning with the gradual decrease in operational voltage.The impact of FC load on by-product heat generation is presented in distributed manner in Figure 5.31.

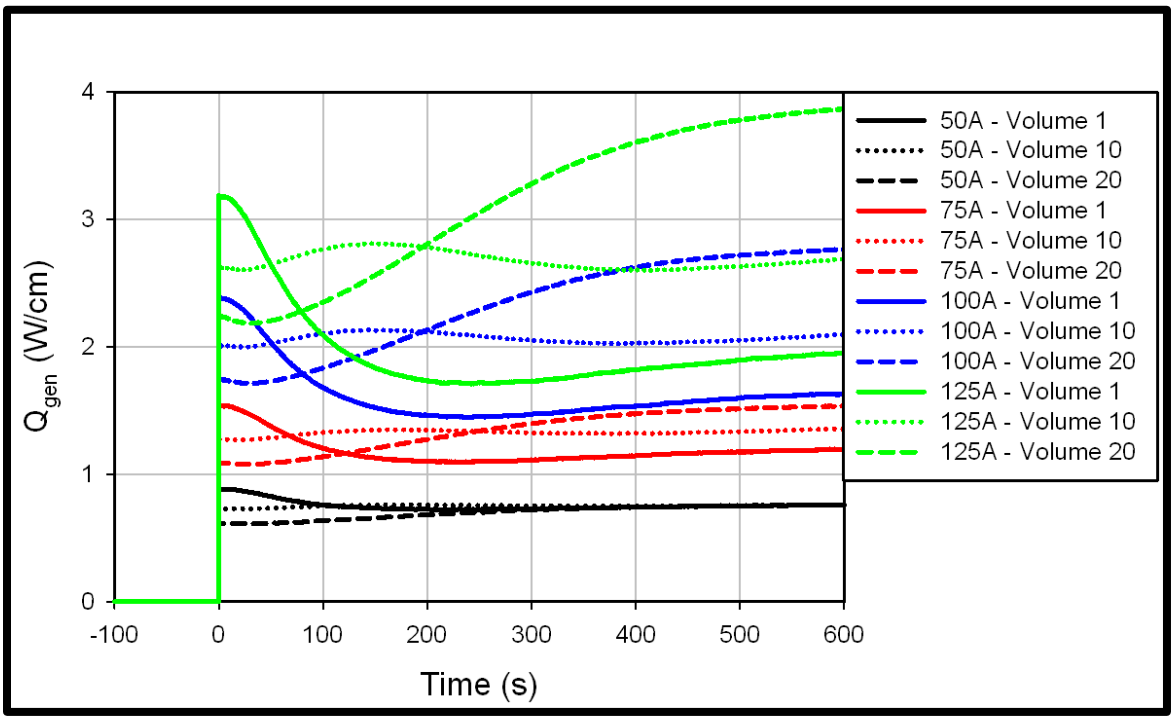

Figure 5.31: Local heat generation along the entire SOFC length – initial FC load comparison, 40% CA by-pass: LBSC

The profiles presented in the figure track very closely with the local current density profiles presented in Figure 5.29, with the impact of the operational voltage again evident, given the upward trend of the dynamic response of the by-product heat. Increases in current draw result in increases in both the magnitude of local heat generation as well as the axial variation in local values for a given load application. Much like the local current density, minimal to no variation between heat generation at the inlet and exit of the FC are observed for an initial load of 50A,whereas a difference of nearly 2

W/cm is observed for 125A of initial load. The opposite trajectories of the local heat generation values at the inlet and exit of the FC, illustrated in Figure 5.30, can be attributed to the dependence of current density illustrated in Figure 5.28. In similar manner, the trends observed, particularly at the inlet and the outlet, are attributed to the evolution of a new temperature profile after the application of load at time=0 and the increase in electrochemical activity in the downstream portion of the cell.

Electrochemical activity, operating temperature and by-product heat all contribute to one of the most significant areas of SOFC operational performance, the characterization of internal temperature dynamics in the SOFC; more specifically, spatial temperature gradients. Given SOFCs' sensitivity to extreme spatial temperature gradients, much research has been dedicated to identifying regimes of safe cell operation and mechanisms to reduce/mitigate the evolution of harmful temperature gradients during SOFC operation. To that end, spatial temperature gradients have been resolved for this characterization study and are presented in Figures 5.32 and 5.33.

Figure 5.32 presents the impact of CA by-pass valve position on local spatial gradients along the axial direction of the SOFC for 100A initial FC load electrochemical start-up. With the competing effects of by-product heat generation as well as cooling from the decreased temperature inlet stream, it is expected that the most significant temperature gradients would exist in the upstream portion of the SOFC. Maximum temperature gradients actually existed across segments 2 and 3 consistently throughout the experiments, but the figure presents profiles at select points throughout the SOFC so that trends can be observed for the entire cell.

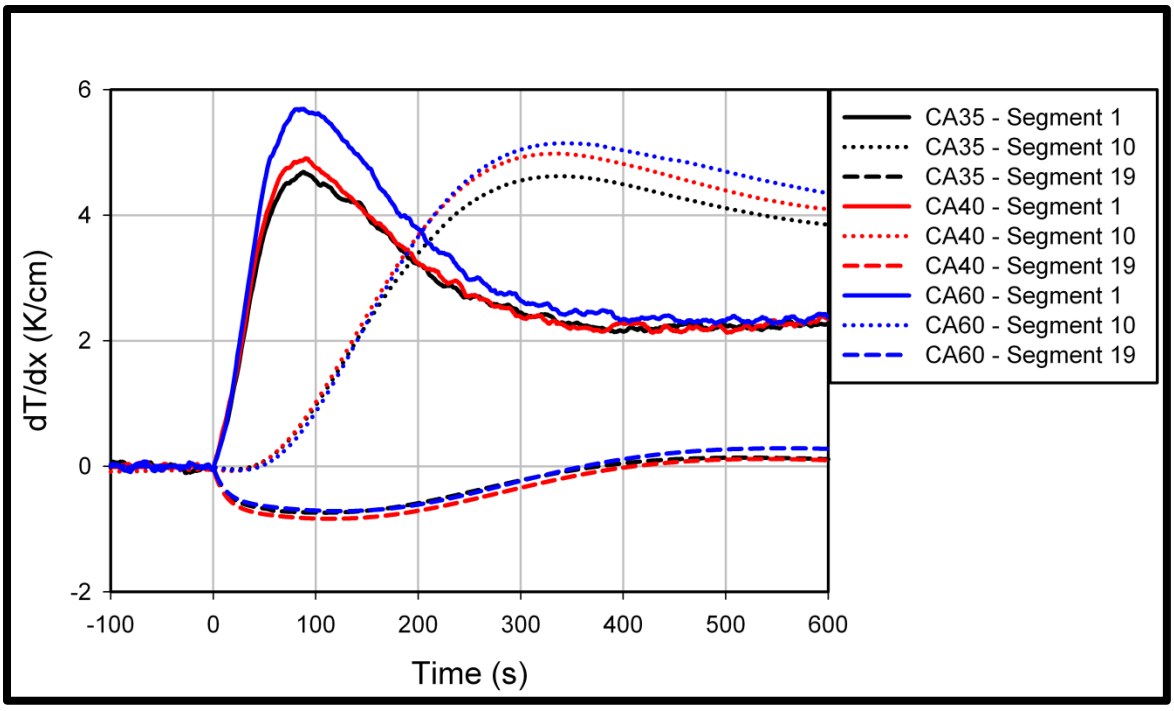

Figure 5.32: Local spatial temperature gradient along the entire SOFC length – CA by-pass comparison, 100A FC load: LBSC

The increase in cathode inlet flow rate for lower CA by-pass valve positions contributes to the mitigation of extreme temperature gradients in the SOFC, particularly in the upstream portion of the cell. As illustrated in Figure 5.32, the magnitude of dT/dx values increases for increasing CA by-pass for segments 1, 5 and 10. Local dT/dx maxima, with respect to time, propagate with respect to spatial location. This propagation of local spatial gradient extrema and the general decrease in their magnitude with respect to spatial position is expected given that the mass flow of the oxidant stream is going to support heat transfer in the downstream direction of the SOFC, which also supports the dampening effect of the thermal mass of the SOFC. The results are generally lower maxima in spatial gradients later in the start-up transient. Again, it is important to note that the 60% CA by-pass experiments were conducted with a new turbine with differing thermal characteristics and a more detailed study utilizing the new turbine would have to be conducted to further substantiate the conclusions drawn from this study. The dT/dx profiles in the downstream portion of the FC appear to approach uniformity due to the

proximity to the adiabatic boundary condition at the exit of the fuel cell. It is important to note that the adiabatic boundary condition is only adiabatic with respect to the solid material and heat transfer due to convection still occurs at the cell outlet. This results in local maxima near to, but not precisely located at, the cell outlet.

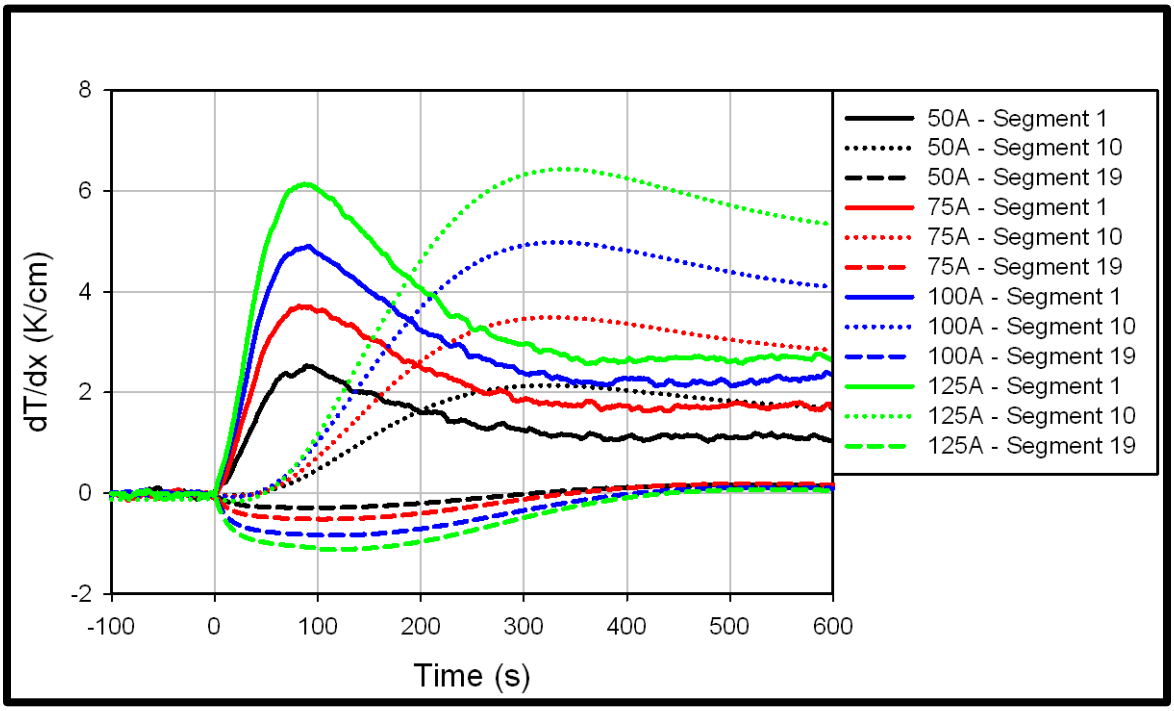

Figure 5.33: Local spatial temperature gradient along the entire SOFC length – initial FC load comparison, 40% CA by-pass: LBSC

Figure 5.33 illustrates the impact of initial FC load on spatial temperature gradient for a 40% CA by-pass setting. As expected, the increase in initial FC load results in an increase in the magnitude of spatial temperature gradient along the entire SOFC. Dynamic response appears to remain consistent for all spatial gradient profiles presented (i.e., regardless of initial FC load application). It is important to note that, although the most significant temperature gradients exit near the upstream portion of the SOFC at early times in the start-up transient response, the most significant spatial gradient values after the transition to cell cooling occurs (at approximately t=300s) is further downstream.

CHAPTER 6

COLD AIR POST COMPRESSOR BY-PASS INVESTIGATION – OPEN LOOP

Similar to the results presented in Chapter 5 of this dissertation work, Chapter 6 presents the results and analysis from characterization studies of electrochemical light-off of an SOFC/GT hybrid system. Chapter 5 presented results from the HyPer facility that employed the use of a LBSC algorithm that afforded the capability to examine the impact of larger initial load steps given the controller's ability to mitigate the effects of decreases in turbine speed beyond the 5% allowable deviation, which could occur for sufficiently large FC initial load. The results and analysis presented in Chapter 6 characterize the system wide and SOFC stack specific dynamic response when no LBSC algorithm is applied. Conducting results in OL (OL) operation limits the amount of load that can be placed on the fuel cell for a given experiment changing the range of initial load applications investigated from a range of 50A – 125A in equal 25A for LBSC to a range of 10A – 40A in equal 10A increments for OL. CA by-pass valve positions of 35%, 40% and 60% open remained consistent between the two investigations. The results of all of the experiments presented in this section operate the virtual FC assuming a humidified hydrogen fuel feed comprised of 90% H_2 and 10% H_2O and an initial nominal operating turbine speed of 40,500 RPM and turbine load of 50kW. Results and analysis from the CA post compressor by-pass investigation for a direct fired, recuperated, SOFC/GT hybrid system employing a OL system configuration are presented in this chapter.

6.1 Base Case – Initial FC Load 30A, CA By-Pass Valve: 40%

For the purpose of investigating and analyzing the impact of initial FC load and CA by-pass on system dynamic response, a base case of 30A of initial fuel cell load and a CA by-pass valve position of 40% open were selected. Given the development of turbine

start-up and stall mitigation strategies with the HyPer facility, 40% cold-air by-pass has been selected as a base CA by-pass position, given its safe operating regime with regards to stall margin and its ability to provide sufficient flow to the virtual SOFC. The 30A initial FC load provides a base line to observe significant system and SOFC dynamics while simultaneously residing within the range of initial FC load values so that comparisons can be made for both larger and smaller initial load step sizes.

Figure 6.1 illustrates the process flow parameters that serve as inputs to the real time SOFC model, which is described in detail in Chapter 4. As outlined in the experimental methodology section and illustrated in the figure, the system was allowed to come to steady state prior to the start of the experiment. The steady state values of the FC model input parameters are illustrated between times -100 and 0 in Figure 6.1. As illustrated the pressure, temperature, and flow of the oxidant stream entering the virtual SOFC stack was approximately 373kPaa, 952K and 1.41 kg/s respectively.

For all of the data presented in this chapter, t=0s signifies the time at which the indicated initial fuel cell load is placed on the virtual SOFC stack. Once load is applied to the FC stack at t=0s, the virtual fuel cell subsystem that was initially only generating thermal energy from the combustion of unutilized fuel is now producing both thermal energy from a combination of unutilized fuel combustion and by-product heat generation from cell operation, as well as electrical energy, produced by the current draw from the SOFC stack. This redistribution of energy transfers results in a decrease in physical heat that is transferred to the working fluid, thus decreasing turbine speed and the process parameters that are inputs to the virtual SOFC.

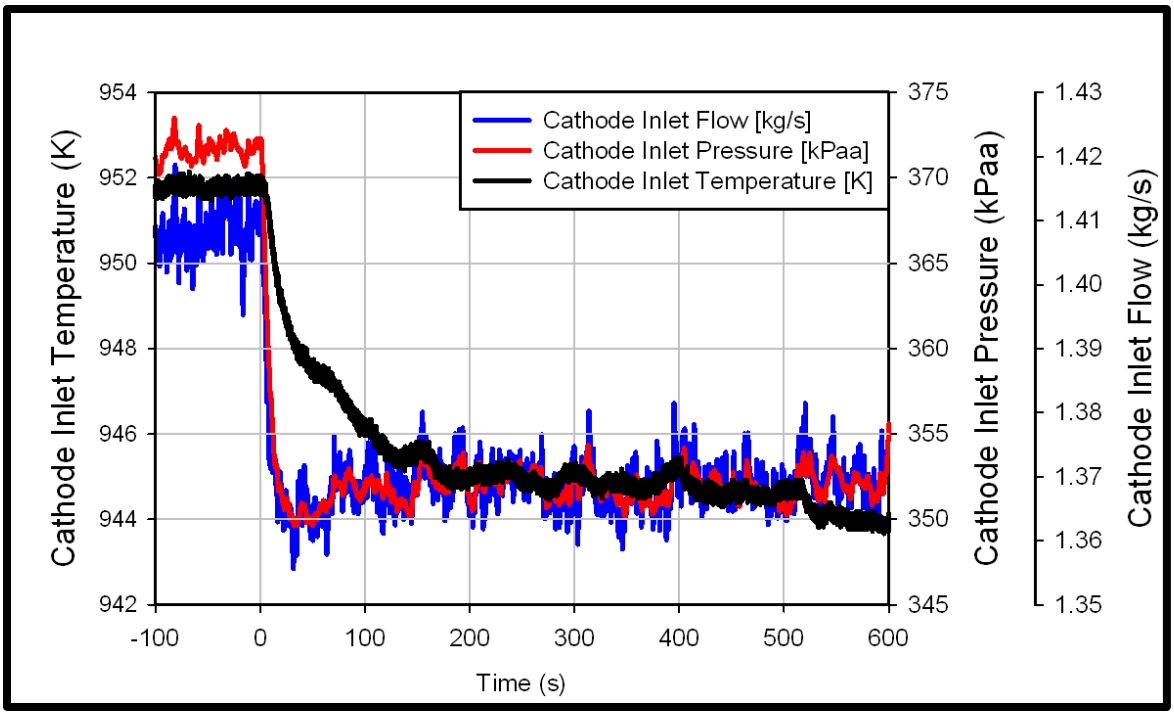

Figure 6.1: Fuel cell inlet parameters - 30A FC load, 40% CA by-pass: OL base case

As presented in the previous chapter, fuel cell inlet parameters such as pressure, temperature and flow are heavily correlated to turbine speed, and consequently FC subsystem thermal effluent. Once the load is applied at t=0s, there is a sharp decrease in the cathode inlet pressure and flow from approximately 373kpaa to 352kpaa and from approximately 1.41 kg/s to 1.37kg/s respectively. These parameters are directly coupled with the turbine speed, thus resulting in the sharp decrease illustrated in Figure 6.1. The cathode inlet temperature is more directly influenced by physical heat provided to the system as opposed to turbine speed. Though the heat provided to the working fluid decreases nearly instantaneously, once load is applied to the SOFC, the impact of system wide thermal transport, including but not limited heat-exchanger dynamics, results in a more gradual decrease in FC inlet temperature as illustrated. FC inlet temperature decreases from approximately 952K prior to approximately 944K, and this is with respect to a timeframe of 600s after the load had been applied.

Unlike the LBSC experiments, once heat is removed from the system, there is no mechanism to force the turbine speed back to its nominal condition. This means that the "increasing-decreasing" dynamic response for system parameters, such as cathode inlet flow and pressure will not be observed during electrochemical start-up where the OL configuration is employed. The increased system thermal transients due to load shedding that were observed in the LBSC case, particularly for FC inlet temperature, will not be present for the OL case. Once load is applied, system parameters quickly approach some steady value and remain at their new respective values throughout start-up. They will not change until load is removed from the FC stack.

At the point of load application, the fuel cell becomes electrochemically active which results in a dynamic response in system process parameters, some which are illustrated in Figure 6.1, as well as internal SOFC stack dynamics. Once electrochemically active, the SOFC stack starts to generate by-product heat due to cell operation. Given the generation of heat in the SOFC stack, the cooling effect at the inlet of the SOFC due to the decrease in temperature of the inlet stream, and a spatial distribution of current density due to variations in hydrogen concentrations along the flow channel, spatial temperature profiles begin to form. Figure 6.2 presents the spatio-temporal temperature plot of the SOFC.

As illustrated in Figure 6.2, the FC temperature was nearly uniform, prior to the load application. At t=0s, 30A of load was place on the SOFC stack which resulted in by-product heat generation from cell operation and a decrease in inlet SOFC temperature, due to a decrease in FC subsystem thermal effluent. At the point of load application, a non-uniform spatial variation in temperature profile begins to form, with the local temperatures decreasing upstream due to inlet cooling and increasing downstream due to generation of by-product heat and diffusion of thermal energy. A maximum local temperature of approximately 953K is observed at the exit of the FC approximately 400s after load application. Once the maximum temperature is achieved at the outlet of the fuel

cell, a cooling effect from the cathode inlet air stream is observed throughout the remainder of the transient response presented.

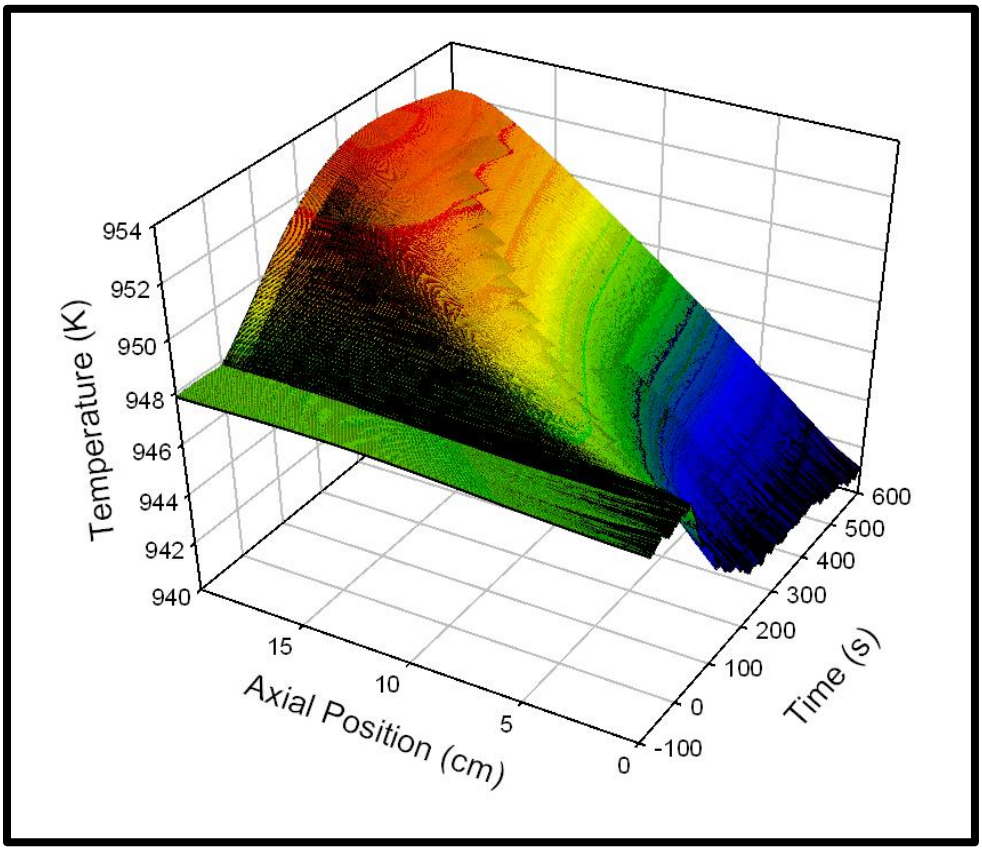

Figure 6.2: Spatio-temporal solid temperature plot – 30A FC load, 40% CA by-pass: OL base case

The spatio-temporal temperature plot presented in Figure 6.2 illustrates the internal SOFC thermal dynamics that are caused by the combination of internal SOFC electrochemistry and system wide thermal transport. This dynamic behavior can cause temperature gradients to form in the SOFC, which can be potentially harmful and threatening to SOFC mechanical integrity and durability (though they are relatively mild for the illustrated base case). To directly analyze the impact of electrochemical start-up on spatio-temporal gradient formation, a plot is presented in Figure 6.3 for the given scenario.

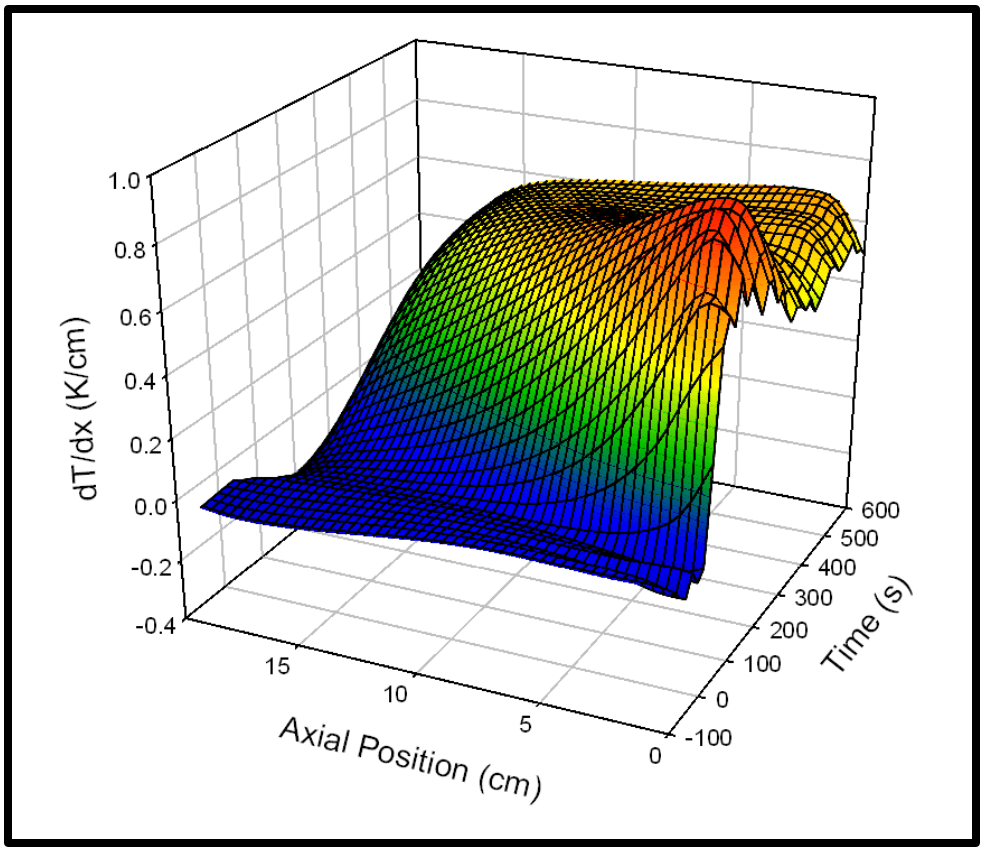

Figure 6.3: Spatio-temporal spatial temperature gradient plot – 30A FC load, 40% CA by-pass: OL base case

The nearly uniform temperature profile prior to the load application, illustrated in Figure 6.2 results in a negligible (nearly zero) spatial temperature gradient, that is illustrated in Figure 6.3, prior to the application of load. Once load is applied, the upstream decrease in local temperature due to inlet cooling and the downstream increase due to by-product heat generation and heat diffusion results in a gradual increase in the spatial gradient profile throughout the initial transient response. Eventually the upstream thermal dynamics begin to dominate and a total maximum spatial gradient of 0.92K/cm is observed across the second segment of the SOFC, approximately 150s after the load had been applied. The combination of elevated local current density at the inlet (see Figure 6.4), which results in larger local by-product heat generation terms, in proximity to the cooling effect of the inlet stream contributed to the formation of an overall maximum spatial temperature gradient. The time of occurrence of the maximum spatial gradient is

closely aligned with the time that the FC inlet temperature reached its minimum ("steady") value of approximately 945K. After approximately the 400s mark, when the maximum local temperature at the exit had been achieved and the FC inlet temperature had arrived at its minimum "steady" value.

The maximum spatial temperature gradient that was observed near the inlet of the fuel cell, approximately 150s into the start-up transient response, was heavily influenced by both the inlet stream cooling effect as well as the by-product heat generation from cell operation. By-product heat generation is directly impacted by local current density, for which a spatio-temporal profile is presented in Figure 6.4. The fuel flow for the 30A OL start-up experiment presented is 23.1 g/s of 90%/10% (H_2/H_2O) humidified hydrogen (HH), resulting in a fuel utilization of 6.2%. Given the low fuel utilization value for 30A of initial load, a fuel flow of 23.1g/s, and relatively evenly distributed temperature profile (ΔT =0K pre-load, ΔT =12K post-load), local current density was primarily influenced by local hydrogen concentration,(see Figure 6.5), resulting a generally linear profile along the axial direction of the FC.

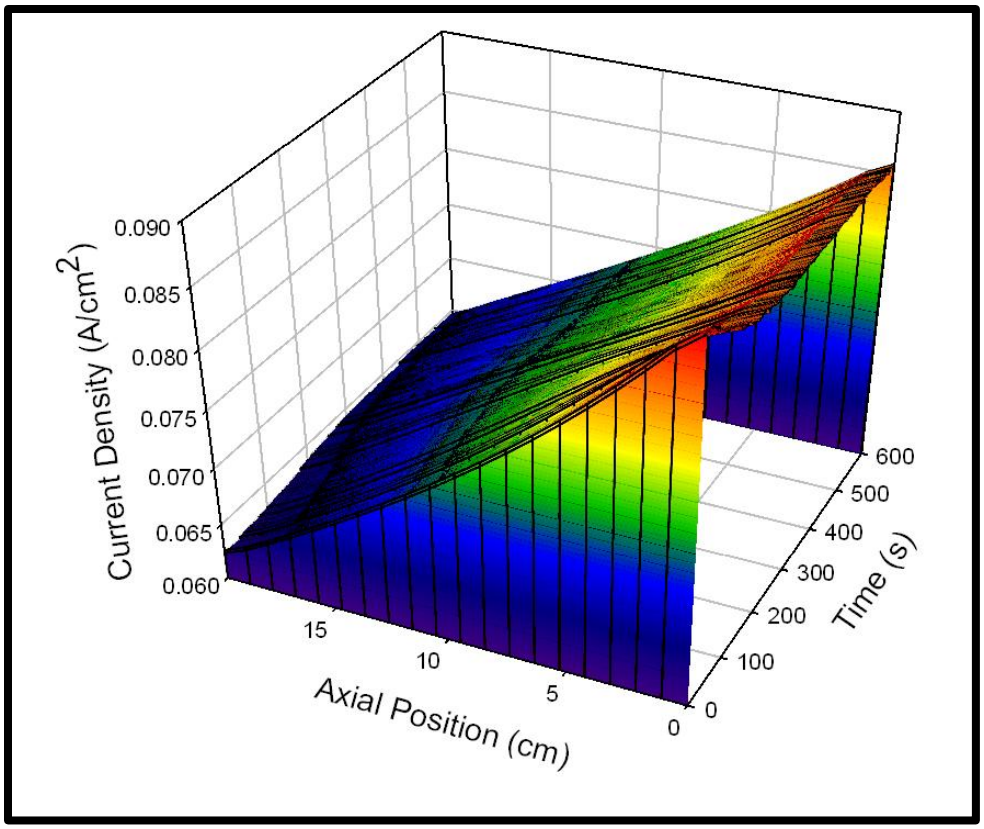

Figure 6.4: Spatio-temporal current density plot - 30A FC load, 40% CA by-pass: OL base case

Near the time of initial current demand, the local current density exhibits a monotonically decreasing profile with a value at the inlet of approximately 0.0875 A/cm^2 and a value at the outlet of approximately 0.0625A/cm^2. From the initial point of start-up, there is a redistribution of local current density in the SOFC due to thermal transient response and the formation of non-uniform spatial temperature profiles in the SOFC solid material. This redistribution results in a decrease in local current densities in the axial locations near the inlet of the SOFC and a gradual increase in local current density downstream, near the exit of the SOFC. Given the low fuel utilization, coupled with the modest thermal transient response, the same general trend of a monotonic decrease in current density from FC inlet to exit is observed after the redistribution, and the effect of the redistribution is minor. The most significant component of the transient response appears to dissipate within the first 200s of start-up, with even more modest redistribution

occurring throughout the remainder of transient response presented. Current density is coupled to hydrogen consumption; thus, the local current density profile is directly coupled to the local hydrogen concentration in the fuel channel of the SOFC. The local H_2 concentration profile for this OL, electrochemical start-up base case is presented in Figure 6.5

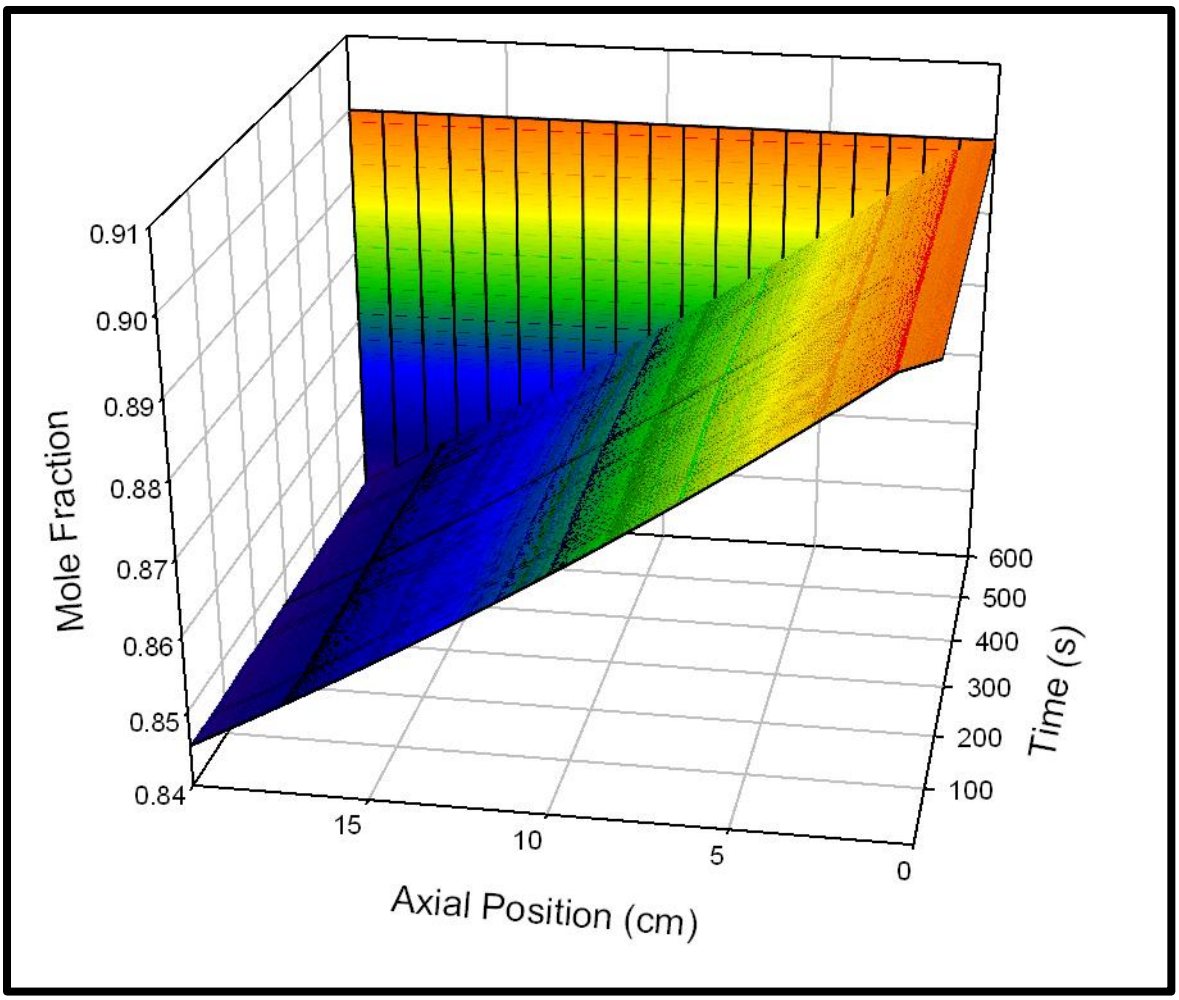

Figure 6.5: Spatio-temporal hydrogen concentration plot – 30A FC load, 40% CA by-pass: OL base case [6]

The H_2 concentration appears to be both linear and generally uniform throughout the entire start-up transient, with a maximum mole fraction at the inlet of 0.90 and a minimum at the exit of approximately 0.845. Low fuel utilization and small thermal

[6] The "wall" effect observed at the 600s mark is due to the removal of load 600s after it was applied

variation in the local SOFC operating temperature (ΔT_{max}=12K after 600s) allow for a minimal effect to be observed on the local hydrogen concentration distribution. The local current density does illustrate redistribution in response to SOFC thermal transport, but the low magnitude of the local current density values for 30A of initial FC load allows for the effect of the redistribution to be small.

6.2 System Performance

The HyPer test facility has been designed to characterize and develop SOFC/GT hybrid systems utilizing HiLS methodology. The HyPer facility captures over 150 system process variables, not including the nearly 300 parameters that are captured by the 1-D, real time SOFC model, when operating "in-the-loop". Though all of those process variables are of notable importance when characterizing and identifying system operation, the parameters of particular interest to SOFC stack operation are turbine speed, and cathode inlet pressure, temperature, and flow. Given their direct impact on SOFC performance and operation, turbine speed, and fuel cell inlet temperature (TE-326 + dTin, which represents the step increase in cathode inlet temperature that is imposed as discussed in Chapter 3), pressure (PT-305) and flow (FE-380) will be presented in addition to the transient response of FC subsystem heat generation and system wide pressure drop.

The increase in the diversion of compressor exhaust from the heat exchanger to the combustion volume that results from increasing CA by-pass open position causes a decrease in airflow to the virtual SOFC. Figure 6.6 illustrates the impact of increasing CA by-pass valve position by presenting the airflow into the cathode of the virtual SOFC for the three CA by-pass valve positions of interest for the 30A initial FC load application.

Prior to the application of load the air flow into the cathode of the virtual SOFC was approximately 1.42kg/s, 1.41kg/s and 1.2kg/s for the respective air flows. This variation in inlet cathode flow prior to the load change demonstrates the capability to

control airflow to the cathode using CA by-pass. There is a much more significant impact of CA by-pass on cathode inlet flow between the 40% to 60% settings as compared to the 35% -40% settings. As a reminder, the rationale is discussed in Chapter 3 of the dissertation and is based upon work conducted by Tucker et. al [14]. It is important to note that the presence of non-linearities will cause changes in CA by-pass to impact other system parameters of interest, such as, but not limited to, cathode inlet temperature and pressure [14-17]; however, given that cathode air flow is the primary means of SOFC thermal management, the ability to control cathode air flow using CA by-pass will be an essential mechanism for control system designers to employ in the design of algorithms. This would be for the purpose of maintaining safe operating conditions for the SOFC with regards to thermal transport.

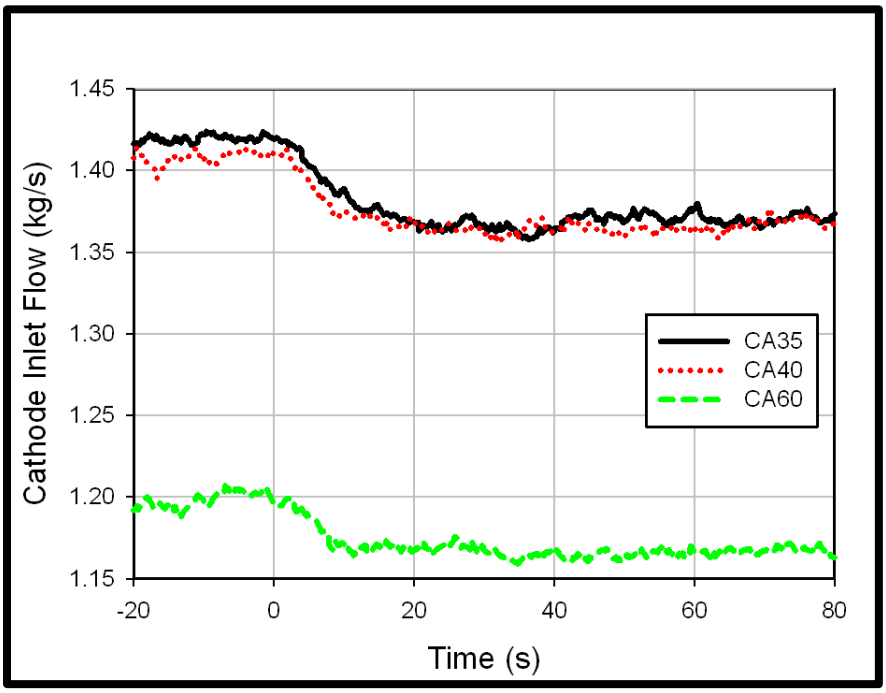

Figure 6.6: Absolute FC inlet flow vs. time – CA by-pass comparison, 100A initial FC load: OL

Once load is applied to the virtual SOFC at t=0s, a quick decrease in cathode inlet flow is observed. For all three CA by-pass cases, a minimum and new steady flow is observed approximately 20s after the initial FC load was applied. With the speed control

mechanism disabled for the OL experiments, the dynamic response to load application varies from the "decrease/increase" dynamic behavior exhibited when LBSC is employed. The dynamic response that is observed for the OL case can be directly attributed to the sustained decrease in turbine speed due to the removal of physical heat from the system once virtual load is applied to the computationally modeled SOFC stack.

To better compare the dynamic impact of CA by-pass on cathode inlet flow for 30A of initial FC load, the start-up transient response is presented in normalized fashion in Figure 6.7.

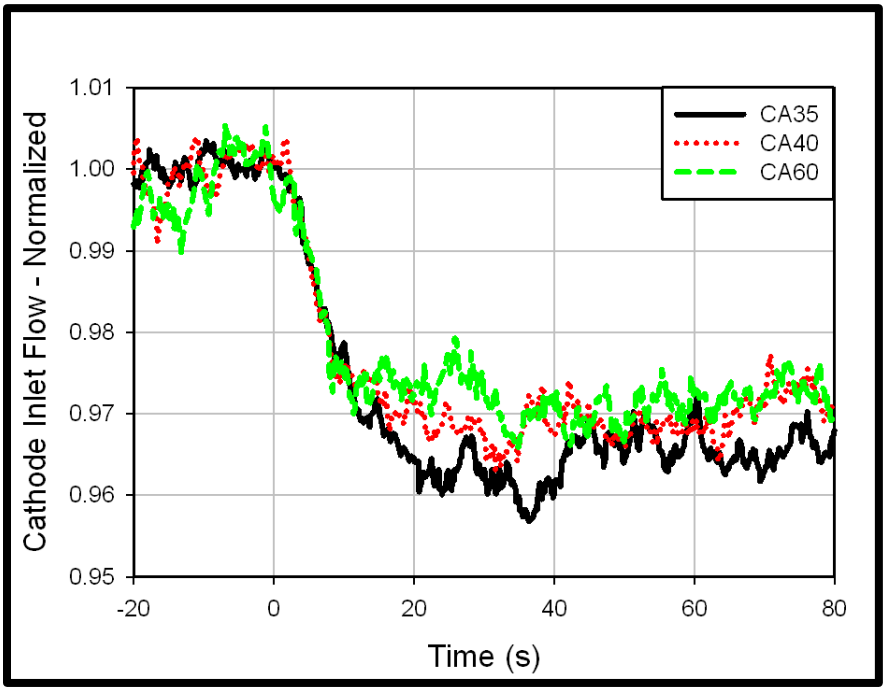

Figure 6.7: Normalized FC inlet flow vs. time –CA by-pass comparison, 100A initial FC load: OL

At the point of load application, the normalized cathode inlet flow decreases to a new "steady" value approximately 20s after the load is applied for each of the CA by-pass cases. For smaller amounts of CA by-pass flow, the percent change in "steady" flow values is greater. Cathode inlet flow appears to decrease nearly 4% for the 35% CA by-pass case compared to an approximate 3% decrease for the 60% case. Given cathode inlet flow's heavy correlation to turbine speed, the variance in post-load flow rates can be

attributed to the variations in fuel flow. Since a decreased amount of working fluid passes through the virtual SOFC subsystem, a greater amount of fuel is required at higher CA by-pass to maintain an initial nominal operating turbine speed of 40,500 RPM. The fuel flow rates for the 90/10 humidified hydrogen mixture were 22.3g/s, 23.1g/s and 25.3g/s for the 35%, 40% and 60% CA by-pass cases, respectively. Since the load application is constant for all three cases, the relative impact on thermal effluent from the fuel cell subsystem is different for all three cases, resulting in more thermal effluent remaining after load has been applied to the system, for larger CA by-pass and consequently elevated post-load cathode inlet flow rates[7]. The impact of initial FC load on normalized cathode inlet flow is presented in Figure 6.8.

As initial FC load increases, so does the amount of heat that is removed from the system, thus resulting in a more significant change in turbine speed and consequently mass flow. The decrease in cathode inlet mass flow is greater with greater initial load application and appears to be impacted by load increase in a relatively linear fashion. The final steady cathode inlet flow decreases from its pre-load values by approximately 1%, 2%, 3% and 4% respectively. Given the low fuel utilization and resulting current density values, the amount of heat that will be generated by the SOFC is minimal relative to the post combustion thus causing the majority of FC subsystem thermal effluent to result from combustion of unutilized fuel. That results in minimal variation in the degree of change for successive increases in FC load, as illustrated in Figure 6.12 and an apparently linear correlation between initial FC load and changes in cathode inlet flow.

[7] Replacement of the turbine compressor assembly that occurred prior to the 60% CA by-pass experiments could contribute to the difference in normalized turbine response for the 60% CA case but calibration studies comparing the dynamic response of the overhauled turbine illustrate very strong agreement in dynamic response between the old and new turbine compressor assemblies.

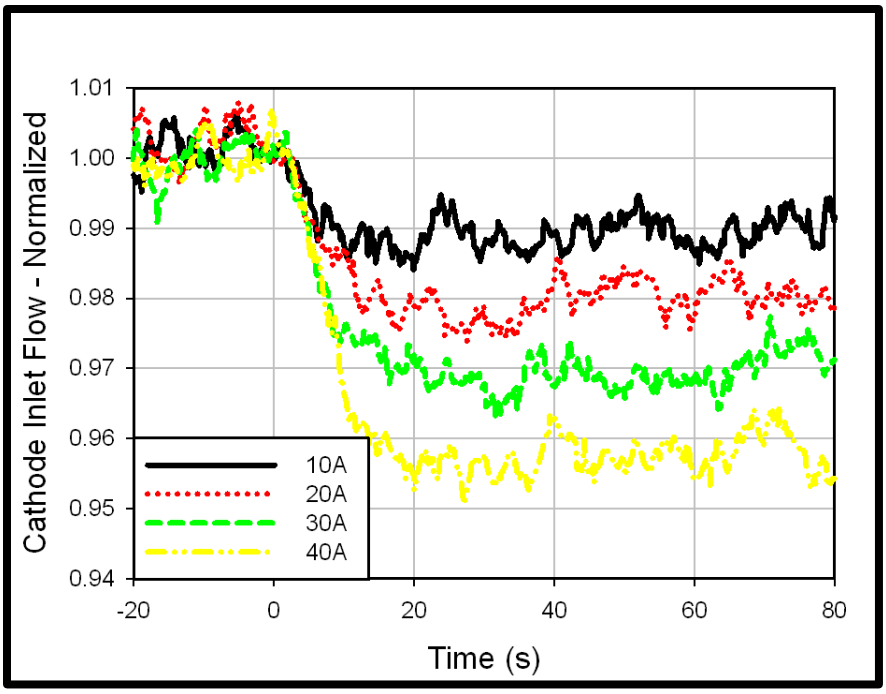

Figure 6.8: Normalized FC inlet flow vs. time –initial FC load comparison, 40% CA bypass: OL

Given the strong correlation between turbine speed and mass flow, the impact of CA by-pass valve position on turbine speed transient response is presented in Figure 6.9. Once load is placed on the SOFC stack at t=0s, heat is removed from the system and the turbine speed begins to decrease. Approximately 20s after the load had been applied; the turbine speed reaches its minimum and steady value, which is approximately 97% of the nominal speed for all three CA by-pass scenarios. Though some differences in the general trends of the turbine speed profiles are observed, with the CA 35% case illustrating the most significant decrease in turbine speed, followed by CA 60% and CA 40%, the final post-load, steady values for turbine speed are all within a 0.5% range (≈200 RPM) of the nominal operating speed. Given the error that is associated with the turbine speed measurement for the OL experiments as presented in Chapter 3, the range does not fall outside of the bounds established by the statistical analysis and thus it is concluded that there is no significant impact of CA by-pass valve position on turbine speed response. The impact of initial FC load on turbine speed is presented in Figure 6.10.

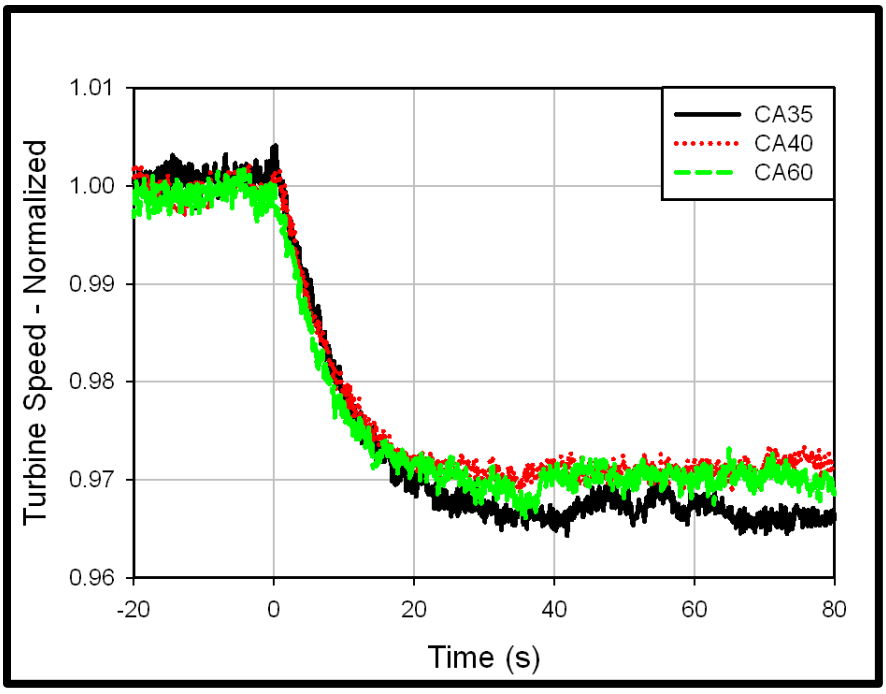

Figure 6.9: Normalized turbine speed vs. time –CA by-pass comparison, 100A initial FC load: OL

Similarly to the cathode inlet flow comparison, presented in Figure 6.8, the turbine speed varies almost linearly with initial FC load. As load increases, more significant decreases in turbine speed are observed, with a 1% decrease from nominal operating speed for 10A of FC load and a 4% decrease for 40A of FC load. For all of the cases, the new steady speed is achieved nearly 20s after the initial load is applied and remains steady throughout the remainder of the start-up period.

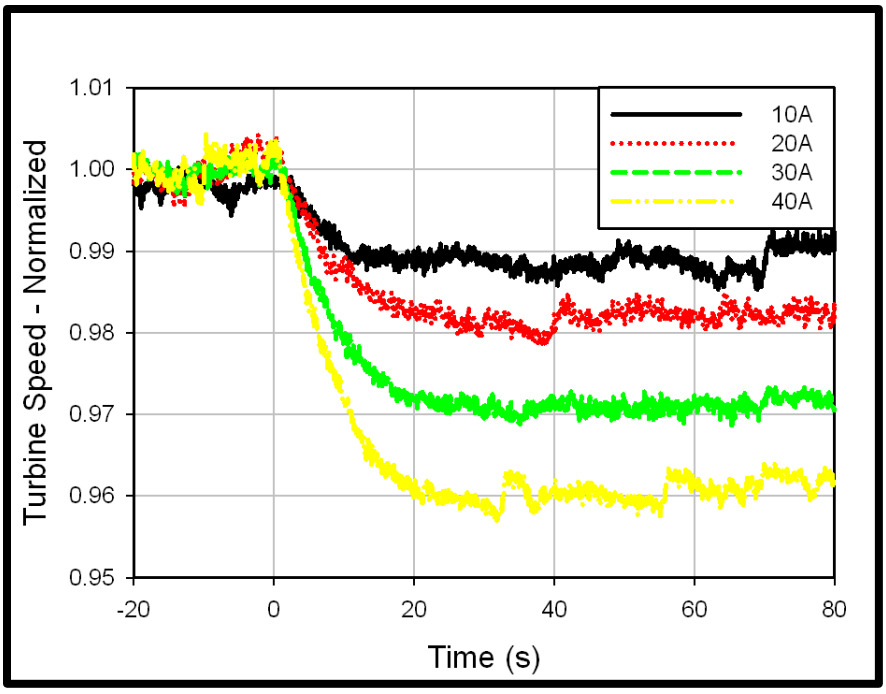

Figure 6.10: Normalized turbine speed vs. time –initial FC load comparison, 40% CA bypass: OL

Cathode inlet flow and turbine speed dynamics are both driven by changes in SOFC subsystem thermal effluent which is presented and discussed in Figures 6.11 and 6.12. As previously discussed, the amount of fuel flow necessary to maintain nominal turbine speed prior to load application is larger for greater amounts of CA by-pass. Given that the load application was a set value, but fuel flow was not, it is expected that the changes in system thermal effluent will vary for each CA by-pass valve position studied. The variation in SOFC thermal effluent dynamics with respect to CA by-pass is presented in Figure 6.11. Elevated fuel flow for the 60% CA by-pass case results in an elevated post-load Q_{gen} value, as compared to the similar values for the 35% and 40% CA by-pass cases. The dynamic response for the 40% case does follow suit with the expected trend producing a value that is slightly higher than the 35% CA by-pass case. The steady value for all three cases is between 94% - 95% of their respective pre-load values. Though the trends observed are expected, given the increase in fuel flow for greater amounts of cold air by-pass, the thermal effluent provided to the system vary by less than 0.1% of the

initial pre-load value for all three cases and is ultimately not significantly impacted by CA by-pass valve position. For the sake or reference, the Q_{gen} values for listed CA by-pass values of investigated, prior to the application of load were approximately 1388kW, 1439kW, and 1582kW respectively.

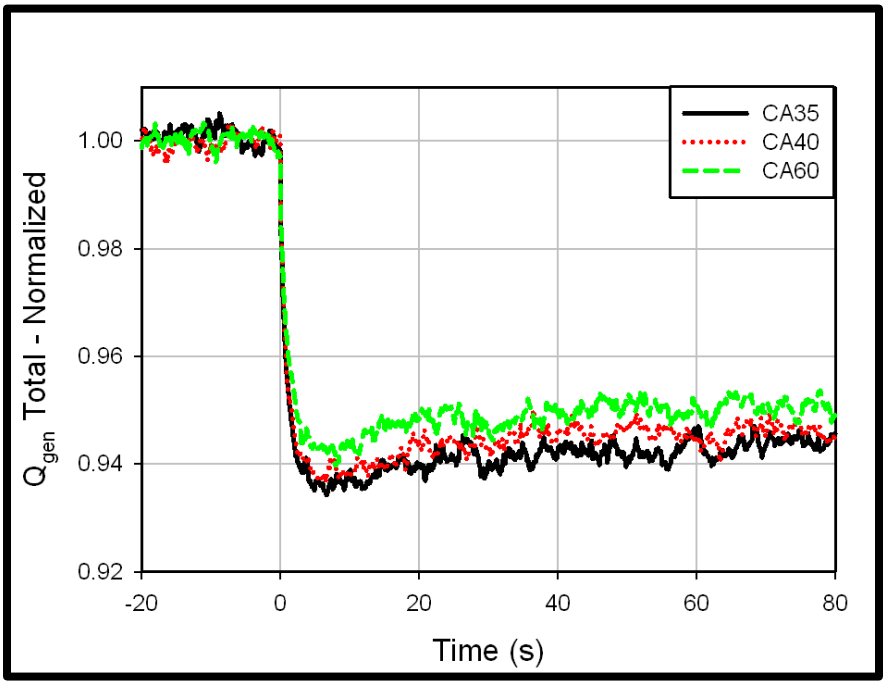

Figure 6.11: Fuel cell subsystem heat generated vs. time –CA by-pass comparison, 100A initial FC load: OL

At the point of load application at t=0s, the total thermal effluent from the fuel cell subsystem decreases rapidly to its minimum value approximately five seconds after load had been applied. Once load had been applied, a gradual increase in the thermal effluent values is observed for all three cases. This increase from the minimal value can be attributed to SOFC by-product heat generation. Once load is placed on the cells, the cells begin to consume hydrogen and thus the amount that is fed to the post combustor decreases. The slight increase in total subsystem thermal effluent is due to the gradual increase in the enthalpy of the combustion products as the amount of by-product heat generated in the SOFCs is further convected to the oxidant stream and increases the enthalpy of the streams in the combustion chamber. The result is increased Q_{gen} from the

SOFC subsystem. After approximately 60 seconds passes after the initial FC load was applied, a steady value of system thermal effluent is observed. The impact of initial FC load on thermal effluent is presented in Figure 6.12.

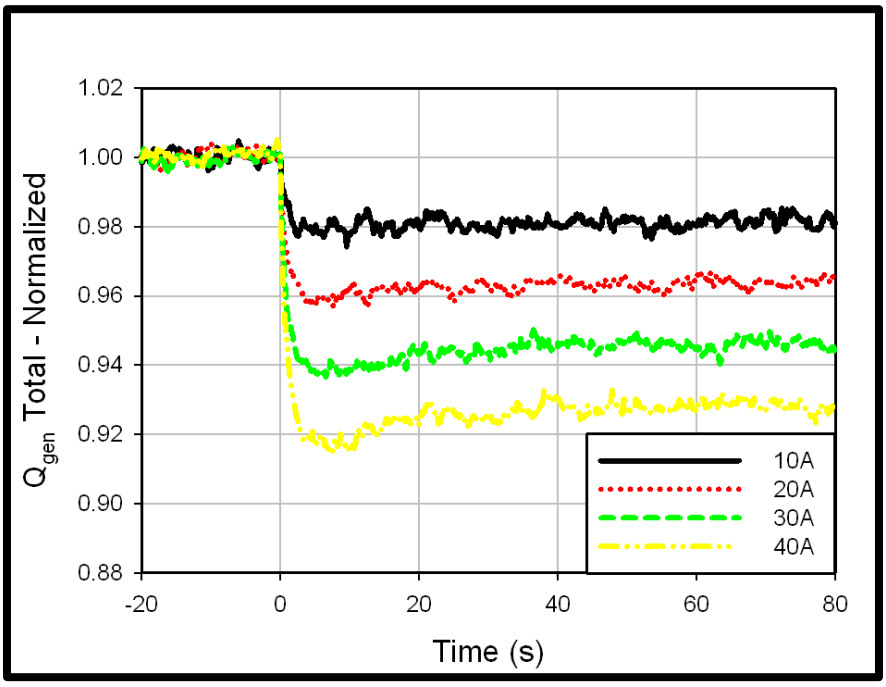

Figure 6.12: Fuel cell subsystem heat generated vs. time –initial FC load comparison, 40% CA bypass: OL

A deviation from the seemingly linear relationship between the initial FC load and the previously presented process parameters is presented by the subsystem thermal effluent case. For an initial FC load of 10A the FC subsystem thermal effluent appears to decrease by 2% as compared to a 7% decrease for the 40A case. The reason for this deviation is the impact of by-product heat generation from cell operation at higher loads. As the amount of initial load increases, the cell produces more by-product heat which results in a longer and more dynamic equilibration process for the FC subsystem. Immediately after load is applied, the cell is producing a significant amount of by-product heat that is partially absorbed by the cell to increase its temperature, but ultimately all of the continued by-product heat generation gets convected from the cell to the oxidant stream. As the thermal transport dynamics transition from partial cell heat up to full-

fledged oxidant stream heating, the enthalpy of the mixture in the combustor is increased, resulting in an increase in Q_{gen} and the gradually increasing profiles observed in Figure 6.12.

As presented in the figure, the minimum Q_{gen} value that is observed in the first 5-10 seconds after load application appears to follow the linear relationship with load. The steady value, approximately 60 seconds after the load has been applied, however, does not. This deviation is due to the previously discussed FC subsystem thermal equilibration phenomena that was previously discussed. The impact of this can be observed in the transient response of the profiles. The 10A FC load Q_{gen} profile is apparently constant once its minimum value has been reached; conversely, the 40A FC load Q_{gen} profile reaches a minimum value which is approximately 92% of its initial value then gradually increases and approaches 93% of its initial value after approximately 40s had passed from the point of load application.

As illustrated by Figures 6.11 and 6.12, increases in FC load ultimately result in decreases in physical heat from the SOFC/GT system which will manifest in decreased stream temperatures throughout the entire system. The stream temperature of particular interest to electrochemical start-up is FC inlet temperature. The impact of CA by-pass setting and initial FC load on FC inlet temperature is presented in Figures 6.13 and 6.14, respectively.

For the 35%, 40% and 60% CA by-pass cases, the pre-load inlet temperatures were 969.6K, 947.1K and 976.6K, respectively[1]**.**Given the relatively low values of initial FC loads (changes in thermal effluent only ranging between 2% - 8%) and thus heat removed from the system, the impact on inlet FC temperature is relatively small, with Figure 6.13 illustrating a maximum effect of approximately a 0.5% decrease in inlet temperature. The transient responses for all three CA by-pass settings are very similar with only a 0.1% difference in final values at 80s; thus, given their statistical

insignificance it can be concluded that control mechanisms of inlet temperature can be decoupled from CA by-pass setting.

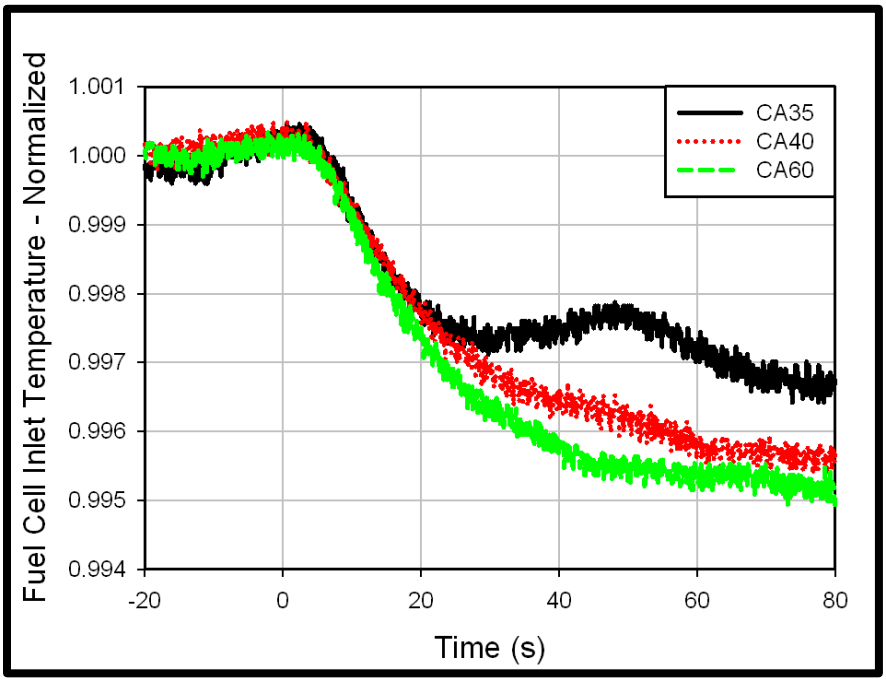

Figure 6.13: FC inlet temperature vs. time –CA by-pass comparison, 100A initial FC load: OL

Approximately 20 seconds after load had been placed on the FC to initiate electrochemical start-up; the decreasing trajectory of the FC inlet temperature for the 35% CA by-pass case quickly changed directions and increased, illustrating a local maxima between t=40s and t=60s, before continuing on its decreasing trajectory. Given the statistical analysis presented in Chapter 3, there is no significant effect of CA by-pass on cathode inlet temperature dynamic response during electrochemical start-up.

Though previously presented system parameters such as turbine speed, cathode inlet flow and system thermal effluent appear to achieve a steady value with in the 80 second transient response presented, the FC inlet temperature is continually responding to the reduction in physical heat from the system, as well as the system's transition to a new operating state. The delay to arriving at a steady value that is presented in both Figures 6.13 and 6.14 also support the presence and impact of heat exchanger dynamics on FC

inlet temperature. As illustrated by the base case, whose process parameters are presented in Figure 6.1, the steady FC inlet temperature value is not achieved after 600s of start-up transient response.

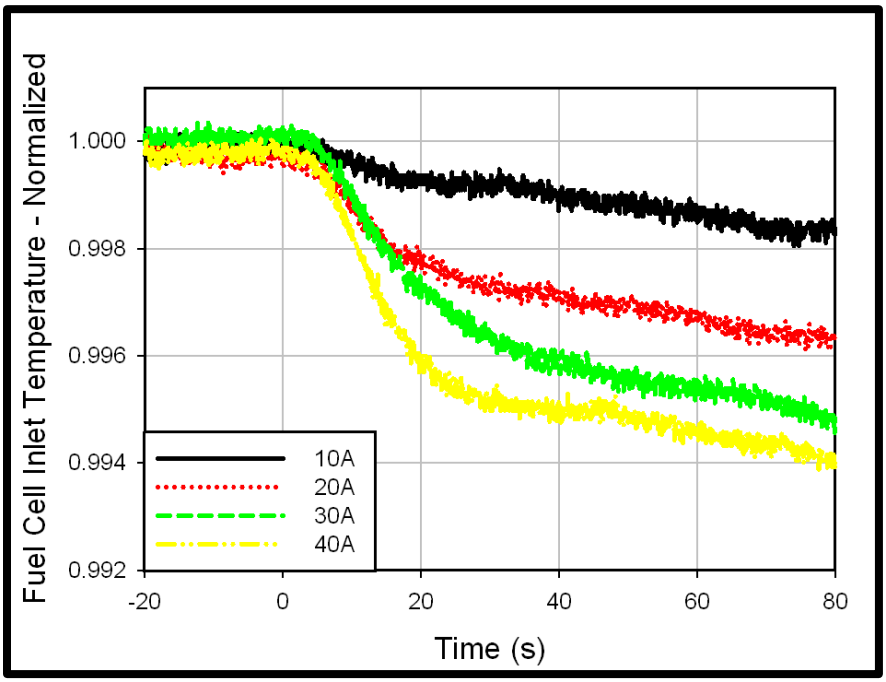

Figure 6.14: FC inlet temperature vs. time –initial FC load comparison, 40% CA bypass: OL

The transient system response during electrochemical start-up is initiated by changes in thermal effluent to the system that sequentially propagate to turbine speed, cathode inlet flow, cathode inlet pressure, and ultimately inlet temperature. As load is applied to the FC, the heat provided to the facility will decrease due to the conversion of what was thermal energy to both thermal energy and (virtual) electrical power. This change in system thermal effluent directly results in a decrease in thermal energy that is provided to the turbine and a subsequent decrease in turbine speed. The decrease in turbine speed initiates decreases in flow and pressure respectively. To illustrate the sequential nature of the decay of these parameters, first order time constants of turbine speed and cathode inlet flow and pressure were calculated. Their values were 7.12s, 7.76s, and 8.96s, respectively. As illustrated in Figure 6.1, the final parameter to reach its

steady value is cathode inlet temperature. The delay that is observed with respect to pressure can be attributed to recuperation between turbine exhaust and cathode inlet which results in a thermal lag due to heat exchanger dynamics. The impact of initial FC load on FC inlet temperature is presented in Figure 6.14. Given the four loads investigated, there is an immediate decrease in the FC inlet temperature at the point of load application due to the immediate removal of thermal energy from the system. The steep decrease in FC inlet temperature is then followed by a gradual decrease to what would be a "steady" FC inlet temperature. This gradual decrease can be primarily attributed to heat exchanger dynamics coupled with slight changes in thermal effluent, especially at higher loads due to the stabilization of by-product heat in the SOFC. The impact of increasing load on the decrease observed in FC inlet temperature appears to decrease at higher loads. This can directly be attributed to the nonlinear relationship between initial FC load and system thermal effluent, discussed in conjunction with Figure 6.12, as well as heat exchanger dynamics. As the initial FC load increases, the SOFC produces more byproduct heat thus resulting in a diminishing effect of increasing load. It is also evident from the investigation of Figure 6.14 that the increase in load also affects the temporal response, given the later occurrence of the transition from steep decrease to gradual decrease in FC inlet temperature values for higher initial FC load, causing a more expedient initial increase for larger initial load applications. Though the observed impact of initial FC load on the cathode inlet temperature is small (0.4% between 10A and 40A of initial FC load), it is within the instrument accuracy of the thermocouple and supports the existence of a correlation between cathode inlet temperature and initial FC load. FC inlet temperature directly impacts the thermal transport in the SOFC. As electrochemical activity is initiated and the cell starts to produce by-product heat, an accurate characterization of the FC inlet temperature transients will be essential in determining ways to mitigate the evolution and formation of harmful temperature gradients in the SOFC due to electrochemical activity. For that reason, analysis and presentation of the

data from Figures 6.13 and 6.14 will be used to address the internal thermal transport sensitivities of SOFC's. As previously stated, the impact of CA by-pass can be decoupled from cathode inlet temperature control can be decoupled from the implemented control strategies, but it is however apparent that the initial FC load will impact, though not significantly, the magnitude of the cathode inlet temperature given that the deviation in the data presented is within the instrument accuracy of the temperature acquisition device.

Another significant SOFC operational sensitivity that must be considered in the design of control strategies for electrochemical start up is changes in cathode inlet pressure. The decrease in turbine speed that results from the application of load on the SOFC results in a decrease in cathode inlet pressure, as illustrated in Figure 6.15. Significant changes in inlet pressure have been shown to contribute to mechanical failure of the SOFC [13].

Cathode inlet pressure is heavily correlated to turbine speed and that correlation is supported by the transient profiles presented in Figure 6.15. As previously discussed with regards to the turbine speed scenario, variation in ambient conditions is the key contributor to the deviation from the expected trend for the 40% CA by-pass experiment. The raw cathode inlet pressure values prior to the application of load are 353.95kpaa, 376.20kpaa and 357.74kpaa for the successive CA by-pass positions, respectively.

When load is applied at t=0s, the cathode inlet pressure, in conjunction with the turbine speed begins to rapidly decrease through the first 20 seconds of electrochemical start-up. At approximately the 20 second mark, the cathode inlet pressure profile starts to level, exhibiting a steady cathode inlet pressure value observed approximately 60 seconds after the application of initial load. The arrival at steady value occurs at approximately t=40s for the 40% and 60% CA by-pass cases, but at approximately t=60s for the 35% CA by-pass case. The "decrease-increase-stabilization" dynamic behavior observed in the

cathode inlet pressure profile for the 35% case is similar to the FC inlet temperature profile presented in Figure 6.13.

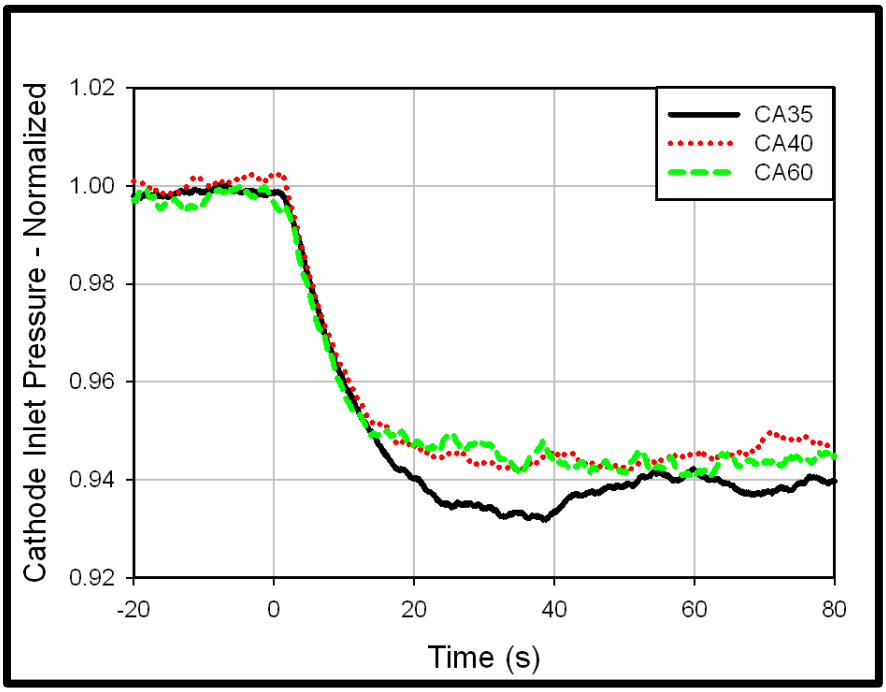

Figure 6.15: Normalized FC inlet pressure vs. time –CA by-pass comparison, 100A initial FC load: OL

It is believed that the transport phenomena presented for 35% CA by-pass occurs due to heat exchanger imbalance, but further investigation with a detailed parametric study around lower ranges of CA by-pass (between 25% and 40%) will be necessary to specifically identify the root cause of the dynamic effect. Once the steady condition is reached, all three CA by-pass cases have a value approximately 94% of their pre-load value. Though there appears to be an impact of CA by-pass setting on dynamic response of cathode inlet pressure, especially given the deviation at the 35% CA by-pass setting, the observed dimensionless changes do not fall outside of the tolerable bounds presented in the statistical analysis in Chapter 3 and thus cannot be deemed statistically significant. It is important to note, however that the impact of CA by-pass on the absolute pressure is significant given that the range between the 35% and 40% cases is nearly 23kPaa and the relative error calculated for the experiment is 2.08%.

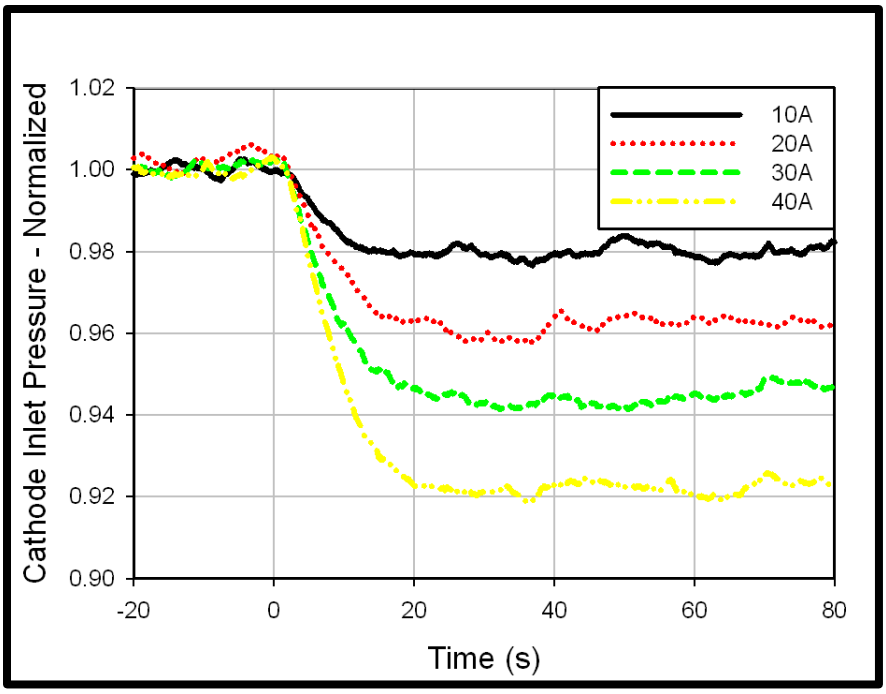

Figure 6.16: Normalized FC inlet pressure vs. time – initial FC load comparison, 40% CA bypass: OL

The dynamic impact of initial FC load on cathode inlet pressure is similar to that for turbine speed as well. As load incrementally increases, turbine speed decreases in a nearly linear fashion, as does cathode inlet pressure. Each 10A increase in FC load results in a 2% decrease in cathode inlet pressure for the 40% CA by-pass experiment. A quick and rapid decrease in cathode inlet pressure is observed for each initial FC load, with arrival at the new steady value occurring at approximately 20 seconds after the FC load had been applied.

6.3 SOFC Performance

This section presents results characterizing the impact of electrochemical start-up of and SOFC/GT hybrid system on SOFC operation and performance with an OL system configuration. Operational parameters such as stack power, operating voltage and polarization losses are presented and analyzed in aggregate or averaged manner for the

entire SOFC stack. Comparisons are made with respect to both CA by-pass valve position as well as initial FC load, as key decision parameters, during electrochemical start-up.

Stack power and operating voltage are key parameters used to characterize SOFC and hybrid system performance. Design and development initiatives for hybrid systems establish desired power production targets, with the majority of the power typically being required from the SOFC stack [1]. Though system and SOFC stack power, performance and efficiency are not of extreme importance when investigating the dynamics of system start-up, characterization of stack power, voltage trajectories and other electrochemical dynamic behavior through the electrochemical start-up period will be pivotal in maximizing speed and efficiency on the path to steady operation, as well as maximizing the operational efficiency once the final operational state has been achieved. Given the underlying purpose of this study, the impact of CA by-pass and initial FC load on operational voltage and stack power is presented and analyzed in Figures 6.17-6.19

The stack power is the product of current, operational voltage and number of cells in the stack. Since current density and the number of cells are fixed, the dynamic response of stack power is heavily influenced by the operational voltage of the stack. Operational voltage is heavily influenced by cell operational temperature, making operational voltage and stack power heavily dependent upon the SOFC internal thermal transport and dynamics.

As discussed in Section 6.2, CA by-pass valve position has an impact on FC inlet temperature and consequently will impact the average cell temperature both before the application of load and throughout the start-up transient. The average cell temperature prior to the application of load for the CA 35%, 40% and 60% cases were 968.1K, 949.5K and 978.3K, respectively[1]. Figure 6.17 illustrates the impact of CA by-pass setting, and thus initial average cell temperature, on SOFC stack power and voltage during start-up. As shown in the figure, once load is placed on the cell, operational voltage decreases in stepwise manner from the Nernst potential to its respective value

depicted in the figure, and stack power increases from zero, while at an electrochemically inactive state, to its respective value which is illustrated. The initial operational voltage at t=0s was approximately 1.037V, 1.032V, and 1.041V for the CA 35%, 40% and 60% cases, respectively. The initial SOFC stack power at t=0s was approximately 71.58kW, 71.22kW, and 71.83kW for the CA 35%, 40% and 60% cases respectively. Though the CA by-pass impacts the initial and average absolute FC temperature, the impact of those thermal states on electrochemical operation is seemingly small. Initial stack power only varies on a range of <1kW with respect to CA by-pass valve position and voltage only varies on a range of <0.1 volts. The dynamic response of these electrochemical parameters also appear to be minimally affected as well

Once load is placed on the cell, these initial electrochemically active values for both operating voltage as well as stack power take effect. Given the system thermal transients, and the cooling effect that the removal of heat from the system has on the SOFC, both the voltage and stack power gradually decrease throughout the first 20 seconds of the start-up transient response. After 20 seconds, the point at which most system operating parameters are near their post-load application steady values, the stack power and operating voltage follow suit and steady values are reached. From inspection, the dynamic response throughout the first 20 seconds of start-up appears to be consistent among all three CA by-pass valve positions.

The dynamic response of both stack power and operating voltage, illustrated in Figure 6.17, appears to be minimal throughout 80 seconds of transient system response, exhibiting an essentially steady profile irrespective of the amount of initial FC load for OL electrochemical start-up. In comparison to Figure 6.17, it is evident that some dynamic response near the beginning of start-up occurs for stack power. Due to scaling, identification of the minor inflection at the beginning of the start-up period is difficult, but furthermore; the amount of change in stack power during that thermal dynamic response (~0.1kW), as illustrated in Figure 6.17, is minor relative to the steady state

values of stack power. The impact of initial FC load on the resulting SOFC stack power during electrochemical start-up is presented in Figure 6.18.

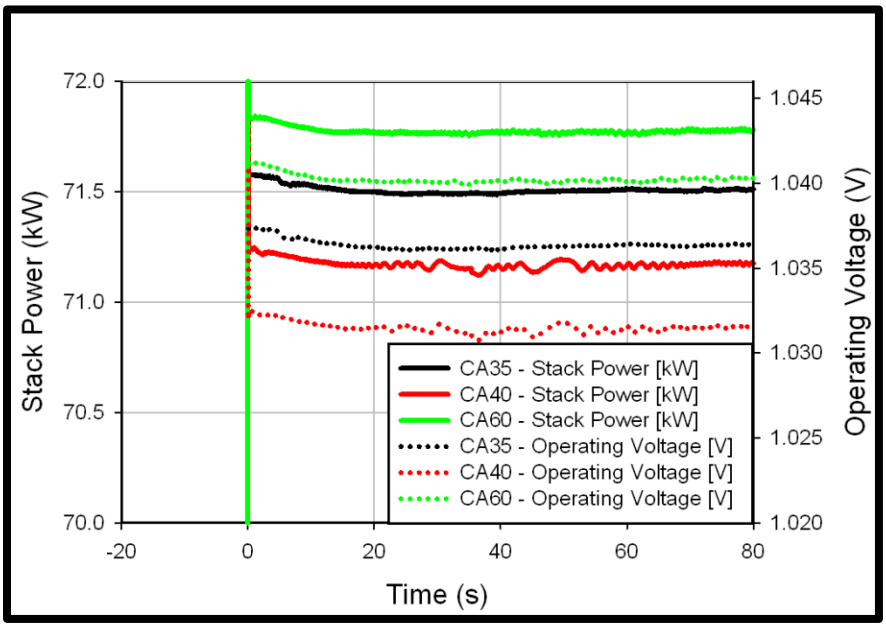

Figure 6.17: Stack power and operating voltage vs. time – CA by-pass comparison, 100A initial FC load: OL

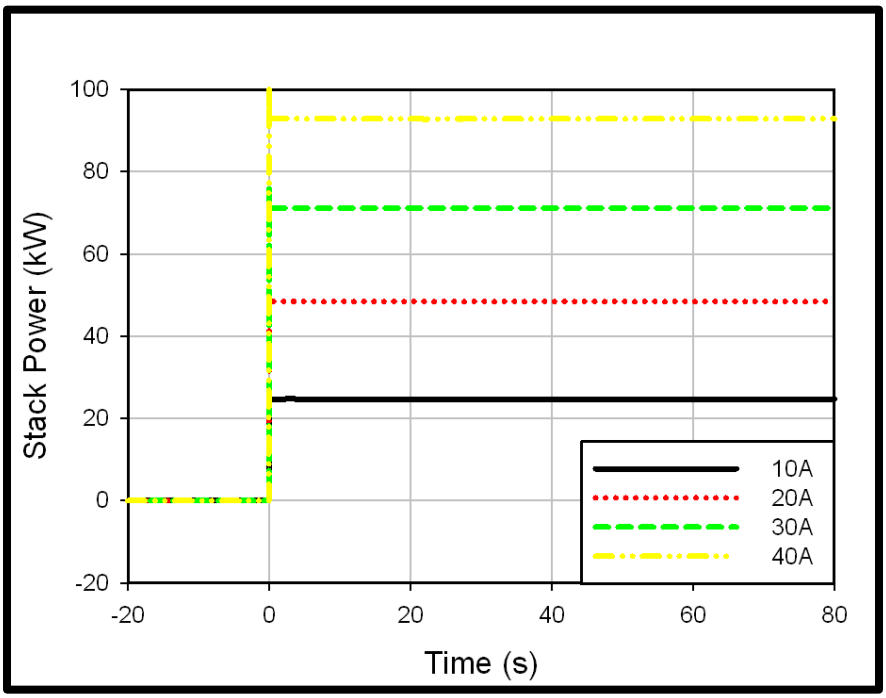

Figure 6.18: Stack Power vs. time – initial FC load comparison, 40% CA bypass: OL

As illustrated, the effect on the secondary dynamic response of stack power is minimal, given the small applications of load investigated and thus the minor effects on system thermal transport. As initial load application increased, more power is drawn from the stack and the relationship between stack power and initial FC load appears to be nearly linear within this 10A – 40A initial FC load regime.

The impact on operating voltage, though modest, is more readily identified. As illustrated in Figure 6.19, once load is placed on the SOFC stack at t=0s, the stack voltage significantly decreases from its Nernst potential down to its operational value. Larger increases in load result in larger decreases in stack voltage due to increased polarization and ohmic losses. At higher loads (30A and 40A) dynamic response of voltage to thermal transients is observed in the first 20 seconds after the load was applied. The elevated level of heat removal from the system for higher initial FC loads coupled with the increased by-product heat generated from cell operation results in a slightly elevated cell temperature.

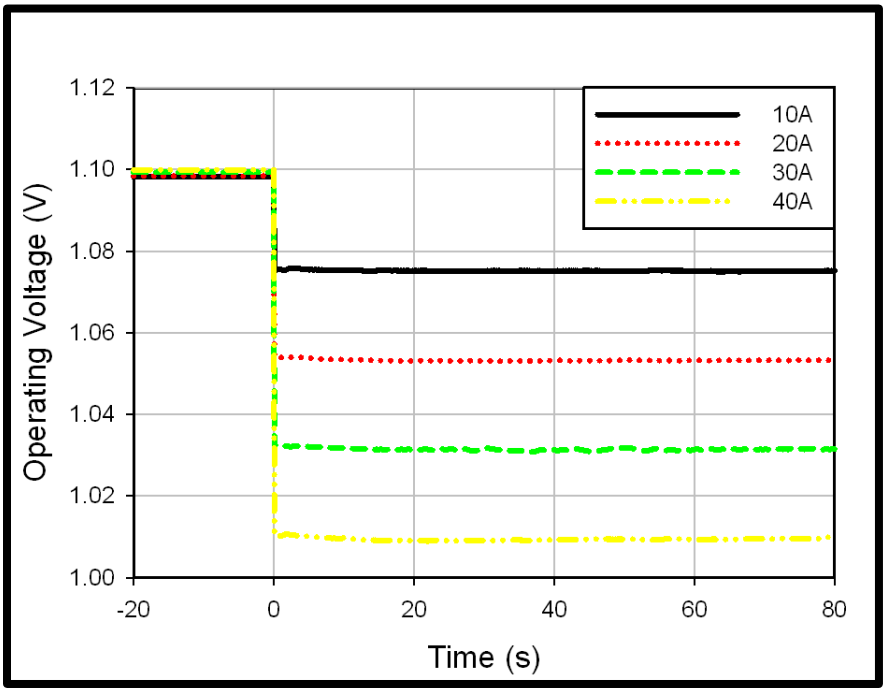

Figure 6.19: Operating Voltage vs. time – initial FC load comparison, 40% CA bypass: OL

The electrochemical component of the 1-D, real time SOFC model calculates operating voltage by determining the maximum possible cell potential, known as the Nernst potential, and subtracting from it electrochemical polarization terms that account for losses due to cell operation. The Nernst potential is primarily influenced by reactant concentration in the fuel and oxidant streams as well as SOFC operational temperature. The impact of CA by-pass valve position and initial FC load on the cell Nernst potential is presented in Figures 6.20 and 6.21 respectively.

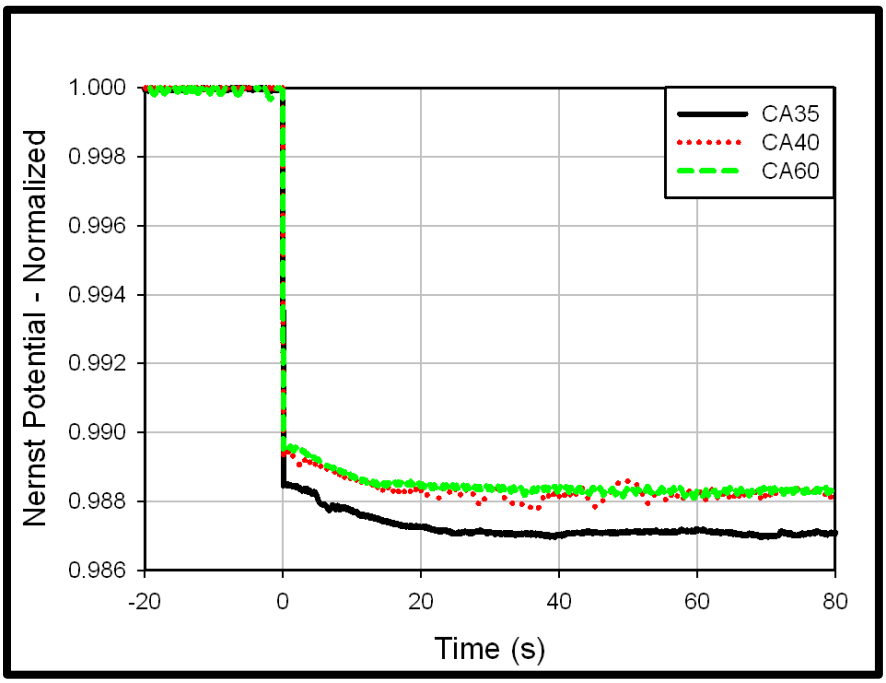

Figure 6.20: Normalized average Nernst potential vs. time – CA by-pass comparison , 100A initial FC load: OL

Prior to the application of load, the SOFC stack Nernst potential for the investigated CA by-pass valve positions cases were 1.093V, 1.098V and 1.091V respectively. Nernst potential is inversely related to cell temperature so the relative Nernst potentials listed are in alignment with the average pre-load cell temperatures listed earlier in this section. Figure 6.20 presents the normalized transient response of stack Nernst potential for a 30A application of initial FC load for the three CA by-pass

positions investigated. The slight decrease in Nernst potential after the 30A load was applied to the SOFC stack was approximately 1.15% for the 35% CA by-pass case.

Both the 40% and 60% CA by-pass cases have very similar normalized responses with regards to transient dynamics and magnitude. Both cases have an initial post-load Nernst potential approximately 1.05% less than their pre-load steady state values. Similar dynamic response from the initial operational Nernst potential values at t=0s to near steady state values at t=20s is observed for all three CA by-pass cases. The similarity in normalized behavior can be attributed to the balancing effect between composition and temperature for each case. The 40% CA by-pass case had the lowest average cell temperature and a fuel flow noticeably lower than the 60% CA by-pass case. The 60% CA by-pass case had the highest average cell temperature and the largest fuel flow rate of the three CA by-pass cases. The fuel flow and average cell temperature values relative to one another, for the 40% and 60% CA by-pass cases, had competing effects and resulted in very similar normalized profiles in both magnitude and transient response. The transient dynamic that occurs from t=0s to approximately t=40s after the 30A of load is placed on the FC is due to SOFC transient response to competing effects of heating due to by-product heat generation from cell operation and cooling due to the decrease in FC inlet temperature. This causes a slight increase in average SOFC temperature resulting in a gradual decrease in Nernst potential with respect to time. Though trends are observed between the Nernst potential profiles for the various CA by-pass settings, they vary in magnitude by less than 0.2% and thus CA by-pass appears to have a minimal effect on cell Nernst potential. Increases in initial FC load resulted in the increased consumption of hydrogen by the fuel cell, thus decreasing Nernst potential as illustrated in Figure 6.21, which presents the impact of initial FC load on the transient response of Nernst potential for electrochemical start-up with 40% CA by-pass.

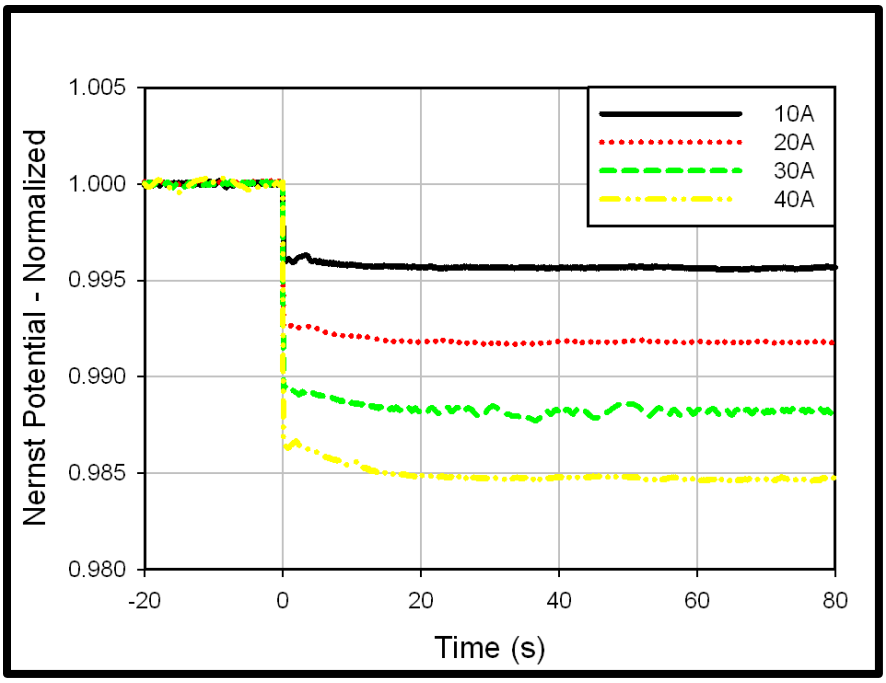

Figure 6.21: Normalized average Nernst potential vs. time – initial FC load comparison, 40% CA bypass: OL

As the magnitude of initial FC load applications increase, the amount of heat removed from the system increases as well, thus initiating more dynamic thermal transients both internally in the SOFC as well as in the working fluid of the system. This behavior is illustrated by the increased curvature in the normalized Nernst potential profiles, presented in Figure 6.21, for larger load applications, between t=0s and t=20s. The steady Nernst potential value is achieved for all loads at 20 seconds after the initial FC load was applied.

The most dominant of the electrochemical polarization terms is activation loss. Activation loss, accounts for the amount of energy utilized to overcome the necessary activation energy for electrochemical activity. SOFC electrochemistry is heavily correlated with temperature, thus activation loss is influenced by the thermal condition of the cell. As illustrated in Figure 6.22, the 40% CA by-pass scenario has the activation loss profile of the greatest magnitude, followed by the 35% case and the 60% case successively. This illustrates the trend of increased activation loss for decreased

temperature[1] as discussed in Section 6.2. The dynamic behavior throughout the first 80s of start-up transient response illustrates a gradual decrease in activation loss for all three cases. This gradual decrease aligns with gradual increase in average cell temperature via by-product heat generation superseding the decreasing FC inlet temperature; stabilization occurs approximately 150s – 200s after the initial FC load has been applied.

As load is applied to the SOFC during electrochemical light off, the average temperature of the SOFC slightly increases through the first 400s of the start-up transient response, resulting in the gradual decrease in activation loss through the first 80 seconds of electrochemical start-up as illustrated in Figure 6.22.

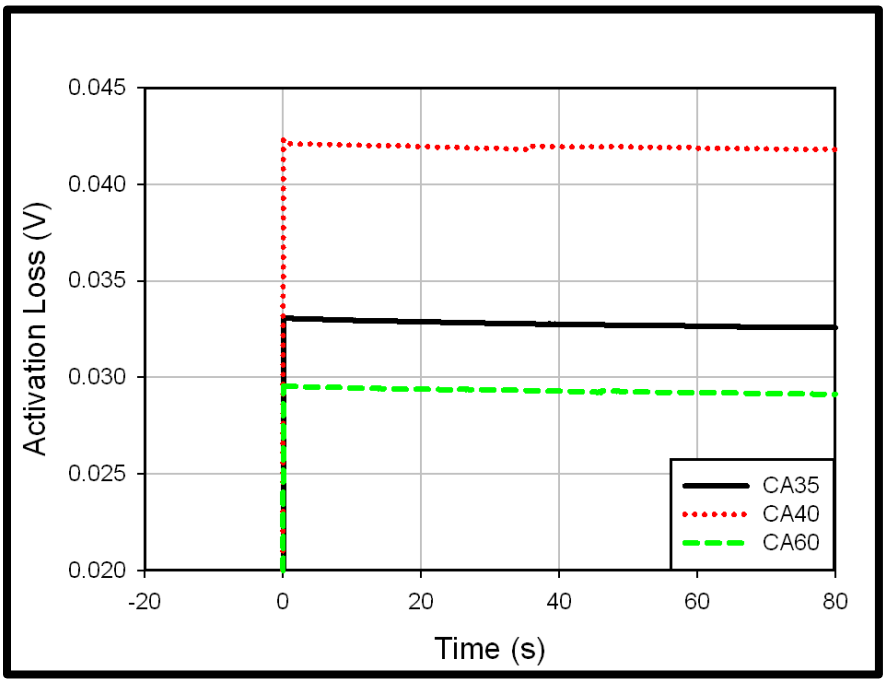

Figure 6.22: Activation loss vs. time – CA by-pass comparison, 100A initial FC load: OL

After approximately 400s of operation a maximum temperature was observed at the FC outlet. Beyond the 400s mark, a gradual decrease in cell temperature was observed due to the downstream cooling effect from the oxidant stream, which suggests that the general decreasing trends of activation loss, presented in Figure 6.22 through the

first 80s of start-up transient response could potentially reverse as the cell cools later in the transient. This is actually the case as illustrated in Figure 6.23.

Figure 6.23 presents the impact of initial FC load on activation loss for electrochemical start-up with 40% CA bypass for 600s after load has been applied. As expected, increased current draw results in increased activation loss and the impact of enhanced thermal transients is observed for higher initial current draw as well. There is initially a decrease in activation loss from the time of load application at t=0s to approximately the 200 – 300s mark, and this is most evident for higher amounts of initial load. At that point, a gradual increase in activation loss is observed. This transient response is primarily due to the impact of thermal transport on SOFC operating temperature. Immediately after start-up is initiated, the average cell temperature slightly and gradually increases until the transition to cell cooling occurs due to the cooling effect of the cathode inlet stream given its decreased temperature, causing a decrease in average cell temperature and consequently activation loss.

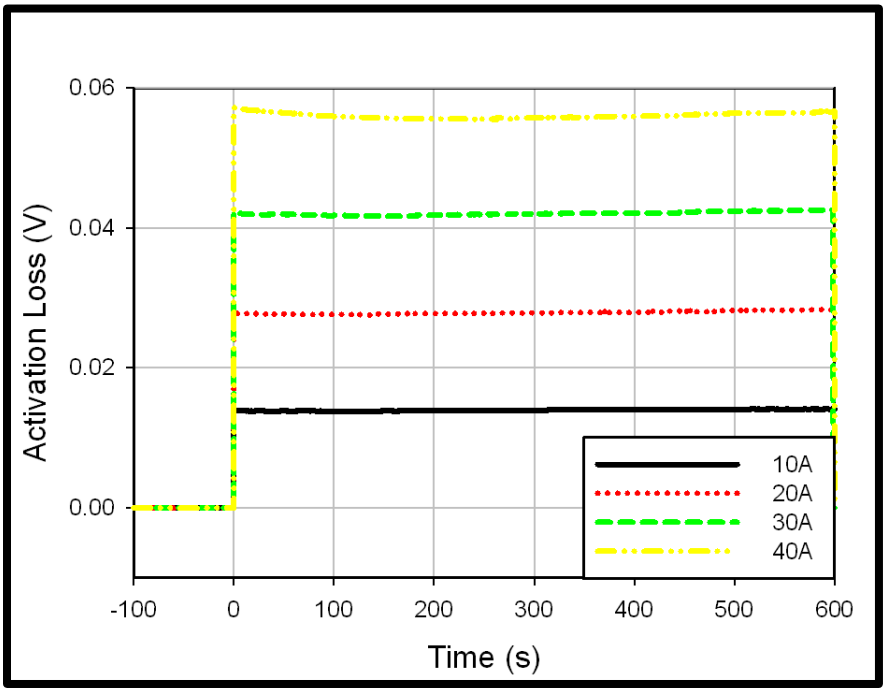

Figure 6.23: Average activation loss vs. time – initial FC load comparison, 40% CA bypass: OL

The impact of CA by-pass valve position and initial FC load on diffusion loss, is presented in Figures 6.24 and 6.25, respectively.

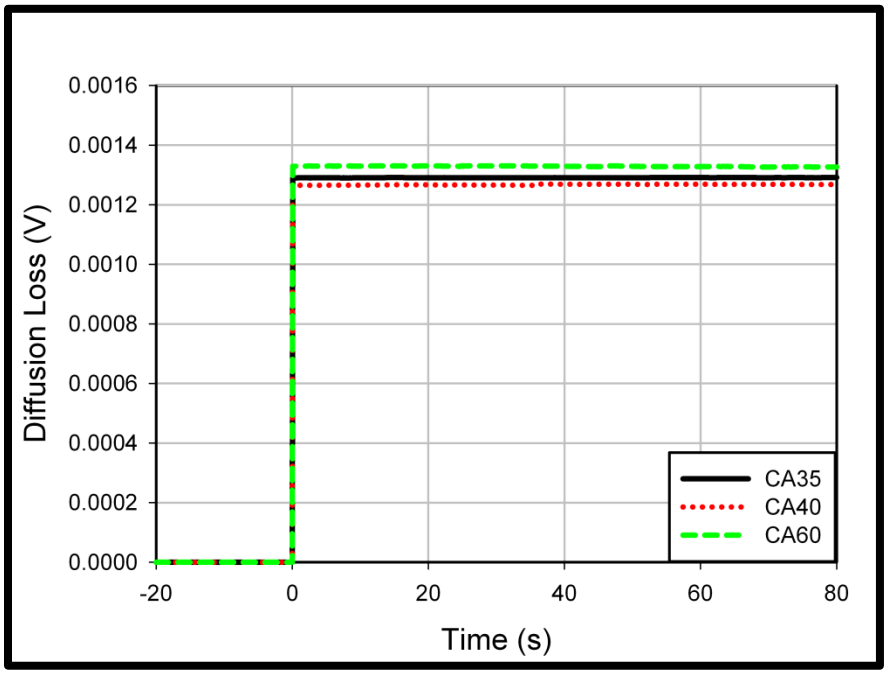

Figure 6.24: Average diffusion loss vs. time – CA by-pass comparison, 100A initial FC load: OL

Diffusion polarization accounts for the loss of concentration of electrochemically active reactants due to diffusion through porous electrodes. As illustrated in Figure 6.24, the diffusion loss profiles are nearly coincident and essentially steady from the point of load application throughout the transient response, with little secondary transients for the given design.

Figure 6.25 presents the impact of initial FC load on diffusion loss for electrochemical start-up with 40% CA by-pass. The steady profiles observed in Figure 6.24 appear to translate to the load comparison plot in Figure 6.25 as well. There is minimal to no effect of thermal transport observed by the diffusion polarization. This can be attributed to the relatively low changes in average cell temperature throughout the transient and the significantly low magnitude of diffusion loss.

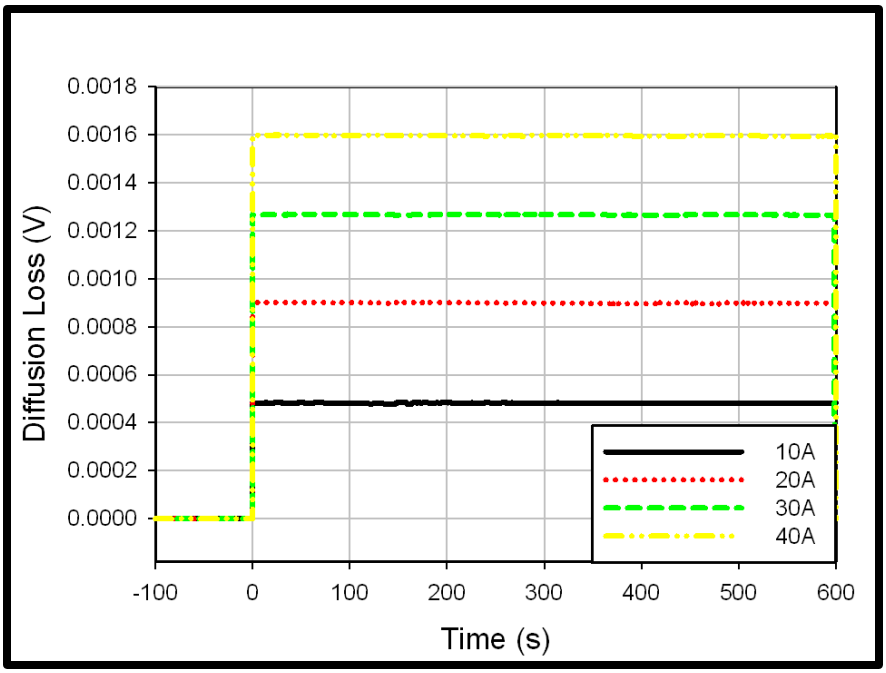

Figure 6.25: Average diffusion loss vs. time – initial FC load comparison, 40% CA bypass: OL

Ohmic loss accounts for the loss in voltage due to the resistance of electrical transport through the SOFC. Similarly to general polarization phenomena, ohmic loss decreases with increasing temperature; additionally, its magnitude is less than that of activation loss. The ohmic loss profiles illustrate very similar trends to those for the activation loss and are presented in Figures 6.26 and 6.27.

As illustrated in Figure 6.26, the ohmic loss decreased with increasing temperature. The ohmic loss profile with the greatest magnitude existed for the 40% CA by-pass case, and the lowest magnitude profile existed for the 60% CA by-pass case; thus supporting the existence of this trend[1] as discussed in Section 6.2. The gradual decrease in loss terms due to slightly increasing cell temperatures early in the start-up phase is observed for the ohmic loss as well.

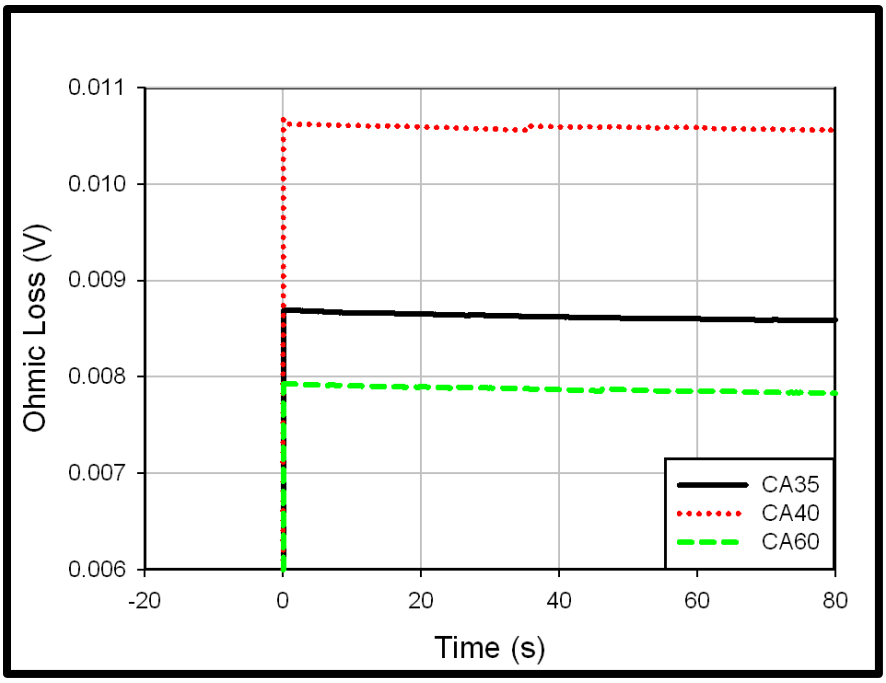

Figure 6.26: Average ohmic loss vs. time – CA by-pass comparison, 100A initial FC load: OL

The impact of initial FC load on ohmic loss profiles, which is presented in Figure 6.27, illustrates the effect of internal SOFC thermal transients on ohmic loss. Unlike Figure 6.26, 6.27 present 600s of transient data which shows the impact of the transition from cell heat up to cell cooling on ohmic loss. Similar to the activation loss profiles, presented in Figure 6.23, as the cell temperature rises, ohmic loss values decrease, but once the cell approaches steady state, cooling from the inlet air stream begins to take effect and ohmic losses begin to slightly increase due to decreasing temperature. This transient response is not glaringly significant, since it is only observed for higher amounts of initial FC load and is minor in nature, but it does however illustrate the impact of system thermal transients on cell operation and performance.

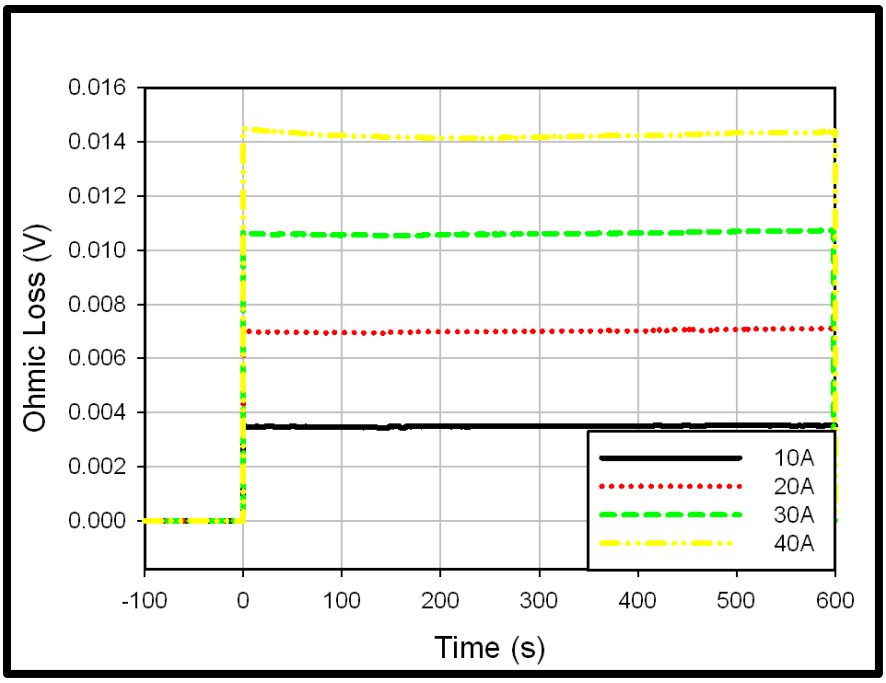

Figure 6.27: Average ohmic loss vs. time – initial FC load comparison, 40% CA bypass: OL

6.4 Distributed Comparison

One of the key characteristics of the 1-D, real-time SOFC model used in the HyPer facility is its ability to provide internal operating diagnostics of a SOFC stack, operating "in-the-loop" with a gas turbine, in distributed manner. This section of the dissertation utilizes that capability by presenting the impact of some key operating parameters such as solid SOFC temperature, current density, spatial temperature gradient and Nernst potential in distributed manner, with accompanying analysis. Figures 6.28 and 6.29 present the solid SOFC temperature while varying CA by-pass valve positions for 30A of initial FC load and while varying initial FC load for 40% CA by-pass, respectively.

As illustrated by the spatio-temporal temperature profile of the base case in Figure 6.1, for all experiments utilizing a humidified hydrogen fuel feed, the SOFC stack is at a uniform temperature prior to initial load application at t=0s. Figure 6.28 demonstrates that uniform, pre-load cell temperatures are different for the different CA

by-pass valve positions given the effect of CA by-pass valve position on inlet FC temperature, which has been previously discussed. Though the pre-load solid temperatures are different for the three by-pass valve position cases, the dynamic behavior appears to be similar irrespective of CA bypass setting.

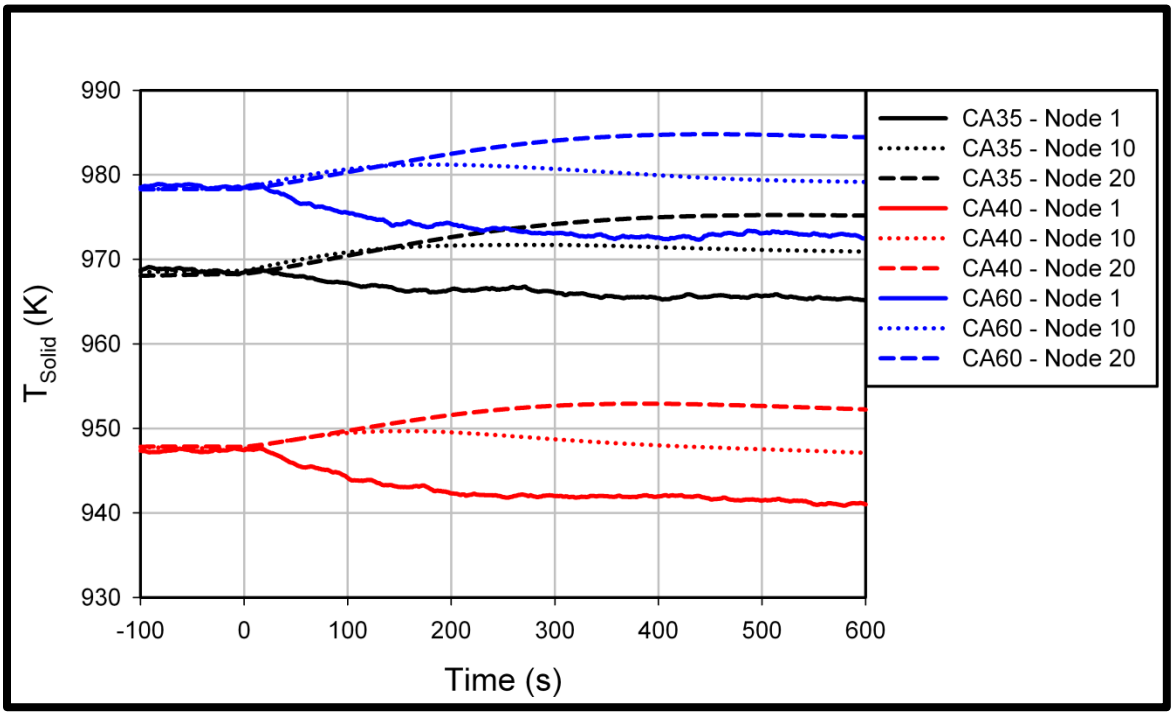

Figure 6.28: Local solid temperatures along the entire SOFC length vs. time – CA by-pass comparison, 100A initial FC load: OL

Application of load on the SOFC initiates the evolution of a non-uniform temperature profile in the SOFC. As previously stated, prior to load being applied to the FC, the SOFC stack had a uniform temperature distribution for all three CA by-pass, cases as illustrated in Figure 6.28. Once load is applied, the combination of by-product heat generation due to cell operation coupled with cooling at the inlet due to decreased FC inlet temperature, results in a profile that monotonically increases from FC inlet to exit. Such a profile is similarly represented in Figure 6.2.

The trends for all five nodes (points of calculation) are very similar for each of the CA by-pass cases of interest. Particularly for the 40% and 60% CA by-pass cases, there is an initial increase in temperatures at node 10 in the downstream portion of the SOFC and

an initial decrease at the inlet of the SOFC that lasts for approximately the first 400s and 300s of start-up respectively. After 400s of startup, when the temperature at the exit of the fuel cell has reached its maximum, a gradual decrease in local cell temperatures along the length of the SOFC is observed (i.e. cooling phase).

For the 35% case, though similar trends are observed, the overall impact on SOFC temperature dynamics appears to be less significant. The decrease at the inlet node appears to be more gradual than the 40% and 60% CA by-pass cases, and the overall cell ΔT from inlet to outlet of the fuel cell appears to be less significant as well. The 35% CA by-pass valve position case has a cell ΔT of approximately 10K, with the 40% and 60% cases having ΔT values of approximately 11K and 14K respectively, 600s after load application. Given that the heat generation terms are very similar for each CA by-pass case, as illustrated in Figure 6.32, and the ΔT difference between 35% CA and 40% CA settings is very small, the trend in variation in ΔT can be primarily attributed to the differences (or lack thereof) in air flow (i.e., oxygen utilization) for the respective CA by-pass valve positions.

As illustrated in Figure 6.6, the pre-load mass flows for electrochemical start-up for 30A of initial load were approximately 1.41kg/s, 1.41kg/s and 1.2kg/s respectively. These result in initial oxygen utilization values of 1.74%, 1.74% and 2.04% as illustrated in Table 6.1. Once the load is applied, the cathode inlet flow decreases thus increasing the O_2 utilization values to 1.79%, 1.79%, and 2.09% respectively, once a steady flow has been attained. These very low oxygen utilization values, especially for the low initial FC load values explored in the OL scenario, provide significant amounts of excess air which contributes to the mitigation of the evolution of potentially harmful temperature gradients and very low cell ΔT.

Table 6.1: O_2 fuel utilization values for electrochemical start up: OL

		10A	20A	30A	40A
CA 35%	t=0s	0.57%	1.15%	1.74%	2.30%
	Post-Load	0.58%	1.17%	1.79%	2.42%
CA 40%	t=0s	0.58%	1.16%	1.74%	2.33%
	Post-Load	0.59%	1.18%	1.79%	2.41%
CA 60%	t=0s	0.69%	1.38%	2.04%	2.71%
	Post-Load	0.70%	1.41%	2.09%	2.83%

Increases in FC load result in an increase in both SOFC stack by-product heat generation as well as removal of heat from the system. These effects combine to stimulate more significant internal SOFC thermal dynamics. The dynamic effect of initial load step size on localized SOFC temperature dynamics during electrochemical start-up with 40% CA by-pass is illustrated in Figure 6.29.

There is a variation of approximately 4K in the initial uniform SOFC temperature as illustrated in Figure 6.29. This variation can be primarily attributed to changes in ambient conditions. As illustrated, the dynamic behavior for all of the various load applications exhibit similar behavior. All of the profiles for the respective increases in load illustrate an evolution of a temperature profile that gradually increases from entrance to exit of the fuel cell. Similarly displayed for the CA by-pass comparison in Figure 6.28, the dominant driver of the thermal dynamic behavior at node one is the cooling from the inlet stream, thus resulting in a gradual decrease in the SOFC temperature at the inlet throughout start-up. A more significant decrease is observed for larger increases in load with approximate decreases in temperature at node one, relative to its pre-load value, ranging between 3K for 10A of initial load to 8K for 40A of initial load, 600s after start-

up. The local temperature at node 10, in the interior of the SOFC, initially increases through the first 100 – 200 seconds of the transient, then the cooling effect from the FC inlet stream starts to take effect near the center of the cell, and the local temperature at node 10 starts to decrease. The local temperatures at node 10 appear to be very close in magnitude, 600s after initial load application, despite the minor offset in pre-load cell temperatures.

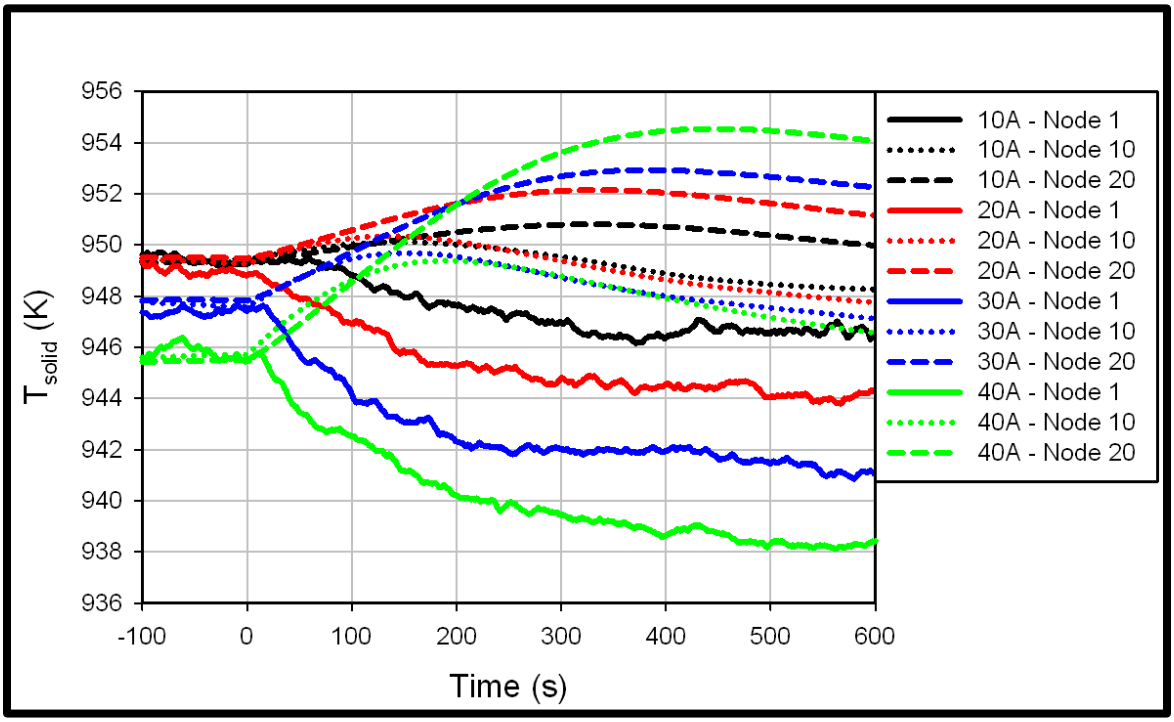

Figure 6.29: Local solid temperatures along the entire SOFC length vs. time – initial FC load comparison, 40% CA bypass: OL

The competing effects of by-product heat generation from cell operation and the cooling effect of the FC inlet stream are best illustrated by the temperature profile at the exit of the SOFC. For all of the load applications, the local temperature at the fuel cell outlet gradually increases through the first 300s-500s after load has been applied, depending on the amount of load that is placed on the SOFC stack. Once a local maximum temperature is reached at the FC exit, the effect of SOFC cooling from the decreased FC inlet temperature begins to take effect downstream and the temperature begins to decrease. At this point the entire cell is in a cooling phase and all local

temperatures along the length of the FC are gradually decreasing. The final cell ΔT values observed at t=600s are approximately 3.5K, 7K, 11K and 16K. This nonlinear relationship between initial FC load and cell ΔT illustrates the combined, non-linear effect of increased cooling due to decreasing inlet cell temperature, the formation of by-product heat in the operating SOFC and decreases in air flow through the cathode due to decreases in turbine speed.

The impact of CA by-pass valve position on current density for electrochemical start-up utilizing 30A of initial load is presented in Figure 6.30. The primary drivers behind the variations observed in this plot are average cell temperature and cell ΔT. As illustrated in Figure 6.28, the average cell temperatures prior to the application of load were approximately 968.1K, 947.6K, and 978.3K for the 35%, 40% and 60% CA by-pass cases, respectively. The 35% and 60% CA by-pass cases have initial average cell temperatures that are very close (~10K difference), with the 40% case being significantly lower. This decrease in initial average temperature, pre-load and throughout the start-up period, results in a more evenly distributed local current density profile. The decreased temperature creates an environment that is less favorable for electrochemical activity which requires a decrease in current density at the inlet and an increase at the exit given similar fuel utilizations, thus the impact on current density profile.

For a given amount of current draw, the amount of fuel that is required is fixed, thus the mole fraction of H_2 both entering and exiting the fuel cell is predetermined, based upon the fuel flow and current draw. A decreased average cell temperature limits the amount of electrochemical activity that can occur at any one location along the fuel cell and requires a more uniform current density distribution at the point of load application. This results in lower amounts of current being drawn in the upstream portion and increased amounts of current being drawn from the downstream portion of the FC, for the 40% CA by-pass case relative to the 35% and 60% cases, forming a more evenly distributed local current density profile for the 40% case.

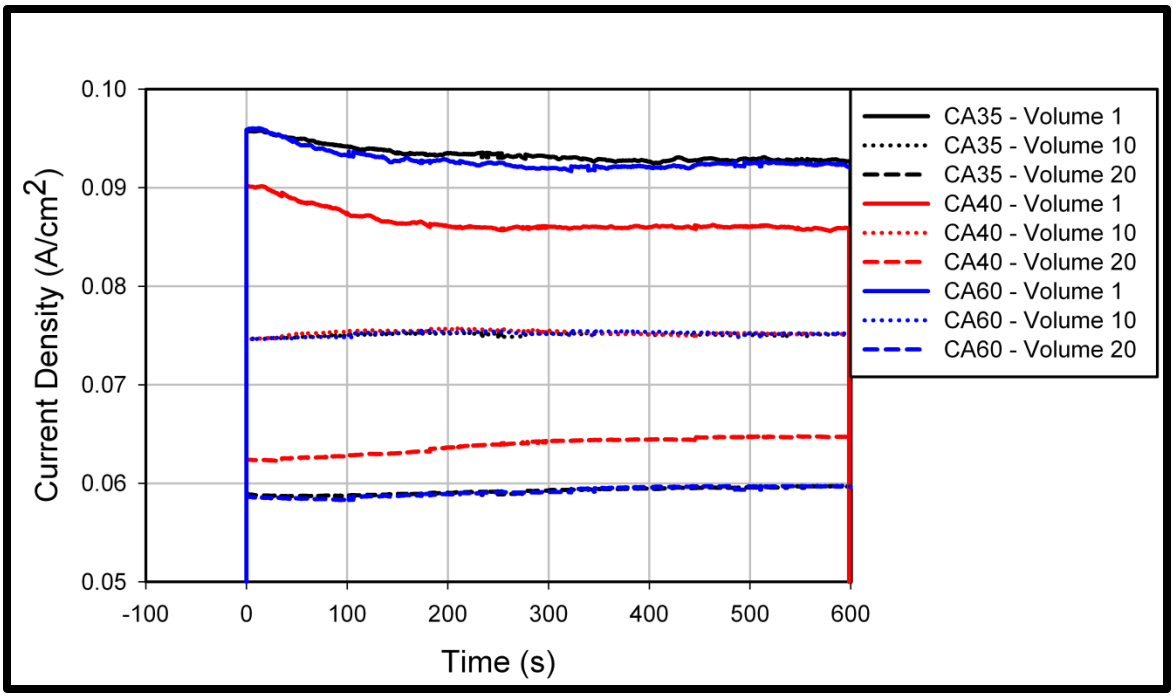

Figure 6.30: Local current density along the entire SOFC length vs. time – CA by-pass comparison, 100A initial FC load: OL

Given the impact of temperature on the local current density distribution for the 40% CA by-pass case it would be expected that more significant variation would be observed between the 35% and 60% CA by-pass cases. This is not the case, however, due to decreased fuel for the electrochemical start-up experiment with 35% CA by-pass. As previously stated, the fuel flow necessary to maintain a nominal turbine speed of 40,500 RPM was higher for start-up with 60% CA by-pass than with 35% CA by-pass. The decreased fuel flow, which results in decreased composition of H_2 at the fuel cell exit initiates a redistribution in the local current density profile, resulting in decreased local current density at the outlet and an increase at the inlet as illustrated in Figure 6.30.

Increases in load will generally impact the magnitude of the current density profile as is illustrated in Figure 6.31. In addition to the increase in magnitude that accompanies increases in current density, a more evident dynamic effect is exhibited for larger amounts of current draw as well. The local current density for volumes 1, 10, and 20 for 10A of initial FC load appear to be nearly constant throughout the 600s of start-up

illustrated, as compared the initial dynamic response that is displayed for 40A of initial load.

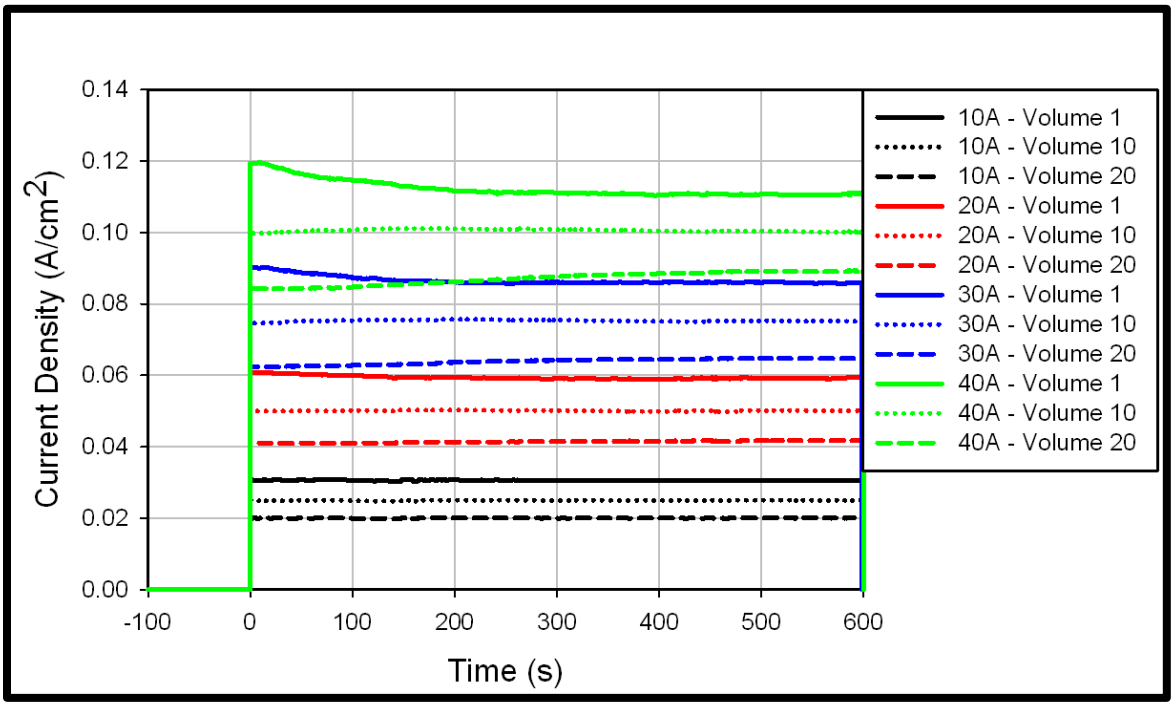

Figure 6.31: Local current density along the entire SOFC length vs. time – initial FC load comparison, 40% CA bypass: OL

For the 40A case illustrated in Figure 6.31, the initial current density at the inlet of the SOFC is approximately 0.12A/cm^2, and the initial current density at the exit is approximately 0.085 A/cm^2. The impact of thermal transients on electrochemical activity are displayed by the decrease in current density at the inlet due to cell cooling and the gradual increase in local current density at the exit of the SOFC due to by-product heat generation. The current density at the exit of the SOFC appears to gradually increase through the first 400s of start-up transient response presented, which aligns with the increase in exit temperature observed in Figure 6.2.

By-product heat generation in an electrochemically active SOFC is directly related to current draw and operating cell voltage as illustrated by equation 4.30 in Chapter 4. As illustrated by the equation, as current draw increases, so does by-product heat, but as voltage increases, by-product heat decreases.

Operating SOFCs produce two types of energy transfers, and they are electrical power and heat. Due to the first law of thermodynamics, the maximum amount of energy that can be converted from the operation of the cell, operating off of a humidified hydrogen feed, is the energy associated with the formation of water. As previously discussed, SOFCs operate more efficiently at higher temperatures, producing more electrical power through an increase in voltage and decreasing the amount of heat dissipated by cell operation.

Accordingly, the key driver behind the amount of by-product heat produced during cell operation remains the local current density, thus the strong similarities in the trends exhibited in Figure 6.32 which illustrates the impact of CA by-pass valve position on by-product heat generation during electrochemical start-up with 30A of load, and Figure 6.30 which presents local current density in the same fashion.

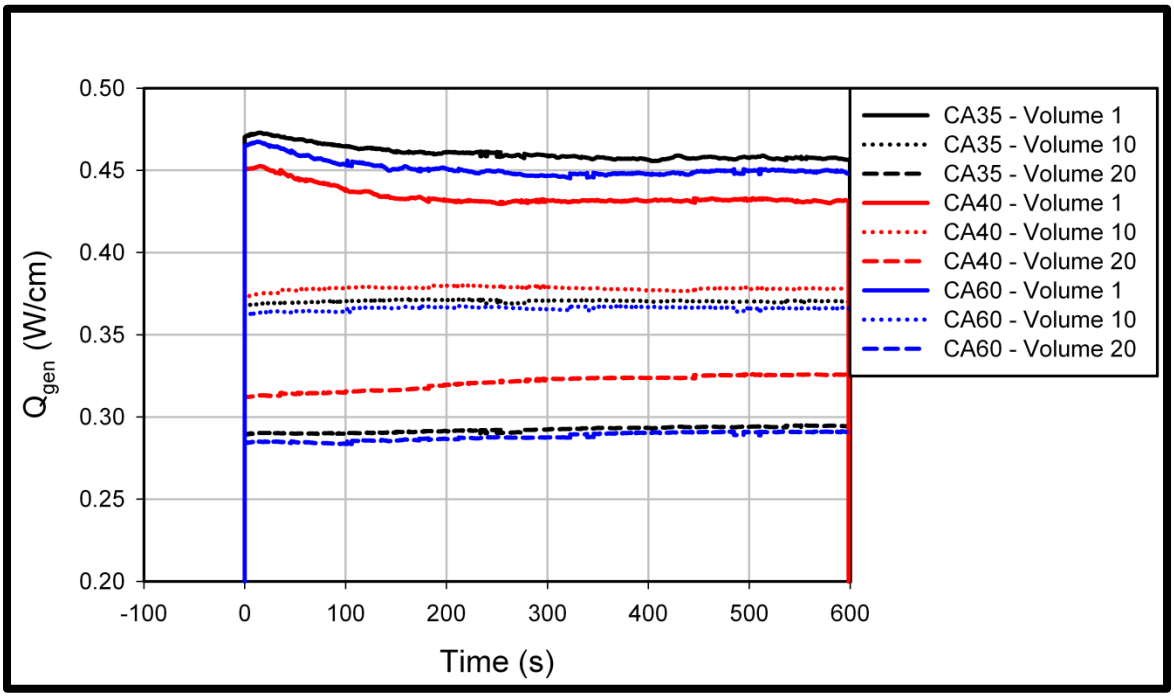

Figure 6.32: Local heat generation along the entire SOFC length vs. time – CA by-pass comparison, 100A initial FC load: OL

The Q_{gen} value for the 35% CA by-pass case is higher than for the 60% CA for all of the locations presented in Figure 6.32. This is due to the higher operating voltage for

the 60% CA by-pass case, presented in Figure 6.17. The higher operating temperature for the 60% CA by-pass start-up results in more efficient SOFC operation, manifested as increased electrical power production and decreased by-product heat generation.

Figure 6.33, presents the impact of initial FC load on the generation of by-product heat during SOFC start-up for 40% CA by-pass. The trends exhibited in Figure 6.33 compare very well with the local current density trends presented in Figure 6.31. As initial FC load increases, so does the impact on local by-product heat generated. As with the local current density profile, the magnitude of Q_{gen} increases with increasing initial FC load, and the impact of the system transients on local current density translate to the behavior illustrated for the by-product heat generation.

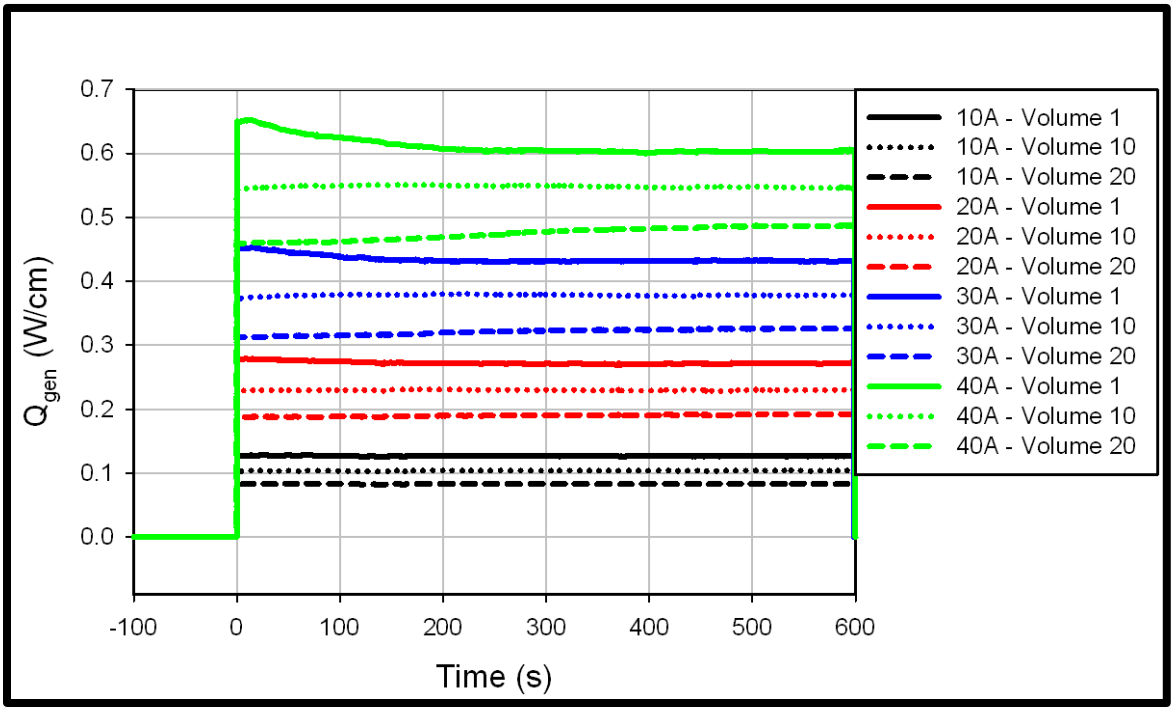

Figure 6.33: Local heat generation along the entire SOFC length vs. time – initial FC load comparison, 40% CA bypass: OL

The thermal and electrochemical behaviors exhibited through start-up, that have been presented thus far, all contributed to characterizing internal transport phenomena in the SOFCs. There was also the characterization of spatial gradient profiles in the fuel cell. Figure 6.34 characterizes the impact of CA by-pass valve position on the evolution of

spatial temperature gradients during electrochemical start-up with 30A of initial FC load. As illustrated, the spatial gradients observed in the fuel cell are not very significant, with the largest one presented being less than 1.0K/cm. The maximum spatial gradient actually occurs across segment 2 and has a value of approximately 1.2K/cm. It is important to note that the "jagged" profiles observed for spatial gradients across segment 1 are caused by noise observed in the transmission of FC inlet temperature from the HyPer facility to the SOFC real-time model. The negative spatial gradients across the last segment of the SOFC can be attributed to the adiabatic boundary condition of the fuel cell solid at the SOFC exit. The combination of the adiabatic solid boundary condition, the convection of heat away from the cell by the oxidant stream, and the changes in by-product heat generation throughout the transient response contributed to the spatial gradients near the exit having a negative value until cell steady state was achieved.

The most significant dT/dx values are observed for the 60% CA by-pass case. Figure 6.6 illustrates that the cathode inlet flow rate is considerably lower for the 60% CA by-pass case, as compared to the 35% and 40% CA by-pass cases. This decreased air-flow results in a larger O_2 utilization throughout the start-up transient, as supported by the data that is presented in table 6.1. The increased oxygen utilization term means that there is decreased air available for cell cooling, relative to the 35% and 40% CA by-pass cases, thus resulting in larger spatial gradient profiles.

The air flow rates for the 35% and 40% CA by-pass experiments are very close, actually having similar O_2 utilization values both at the time of load application, and once a new "steady" flow is achieved. Though the cathode inlet flow for 35% CA by-pass is slightly higher than for 40% CA by-pass, the key driver behind the reduction in temperature gradients is the dynamic response of FC inlet temperature, presented in Figure 6.13, during response to electrochemical start-up. For electrochemical start-up with 35% CA by-pass, the FC inlet temperature did not decrease as much as the 40% and 60% CA by-pass case, and exhibited some nonlinear behavior that could potentially be

due to heat exchanger imbalance. FC inlet temperature through 600s of start-up transient response is presented in Figure 6.35.

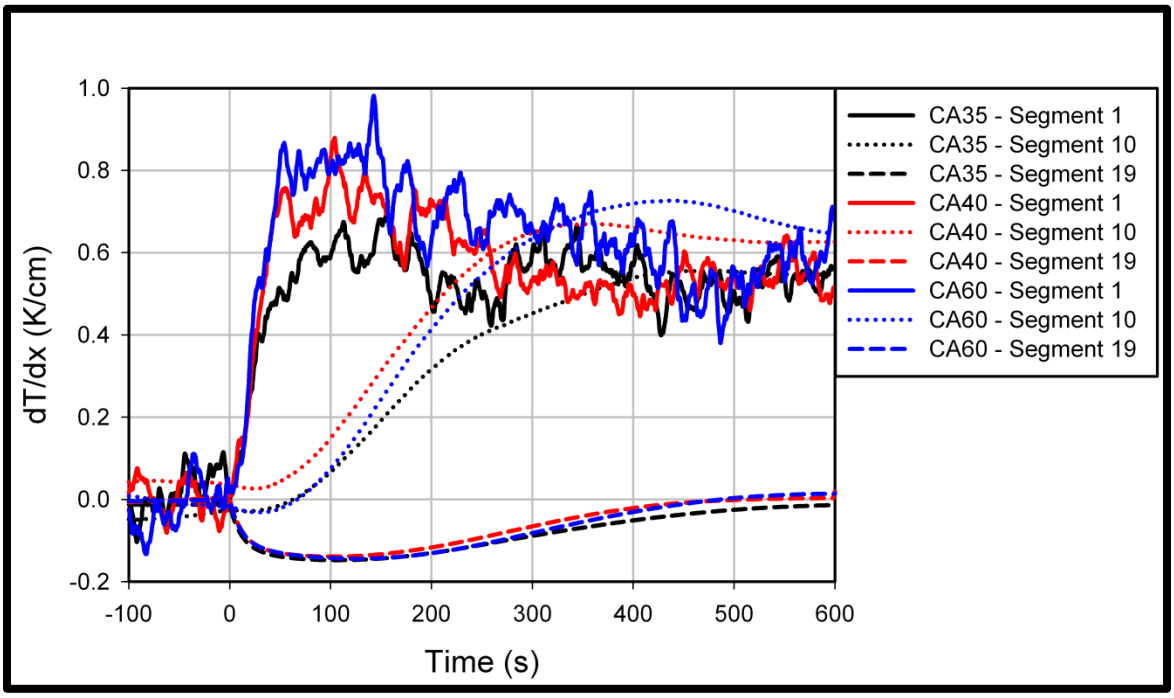

Figure 6.34: Local spatial temperature gradient along the entire SOFC length vs. time – CA by-pass comparison, 100A initial FC load: OL

As illustrated in Figure 6.35, the nonlinear response discussed in Section 6.2 occurs in the first 100s of the transient response. A key contributor to the larger temperature gradients near the inlet of the SOFC is the competing effect of by-product heat generation and enhanced cell cooling at the inlet of the SOFC. The relative increase in FC inlet temperature, combined with the more significant decrease in relative air flow, as illustrated by Figure 6.7, results in a higher level of thermal energy being provided to the FC for the 35% CA by-pass case relative to the 40% CA by-pass case, which ultimately causes leveling of the SOFC temperature profile and the decreased magnitude of temperature gradients.

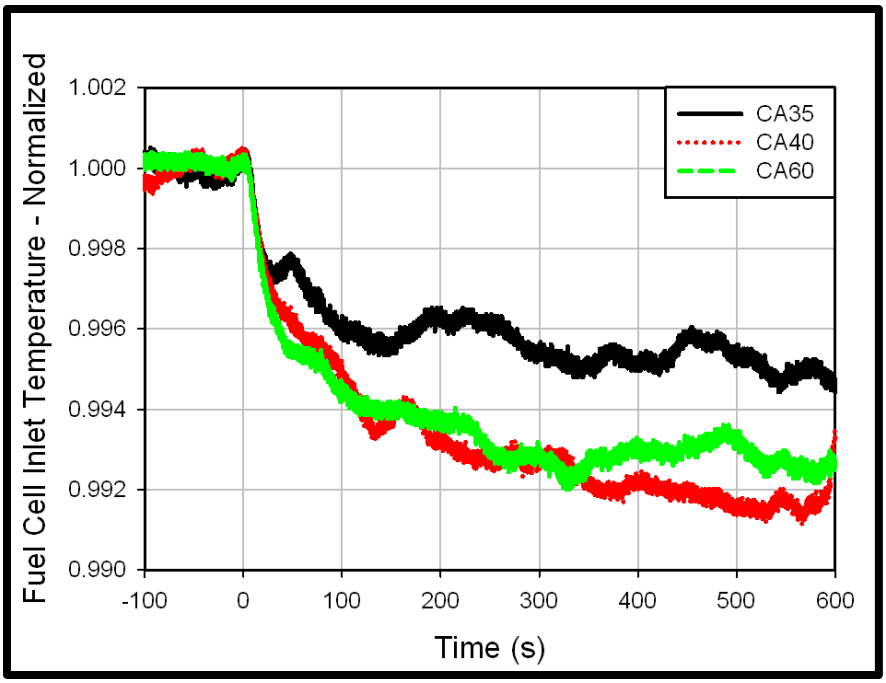

Figure 6.35: FC inlet temperature vs. time – CA by-pass comparison, 100A initial FC load: OL (600s)

At interior locations of the SOFC, spatial gradients for the 40% CA by-pass have larger magnitudes than for the 60% CA by-pass case. This is particularly observed at nodes 10 and 15, where the local heat generation is higher for the 40% CA by-pass case. Though the O_2 utilization is higher for the 60% case, during the transient response, the local by-product heat generation and internal heat diffusion dynamics dominate the spatial gradient profile for the 40% CA by-pass case. At the 400s and 500s marks, the magnitude of the local spatial gradients for nodes 10 and 15 respectively for the 60% CA by-pass case overtake the magnitude of the 40% case due to the dominant effect of increased mass flow that late in the start-up transient.

Increases in load increase the magnitude and the dynamic response of spatial gradients in SOFC's. Figure 6.36 presents the impact of initial FC load on spatial temperature gradients in the SOFC. Consistent increases across segments 1 and 10 are observed for increases in load, accompanied with similarly consistent decreases across segment 20. The impact of load application on the length of start-up transient response is

best illustrated by the dynamic response of the spatial gradient across segment 10. All 4 cases demonstrate slightly different dynamic behavior. For the 10A case, the spatial gradient gradually increases and begins to decrease at approximately t=400s. For the 20A and 30A cases, the spatial gradients across segment ten gradually increases and start to decrease between the 300s and 400s mark, but are then appear to begin to stabilize at t=500s. For the 40A case, the spatial gradient profile increases and essentially levels at t=400s, with a slight decrease observed between 500s and 600s after load application.

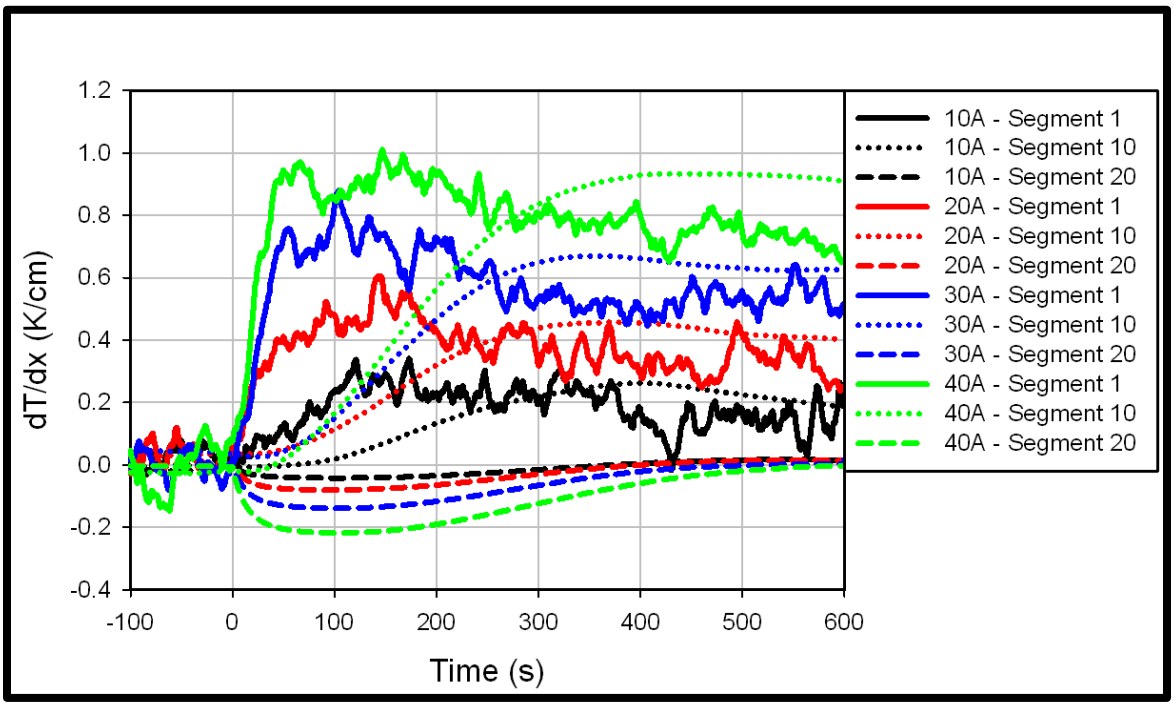

Figure 6.36: Local spatial temperature gradient along the entire SOFC length vs. time – initial FC load comparison, 40% CA bypass: OL

These dynamic responses observed, with regards to initial FC load are due to both internal SOFC thermal and electrochemical transients as well as the effects of load perturbation on system dynamics. The increase in by-product heat generation and decrease in inlet temperature and flow at increased load supports the significant increases in magnitude of the dT/dx profiles. The impact of dynamic behavior can be attributed to the nonlinear relationship of load and increases in heat provided to the system, which is illustrated in Figure 6.12. A detailed study focused on isolating all variables that impact

internal SOFC temperature gradients will have to be conducted to identify the root cause of the dynamic behavior observed.

CHAPTER 7

HUMIDIFIED HYDROGEN – SYNGAS FUEL FEED COMPARISON

7.1 Load Based Speed Control Comparison

One of the characteristics of SOFCs that makes them attractive for GT hybridization as well as integration into our current energy framework is their fuel flexibility. Although hydrogen is reasonably assumed to be the only electrochemically active specie in the SOFC model used for this study, the capability of the anode to catalyze direct internal reformation (DIR) of methane (CH_4) and water gas shift (WGS) facilitates using methane-containing syngas fuel feeds, in addition to humidified hydrogen (HH). To investigate the impact of using syngas on dynamic response during electrochemical start-up, simulations utilizing a methane rich syngas fuel feed (26.26% H_2, 17.1% CH_4, 2.94% CO, 4.36% CO_2, 49.34% H_2O) at the base CA by-pass valve position of 40% open were conducted. Comparative studies were conducted for the LBSC configuration, with an initial FC load of 100A. In this chapter, data from both base cases will be presented as well as comparisons of system operating parameters, SOFC performance parameters and select SOFC thermal data in distributed fashion.

7.1.1 Base Case – Initial FC Load 100A, Cold Air By-Pass Valve: 40%

For the purpose of investigating, analyzing and comparing the difference in system and SOFC behavior for HH vs. syngas, electrochemical light-off experiments with 40% CA by-pass were conducted with the IEA syngas benchmark fuel feed (26.26% H_2, 17.1% CH_4, 2.94% CO, 4.36% CO_2, 49.34% H_2O) utilizing 100A of initial load.

Figure 7.1 illustrates the system process flow parameters that serve as inputs to the real time SOFC model for a scenario of 100A initial load, 40% CA by-pass, electrochemical start-up with a syngas fuel feed. As outlined in Chapter 3, the system was allowed to come to steady state prior to the experiment and pre-load, steady state values

of the FC model input parameters are illustrated between times -100 and 0 in the figure. The pressure of the oxidant stream entering the virtual SOFC stack was approximately 373kPaa, the temperature was approximately 952K and inlet air flow was approximately 1.41 kg/s prior to the application of load.

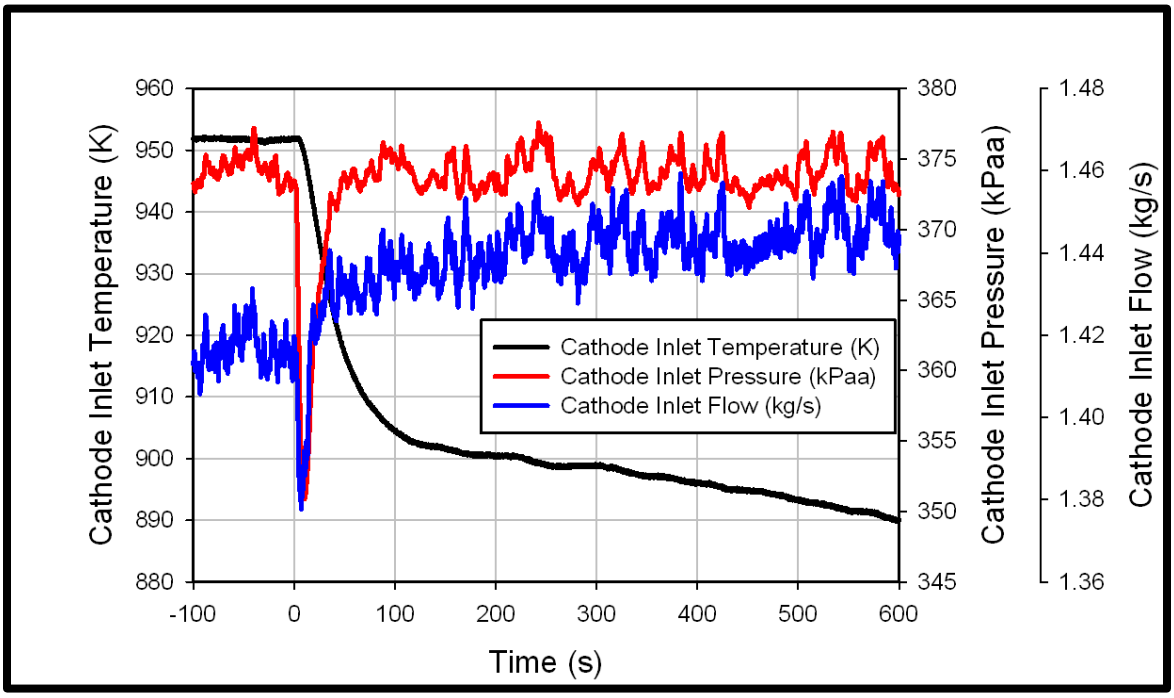

Figure 7.1: Fuel cell inlet parameters - 100A FC load, 40% CA by-pass: LBSC syngas base case

The application of FC load causes a decrease in thermal effluent to the system and consequently the turbine. This results in a decrease in all of the process parameters that serve as inputs to the virtual SOFC.

The decrease in physical heat or Q_{gen} total from the fuel cell subsystem that results from the application of load causes a sharp decrease in turbine speed which results in a decrease in cathode inlet pressure and flow as presented in Figure 7.1. Inlet pressure decreases by approximately 22kPa to 351kPaa and the inlet flow reaches a minimum value of approximately 1.38 kg/s. The decrease in turbine speed also activates the LBSC algorithm. Once activated, the controller begins to decrease the amount of electric turbine load (initially 50kW) to maintain the nominal turbine speed of 40,500 RPM. After the

LBSC algorithm starts to take effect, given the realized decrease in turbine speed, the rotational speed eventually reaches a minimum and starts to increase in response to the shedding of turbine load, resulting in a similar transient response for both pressure and flow to the SOFC cathode. The stable values of both pressure and flow observed appear to slightly decrease and increase, respectively. When the load is placed on the fuel cell there is a decrease in physical heat in the system due to decreased fuel flow and turbine electric load, which manifests itself in a decrease in fuel cell inlet temperature. This decrease in FC inlet temperature results in a decrease in compressor back pressure which increases mass flow through the compressor and the entire system.

As previously stated, the fuel cell inlet temperature decreases in response to the decrease in system thermal effluent from load application at the point the initial load is placed on the fuel cell. As illustrated in Figure 7.1, FC inlet temperature has a sharp initial decrease, which transitions into a more gradual decrease, shortly after the turbine speed returns to its nominal 40,500 RPM value. The impact of this transient response of the FC inlet temperature is observed by the solid FC material.

Prior to the application of load, the prescribed IEA benchmarking syngas mixture was fed into the SOFC, and both the fuel cell and system were allowed to reach steady state. The cell was not electrochemically active prior to t=0s, but the presence of DIR and WGS in the fuel channel resulted in a consumption of thermal energy and a gradual decrease in SOFC temperature in the flow direction. The source of thermal energy for the fuel stream chemistry is the hot air supply on the cathode side of the SOFC. The fuel stream composition with respect to axial position, prior to the application of load, is presented in Figure 7.2. As illustrated in the figure, there is a gradual decrease of both methane (CH_4) and water (H_2O) along the length of the fuel channel due to DIR and WGS. The sharp decrease and increase of carbon monoxide (CO) and carbon dioxide (CO_2), respectively, at the entrance of the fuel cell, signifies the presence of the WGS and the reaction going to equilibrium. The concentrations of both CO and CO_2 gradually

increase along the length of the SOFC. The increase of CO_2 supports that WGS is occurring, however; the increase in CO supports that though WGS, which consumes carbon monoxide, is occurring, DIR which produces carbon monoxide is occurring simultaneously as well. Given the elevated concentration of CH_4 relative to CO, the kinetics of steam reformation dominate, thus the net CO increase. Both of these reactions contribute to the gradual increase in hydrogen concentration along the length of the fuel cell. The mole fraction of H_2 increases from its inlet value of 0.2626 to its outlet concentration of 0.4631.

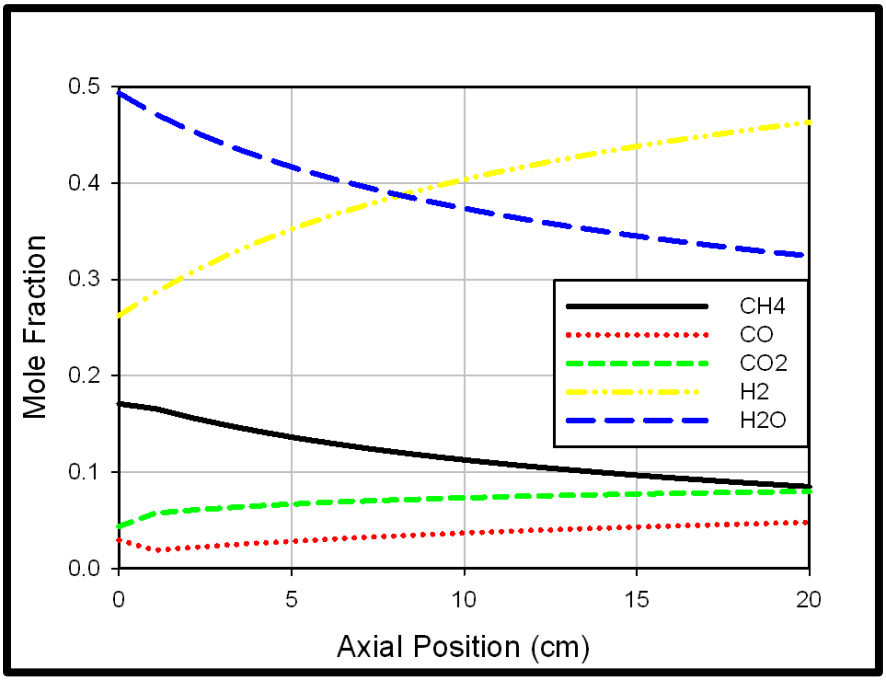

Figure 7.2: Initial steady-state axial fuel composition prior to electrochemical start-up – syngas

The presence of reactant stream chemistry, which is illustrated by Figure 7.2, results in the evolution of a non-uniform temperature profile. The chemical activity results in a net consumption of thermal energy and thus negative local heat generation terms along the axial length of the fuel cell. This causes a decrease in SOFC temperature from FC inlet to exit. Prior to load application a cell ΔT from inlet to outlet of a magnitude greater than 50K is present in the fuel cell. The effect of reactant stream

chemical activity on the temperature and local heat generation profiles prior to the application of load is illustrated in Figure 7.3. As illustrated in the figure the local heat generation has a value of approximately -2.0 W/m at the inlet of the fuel cell followed by a sharp decrease with a value of -4.0 W/m observed at node 2. This steep decrease can be attributed to the assumption that the WGS reaction occurs at equilibrium and a resulting significant release of heat across the first half volume of the fuel cell. Once the minimum local heat generation value of -4.0 W/m is observed at node 2, the axial heat generation profile exhibits a monotonic increase through the remaining portion of the fuel cell arriving at a maximum of approximately -1.25 W/m at the fuel cell exit. This trend can be primarily attributed to the decreasing presence of DIR in the fuel stream due to methane consumption. The FC solid profile illustrates a monotonic decrease along the length of the fuel cell with a local and absolute minima observed at the end of the fuel cell exit. The general decreasing trend is due to the cooling effect of DIR along the length of the fuel cell and the local and absolute minima at the exit is attributed to the adiabatic boundary condition at the exit of the fuel cell.

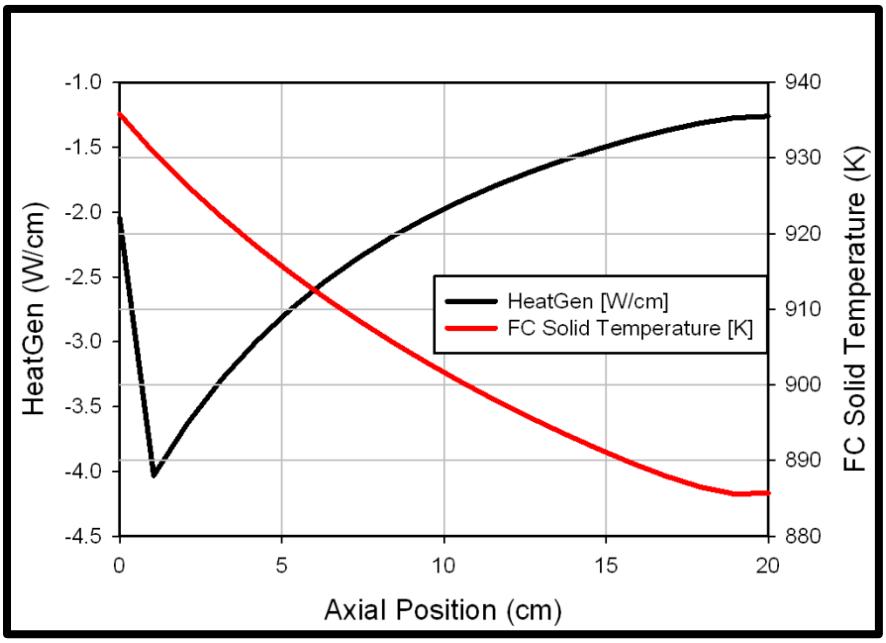

Figure 7.3: Steady-state, axial local heat generation and FC solid temperature prior to electrochemical start-up

As previously stated, the FC temperature at the inlet was approximately 937K and given the stated thermal effect of reactant stream chemistry, the temperature at the exit of the fuel cell is approximately 885K. The local heat generation term at the inlet is approximately -2 W/cm, which steeply decreases to approximately -4W/cm. Figure 7.2 presents a noticeable decrease and increase in the concentrations of CO and $CO_{2,}$ respectively, which illustrates the significance of the water gas shift reaction near the inlet of the FC. The concentrations of the constituents move directly towards equilibrium based upon the equilibrium chemistry model. Given the exothermic nature of WGS, its production of heat initially counters the consumption of thermal energy by DIR; and thus a significantly decreased magnitude of the inlet heat sink effect occurs. Decreases in methane concentration along the length of the fuel cell results in decreased reaction rates and a decrease in the magnitude of the negative Q_{gen} local values along the length of the reactant channel.

The spatio-temporal temperature profile for 100A, 40% CA by-pass electrochemical start-up employing LBSC is presented in Figure 7.4. At time t=0s, load is applied to the fuel cell which results in electrochemical activity, the generation of by-product heat from cell operation and an increase in average SOFC temperature. The formation of a local temperature maximum at the outlet of the SOFC is observed approximately 300s after the load is placed on the virtual SOFC, similar to the humidified hydrogen case that is presented in Chapter 5. After the local temperature maximum is observed, the cooling effect of the decreased inlet air temperature, illustrated in Figure 7.4, and increased mass flow is observed along the entire SOFC. Similarly to the humidified hydrogen case, the SOFC eventually transitions into a cooling phase, where the impact of by-product heat generation and cell operation is no longer causing the local SOFC temperatures to increase. After 600s of start-up, the cell ΔT, which represents the difference in temperature from cell inlet to exit, is approximately 25K, with a solid FC temperature of 889K at the inlet and of approximately and 915K at the exit. The cell ΔT

observed for the syngas case is significantly lower than the nearly 71K value observed for the humidified hydrogen case as illustrated in Figure 5.2. As illustrated by the continually decreasing FC inlet temperature after 600s of start-up in Figure 7.1, it is evident that the system has yet to reach a steady condition; yet, the solid temperature profile of the SOFC illustrates that after approximately 300s the internal dynamics of SOFC operation due to start-up have subsided and the SOFC stack is primarily responding to thermal transients caused by other system parameters.

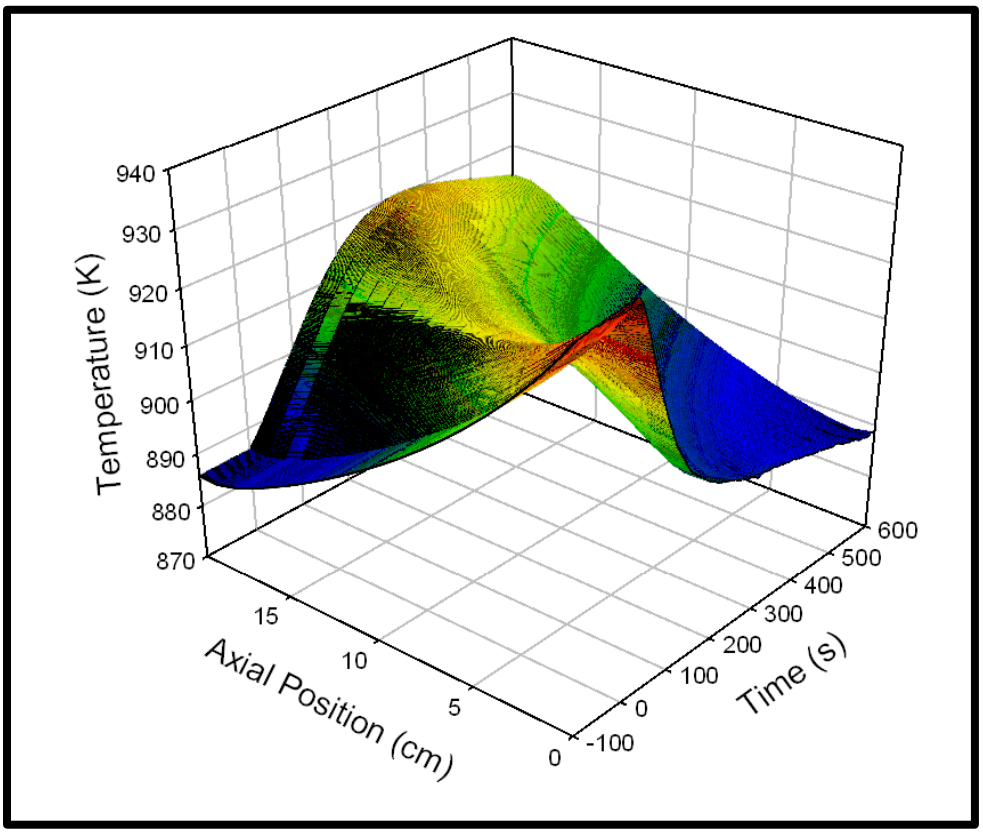

Figure 7.4: Spatio-temporal solid temperature plot – 100A FC load, 40% CA by-pass: LBSC syngas base case

It is apparent that the presence of constituents in the fuel stream that support the presence of endothermic chemical activity aid in the management of potentially harmful thermal transport and dynamics in operating SOFCs. Though prior to the application of load, the presence of internal reactant stream chemistry contributed to existence of a significant and potentially harmful SOFC axial temperature profile, the reactant stream

chemistry actually provided a cooling effect which assisted in the management of thermal transport during electrochemical start-up.

The combined effect of all of the thermal energy transfers present during start-up has the potential to initiate some significant internal thermal dynamics during electrochemical start-up. To investigate the impact of these coupled and competing effects on internal thermal transport and dynamics, a spatio-temporal plot of the spatial temperature gradient was produced and is presented in Figure 7.5. The figure has a similar form to that of the LBSC HH case, presented in Figure 5.3.

Prior to the application of load, as illustrated in Figure 7.4, the spatial temperature gradient of the most significant magnitude (approximately 4.8K/cm) existed at the inlet of the SOFC. The presence of this significantly negative dT/dx value is attributed to the heightened level of upstream cell cooling that takes place primarily due to the presence of DIR. The dT/dx values are negative along the remainder of the cell prior to electrochemical start-up due to the prescribed cooling effect, but the decrease in local "heat sink" effect due to the consumption of methane results in a decrease in the magnitude of the spatial gradient along the length of the FC, as it appropriately approaches zero at the outlet due to the adiabatic boundary condition.

The spatial temperature gradient initially has the pre-load profile which was previously discussed. At t=0s, there is a minor decrease in spatial gradient profile which could possibly be attributed to the competing effect of heat generation from SOFC operation as well as intra-stack cooling from DIR which creates a more favorable thermal environment by decreasing the magnitude of the pre-load temperature gradients in the SOFC. As the start-up response continues, a gradual increase in dT/dx values along the length of the fuel cell are observed. Larger values arise in the downstream portion of the FC given the decreased effect of cathode inlet cooling at downstream locations, the end-of-cell adiabatic boundary condition and ultimately the growing impact of downstream by-product heat generation. An overall maximum temperature gradient magnitude is

observed near the inlet of the FC approximately 135s into the transient response due to the competing effects of thermal energy generation and FC inlet stream cooling effects. Once that maximum value is observed, the spatial gradient near the inlet decreases to an apparent steady value for the remainder of the transient response. This is one of the included results in the significant redistribution of the SOFC temperature profile as conveyed in Figure 7.4. The spatial dT/dx profile does not appear to significantly change with time throughout the final 250-300 seconds of the experiment. As similarly concluded from the temperature profile analysis, the SOFCs' dynamic response to the application of load appears to dissipate and the internal transients observed appear to be primarily due to the dynamic response of the SOFC to system parameters.

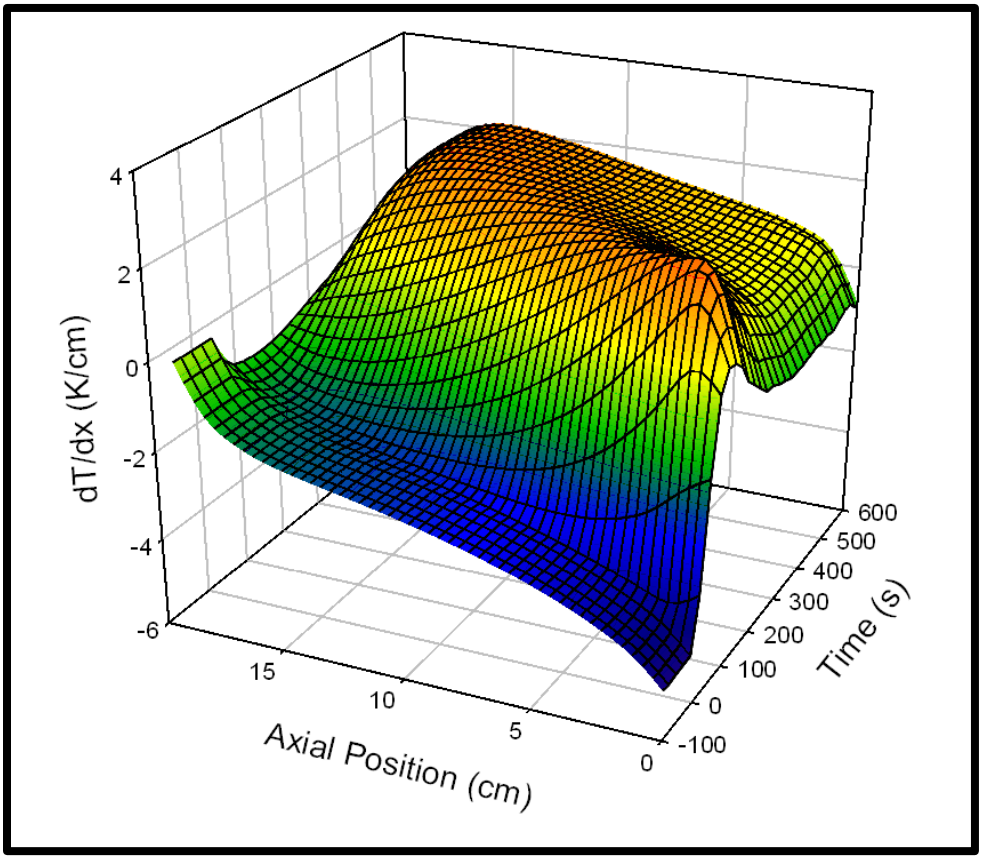

Figure 7.5: Spatio-temporal spatial temperature gradient plot – 100A FC load, 40% CA by-pass: LBSC syngas base case

As discussed above, the combined cooling and heating effects of the decreased thermal energy of the inlet stream coupled with the formation of by-product heat in the fuel cell contributes to the formation of the maximum positive dT/dx value of 2.54K/cm approximately 2.5cm from the inlet of the fuel cell, 138.56s after load application. Though it is important to note the presence and of an overall maximum post-load dT/dx near the inlet of the SOFC, the spatial gradient of the greatest magnitude actually occurs at the inlet of the SOFC prior to load being applied. This illustrates the thermal impact of reactant stream chemistry on internal thermal transport in the SOFC. Though methane containing syngas can be used to manage SOFC thermal transport, this pre-load phenomena illustrates the potentially negative effect that it can have if mismanaged and not appropriately utilized. Though relative to the spatial gradient values prior to the application of load on the SOFC the magnitude of increase could be deemed significant , the magnitude of this peak value is much less that the peak post load value of approximately 6.20K/cm for the 100A, LBSC HH case. The decrease in this maximum temperature gradient can be attributed to the cooling effect of the reactant stream chemistry which counteracts the generation of by-product heat due to cell operation. This results in a more evenly distributed temperature profile and a decreased magnitude of spatial gradients during electrochemical start-up.

The electrochemical activity of the cell is heavily influenced by internal transport phenomena within the SOFC. The transient response of local current density profiles throughout the start-up period is presented in Figure 7.6. At the initial time of load application, the local current density is highest at the inlet of the SOFC and monotonically decreases along the length of the fuel cell. This is largely due to the elevated inlet temperature that is illustrated in Figure 7.3. The initial local current density profile for the syngas experiment illustrates more variation than the HH experiment, with current densities ranging from 0.33A/cm^2 to 0.20A/cm^2 for the syngas case as compared to 0.29A/cm^2 to 0.21A/cm^2 for the HH case, from inlet to outlet, respectively. This is also

due to the presence of a monotonically decreasing FC solid temperature profile prior to load application for the syngas experiment as compared to the uniform profile prior to load application for the HH experiment. After start-up is initiated at t=0s, the gradual progression of the SOFC temperature profile is similar to the HH case. The maximum current density transitions from inlet to exit with a more evenly distributed current density profile forming for the syngas case as compared to the HH case. The local current densities 600s after the application of load ranged from approximately 0.21A/cm^2 to 0.29A/cm^2 for the HH case as compared to 0.19A/cm^2 to 0.32A/cm^2 for the syngas case, from inlet to outlet, respectively. This further illustrates the impact of the SOFCs thermal condition on electrochemical activity. Those fuel stream conditions that promoted more evenly distributed temperature profiles at t=0s and t=600s, respectively, also promoted more uniformity in current density distribution.

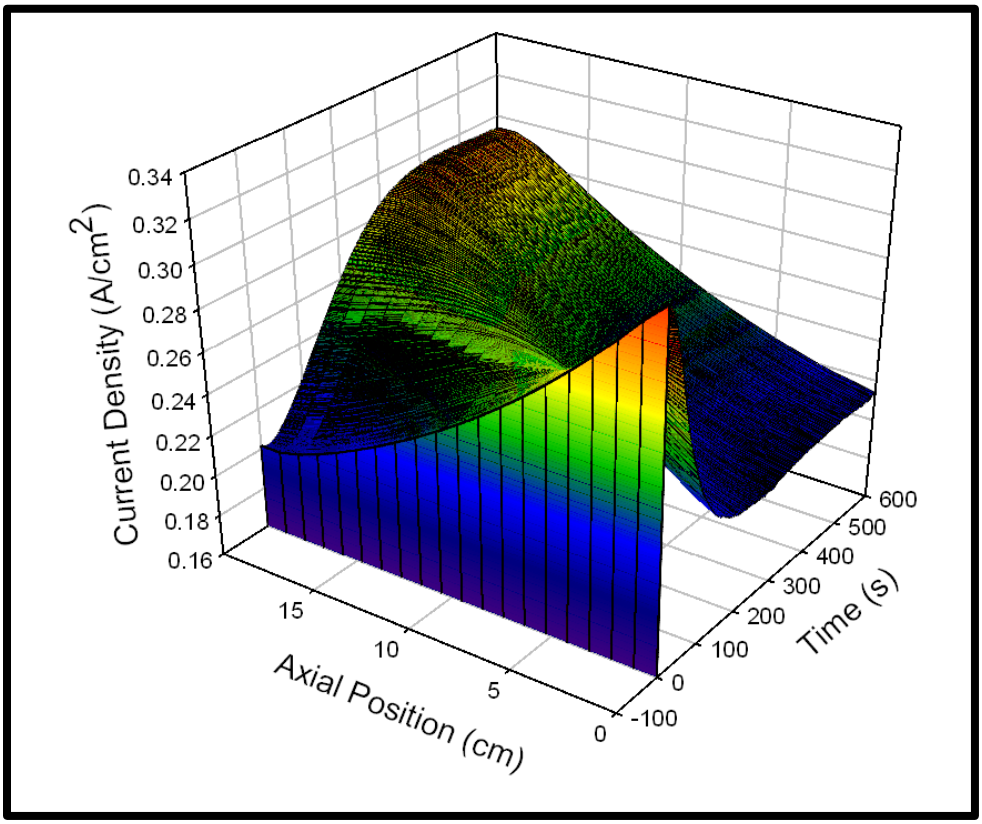

Figure 7.6: Spatio-temporal current density plot – 100A FC load, 40% CA by-pass: LBSC syngas base case

Another driver behind the electrochemical activity of the cell is the amount of electrochemically active species available for consumption by the SOFC for the production of electrical power, (i.e. H_2 concentration). Once load is placed on the FC, the magnitude of the overall hydrogen concentration profile, initially illustrated in Figure 7.2, decreases to the profile illustrated in Figure 7.7, t=0s, with a local concentration at the exit of the FC of approximately 33% as compared to 46% prior to the application of load.

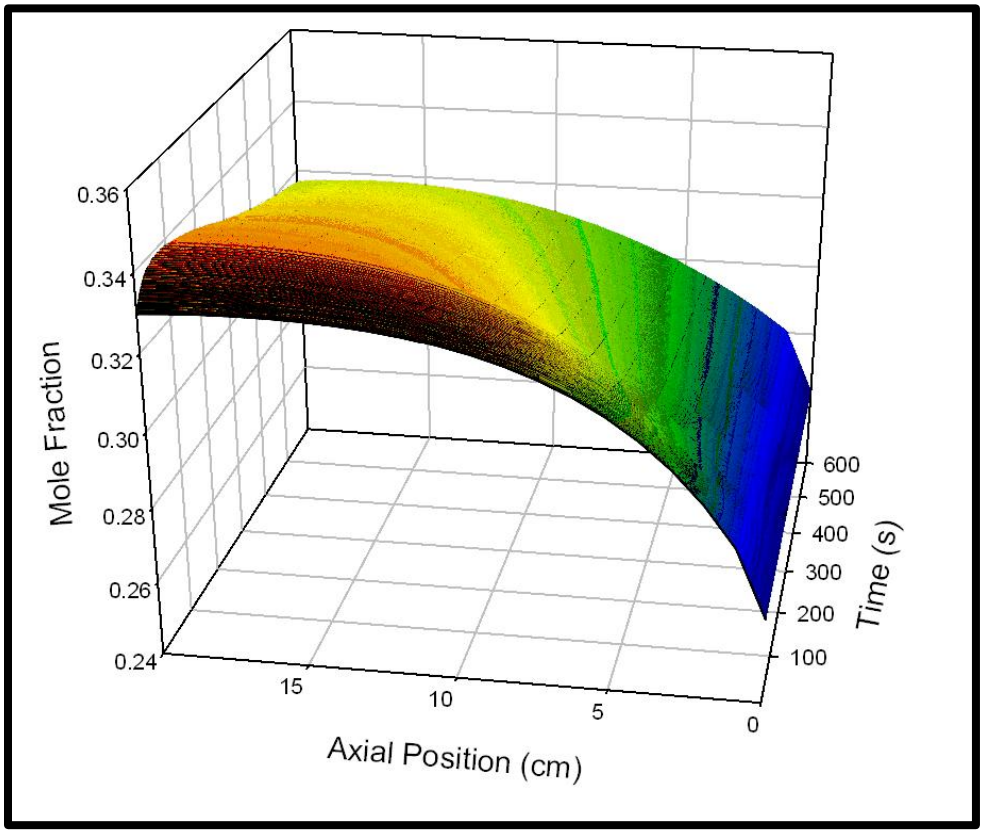

Figure 7.7: Spatio-temporal hydrogen concentration plot – 100A FC load, 40% CA by-pass: LBSC syngas base case

The decrease in H_2 concentration is due to the consumption caused by the new load demand. In the HH experiments, the amount of hydrogen present at the exit of the FC was fixed. The amount of load that was applied directly correlated to an amount of H_2 that must be consumed, and since none was being formed in the reactant stream fuel channel, the amount at the exit had to be fixed. This is not the case for the syngas fuel

feed. As illustrated by Figure 7.2, H_2 is formed along the length of the fuel cell, resulting in an increased concentration at the exit as compared to the inlet.

The thermal and electrochemical condition of the cell contributes to the amount of H_2 that will be produced and or consumed for the syngas case; thus, the H_2 concentration at the exit of the cell as well as its general profile is not exclusively dependent upon current draw and local current density profile, but also local temperatures, given their impact on the reaction rate and equilibrium constant of DIR and WGS, respectively.

A gradual increase in the H_2 concentration along the length of the FC from entrance to exit is observed throughout the start-up transient response. The increase in local SOFC temperature downstream, which results in an increase in local current density downstream, increases the amount of H_2 consumption near the exit of the FC. The mole fraction at the exit eventually decreases to less than 0.32 after 600s of start-up, from its maximum value of approximately 0.34 within the first 100s of start-up. The initial increase in the hydrogen concentration profile immediately after load is applied to the FC is due to the increasing temperature as illustrated in Figure 7.4, which results in increased reactant stream chemistry and production of hydrogen. Additionally, the local current density profile was initially illustrating that the majority of current production was occurring in the upstream portion of the SOFC; but the profile transitions to a local maximum at the exit of the cell. The subsequent gradual decrease in H_2 observed at the exit is due to a combination of increasing cell temperature at the exit which results in increased hydrogen production as well as increased electrochemical activity with results in increased hydrogen consumption.

7.1.2 System Performance – LBSC – HH/Syngas Comparison

Again characterizing the impact of electrochemical start-up on system operational parameters is essential to capturing the overall behavior of the system during this initial phase of operation. In complementary fashion to the study that was presented in Chapter

5, this section presents results that compare the impact of electrochemical start-up on cathode inlet air flow, temperature, and pressure, as well as turbine speed to illustrate the coupled effects.

Cathode air flow is the primary mechanism used to manage by-product thermal energy generation in the SOFC. Furthermore, given the evolution of potentially harmful temperature gradients in SOFCs during the electrochemical start-up of SOFC/GT hybrid systems, it has particular importance in mitigating the evolution of potentially harmful thermomechanics in SOFCs during the start-up period. For that purpose, the dynamic response of cathode inlet flow to electrochemical start-up is characterized. The absolute cathode inlet flow for the 100A LBSC base case utilizing both syngas and HH fuel feeds is presented in Figure 7.8.

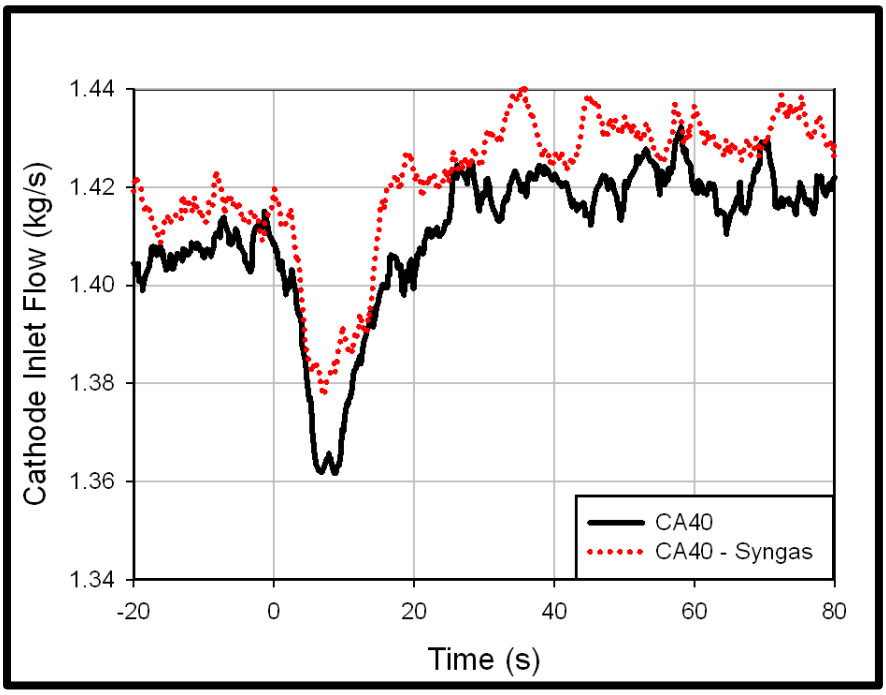

Figure 7.8: Raw FC inlet flow vs. time – HH/syngas comparison: LBSC

The syngas experiment has a slightly higher airflow prior to the application of load and throughout the transient response. This can be attributed to a combination of different ambient conditions, which impact system operation, as well as slightly unequal FC subsystem heats released prior to the initiation of start-up. As illustrated, the dynamic

response of both profiles appears to be comparable but the decrease in air flow through the cathode is noticeable less for the syngas case than it is for the HH case.

To further investigate the impact of electrochemical light-off on cathode inlet flow dynamic response, the normalized cathode inlet flow is presented in Figure 7.9. The cathode inlet flow decreased by over 3% for the humidified hydrogen case as compared to approximately 2.75% for the syngas case. Aside from the deviation in the percent decrease from the nominal value observed approximately 8s into the transient response, the dynamic response of the cathode inlet flow for electrochemical start-up with the humidified hydrogen and syngas fuel feeds, illustrated by Figure 7.9, compare very well.

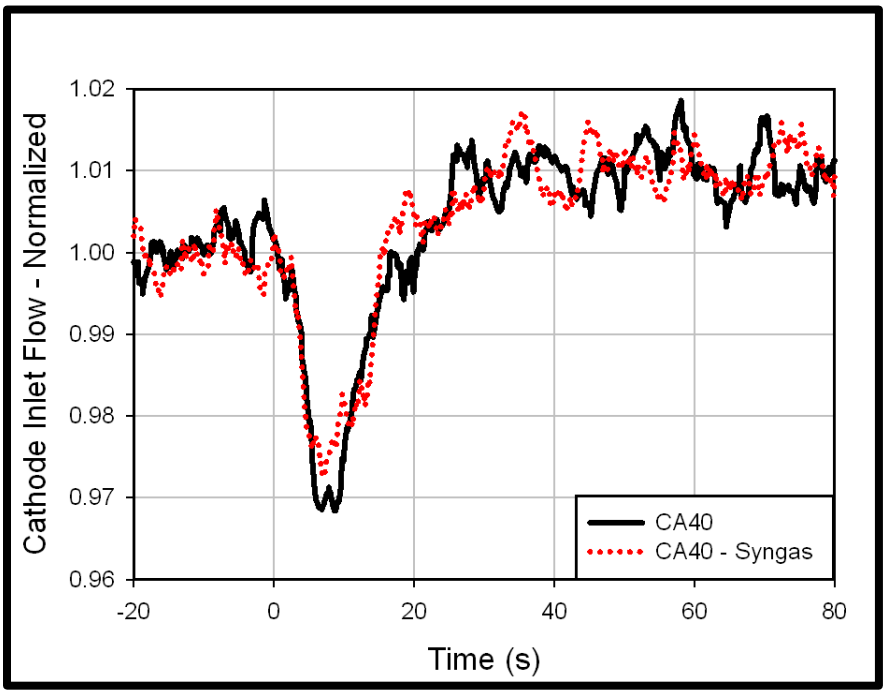

Figure 7.9: Normalized FC inlet flow vs. time – HH/syngas comparison: LBSC

This impact of fuel feed on the percent decrease of cathode air flow that is illustrated in Figure 7.9 can be supported and further illustrated by the normalized turbine speed transient profile illustrated in Figure 7.10. A similar trend of a decreased minimum value of turbine speed for the HH fuel feed, as compared to the syngas fuel feed is observed. The minimum turbine speed for the HH experiment is nearly 3.5% less than the nominal value as compared to the syngas case that is approximately 2.75% less than the

nominal value. The return to nominal speed also appears to be more gradual (i.e. less "sharp") for the syngas case as opposed to the HH case. The tip of the profile for the syngas case presents a more rounded contour as compared to the HH case that has a very "sharp" transition back to nominal speed.

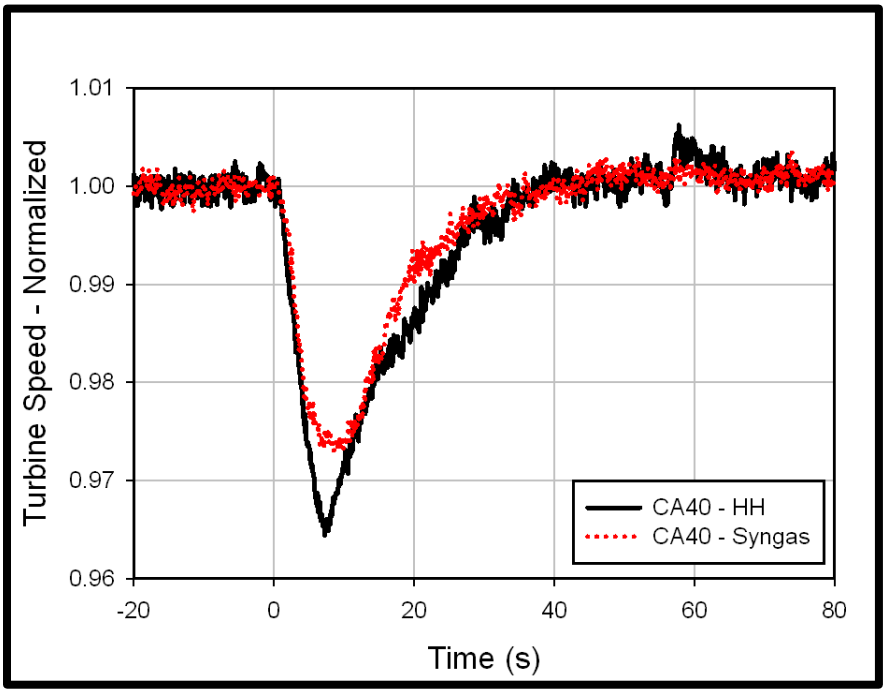

Figure 7.10: Normalized turbine speed flow vs. time – HH/syngas comparison: LBSC

The existence of the more contoured transition to nominal operating speed for the syngas case, as compared to the HH case, suggests that the use of syngas fuel feed and the presence of inter reactant stream chemistry can affect the transient thermal response of the SOFC subsystem. The transient impact of heat generated from the subsystem during 100A electrochemical start-up, in conjunction with a 40% CA by-pass setting, is presented in normalized fashion in Figure 7.11. The Q_{gen} total values, prior to the application of load at t=0s, was approximately 1450kW for the syngas experiment and 1435kW for the HH experiment, thus supporting the slight deviation in magnitude of cathode inlet flow observed in Figure 7.8. The Q_{gen} total represents the total amount of heat generated from the FC subsystem, which includes heat produced due to post

combustion of unutilized fuel as well as from by-product heat generation from cell operation.

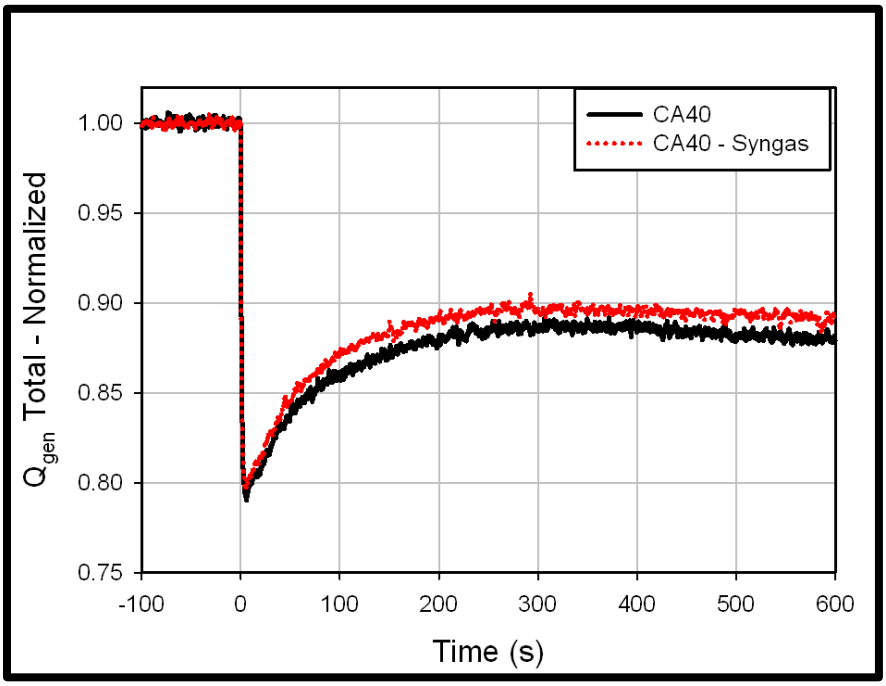

Figure 7.11: FC cell subsystem heat generated vs. time – HH/syngas comparison: LBSC

As illustrated in Figure 7.1, both the syngas and HH case illustrate similar dynamic trends. Prior to the application of load, the SOFC subsystem only produces thermal energy via combustion of unutilized fuel. Once the load is placed on the fuel cell, the SOFC starts producing power which means that the SOFC subsystem is now producing electrical power from SOFC operation as well as thermal energy from a combination of SOFC by-product heat as well as the combustion of unutilized fuel. Ultimately the amount of physical heat provided to the system decreases, due to the conversion, of what was originally thermal energy from the combustion of fuel, into a combination of thermal energy and electrical power. Once the load is applied, the SOFC also starts to generate by-product heat, which results in a counter-response of partial recovery of Q_{gen} total. The stable value of Q_{gen} total, relative to its pre-load value, is higher for the syngas case, as compared to the HH case. This suggests that the SOFC

stack produces more by-product heat for the syn-gas case than for the HH case, which is actually the case.

Prior to load application, the reactant stream was consuming 100.19kW of thermal energy for the syngas case, and none was being produced or consumed for the HH case. The SOFC stack was producing approximately 33.90kW of thermal energy for the syngas case, compared to 130.60kW for the HH case; 600s after load was applied. This resulted in an increase in Q_{gen} stack of 134.09kW for the syngas case and 130.60kW for the HH case. Though syngas fuel feeds consume thermal energy and produce potentially harmful temperature gradients in the SOFC prior to operation, utilizing a fuel feed of this nature actually has the ability to mitigate the evolution of harmful gradients during operation as well as ease the systems dynamic response to electrochemical start-up and load perturbations during system operation. It is also important to note that in addition to the SOFC stack producing more thermal energy relative to its initial value, the exit composition of the SOFC stack is changing throughout start-up and thus impacting the heat generated via post combustion as well.

The impact on cathode inlet temperature and pressure are illustrated in Figures 7.12 and 7.13. As illustrated, the temperature compares very well with the system thermal effluent as slight deviations between the HH and syngas profiles are observed approximately 150s after load is applied. The cathode inlet pressure compares very well with the turbine speed, which is illustrated in Figure 7.10, as expected given the strong correlation between the two system parameters. The turbine speed profile for the syngas experiment illustrates a larger and less sharp maximum than the HH case. This is also observed for the cathode inlet pressure as well. The dynamic responses compare very well with both the dynamic response of the turbine speed as well as the air flow.

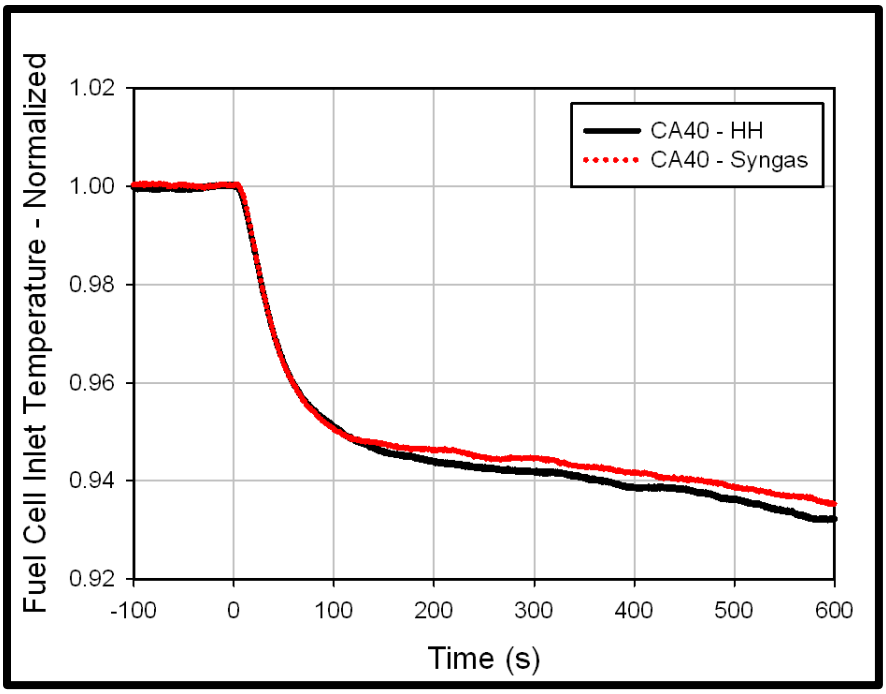

Figure 7.12: Normalized FC inlet temperature vs. time – HH/syngas comparison: LBSC

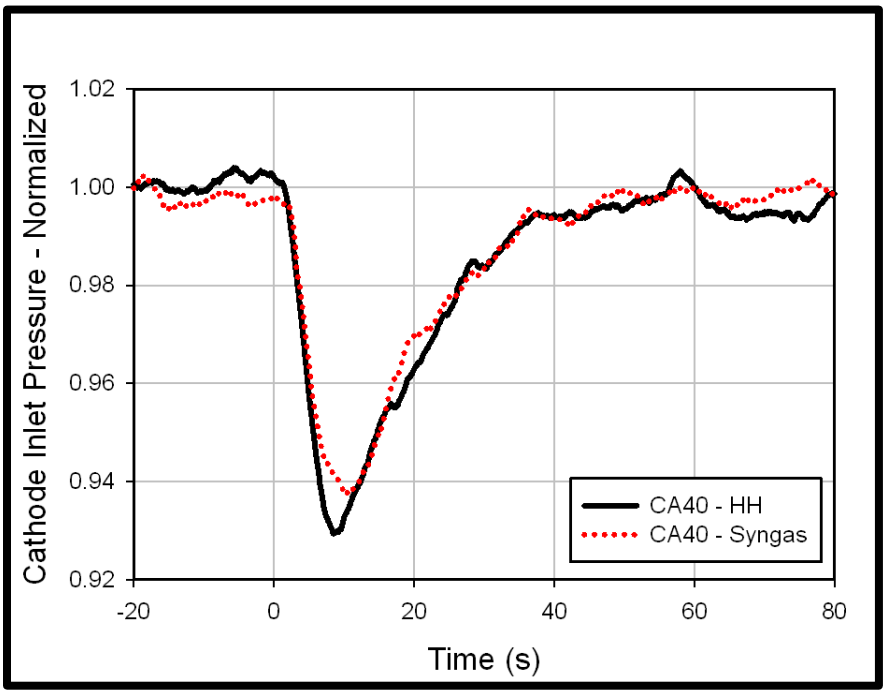

Figure 7.13: Normalized FC inlet pressure vs. time – HH/syngas comparison: LBSC

7.1.3 SOFC Performance – LBSC – HH/Syngas Comparison

As discussed in Chapter 5, a key condition that influences the amount of power produced by the stack is its operating voltage. Stack power is resolved by determining the product of the operating voltage, current draw and number of cells in the stack, and the voltage is the simulated dependency. The operational voltage is dependent upon a number of different thermal and electrochemical parameters which contribute to the value of Nernst potential and electrochemical losses in the SOFC stack. Though the syngas fuel feed positively impacts thermal transport during electrochemical start-up, in comparison to humidified hydrogen, it herein has a negative impact upon stack power and operating voltage. As previously stated in the experimental set-up method of chapter 3, the amount of fuel (i.e., whether HH or syngas) that is fed to the SOFC subsystem is enough to ensure a turbine rotational speed of 40,500 RPM with 50kW of turbine load prior to the draw of current from the SOFC.

As illustrated in Figure 7.14, the stack power is approximately 25kW less for the syngas case as compared to the HH case and operating voltage is approximately 0.125V less for the syngas case as compared to the HH case. This can be directly attributed to the decreased Nernst potential and increased electrochemical polarization loss terms for the syngas simulation. Given the significant decrease in H_2 concentration prior to the application of load (90% for HH and 26%-49% for syngas), the Nernst potential is consequently decreased for the syngas case as compared to the HH case. The pre-load Nernst potential for the SOFC stack is nearly 1.1V for the HH case as compared to 1.0V for the syngas case. In addition, the decreased average operational temperature once the cell is electrochemically active, due to the decreasing cathode inlet temperature, results in an increase in activation and ohmic loss terms which further impact the operating voltage of the SOFC stack while using a syngas fuel feed. The decreased average operating temperature increases electrochemical loss terms which results in a lower operating voltage, and thus decreased stack power, when using the syngas fuel feed investigated.

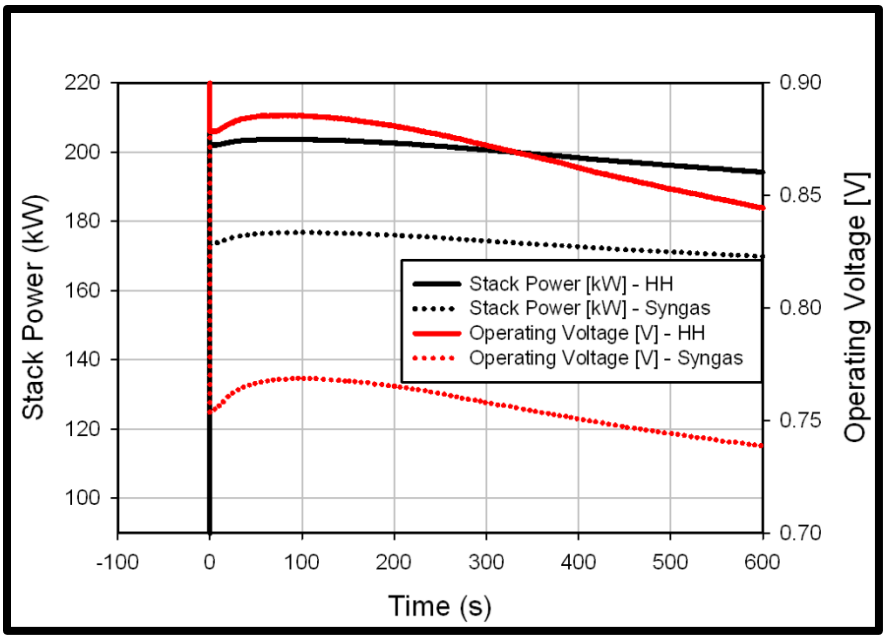

Figure 7.14: Stack power and operating voltage vs. time – HH/syngas comparison: LBSC

Aside from the impact on actual operating voltage and stack power values, there appears to be minimal effect on the dynamic response of either of the parameters of interest. The stack power and operating voltage for each case exhibit the same dynamic behavior through the first 600s of start-up transient response. Though the different fuel feeds create different initial operating states, the dynamic response of the thermal transport between the start-up with the varying fuel feeds is very similar, thus translating to the electrochemical regime as well. The similarities between the thermal trends are discussed later in the chapter.

7.1.4 Distributed Comparison – LBSC – HH/Syngas Comparison

To maximize utilization of the full set of capabilities of the real time, 1-D SOFC model, a comparison of key operating parameters and diagnostics on a distributed basis was conducted. Though the model gives us the capability to characterize a number of thermal and electrochemical operating parameters of SOFCs operating in a hybridized fashion with a GT, the major premise of this work is to characterize SOFC and system

dynamic response during electrochemical start-up so that control strategies can be developed to preserve the mechanical integrity of the SOFC through significant dynamic transients. To that end, this section primarily focuses on distributed parameters that most directly impact the thermal dynamic operation of the SOFC. Solid SOFC temperature, current density, by-product heat generation and spatial temperature gradient will all be presented in distributed fashion. Figure 7.15 illustrates the local SOFC solid temperatures at equidistant nodes along the length of the SOFC for electrochemical light off with 100A of initial FC load and 40% CA by-pass setting. LBSC was employed for both HH and syngas fuel feeds.

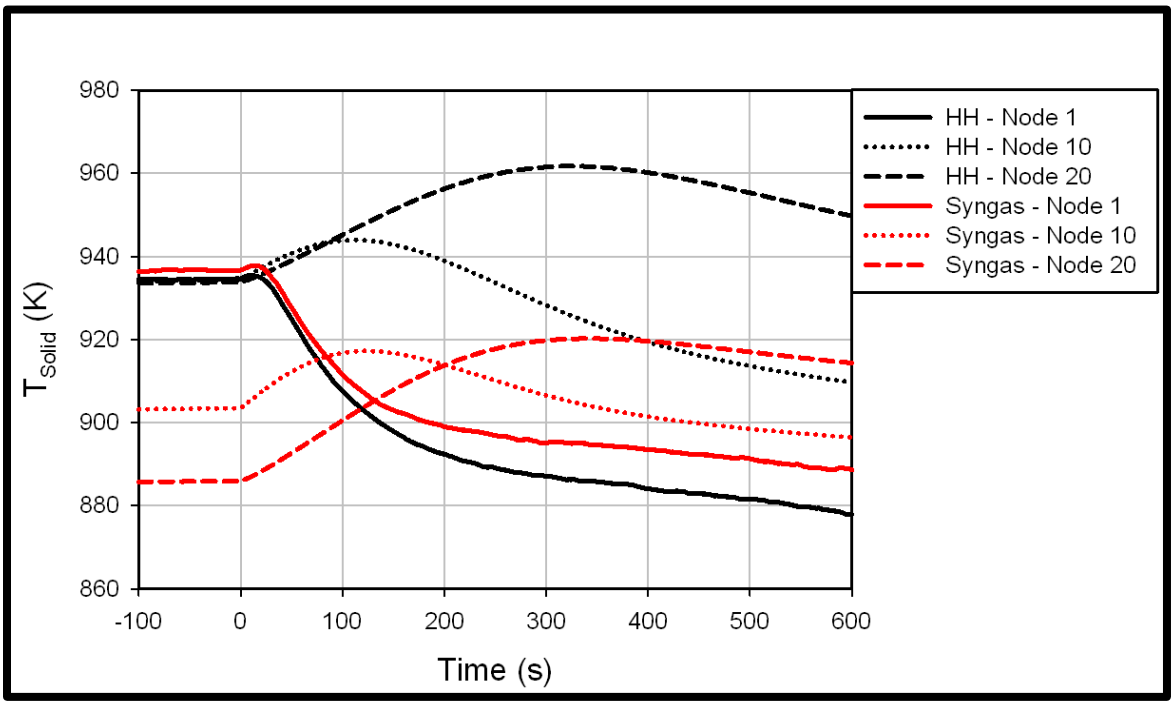

Figure 7.15: Local solid temperature along the entire SOFC length vs. time – HH/syngas comparison: LBSC

As previously discussed and illustrated, prior to the application of load both systems were allowed to come to a steady condition. Given the absence of the occurrence of reactant stream chemistry, that steady condition results in an essentially uniform temperature profile for the HH fuel feed experiment, as illustrated by the overlapping of the local temperature profiles for all of the HH nodes in Figure 7.15. The steady

condition for the syngas fuel feed, however, results in a monotonically decreasing temperature profile, due to the dominance of the extremely endothermic DIR reaction occurring in the reactant stream. That results in localized initial temperatures ranging from 947K to 885K for the syngas case.

Though the magnitude of the localized temperatures are generally lower for the syngas case than the HH case, the general dynamic trends and shape of the profiles appear to compare very well. Once load is applied to the cell at t=0s, all of the downstream localized temperatures (every node accept node one) exhibits an increase in temperature. Node one exhibits a slight increase followed by a prompt decrease due to decreasing FC inlet temperature. The remainder of the local SOFC solid temperatures gradually increase and eventually decrease, with this arrival at a maximum local temperature and transition to cooling occurring more quickly for nodes that are closer to the inlet of the FC. As the SOFC experiences its dynamic response to electrochemical start-up, there is a gradual progression of the formation of the temperature profiles as presented in Figures 5.2 and 7.4 for the HH and syngas experiments, respectively. As the cell responds, the temperatures of the greatest magnitude begin to transition to downstream locations of the cell and the temperatures of the lowest magnitude transition to the upstream portion of the cell. Once the temperature at the exit of the FC reaches it maximum, the entire cell transitions to a cooling state, where every local temperature has a downward trajectory illustrating removal of thermal energy from the SOFC stack. This transition occurs at approximately the same time, between 300s and 400s after the start-up was initiated.

The temperatures at the inlet of the FC were approximately equal for the two different fuel feeds, but at the 600s mark after the load has been applied, a temperature difference of nearly 10K is observed between the two values. This can be attributed to the decreased impact on inlet temperature observed for the syngas case as compared to the

HH case, as illustrated in Figure 7.12, as well as an increased effect in stack by-product heat for the syngas case as compared to the HH case, as illustrated in Figures 7.11.

There appears to be a relatively uniform temperature distribution in the upstream portion of the SOFC, for the syngas fuel feed case, as illustrated by the spatio temporal profile in Figure 7.4 and by the proximity of the temperature profiles of nodes 1 and 5 approximately 300s after the load application in Figure 7.15. The close proximity of these local temperature profiles can be attributed to the enhanced cooling effect of the FC inlet stream, coupled with the internal cooling from DIR, which results in a more evenly distributed temperature distribution in the upstream portion of the SOFC. In addition to leveling out the temperature distribution in the upstream portion of the SOFC, the use of the syngas fuel feed decreases the ΔT across the entire fuel cell.

The temperature profile is directly impacted by the electrochemical activity of the cell, which is illustrated through the temporal profiles of local current density values along the entire axial length of the SOFC during electrochemical start-up. This is again with 100A of initial FC load and a 40% CA by-pass setting. The presence of a significant temperature distribution prior to the application of load on the SOFC results in a more broadly distributed initial current density profile, with a local current density of approximately 0.33A/cm^2 at the inlet of the FC and approximately 0.20 A/cm^2 at the exit of the FC, for the syngas fuel feed case.

The essentially uniform HH pre-load temperature profile results in a local current density of approximately 0.29 A/cm^2 at the inlet and approximately 0.22 A/cm^2 at the exit. The local current densities 600s after the application of load ranged from approximately 0.21A/cm^2 to 0.29A/cm^2 (inlet to exit) for the syngas case as compared to 0.19A/cm^2 to 0.32A/cm^2 (inlet to exit) for the HH case.

Once load is applied, the local current density profiles follow the general trends of increasing local current density in the downstream portion of the FC and decreasing local current density in the upstream portion of the FC, which results in a more compact local

current density profile for the syngas fuel feed case and a more widely distributed current density profile for the humidified hydrogen case. This is heavily influenced by the larger cell temperature variation at the 600s mark for the HH case as compared to the smaller cell temperature variation for the syngas case.

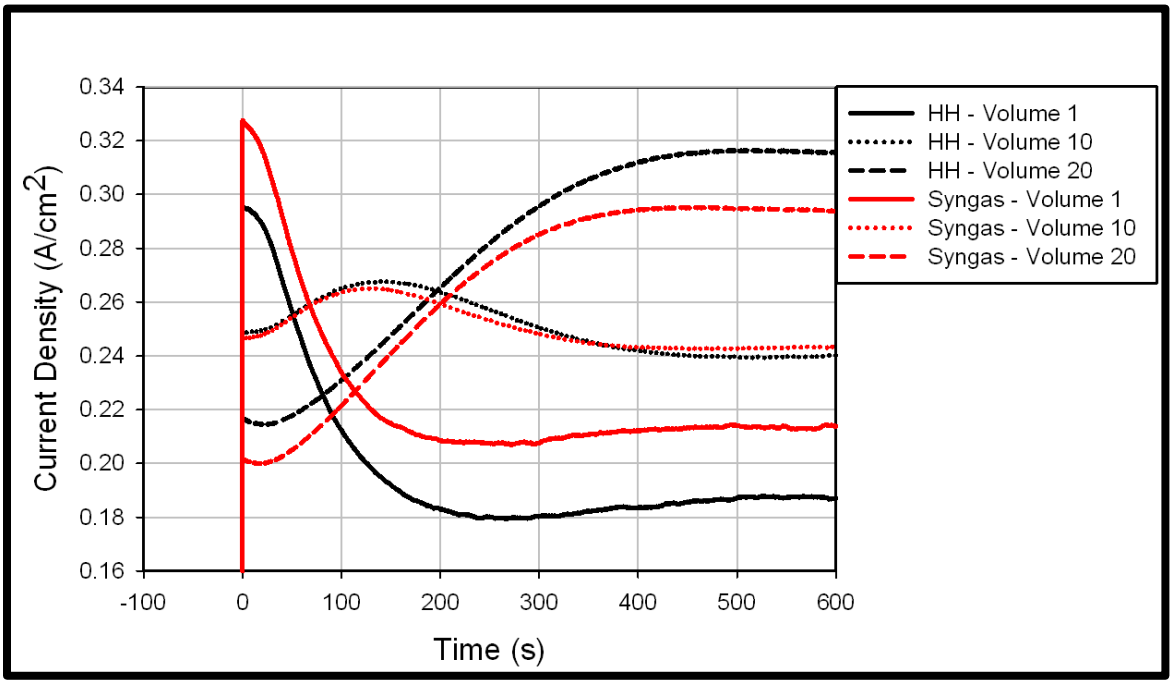

Figure 7.16: Local current density along the entire SOFC length vs. time – HH/syngas comparison: LBSC

The local heat generation profiles are heavily influenced by local current density but as previously addressed in the discussion regarding the transient response of the SOFC system thermal effluent, the heat generation term for the syngas fuel feed case must also consider the heat produced and/or consumed due to reactant stream chemistry. The local heat generation profiles for the HH and syngas experiments throughout the start-up response are illustrated in Figure 7.17. The local heat generation profiles for both the HH and syngas cases closely follow the general current density trends illustrated in Figure 7.16. Without the presence of local reactant stream chemistry, the heat generation in the SOFC stack is primarily influenced by current draw and operating voltage, and though voltage will trend with average operating temperature, local current density

remains the primary driver in the dynamic behavior of the local heat generation, as illustrated by the figure.

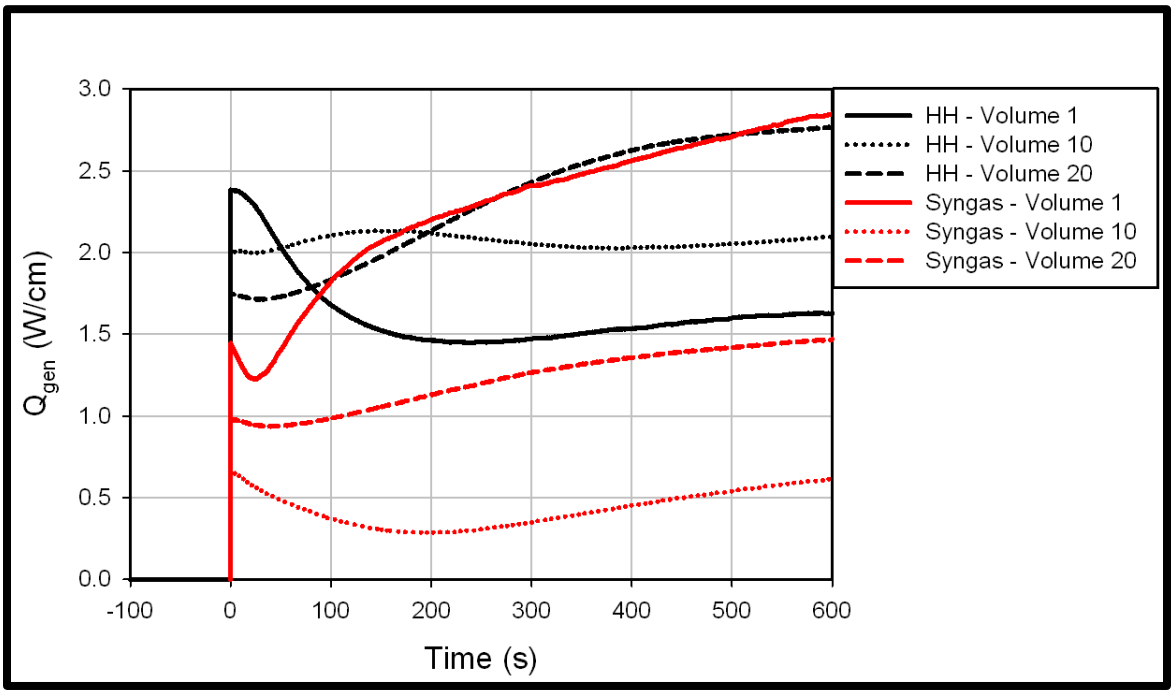

Figure 7.17: Local heat generation along the entire SOFC length vs. time – HH/syngas comparison: LBSC

The natural coupling between local current and heat generation is less prevalent from the dynamic response of the electrochemical start-up, illustrated in Figure 7.17, for the syngas fuel feed scenario. The profile for the local heat generation at the entrance of the FC has the largest magnitude throughout start-up. This is due to the generation of by-product heat from cell operation as well as the release of heat from the water gas shift reaction as it goes to imposed equilibrium. Upon entrance into the fuel channel, there is also consumption of heat due to the endothermic nature of DIR, but the coupled effect of WGS and by-product operational heat dominate as the maximum amount of heat is generated at the inlet. The initial decrease in the Q_{gen} local profile at the inlet node, that is observed shortly after load is applied, is due to the sharp decrease in current density. The sharp decrease in current density is due to the transition of the solid temperature profile,

presented in Figure 7.4, soon after load application, as illustrated in Figure 7.16. The prompt decrease in local current density decreases operational by-product heat and thus the Q_{gen} local value at the inlet. Once the cooling starts to take effect, the rate of reaction of DIR begins to decrease, and operational by-product heat begins to increase due to decreasing voltage, thus the observed sharp increase in the local heat generation profile at the FC inlet. Once the WGS goes to initial equilibrium at the inlet of the SOFC, the impact of the endothermic nature of DIR is prevalent along the length of the cell, with more heat being consumed by DIR in the upstream portion of the fuel channel, given more available constituents for reaction. As illustrated in Figure 7.3, Q_{gen} local value is at its minimum (maximum magnitude, negative value) near volume 2. Since WGS goes to equilibrium at the entrance, the heat generation across the entrance volume presents a different trend than the downstream portion of the cell with the remainder of the chemical activity downstream from volume 1 is dominated by DIR along the reactant channel. Since methane will have its highest concentration upstream, the min Q_{gen} local value will reside across volume 2. Methane concentration decreases; thus, DIR reaction rate decreases and causes an increase in Q_{gen} local profiles in the flow direction, as illustrated by the values at nodes 10 and 20 increasing successively.

The furthest upstream node aside from the inlet node, node 5, illustrates the minimum amount of heat generated from all of the nodes displayed. Its Q_{gen} values are actually negative, throughout the first 400s of the start-up transient response, which signifies a cooling effect on the SOFC. As the local temperature decreases, and thus the operating voltage, the magnitude of the by-product heat generation from cell operation increases, thus moving that localized value from the negative to the positive regime. The impact of decreasing temperature, which results in decreasing voltage and thus increasing by-product operational heat and increased localized Q_{gen} values, is evident at all of the nodes illustrated. The effect of DIR is progressively less apparent at nodes further downstream. This is due to the decrease in methane concentration in the axial direction of

the flow and thus decreased reaction rates, given the model's employment of a rate law that is first order with respect to methane. After approximately the 300 second mark, when the SOFC has transitioned to its cooling regime and the temperature at every node is decreasing, by-product heat generation across the entire cell is increasing.

The solid temperature profile contributes to the evolution of local current density distributions, which ultimately affects cell by-product heat generation and ultimately spatial temperature gradients in the SOFC material. If inappropriately managed, the evolution of these gradients can contribute to material failure. As illustrated in Figure 7.18, the trends for the syngas case are very similar to the HH case, with the local maximum temperature gradient occurring later in time for successive segments and with the minimum, always occurring across the final segment. The dynamic behavior of the spatial gradient for the syngas fuel feed selected appears to operate very similarly to HH, the major difference is the magnitude of the spatial gradient values.

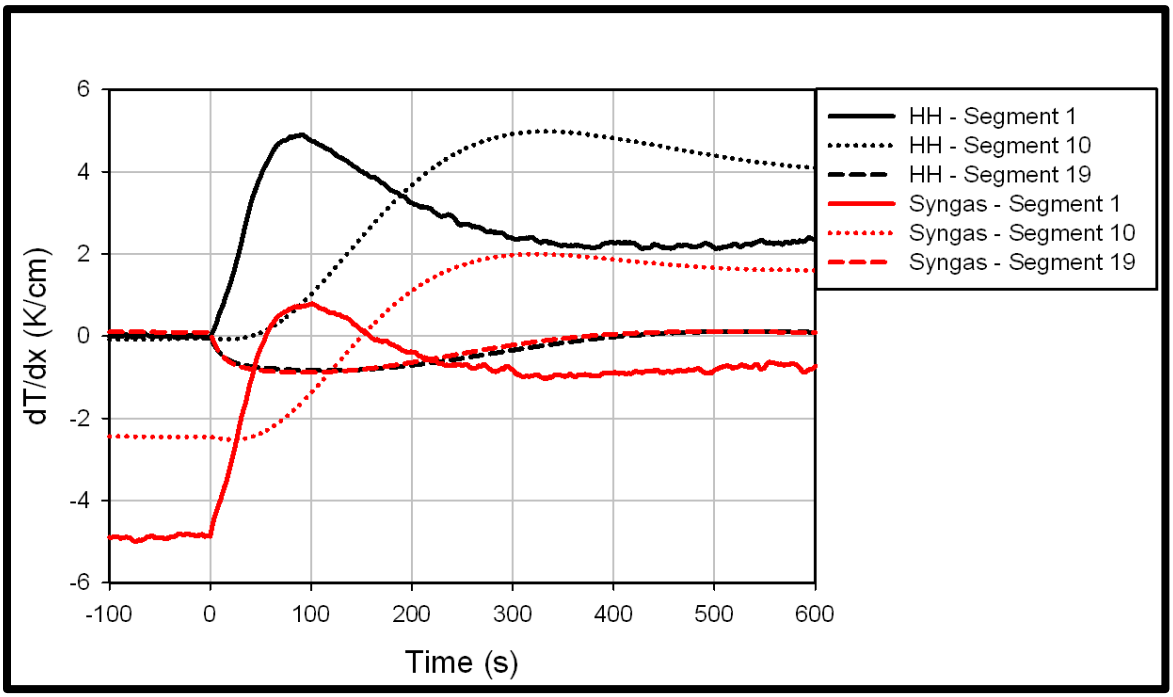

Figure 7.18: Local spatial temperature gradient along the entire SOFC length vs. time – HH/syngas comparison: LBSC

Prior to the application of load, the spatial gradient values for the syngas fuel feed are significantly negative, with a value of nearly -5K/cm at the inlet of the fuel cell. After load is applied, the profiles are very similar but the magnitude of the profiles are significantly lower for the syngas case as compared to the HH case. The HH case exhibits maximum dT/dx value greater than 6K/cm and the syngas case exhibts values just above 2K/cm. Ultimately, the DIR present in the syngas feed contributes significantly to decreasing the intensity of spatial temperature gradients during electrochemical light off and also decreases the average operating temperature of the SOFC.

7.2 Open Loop Comparison

LBSC based speed control is an effective mechanism to ensure that the rotational speed of the turbine in this hybrid system does not deviate excessively from its setting; however, it may be unreasonable or infeasible to decrease the amount of electrical power that is released to the grid by the power plant, and thus the turbine speed must be allowed to vary. In addition to feasibility of operation, the results from Chapter 5 and Section 7.1 illustrated that removal of turbine load has a sustained impact on the thermal state of the system, with no thermal steady condition being reached even 600s after the start-up was initiated. An investigation on the impact of SOFC/GT electrochemical start-up on system and SOFC dynamic response was thus conducted. A detailed parametric study, investigating the impact of CA by-pass valve position and initial FC load on dynamic response during electrochemical start-up, using a HH fuel feed was conducted and presented in Chapter 6. Section 7.2 presents a preliminary case study comparing the system and SOFC dynamic response during electrochemical start up with 30A of initial FC load and 40% CA by-pass for HH and syngas fuel feeds for an OL system configuration. Given that the HH base condition has already been presented in Chapter 6, Section 7.2.5 will present select process parameter and spatio-temporal data from the start-up experiment utilizing a syngas fuel feed.

7.2.1 Base Case – Initial FC Load 30A, Cold Air By-Pass Valve: 40%

For the purpose of investigating, analyzing and comparing the difference in system and SOFC behavior for humidified hydrogen vs. methane rich syngas, electrochemical light-off experiments with 30A of FC load and 40% CA by-pass were conducted with the IEA syngas benchmark fuel feed (26.26% H_2, 17.1% CH_4, 2.94% CO, 4.36% CO_2, 49.34% H_2O).

Figure 7.19 illustrates the system process flow parameters that serve as inputs to the real time SOFC model. The system was allowed to come to steady state prior to the application of load. Pre-load, steady state values of the FC model input parameters are illustrated between times -100 and 0 in the figure. As illustrated the pressure of the oxidant stream entering the virtual SOFC stack was approximately 375kPaa, the temperature was approximately 947K and inlet air flow was approximately 1.42 kg/s.

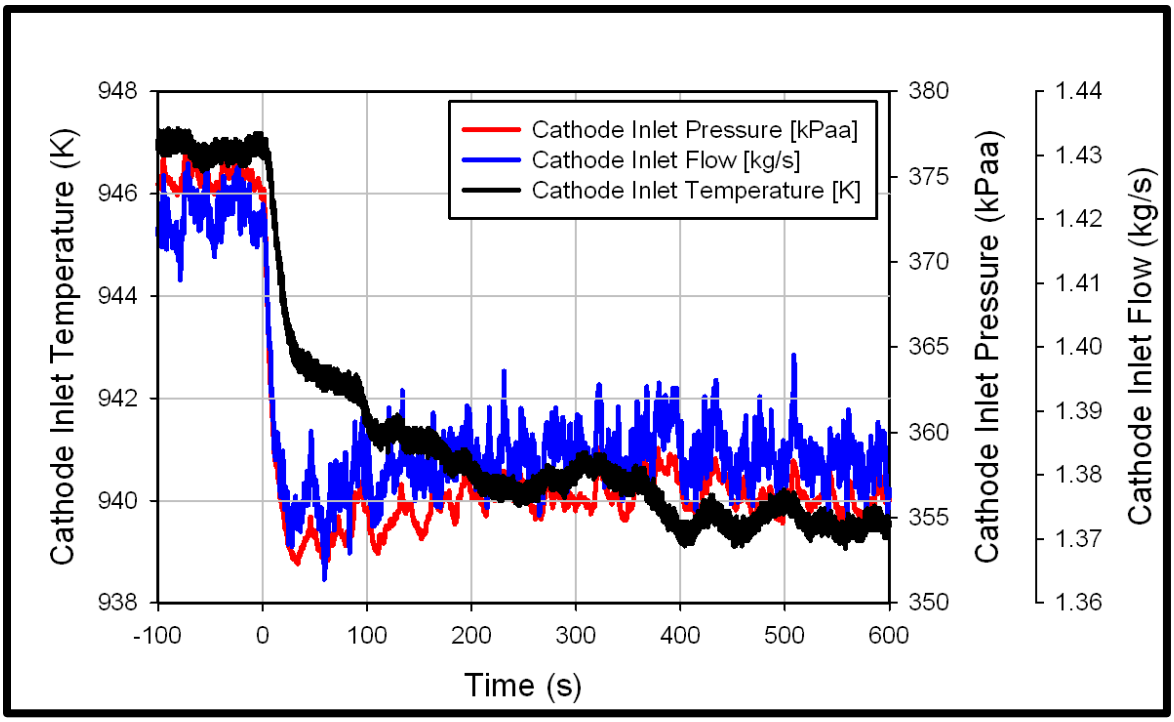

Figure 7.19: Fuel cell inlet parameters - 30A FC OL: base case - syngas

The decrease in physical heat from the system that resulted from the stepwise increase in FC load from 0A to 30A at t=0s, caused a steep decrease in all of the process

parameters that serve as inputs to the fuel cell model, as illustrated in Figure 7.19. The decrease in physical heat or Q_{gen} total from the fuel cell subsystem results in a sharp decrease in turbine speed which causes the decrease in cathode inlet pressure and flow. Inlet pressure decreases by approximately 23kPa to a minimum value of 352kPaa and the inlet flow reaches a minimum value of approximately 1.37 kg/s. At the point of load application, the pressure and mass flow quickly approach the minimum values listed above, approximately 25s after load application. Once those minimum values are achieved, a gradual increase to steady values of 1.38kg/s and 358kPaa are achieved. The gradual increase observed after the minimum values are attained, is attributed to the gradual increase in SOFC sub-system thermal effluent after load is applied to the cell due to by-product heat generation from cell operation. Similar trends for the HH case, as presented in Chapter 6 in Figure 6.1, are present for the cathode inlet parameters that are presented here in Figure 7.19.

The transients observed with regards to pressure and flow can be directly connected to turbine speed. Once load is placed on the virtual SOFC at t=0s, the amount of thermal effluent that is provided by the SOFC subsystem is decreased and thus the rotational speed of the turbine follows suit. Cathode inlet pressure and flow are heavily correlated with turbine speed and thus changes in turbine speed, typically initiated from changes in system thermal effluent, manifest in a dynamic response in cathode inlet flow and inlet pressure. It is for this reason that the slow evolution of the generation of by-product heat from the SOFC stack after the application of load on the fuel cell translates to gradual increases in cathode inlet pressure and flow during the start-up transient response. The decrease in system thermal effluent also manifests as a decrease in fuel cell inlet temperature as well, which is illustrated in Figure 7.19. Similarly to the pressure and flow profiles, the inlet temperature exhibits a sharp decrease at the point of load application and then illustrates a gradual downward trajectory towards some steady value that is not fully achieved by the 600s mark, after the load had been applied to the SOFC

stack. By the 600s mark, the temperature had decreased by approximately 7K to just below 940K. For the LBSC experiments, this decrease in FC inlet temperature was very significant, ultimately contributing to a significant increase in the density of fluid passing through the turbine and thus increasing mass flow and decreasing pressure after the initial transient response. Given the relatively modest decrease in FC inlet temperature for the OL case, its impact on fluid density and pressure is minimal and the increase in pressure and flow throughout the transient response is primarily a function of increased Q_{gen} total from the SOFC subsystem.

The FC inlet temperature has a sharp initial decrease, which transitions into a new steady value shortly after the turbine speed reaches its new steady value. The impact of this transient response of the FC inlet temperature directly impacts the temperature fields in solid FC material, for which a spatio-temporal profile is presented in Figure 7.20. As illustrated in the figure, temperature at the inlet of the SOFC has a very similar profile, with respect to time, as that of the FC inlet temperature presented in Figure 7.19.

Prior to the application of load, the prescribed IEA benchmarking syngas mixture was fed to the virtual SOFC, and both the simulated fuel cell and system were allowed to reach steady state. The cell was not electrochemically active prior to t=0s, but the presence of nickel in the anode as well as suitable temperatures resulted in a consumption of thermal energy and a gradual decrease in SOFC temperature in the axial direction of the flow. This is very similar to the LBSC case for which the fuel stream composition profile, prior to the application of load, is presented in Figure 7.2.

Given relatively low initial load application, a modest amount of by-product heat from cell operation is produced and a minor change in magnitude of the SOFC solid temperature profile is observed post-load. As illustrated in Figure 7.20, the temperature at the exit of the SOFC increases from 885K to approximately 890K, as compared to the LBSC case that exhibits an increase at the SOFC exit of nearly 35K for 100A of initial load. As a reminder, it is important to note that the 30A loading for the OL case was

employed given the turbine's inability to operate at rotational speeds outside of the ±5% window, thus limiting the amount of load that can be placed on the turbine without turbine speed control. Another difference between the OL and LBSC scenario is that there is no apparent transition to a cooling regime for the SOFC. The temperature of the SOFC exhibits a gradual increase once load is applied at t=0s, but no reversed trajectory as illustrated in the LBSC case across the length of the SOFC is readily observed. This is again due to the relatively small initial FC loading which had a very minor effect on the SOFC temperature profile and thermal transport. As illustrated by the small increase in solid temperature at the outlet of the FC, this can be attributed to the low level of by-product heat generation that can be readily balanced by the presence of endothermic DIR in the SOFC fuel channel.

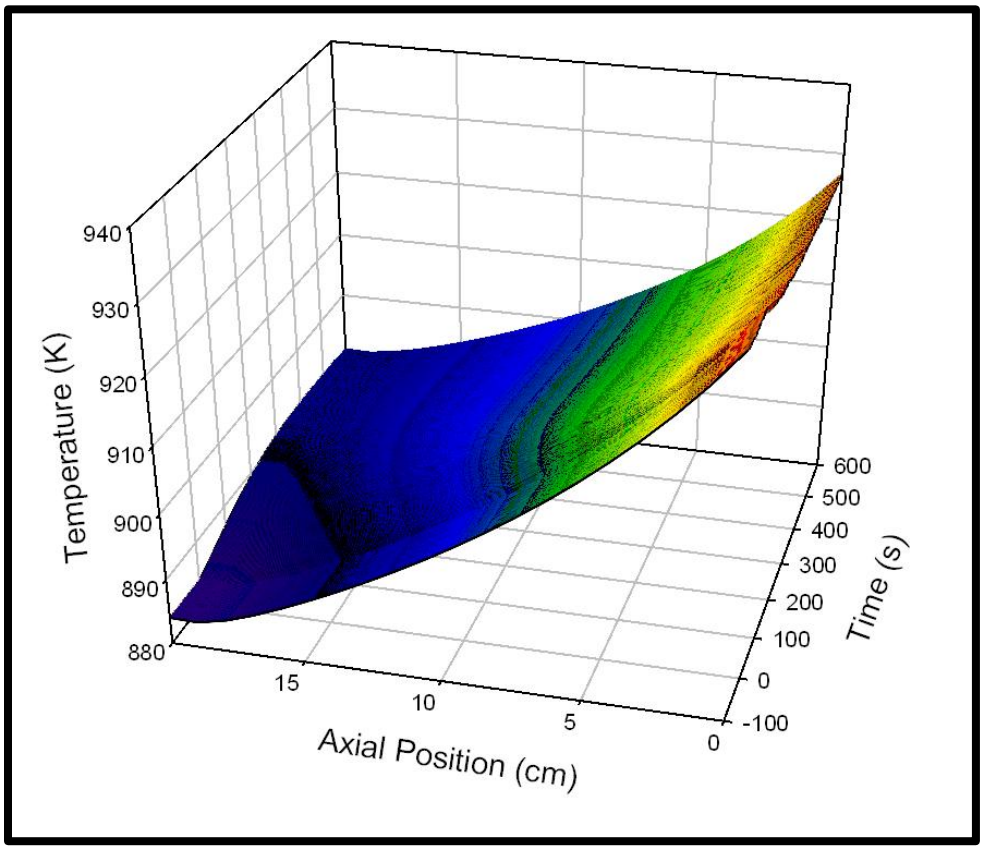

Figure 7.20: Spatio-temporal temperature plot – 30A FC OL: base case – syngas

The LBSC syngas experiment, presented in Section 7.1, illustrated that utilization of a syngas fuel feed provides a cooling effect that could contribute to reduction of potentially harmful gradients during electrochemical start-up. To examine this effect for the OL experiment, the spatio-temporal spatial gradient plot is presented in Figure 7.21.

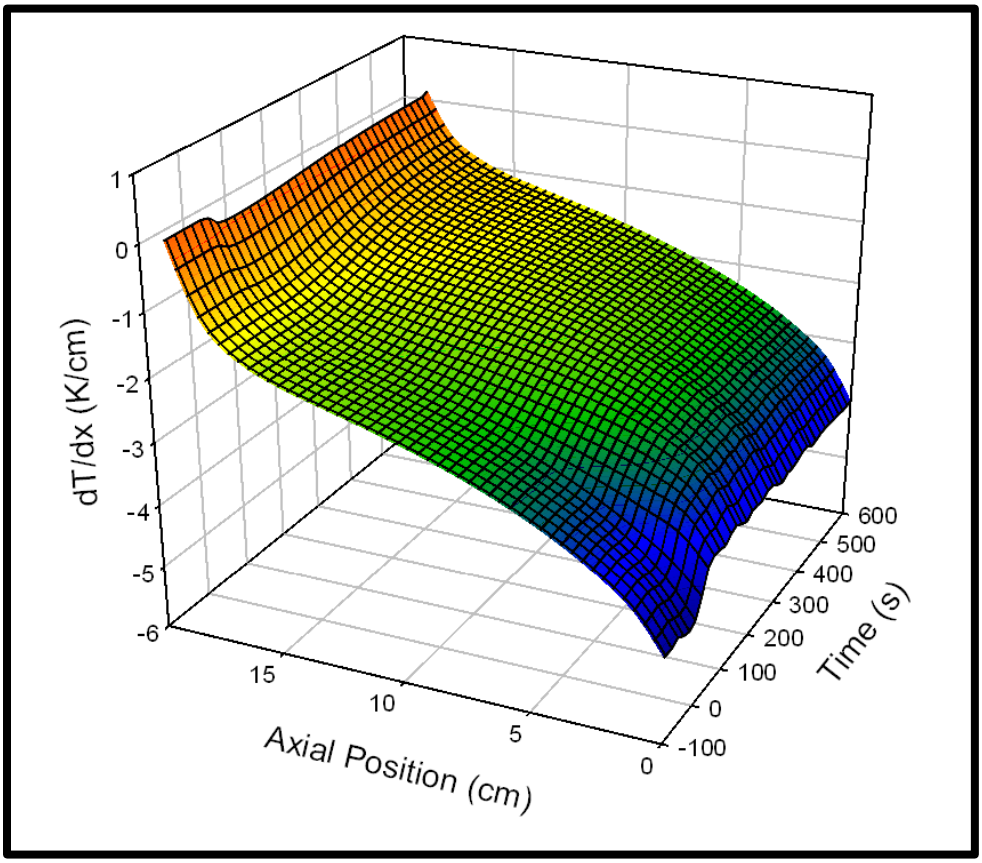

Figure 7.21: Spatio-temporal spatial temperature gradient plot – 30A FC OL: base case – syngas

Given the IEA, methane-rich syngas serving as the fuel feed to the SOFC prior to the application of load, there was significant cell cooling along the length of the fuel channel resulting in a monotonically decreasing temperature profile from entrance to exit of the fuel cell, as illustrated in Figure 7.20. Given the higher concentrations of methane in the upstream portions of the SOFC, enhanced cooling effects are present near the entrance of the fuel cell resulting in negative temperature gradients of decreasing magnitude from inlet to exit. Before load is applied to the fuel cell, the dT/dx value at the

inlet of the SOFC is approximately -5 K/cm. The local spatial gradient terms gradually increase in the axial direction of the flow, with a steep incline observed in the downstream portion of the fuel cell as a spatial temperature gradient of zero is approached given the adiabatic boundary condition at the cell exit.

At the point of load application, at t=0s, the cell becomes electrochemically active and starts to generate by-product heat from cell operation. The competing effect of the heating due to cell operation against the cooling due to inter reactant stream chemistry results in an increase in the overall spatial temperature profile and consequently a decrease in the magnitude of the local spatial gradients, along the length of the FC. The small amount of current draw results in relatively low values of operational by-product heat generation, thus resulting in relatively minor changes in the spatial gradient spatio-temporal profile.

The dynamic behavior of local spatial gradient, illustrated in Figure 7.21, for OL electrochemical start-up with a syn-gas fuel feed, is much different than the resulting profile that is presented in Figure 6.3 for the HH fuel feed case. At the point of load application for the HH case, the spatial gradient profile gradually increases with an overall maximum value being observed near the inlet, approximately 150s after load was applied and a “steady” dT/dx profile that gradually decreases in the axial direction of the flow. Prior to load being applied, the local dT/dx profile is essentially uniform with a value of 0K/cm, but after the application of load the majority of the profile is positive, which means that temperature is primarily increasing in the flow direction.

The syngas fuel feed case illustrates no distinct local, interior maxima near the inlet of the fuel cell, but the overall maximum magnitude is consistently present at the inlet due to the effect of reactant stream chemistry. This demonstrates the impact of the DIR cooling on the thermal transport in the SOFC as well as the impact of low levels of by-product heat generation on the electrochemical start-up process when using a syngas fuel feed. Ultimately the cooling effect of DIR provides a benefit in the leveling of local

temperature and spatial temperature gradient profiles, if the magnitude of FC load is sufficient to generate enough by-product heat to overcome the cooling effect of the reactant stream chemistry. This means that the appropriate balance between fuel feed composition and initial FC load will have to be empirically identified to properly utilize reactant stream chemistry to counteract the thermal transport initiated by electrochemical start-up.

The local current density spatio-temporal plot is presented in Figure 7.22. The current density trend, at the point of initial load, is significantly different from both the LBSC syngas fuel feed profile as well as the OL HH fuel feed profile. The current density for the LBSC syngas fuel feed experiment, which is illustrated in Figure 7.6, has a maximum current density at the entrance of the FC, which monotonically decreases along the length of the FC to the exit, at the point of load application. Though the H_2 concentration was not at a maximum at the inlet of the fuel cell for the LBSC syngas fuel feed case, temperature had a dominant effect over the local current density at the higher level of current draw and a monotonic decrease was observed. The local current density profile for the OL HH fuel feed start-up has a local maximum at the inlet of the FC and exhibited a nearly linear decrease to the exit of the FC at the point of load application. Given the uniform nature of the temperature profile prior to load application, the observed profile was heavily influenced by reactant concentrations. The OL syngas fuel feed case, presented in Figure 7.22, illustrate local current density maxima approximately 5cm downstream from the inlet of the fuel cell, with a gradual decrease in the axial direction of the flow.

The trend observed for the OL syngas case illustrates the coupled effect of local hydrogen concentration and SOFC temperature on electrochemical current density. As illustrated in Figure 7.20, local SOFC temperatures are monotonically decreasing downstream but, as illustrated in Figure 7.23, local H_2 concentration is increasing

downstream. These competing effects result in the presence of a local current density maximum in the interior of the SOFC.

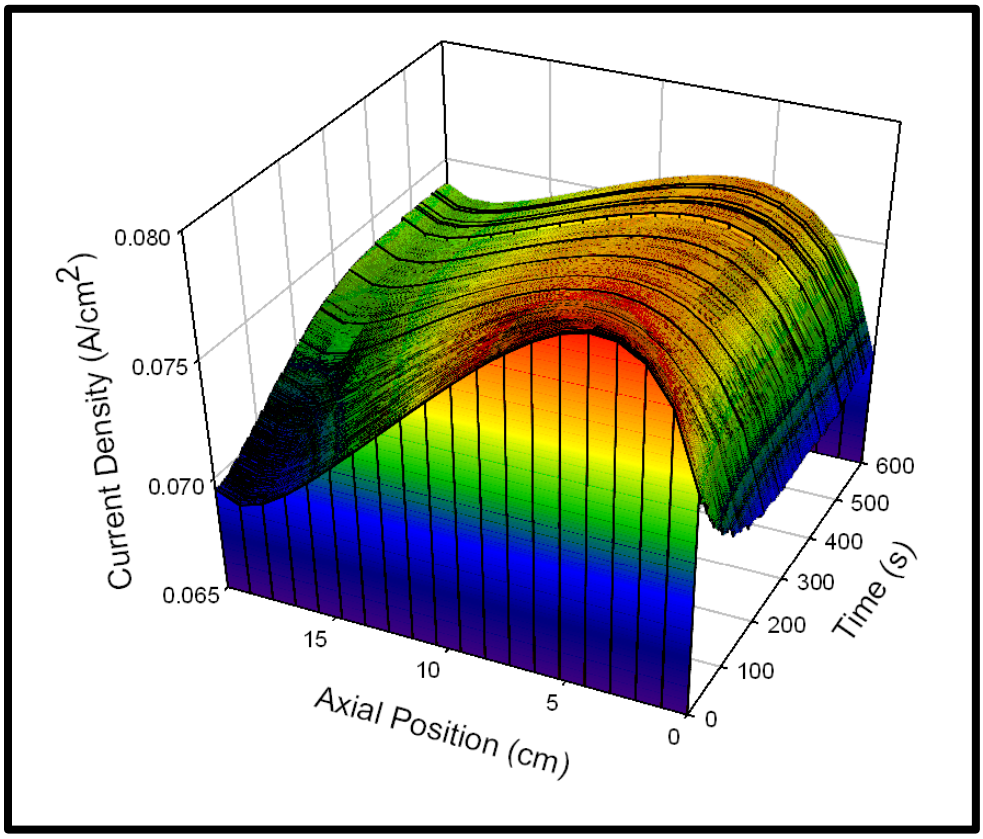

Figure 7.22: Spatio-temporal current density plot – 30A FC OL: base case – syngas

As the system and the SOFC respond to the electrochemical start-up, the redistribution of the temperature profiles impacts the local current density profiles as well. The magnitude of the maximum local current density gradually decreases. The downstream current densities significantly increase due to increasing temperature from by-product heat generation, while the upstream current densities decrease due to the cooling effect of the inlet stream. Despite the redistribution of the current density profile due to changes in the temperature distribution of the SOFC, and current density dynamics, the low current draw and subsequently low fuel utilization results in a nearly constant H_2 concentration profile that is illustrated in Figure 7.23.

The hydrogen concentration monotonically increases in the axial direction of the flow throughout the entire transient response to electrochemical start-up, with an inlet concentration of 26.26% and an exit concentration of approximately 42% throughout the entire start-up period. It is apparent that the low current and fuel utilization values result in minimal dynamic impact on the spatio-temporal composition profile as it doesn't change as an effect of the transient response of temperature during start-up.

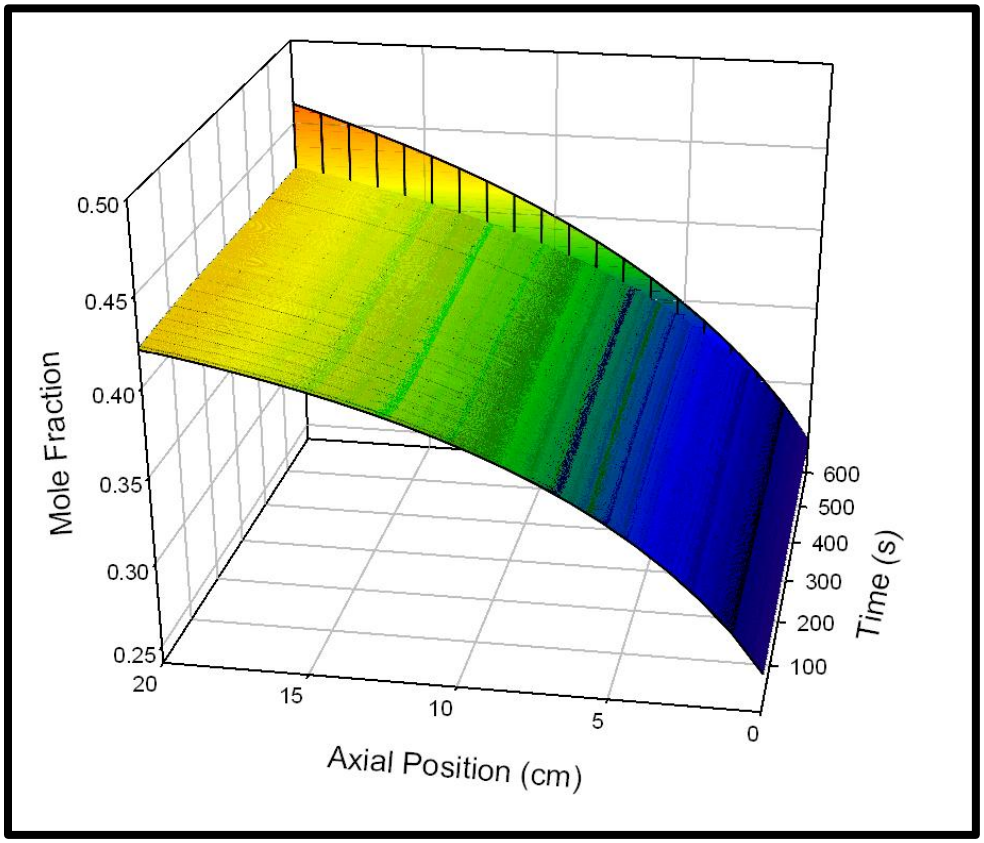

Figure 7.23: Spatio-temporal hydrogen concentration plot – 30A FC OL: base case – syngas

7.2.2 System Performance – OL – HH/Syngas Comparison

The application of load on the virtual SOFC subsystem results in an instantaneous decrease in the amount of thermal effluent provided to the HyPer facility. This decrease in physical heat results in a decrease in turbine speed, and the input parameters for the virtual SOFC of pressure, temperature and flow. This section presents and analyzes the

transient system parameter data of interest for the 30A, 40% CA by-pass, OL electrochemical start-up with a syngas fuel feed in comparison to the HH scenario.

Figure 7.24 presents the cathode inlet flow as a function of time for electrochemical start-up based upon applying 30A of initial FC load with 40% CA by-pass. The pre-load cathode flow for the syngas fuel feed case appears to be slightly larger than the HH case, and the difference in magnitude remains throughout the 80 seconds of the start-up transient response that is presented in the figure. The deviation in the pre-load cathode flow can be attributed to differences in ambient conditions and the slightly different pre-load Q_{gen} total values discussed earlier in Section 7.2.

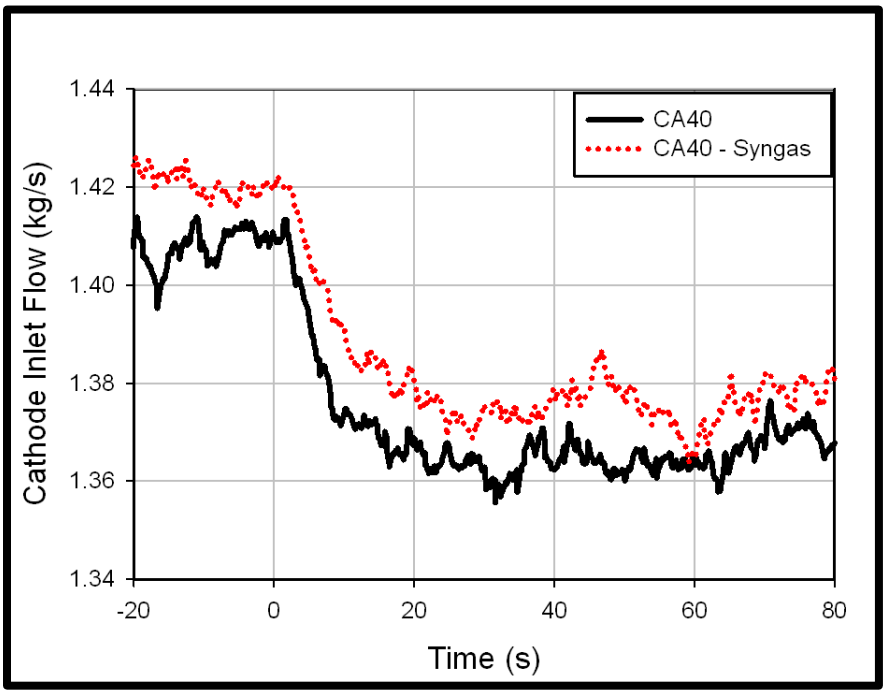

Figure 7.24: Absolute FC inlet flow vs. time – HH/syngas comparison, initial FC load 30A, 40% CA by-pass: OL

From inspection of Figure 7.24, it appears that the dynamic response of cathode inlet flow is very similar for both the syngas case as well as the HH case, but the comparison can be discerned more clearly by the presentation of the normalized cathode inlet flow profiles presented in Figure 7.25.

The normalized cathode inlet flow profiles illustrate a nearly identical dynamic response to the initial application of 30A of load during the start-up experiment. Once load is applied at t=0s, the cathode inlet flow begins to decrease due to the decrease in turbine speed initiated by the decrease in thermal effluent from the SOFC subsystem. Approximately 25 seconds after the load was applied, the minimum value of cathode inlet flow, for both the HH and syngas experiment is observed, approximately 3.5% less than the pre-load steady state value. The cathode inlet flows appear to start to increase approximately 60s after the application of load. This gradual increase to a new "steady" value is expected given the gradual increase in thermal effluent from the system (see Figure 7.27). This dynamic behavior is also illustrated in the base case process parameter plot in Figure 7.19.

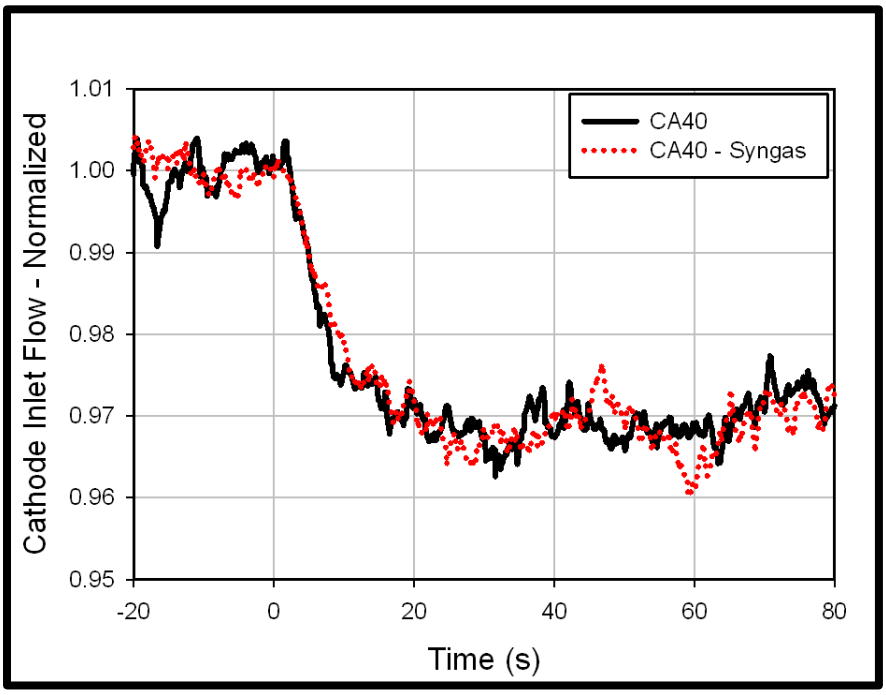

Figure 7.25: Normalized FC inlet flow vs. time – HH/syngas comparison: OL

Cathode inlet flow is highly coupled to the rotational speed of the turbine, which is presented for both the HH and syngas 30A, 40% CA by-pass electrochemical start-up experiments in Figure 7.26. The nominal, pre-load, rotational speed of the turbine is 40,500 RPM. Similarly to the cathode inlet flow, the dynamic behavior of the turbine

speed for both the HH and syngas fuel feed experiments compares very well. At t=0s, load is applied to the SOFC subsystem which decreases the amount of thermal effluent that it provides to the system and thus decreases turbine speed. At the point of load application, the turbine speed quickly decreases to approximately 97.5% of its initial value and then gradually approaches its minimum value, which is approximately 3% less than nominal operating speed approximately 30s after the application of load. Approximately 60s after start-up (i.e. load application), the turbine speed starts to increase in response to the increase in system thermal effluent due to by-product heat generation from cell operation as illustrated in the SOFC subsystem thermal effluent plot illustrated in Figure 7.27

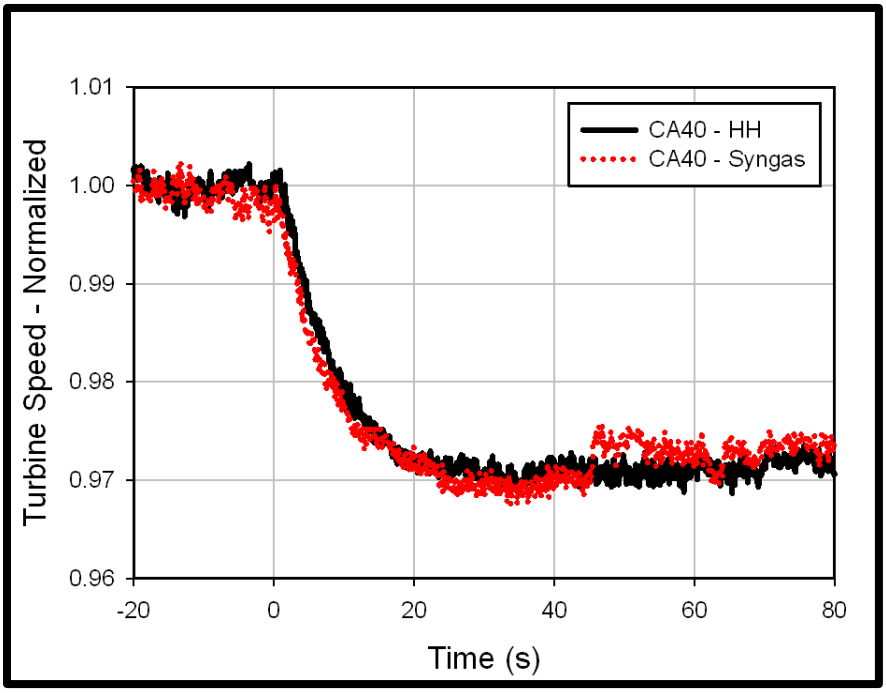

Figure 7.26: Normalized turbine speed vs. time – HH/syngas comparison: OL

In complementary fashion to the cathode inlet air flow and turbine speed, the dynamic response of the SOFC subsystem thermal effluent for both the HH and syngas fuel feed experiments compare very well. The pre-load Q_{gen} total values for the HH and syngas cases are 1439kW and 1432kW, respectively. At t=0s, the virtual SOFC starts to consume fuel, which is used to produce a combination of electrical power and by-product

heat from cell operation. The load application thus results in a decrease in the amount of fuel that is fed to the post combustor and the sharp decrease to a Q_{gen} total value that is less than 94% of its original value for both the HH and syngas experiments, and these minima occur approximately 5 seconds after load is applied. Once the minimum Q_{gen} total value is observed, the profile illustrates a gradual increase due to the generation of by-product heat in the SOFC stack. The thermal effluent profile illustrates the arrival at a steady value that is approximately 94.5% of the initial Q_{gen} total value, for both the HH and syngas fuel feed experiments, approximately 60s after initial load application

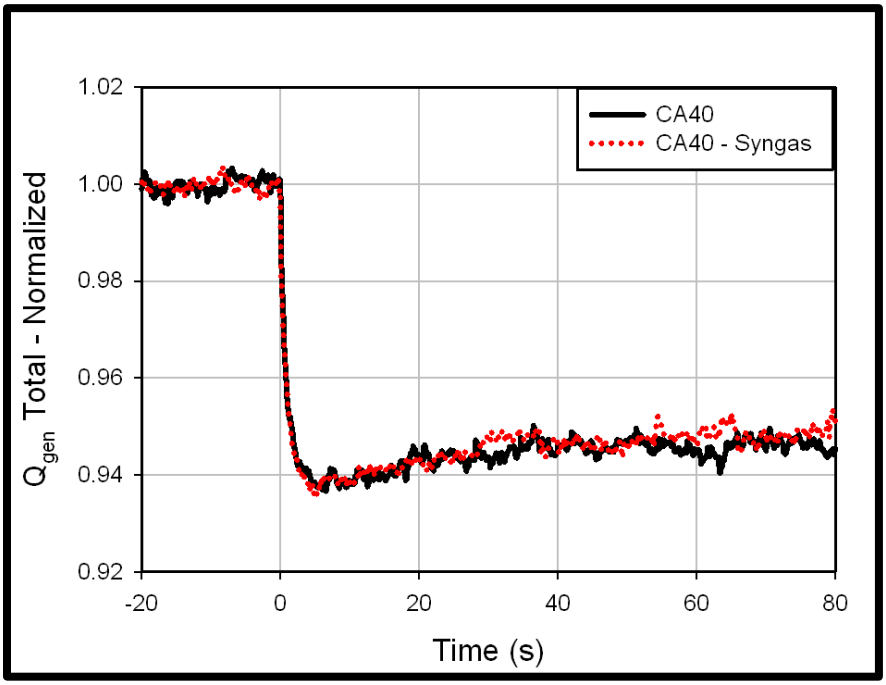

Figure 7.27: Normalized FC subsystem heat generated vs. time – HH/syngas comparison: OL

The transient response of the SOFC sub-system thermal effluent is very fast relative to both the turbine speed and cathode inlet mass flow previously presented. Essentially, applying load to the SOFC is the equivalent of decreasing the fuel flow to the system combustor in stepwise fashion, thus the steep and sharp trajectory to the minimum thermal effluent value. In comparing thermal effluent to turbine speed, there is approximately a delay of more than 20s in the occurrence of thermal transients in the

thermal effluent to the impact of those transients being exhibited by the turbine speed. For example, the minimum thermal effluent value occurs approximately 5 seconds after the application of load whereas the minimum turbine speed occurs approximately 30 seconds after the load application. Fully characterizing these delay times and combined effects between coupled system transients will be essential in the development of control strategies for safe and reliable system operation.

The decrease in system thermal effluent that is caused by the application of electrical load on the SOFC, removes thermal energy from the system and thus decreases inlet temperature to the virtual SOFC, which is illustrated for both the HH and syngas experiments in normalized fashion in Figure 7.28. The pre-load FC inlet temperatures were 945.3K and 939.1K for the HH and syngas fuel feeds, respectively. At the point of load application, the FC inlet temperature profile illustrates a sharp downward trajectory through the first 20s of start-up. Approximately 20s after start-up, a change in concavity of profiles is observed, with the steep decrease transitioning to a gradual decrease between t=20s and t=40s. A slight variation in the profiles is observed between the t=20s and t=40s range, with the syngas profile exhibiting a more pronounced transition from sharp decrease to gradual decrease than the HH profile. Though this deviation is identifiable given the scale of the graph, the statistical analysis supports that the deviation between the two profiles in the 20s – 40s regime is within a standard deviation as presented in Chapter 3, and the difference between the HH and syngas cases is not statistically significant. Ultimately, the normalized cathode inlet temperature for an OL system configuration utilizing 40% CA by-pass and 30A of initial FC load have the same dynamic response for both HH and syngas fuel feeds.

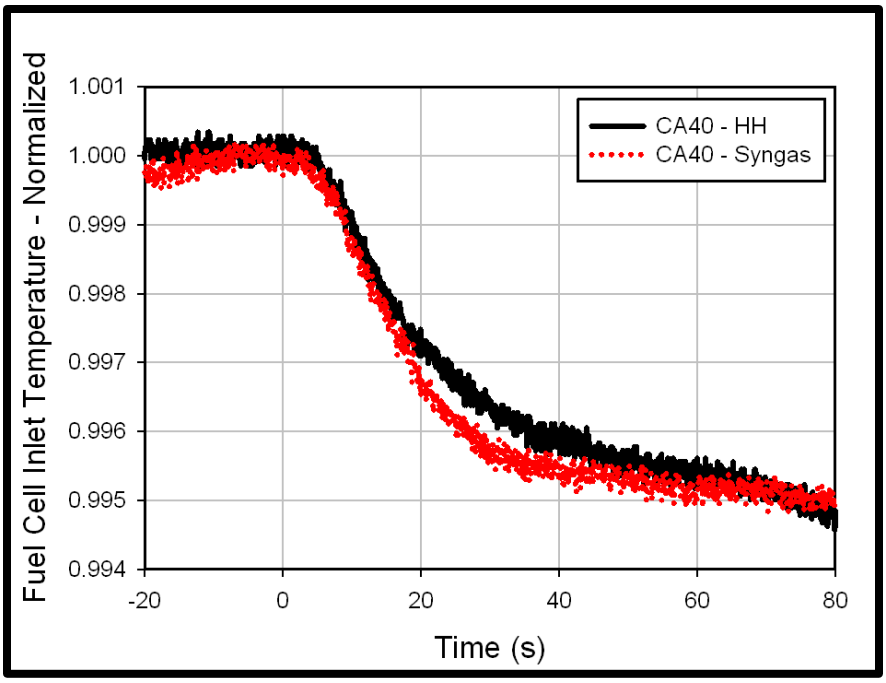

Figure 7.28: Normalized FC inlet temperature vs. time – HH/syngas comparison: OL

The normalized cathode inlet pressure for the electrochemical start-up experiments employing 30A of initial load and 40% CA by-pass is presented in Figure 7.29. The pre-load cathode inlet pressure was 376.0kPaa and 376.9kPaa for the HH and syngas cases, respectively. The dynamic behavior illustrated in the figure, is very similar to both the turbine speed and cathode inlet flow normalized profiles. The cathode inlet pressure exhibits a steep and sharp decline at the time of load application, and its minimum of 94% of the pre-load value is reached approximately 30s after the load is applied to the SOFC. Once that minimum is reached, a gradual increase in cathode inlet pressure is observed throughout the 80s illustrated in Figure 7.29. This gradually increasing trend of cathode inlet pressure, after the minimum is achieved is also illustrated in the base case process parameters illustrated in Figure 7.19. This, again, can be attributed to changes in turbine speed.

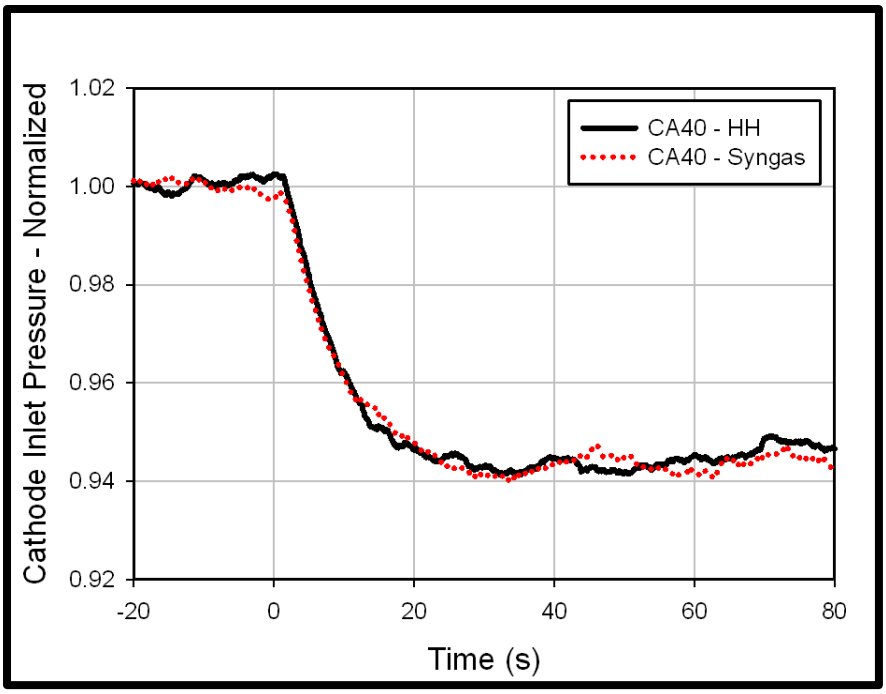

Figure 7.29: Normalized FC inlet pressure vs. time – HH/syngas comparison: OL

7.2.3 SOFC Performance – OL – HH/Syngas Comparison

Figure 7.30 presents the SOFC stack power and operating voltage throughout the first 600 seconds of 30A, CA 40% electrochemical start-up, for both HH and syngas fuel feeds. Once load is placed on the cell, operational voltage decreases in stepwise manner from the Nernst potential to its respective value depicted in the figure, and stack power increases from 0 while at an electrochemically inactive state, to its respective value which is illustrated. The initial operational voltages at t=0s were approximately 1.086V and 1.017V, respectively, for the HH and syngas fuel feed cases. The initial SOFC stack power at t=0s was approximately 71.22kW and 63.75kW, respectively.

Prior to placing load on the cell, the cell's voltage is its Nernst potential, which is the theoretical maximum voltage attainable given the presence of reactants available for electrochemical activity as well as the temperature of the SOFC. Once load is placed on the cell, an actual operating voltage is attained, which accounts for changes in concentration of reactants and temperature as well as the electrochemical loss terms that will arise with the drawing of current from the cell. The initiation of electrochemical

activity from current draw also initiates the production of stack power. Stack power is merely the product of the current, the operational voltage, and the number of cells in the SOFC stack.

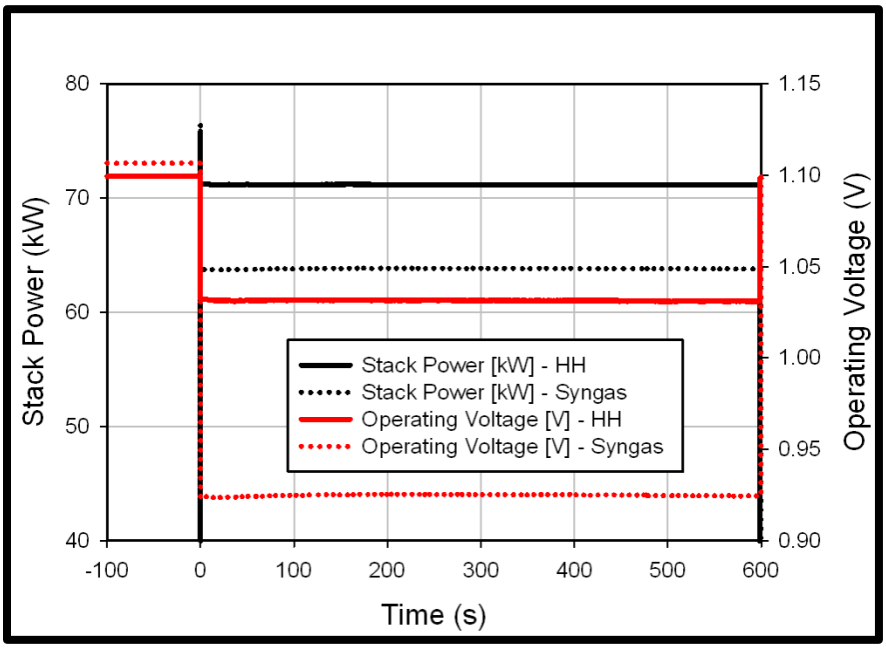

Figure 7.30: Stack power and operating voltage vs. time – HH/syngas comparison: OL

Both the stack power and the operational voltage for both fuel feeds of interest are essentially uniform throughout the 600 seconds of start-up transient response presented in Figure 7.30. This is due to the relatively small application of load and the minor to moderate thermal transient response. Once load is applied to the cell, the cell's voltage decreases from the Nernst potential to its actual operating value, and electrical power is being produced. As previously discussed, both the stack power and the operating voltage for the syngas fuel feed is lower than for the operating stack with HH fuel feed. This can be attributed to the decreased average operating temperature which results in increased electrochemical losses for the syngas fuel feed, as well as increased Nernst potential for the HH case due to greater concentrations of hydrogen in the fuel stream.

As previously discussed in section 7.2.2, the pre-load thermal effluent values were very comparable between the syngas and HH cases, but given the different fuel feed

compositions, the fuel flow rates were much different. The amount of fuel fed to the SOFC stack for the HH and syngas experiments was 23.1g/s and 98.5g/s respectively. The variation in fuel flow rates is associated with their respective heating values and the amount of thermal energy required to maintain a turbine sped of 40,500 RPM prior to electrochemical start-up. Once load is applied to the cell at t=0s, the fuel utilization for the two experiments is 6.2% and 17.8% for the HH and syngas fuel feeds, respectively. This illustrates that the amount of H_2 (and H_2 equivalents) available for electrochemical activity is significantly less for the syngas case as compared to the HH case and thus a lower Nernst potential for the syngas fuel feed. The average cell temperature is lower as well. The average pre-load cell temperatures for HH and syngas cases are 947.8K and 902.5K respectively. Given the direct relationship between temperature and electrochemical activity, this difference in temperature should result in a significantly lower operating voltage which is exhibited in Figure 7.30.

From inspection of the operating voltage and stack power profiles, there is essentially no dynamic behavior observed throughout start-up. All of the response variables are essentially invariant for the 600s presented. Given the known dependence on temperature of both operating voltage and stack power, it is expected that a smaller scale may delineate this dynamic behavior more readily; but aside from minor (± 1% deviation from the steady value) dynamic trends, immediately after the application of load, both stack power and operating voltage are essentially invariant due to the relatively small application of load and the minor to moderate temperature variation throughout the 600s following the application of load**.**

7.2.4 Distributed Comparison – OL – HH/Syngas Comparison

Figure 7.31 presents local temperatures of the SOFC at selected nodes along the entire length of the cell for the 30A, 40% CA by-pass electrochemical start-up. These were simulated for both HH and syngas fuel feeds. The local temperature profiles prior to

the load change illustrate the same behavior that was exhibited in Figure 6.2 and 7.21 for the HH and syngas fuel feeds, respectively. The SOFC had a nearly uniform temperature profile along the length of the fuel cell for the HH fuel feed experiment, which is illustrated by all of the overlapping local temperature profiles illustrated in Figure 7.31. For the syngas case, the temperature monotonically decreases along the length of the cell, as illustrated by the pre-load local temperatures ranging between approximately 933K at node one to 885K at node twenty. The magnitude of temperature decrease at successive nodes in the direction of the fuel flow decreases, exhibiting that the cooling from DIR decreases downstream due to the decrease in methane concentration, as well as temperature, in the direction of the flow.

The temperature profiles of the SOFC illustrate similar dynamic behavior in response to the load application. Nodes one and five for both cases exhibit a decrease in temperature, early in the start-up transient response, in response to the application of load. Node five does present a slight initial increase, but it is quickly followed by a decreasing profile. The decrease observed upstream is due to the dominating cooling effect of decreasing inlet temperature due to removal of physical heat from the system. The temperatures in the downstream portions of the cell, nodes fifteen and twenty, start to increase at the point of load application due to by-product heat generation from cell operation and the buffered downstream effect of oxidant stream cooling. The temperature profile near the center of the SOFC, node ten, is nearly uniform, illustrating a slight increase at the point of load application, followed by a gradual decrease to a temperature close to its pre-load value for both cases.

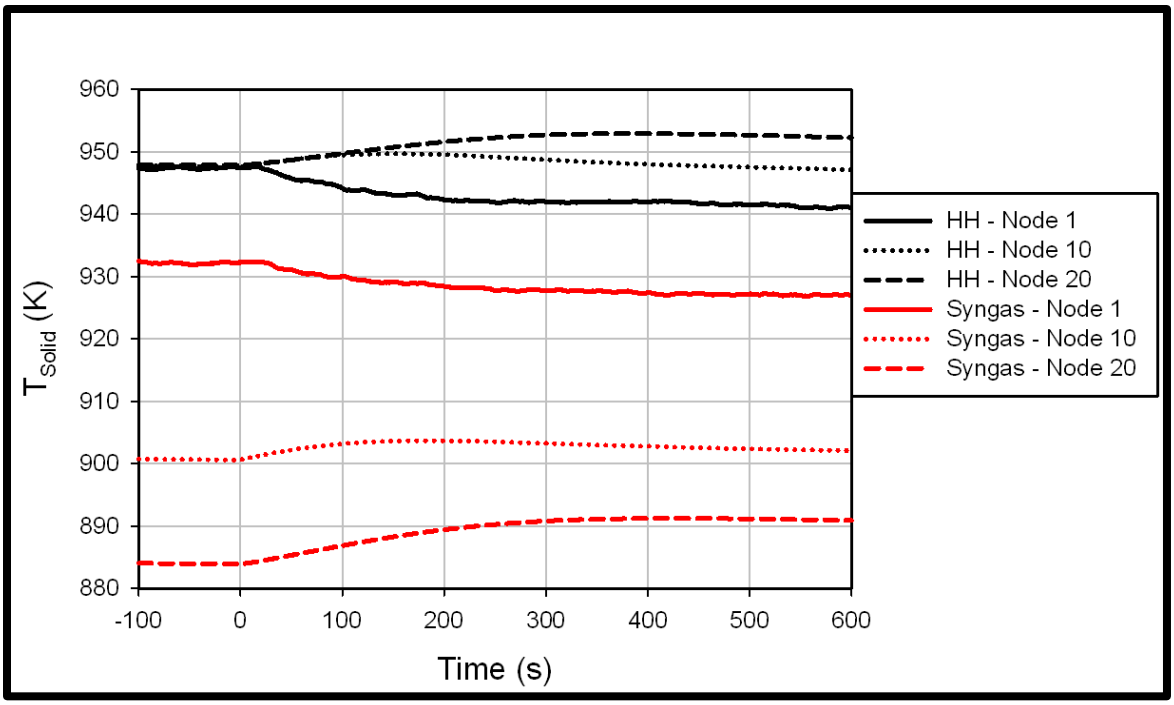

Figure 7.31: Local solid temperature along the entire SOFC length vs. time – HH/syngas comparison: OL

The dynamic behavior and response for each local temperature is very similar between both the HH and syngas fuel feed experiments. The most significant difference between the two temperature profiles is cell ΔT, which represents the difference between outlet and inlet cell temperatures. Prior to start-up the cell ΔT for the HH and syngas cases were approximately nil and 50K, respectively. After load is applied, the cell ΔT for the HH experiment increases to approximately 15K and decreases to approximately 35K for the syngas experiment. As illustrated by the leveling of the temperature profile after load was applied, for the syngas experiment, the cooling effect of DIR can assist in the leveling of temperature profiles during electrochemical start-up. In the case of the OL experiment, the current draw is so low that the cooling effect of DIR dominates the by-product heat generation from cell operation and thus a monotonically decreasing profile with a significant cell ΔT still exists. As initial FC load increases, the role of DIR cooling can play a significant role in managing temperature gradients but for low levels of current draw, and thus minimal by-product heat, the use of a methane rich syngas mixture can

have a deleterious effect on thermal stresses, both before and after the application of load during electrochemical start-up. This is illustrated by the sustained existence of significant temperature variation.

Though the syngas feed causes DIR, which significantly impacts the temperature profile, the combination of axial temperature and H_2 concentration variations cause the formation of an internal local current density maximum, as illustrated in Figure 7.22, as well as a more evenly distributed CD profile that is best exhibited in Figure 7.32. From inspection of Figure 7.22, the local CD maxima for the syngas case occurs at approximately node five, which has a value of 0.080 A/cm^2 at the point of load application. The range of CD values for the syngas is relatively small, ranging between 0.080A/cm^2 and 0.069 A/cm^2. Once the CD profile reaches its steady condition, the range decreases to approximately 0.077A/cm^2 and 0.070 A/cm^2. The profile for the HH case has a much greater range, varying between 0.090 A/cm^2 and 0.062 A/cm^2 at the point of load application and decreasing to values between 0.086 A/cm^2 and 0.065 A/cm^2 after the steady profiles had been reached.

Similarly to the temperature profiles, the magnitudes of the local current density profiles is much different for the two fuel feed cases, but the dynamic behavior between the two cases is very similar. The local CD at node one monotonically decreases throughout the transient for both cases. Nodes five and ten illustrates slight increases followed by gradual decreases through the remainder of start-up. Nodes fifteen and twenty gradually increase and arrive at an apparent steady value prior to the 600s mark. The major difference in the local CD profiles lies in the magnitude of the values and range between the maximum and minimum values and not in the dynamic behavior. This supports the stated similarity in the thermal dynamic behavior, regardless of fuel feed, and the competing effects of operating temperatures and hydrogen concentrations on the current density profile for the syngas case; the latter of which results in formation of internal local maxima. The strong similarity in the dynamic behaviors of the current

densities can be attributed to similarities in thermal dynamics for the "start-up" experiments of the two fuel feeds.

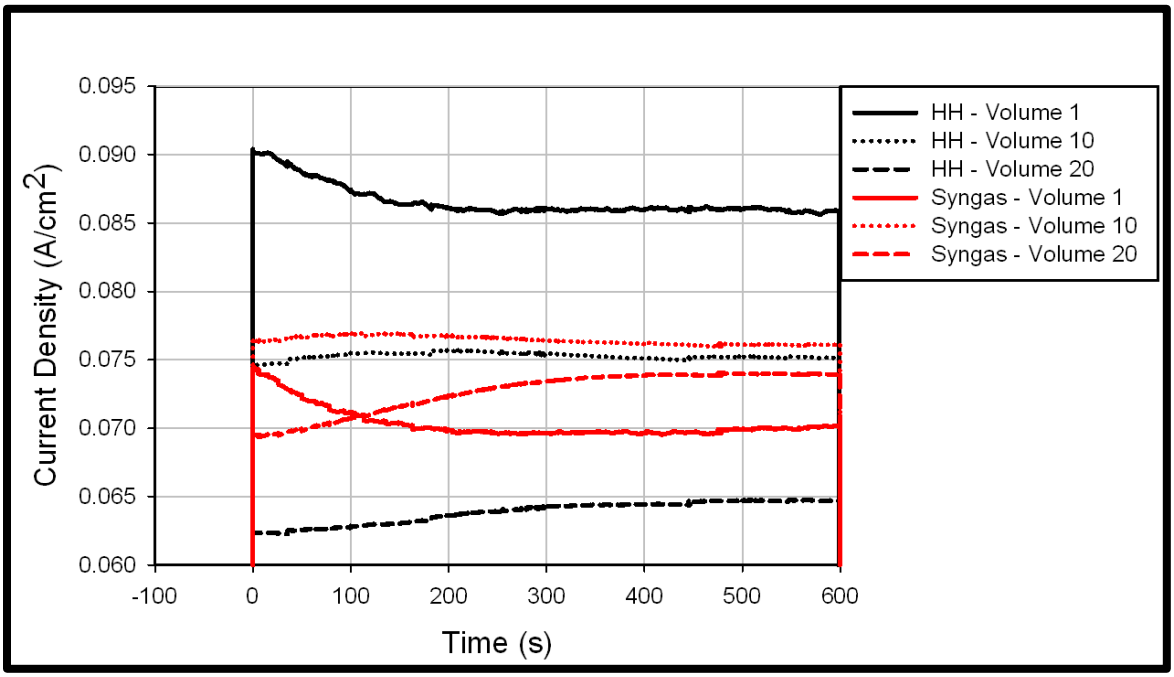

Figure 7.32: Local current density along the entire SOFC length vs. time – HH/syngas comparison: OL

The local current density profile directly influences local heat generation in the SOFC which is presented in Figure 7.33. The HH case has a nearly uniform local heat generation profile along the length of the SOFC. All of the local values appear to be centered around the 0.5W/cm value. The low levels of current draw and relatively small cell axial temperature variation allow for this nearly uniform local heat generation distribution.

The syngas case has negative Q_{gen} local terms for all of the volumes presented prior to the application of load. This is due to reactant stream chemistry (primarily DIR) that results in cell cooling. Excluding volume one, given the shifting of CO to equilibrium at the cell entrance, the local Q_{gen} values decrease in the downstream direction given that methane is being consumed as it flows through the fuel channel.

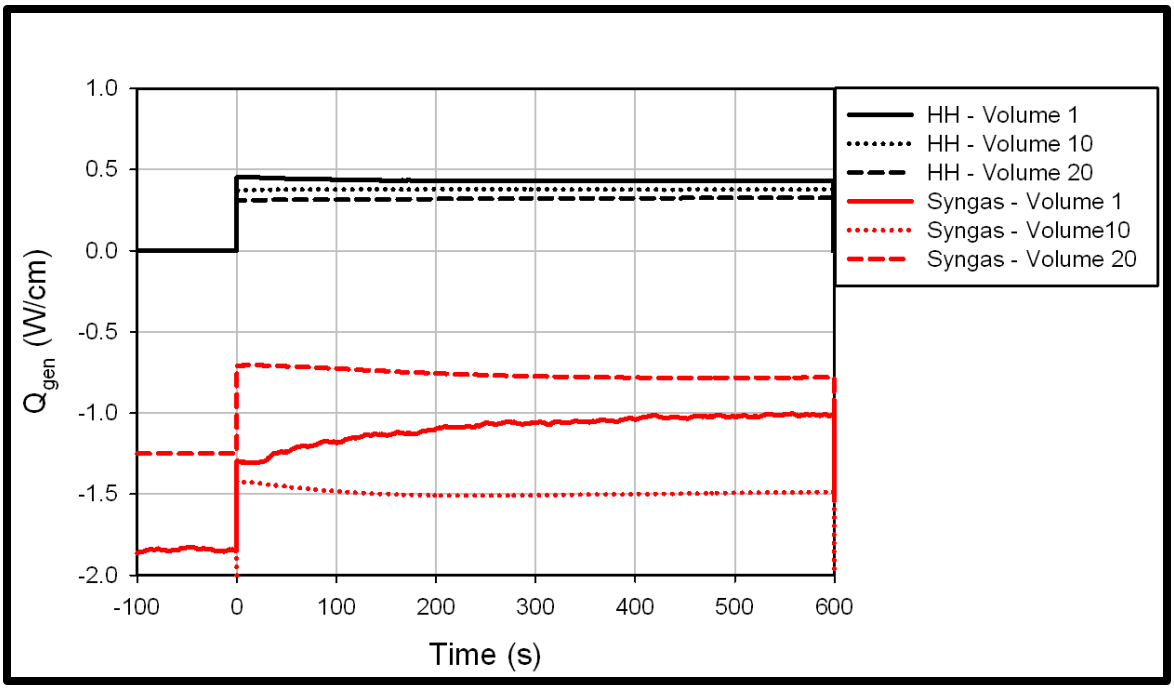

Figure 7.33: Local heat generation along the entire SOFC length vs. time – HH/syngas comparison: OL

At the point of load application, a step increase in local Q_{gen} is observed due to the generation of by-product heat. For nodes five through twenty, some slight dynamic behavior is observed within the first 200s of start-up, which is due to the thermal transients in the SOFC and their impact on both current density and the rate of reaction. For example, the decrease that is observed in the local heat generation term at volume five can be attributed to the decrease in local current density, illustrated in Figure 7.32. The most distinguishable transient response is illustrated for volume 1. After the application of load, the Q_{gen} local profile for volume one exhibits a step increase from approximately -1.9W/cm to -1.3W/cm. After the start-up is initiated the, the local heat generation value gradually increases until a steady value of –1.0W/cm is achieved. This gradual increase is due to the upstream cooling of the SOFC and its impact on the WGS reaction. As the temperature decreases, the equilibrium constant increases, thus resulting in more heat released due to the reaction and an increase in the Q_{gen} local profile at volume one. Since WGS reaction goes to equilibrium, the impact of temperature on the

Q_{gen} local profile is more pronounced at the inlet than at other locations along the length of the cell.

All of the distributed parameters presented contribute to the evolution of temperature gradients in the SOFC, for which local profiles are presented for electrochemical start-up employing both the HH and syngas fuel feeds in Figure 7.34. As with the other profiles, the dynamic behavior is very similar between the HH and syngas cases, but the magnitudes vary significantly. The one difference in the dynamic response is the absence of the "overshoot" effect for the syngas fuel feed. As is most pronounced for segments one and five of the HH case, the local dT/dx profile initially increases once load is applied, reaches some respective local maxima, then gradually decreases toward its steady value as discussed in Chapter 6. For the syngas case, the dT/dx values increase once load is applied but no "overshoot" is observed and the profile quickly arrives at its steady value. This can be attributed to the intra stack cooling effect from DIR that further influences the competing effects of by-product heating from SOFC operation and cell cooling from the decreased temperature of the cathode inlet air. As illustrated in Figure 7.21, the dT/dx profile of the syngas case was decreasingly negative from inlet to exit of the fuel cell prior to the application of load. After load was applied, the local values were still noticeably negative, but slightly increased. As illustrated in Figure 7.34, the spatial gradient is most negative across segment one and approximately 0K/cm across segment 19. The larger increase between segments 15 and 19 is due to the adiabatic boundary condition at the exit and the steep increase towards the adiabat due to elevated cell temperatures downstream. The by-product heat generation does decrease the average dT/dx value in the cell but given the low current draw, the DIR overcompensates for the by-product heat generation and causes more significant temperature gradients after the application of load than exist for the HH case.

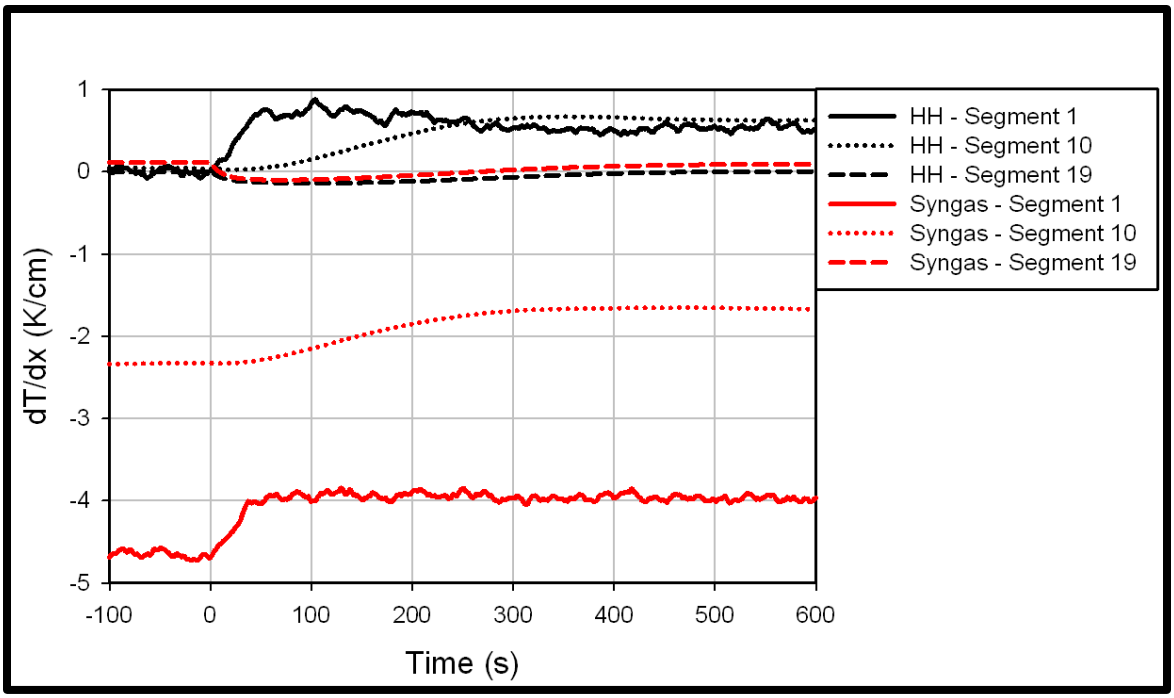

Figure 7.34: Local spatial temperature gradient along the entire SOFC length vs. time – HH/syngas comparison: OL

CHAPTER 8

CONCLUSION

The primary focus of the efforts set forth in this dissertation was to develop a 1-D solid oxide fuel cell (SOFC) model that was capable of operating in real time for use in a hardware-based simulation facility of a solid oxide fuel cell/ gas turbine (SOFC/GT) hybrid system. The operational emphasis was to characterize electrochemical start-up. The 1-D, real-time, SOFC model was successfully developed and verified via benchmarking with the IEA SOFC modeling protocol [45] as well as comparisons with other pre-published modeling data [44]. The model was then successfully coupled with the hardware-based Hybrid Performance Project (HyPer) simulation facility at the NETL in Morgantown, WV to initially investigate the impact of initial fuel cell FC load and cold air (CA) post-compressor by-pass on dynamic response of electrochemical start-up. The developed model was used to predict SOFC internal dynamic behavior while operating with the gas turbine (GT) in "direct" hybridized manner. This model will be used to drive the development of FC's capable of withstanding the projected system dynamics caused by gas turbine hybridization. Furthermore, simulations with the model can be used to develop system control strategies to mitigate the potentially harmful dynamic and transient effects upon SOFC durability and reliability. The findings from the CA by-pass and initial FC load investigation will further contribute to the advancement of addressing the issues of systems integration, for the essential start-up mechanism of SOFC/GT hybrid systems.

8.1 Project Developments

A robust, 1-D, real-time SOFC model was developed and integrated into the HyPer facility for hardware-based simulation of a SOFC/GT hybrid system. The model is

capable of characterizing a number of important SOFC operating parameters such as: SOFC temperature, oxidant temperature, current density, fuel stream composition, spatial temperature gradient, temporal temperature derivatives and polarization losses in spatio-temporal manner. The model was coupled to the facility using the dSpace control desk software, so that real-time operational parameters of pressure, temperature, and flow into the (virtual) SOFC subsystem can be directly fed into the model, and the SOFC internal characterization along with a subsystem thermal effluent value is returned. The thermal effluent allows the system to mimic (i.e. simulate) the amount of heat that would be provided to the system and, in coupled manner, the effect of dynamic response of the balance of plant (BOP) on SOFC operation.

To ensure the validity of the model, comparative benchmarking studies were conducted with the IEA SOFC modeling framework as well as pre-published data in the SOFC modeling arena. As presented in Chapter 4, the operational metrics of peak current density, stack power, max PEN temperature, exit air temperature, etc. compared well with both the IEA benchmark [45] as well as the NFCRC work from the University of California at Irvine [44].

The developed model was then used to characterize system wide and SOFC dynamic response to electrochemical start-up of the SOFC. During the investigation, the entire facility was allowed to come to a steady condition, at which point an initial load was applied to the virtual fuel cell stack. This load application, whether operating in open loop (OL) or load based speed control (LBSC) system configuration, resulted in a decrease in thermal effluent provided to the system, thus a decrease in turbine speed, and a resulting dynamic response that was observed throughout the entire system. The work presented in this dissertation presents a complete characterization of CA by-pass and initial FC load on system start-up during electrochemical start-up. CA by-pass valve positions of 35%, 40% and 60% were investigated along with initial FC loads of 50A, 75A, 100A, and 125A for LBSC configuration and 10A, 20A, 30A, and 40A for the OL

configuration. The impact on CA by-pass as well as initial FC load on system parameters that directly affect SOFC operation, such as inlet temperature, pressure, and flow, along with turbine speed and thermal effluent dynamics are presented and discussed in the dissertation. In addition to system parameters, SOFC performance metrics such as stack power, operating voltages and electrochemical losses are presented. Finally, the full spatio-temporal capability was exhibited and utilized in examining the impact of electrochemical start-up upon SOFC temperature, spatial gradient, current density and by-product heat generation. Ultimately a comprehensive parametric study, characterizing SOFC and hybrid system response to electrochemical start-up along the decision variable values of initial FC load as well as CA by-pass valve position was completed for LBSC and OL configurations. The impact of the given process variables on the dynamic behavior of the system was captured, and for the first time an empirically enhanced quantitative assessment of the impact of electrochemical start-up on system and SOFC dynamic response is presented.

8.2 Insights and Recommendations

Though the study focused on characterization of the system, results and prior research illustrates that the most significant effect or impact to consider during electrochemical start-up is the evolution of potentially harmful temperature gradients in the SOFC. The results specific to this study further illustrate that internal thermal transport of the SOFC is dependent upon both thermal dynamics of the system and electrochemical dynamics of the SOFC. Although transient response has an impact on electrochemical performance of the cell throughout the start-up event, the system efficiency and the amount of power production during start-up were not emphasized in light of “health” cautions and concerns associated with SOFC mechanical reliability and durability.

8.2.1 CA By-pass Variation

The results show that decreased levels of O_2 utilization as well as higher operating temperatures result in decreased impact of spatial temperature gradient formation in the SOFC. At higher operating temperatures, SOFC's operate more efficiently and thus less by-product heat generation is formed. Decreased localized by-product heat results in a more evenly distributed temperature profile through the transient response and thus a decrease in maximum temperature gradients is realized.

Decreased oxygen utilization in the SOFC results in an enhanced cooling effect during the start-up transient. This can be attributed to an increased amount of airflow relative to cell current draw. This increased cooling effect, in conjunction with the generation of by-product heat results in the leveling of the spatial temperature profile and thus minimizes temperature gradients.

Increasing CA by-pass results in decreases in both air-flow and cell operating temperature (excluding the CA 60% case given the fact it was a new turbine), so that suggests that increasing CA by-pass has competing effects with regards to internal SOFC temperature gradient mitigation strategy given the decreased SOFC operating temperature which makes the cell less efficient and thus increases the amount of by-product heat generation and increased cathode airflow, which enhances cell cooling.

Though the impact on the thermal cell dynamics appears to be qualitatively inconclusive regarding the CA by-pass, it is important to not overlook the impact of system dynamic response. As CA by-pass flow increases, turbine inlet temperature decreases and the system requires more fuel to maintain the desired turbine speed and steady operating state prior to the application of load onto the FC. The increased fuel flow results in a lower percentage decrease in thermal effluent from the SOFC sub-system which ultimately results in a decreased dynamic system response. This lower percent decrease results in less significant changes in turbine speed, cathode inlet pressure and can potentially be used as a mechanism to minimize the existence of

harmful pressure changes in the SOFC cathode air channel as well. Ultimately, decreasing CA by-pass had the most significant impact on the magnitude of the largest local temperature gradients in the SOFC.

8.2.2 Initial FC Load and Fuel Feed

Load step size played a significant role in the evolution of temperature gradients and system dynamics as well. Increased changes in load resulted in more by-product heat generation due to cell operation, more significant decreases in air flow (with a subsequent increase for LBSC) and a more significant and sustained decrease in cathode inlet temperature. The decrease in airflow and cathode inlet temperature coupled with the increase in the generation of byproduct heat both contribute, or do not deter, from the formation of temperature gradients and thus have a compounding effect on their evolution. This effect was more readily observed for LBSC experiments given the flexibility afforded with respect to initial FC load step size for the LBSC case as compared to OL.

The system configuration (LBSC vs. OL) had a significant impact on the magnitude of temperature gradients observed. Given the base cases for the system configurations, LBSC had a max temperature gradient of approximately 6K/cm, compared to approximately 1K/cm for the OL case. This is attributed directly to the magnitude of the initial FC load size. Since LBSC can allow for higher initial loads the dynamic response is more significant, and a greater impact on the evolution of temperature gradients is realized.

The impact of load system configuration, and consequently load step size on SOFC internal thermal dynamics, was strongly exhibited with the HH/syngas fuel feed comparison. For the 100A, LBSC case, the peak cell temperature gradient decreased to approximately 2K/cm due to reactant stream cell cooling. The DIR from the methane rich stream was able to counteract the generation of by-product heat and aid in the mitigation

of temperature gradients during start-up. It is important to note, however, that prior to the application of load the SOFC exhibited a significant decrease in local cell temperature in the direction of the flow due to DIR, and this resulted in significant temperature gradients prior to start-up. Given the low levels of by-product heat generation for the 30A case, the DIR from the syngas fuel feed not only counteracted the formation of by-product heat, but it significantly superseded it, resulting in a temperature profile of monotonic decrease even after the application of load. Though the HH/syngas fuel feed study illustrated that the fuel feed can be used as an effective mechanism to mitigate the presence of harmful temperature gradients, determination of the fuel feed composition should ultimately consider the desired operating state, path to that desired state, and expected generation of by-product heat.

8.3 Original Contribution and Significance

The key fundamental research challenges and questions addressed by this dissertation are as follows:

- Development of a tool to address the system integration issues associated with SOFC/GT hybrids with sufficient fidelity while mitigating the fiscal risk associated with empirical investigation of SOFC stacks.
- What are the effects of electrochemical start-up of SOFC/GT hybrid system dynamic response, specifically with respect to internal SOFC thermal dynamics?
- How can control strategies be developed to ensure that system and SOFC mechanical durability and reliability can be preserved during electrochemical start-up.

This dissertation project involved the development of a 1-D, real-time operating planar SOFC model that was coupled to an operating gas turbine facility to simulate SOFC operation using hardware-based simulation, while operating “in-the-loop” with a

gas turbine in a hybrid environment. This 1-D model was a significant upgrade from the 0-D, lumped model previously used at the HyPer facility. Its coupling with the facility allows for feedback dynamics from the system to be directly observed by the model and accounted for in the simulation. The coupling of hardware and software provides a combination of sufficient accuracy from the flow dynamics of the physical system and flexibility with use of a computational tool such as the SOFC model. The model has significant novelty, being the first one identified in literature that is capable of distributed characterization, operating in real time, and coupling to a gas turbine using hardware-in-the-loop simulation (HiLS). It includes a set of temperature dependent thermophysical properties over an extensive range of temperatures that allows it to simulate inert heating, electrochemical start-up, on design operation and extreme off design conditions as well.

This model is used, in conjunction with the HyPer facility to conduct a parametric study analyzing the impact of CA by-pass and initial FC load on initial electrochemical start-up in a hybrid environment. Though some pilot scale SOFC/GT hybrids have been developed and operated, the characterization of the impact of varying system operating states on system dynamic response during initial electrochemical start-up, either empirically or using hardware based simulation has not been identified in literature as well. The results of this parametric characterization study are presented in this dissertation work and may be used by control system designers to develop transfer functions for the system so that it can be theoretically characterized and control strategies can be employed to ensure safe and reliable start-up.

To that end, the novel contributions of this dissertation project are as follows:

- Development of a robust, real-time operating, 1-D SOFC model capable of being coupled with a hardware facility for HiLS. As identified in literature, it is the first of its kind. The model has an extensively broad operating range as compared to other models that have been developed, harnessing the capability to characterize

inert heating, electrochemical start-up, on design operation, and off design operation.

- A comprehensive parametric evaluation and characterization of initial electrochemical light-off of an SOFC/GT hybrid system, varying CA by-pass valve position and initial FC load for both LBSC and OL system configurations. As compared to pre-existing literature and prior art, it is the first time a thorough and detailed study of initial electrochemical start-up has been conducted.

8.4 Future Work

As suggested through the explanation and justification of this work, the tool developed and the results presented only represent one component of a number of endeavors that still need to be addressed prior to the full integration of these system into the energy framework. With regards to electrochemical start-up characterization, a number of characterization studies still need to be investigated for variation of the system parameters as follows.

- Lower amounts of CA by-pass (25% - 35%)
- Hot air (HA) by-pass variance
- Bleed air (BA) by-pass variance
- Initial turbine load variance
- Coupled effects of varied by-pass valve positions and initial turbine load

Once the impact of operating state control parameters have been resolved, determining the impact of both simulated and physical pre-heat components such as a pre-combustion system, heat exchanger, electric heaters, etc. upstream of the SOFC needs to be evaluated as well. Investigations on the impact of load application methodology (step vs. ramp) as well as airflow management and control through start-up are also necessary areas of investigation. Finally, once the initial phase of electrochemical start-up is understood, characterized and controlled, development of a pathway to full load, nominal conditions must be developed.

With regards to the SOFC model, reactant stream chemistry needs to be further investigated and developed. Assuming that the governing rate law for direct internal reformation (DIR) is first order with respect to methane and that water gas shift (WGS) occurs at equilibrium may be valid for standard presumed operating states, but given the scope of the HyPer project and this desire to investigate extreme operating states and regimes, further evaluation of the governing chemical equations, included in the model, must be done to increase the level of accuracy and fidelity of the system at off design conditions.

REFERENCES

1. Kameswaran, S., H. Xi, S.T. Junker, S. Peles, J. Yamanis, and E. Sun, *Model-Based System Design of Highly-Efficient Integrated Gasification Fuel Cell Power Plants*, in *ASME 2010 Enght International Fuel Cell Science, Enginering and Technology Conference*, ASME, Editor. 2010, ASME: Brooklyn, New York.

2. U.S.DOE, *Cost and Performance Baseline for Fossil Energy Plants - Volume 1: Bituminous Coal and Natural Gas to Electricity*, U.S. DOE, Editor. 2007, U.S. DOE: Morgantown, WV.

3. Williams, M.C., J.P. Strakey, and W.A. Surdoval, *The U.S. Department of Energy, Office of Fossil Energy Stationary Fuel Cell Program.* Journal of Power Sources, 2005. **143**: p. 191-196.

4. Agency, E.I., *Electrical Power Annual 2009*, U.S.E.I. Administration, Editor. 2010, U.S. DOE: Washington, DC. p. 108.

5. Association, W.C. *Improving Efficiencies*. 2011 [cited 2010 September 1]; Available from: http://www.worldcoal.org/coal-the-environment/coal-use-the-environment/improving-efficiencies/.

6. Nelson, G.J. and C.L. Haynes, *Continuum-Level Solid Oxide Electrode Constriction Resistance Effects.* Journal of Power Sources, 2008. **185**: p. 1168-1178.

7. U.S.DOE, *Fuel Cell Handbook*. Seventh ed, ed. DOE/NETL. 2004, Morgantown, WV: DOE/NETL.

8. Larminie, J. and A. Dicks, *Fuel Cell Systems Explained*. 2nd ed. 2003: John Wiley & Sons.

9. U.S.DOE. *Fuel Cells: Hybrids*. 2011 [cited 2001 March, 1]; Available from: www.netl.doe.gov/technologies/coalpower/fuelcells/hybrids.html.

10. Selimovic, A., M. Kemm, T. Torisson, and M. Assadi, *Steady State and Transient Thermal Stress Analysis in Planar Solid Oxide Fuel Cells.* Journal of Power Sources, 2005. **145**: p. 463-469.

11. Tucker, D., A. Tsai, P. Jablonski, D.O. Hughes, C. Haynes, and J. Sellers, *Initial Transient Response during Fuel Cell Turbine Hybrid System Startup*, in *International Colloquium on Environmentally Preferred Advanced Power Generation*, ASME, Editor. 2010, ASME: Costa Mesa, Califorina. p. 11.

12. Nakajo, A., Z. Wuillemin, J. Van herle, and D. Favrat, *Simulation of thermal stresses in anode-supported solid oxide fuel cell stacks. Part I: Probability of failure of the cells.* Journal of Power Sources, 2009. **193**: p. 203-215.

13. Lim, H.-T. and A.V. Virkar, *A Study of Solid Oxide Fuel Cell Stack Failure by Inducing Abnormal Behavior in a Single Cell Test.* Journal of Power Sources, 2008. **185**: p. 790-800.

14. Tucker, D., L. Lawson, and R. Gemmen. *Characterization of Air Flow Management and Control in a Fuel Cell Turbine Hybrid Power System Using Hardware Simulation*. in *2005 ASME Power Conference, April 5, 2005 - April 7, 2005*. 2005. Chicago, IL, United states: American Society of Mechanical Engineers.

15. Tucker, D., E. Liese, and R. Gemmen. *Determination of the Operating Envelope for a Direct Fired Fuel Cell Turbine Hybrid Using Hardware Based Simulation*. in *International Colloquium on Environmentally Preferred Advanced Power Generation*. 2009. Newport Beach, Califorina: ASME.

16. Tucker, D., L. Lawson, R. Gemmen, and R. Dennis. *Evaluation of Hybrid Fuel Cell Turbine System Startup with Compressor Bleed*. in *ASME Turbo Expo 2005 - Gas Turbie Technology: Focus for the Future, June 6, 2005 - June 9, 2005*. 2005. Reno-Tahoe, NV, United states: American Society of Mechanical Engineers.

17. Tucker, D., L. Lawson, T.P. Smith, and C. Haynes. *Evaluation of Cathodic Air Flow Transients in a Hybrid System using Hardware Simulation*. in *4th International ASME Conference on Fuel Cell Science, Engineering and Technology, FUELCELL2006, June 19, 2006 - June 21, 2006*. 2006. Irvine, CA, United states: American Society of Mechanical Engineers.

18. Hughes, D.O., C. Haynes, L., D. Tucker, A. Tsai, and E. Liese, *Transient Behavior of a Fuel Cell/Gas Turbine Hybrid Using Hardware Based Simulation With a 1-D Distributed Fuel Cell Model*, in *International Colloquium on Environmentally Preferred Advanced Power Generation*, ASME, Editor. 2010, ASME: Costa Mesa, CA. p. 10.

19. Liese, E.A., R.S. Gemmen, T.P. Smith, and C.L. Haynes. *A Dynamic Bulk SOFC Model Used in a Hybrid Turbine Controls Test Facility*. in *2006 ASME 51st Turbo Expo, May 6, 2006 - May 11, 2006*. 2006. Barcelona, Spain: American Society of Mechanical Engineers.

20. Smith, T.P., C.L. Haynes, W.J. Wepfer, D. Tucker, and E.A. Liese. *Hardware-Based Simulation of a Fuel Cell Turbine Hybrid Response to Imposed Fuel Cell Load Transients*. in *2006 ASME International Mechanical Engineering Congress and Exposition, IMECE2006, November 5, 2006 - November 10, 2006*. 2006. Chicago, IL, United states: American Society of Mechanical Engineers.

21. Smith, T.P., *Hardware Simulation of Fuel Cell/Gas Turbine Hybrids*, in *George W. Woodruff School of Mechanical Enginering*. 2007, Georgia Institute of Technology: Atlanta, GA. p. 251.

22. Johnson, J. and J. Qu, *Effective Modulus and Coefficient of Thermal Expansion of Ni-YSZ Porous Cermets.* Journal of Power Sources, 2008. **181**: p. 85-92.

23. Liu, S.X., C. Song, and Z.J. Lin, *The Effects of the Interconnect Rib Contact Resistance on the Performance of Planar Solid Oxide Fuel Cell Stack and the Rib Design Optimization.* Journal of Power Sources, 2008. **183**: p. 214-225.

24. Liu, W. and J. Qu. *Creep Deformation of Ni/YSZ Cermet in SOFCs*. in *29th International Conference on Advanced Ceramics and Composites, January 23, 2005 - January 28, 2005*. 2005. Cocoa Beach, FL, United states: American Ceramic Society.

25. Ackmann, T., L.G.J. de Haart, W. Lehnert, and D. Stolten, *Modeling of Mass and Heat Transport in Planar Substrate Type SOFCs.* Journal of the Electrochemical Society, 2003. **150**: p. A783-A789.

26. Campanari, S., *Thermodynamic Model and Parametric Analysis of a Tubular SOFC Module.* Journal of Power Sources, 2001. **92**: p. 26-34.

27. Campanari, S. and P. Iora, *Definition and Sensitivity Analysis of a Finite Volume SOFC Model for a Tubular Cell Geometry.* Journal of Power Sources, 2004. **132**: p. 113-126.

28. Chyou, Y.P., T.D. Chung, J.S. Chen, and R.F. Shie, *Integrated Thermal Engineering Analyses with Heat Transfer at Periphery of Planar Solid Oxide Fuel Cell.* Journal of Power Sources, 2005. **139**: p. 126-140.

29. Sudaprasert, K., R.P. Travis, and R.F. Martinez-Botas, *A Study of Temperature Distribution Across a Solid Oxide Fuel Cell Stack.* Journal of Fuel Cell Science and Technology, 2010. **7**: p. -.

30. Achenbach, E., *Three-Dimensional and Time-Dependent Simulation of a Planar Solid Oxide Fuel Cell Stack.* Journal of Power Sources, 1994. **49**: p. 333-348.

31. Achenbach, E., *Response of a Solid Oxide Fuel Cell to Load Change.* Journal of Power Sources, 1995. **57**: p. 105-109.

32. Pei-Wen, L. and M.K. Chyu, *Simulation of the Chemical/Electrochemical Reactions and Heat/Mass Transfer for a Tubular SOFC in a Stack.* Journal of Power Sources, 2003. **124**: p. 487-98.

33. Xue, X., J. Tang, N. Sammes, and Y. Du, *Dynamic Modeling of Single Tubular SOFC Combining Heat/Mass Transfer and Electrochemical Reaction Effects.* Journal of Power Sources, 2005. **142**: p. 211-22.

34. Jiang, W., R. Fang, R.A. Dougal, and J.A. Khan, *Thermoelectric Model of a Tubular SOFC for Dynamic Simulation.* Journal of Energy Resources Technology, 2008. **130**: p. 022601-10.

35. Mollayi Barzi, Y., M. Ghassemi, and M.H. Hamedi, *A 2D transient numerical model combining heat/mass transport effects in a tubular solid oxide fuel cell.* Journal of Power Sources, 2009. **192**: p. 200-207.

36. Salogni, A. and P. Colonna, *Modeling of solid oxide fuel cells for dynamic simulations of integrated systems.* Applied Thermal Engineering, 2010. **30**: p. 464-477.

37. Ferrari, M.L., A. Traverso, L. Magistri, and A.F. Massardo, *Influence of the Anodic Recirculation Transient Behaviour on the SOFC Hybrid System Performance.* Journal of Power Sources, 2005. **149**: p. 22-32.

38. Jiang, W., R.X. Fang, J. Khan, and R. Dougal, *Control Strategies for Start-Up and Part-Load Operation of Solid Oxide Fuel Cell/Gas Turbine Hybrid System.* Journal of Fuel Cell Science and Technology, 2010. **7**: p. -.

39. Magistri, L., M. Bozzolo, O. Tarnowski, G. Agnew, and A.F. Massardo, *Design and Off-Design Analysis of a MW Hybrid System Based on Rolls-Royce Integrated Planar Solid Oxide Fuel Cells.* Journal of Engineering for Gas Turbines and Power, 2007. **129**: p. 792-797.

40. Shelton, M., I. Celik, E. Liese, and D. Tucker, *A Study in the Process Modeling of the Startup of Fuel Cell/Gas Turbine Hybrid Systems.* Journal of Engineering for Gas Turbines and Power-Transactions of the Asme, 2010. **132**: p. -.

41. Traverso, A., A. Massardo, R.A. Roberts, J. Brouwer, and S. Samuelsen, *Gas Turbine Assessment for Air Management of Pressurized SOFC/GT Hybrid Systems.* Journal of Fuel Cell Science and Technology, 2007. **4**: p. 373-383.

42. Haynes, C.L. and J.C. Ford. *A Simulation of the Solid Oxide Fuel Cell Electrochemical Light Off Phenomenon*. in *2005 ASME Summer Heat Transfer Conference, HT 2005, July 17, 2005 - July 22, 2005*. 2005. San Francisco, CA, United states: American Society of Mechanical Engineers.

43. Chyou, Y.P., J.S. Chen, and T.D. Chung, *A Methodology for Optimizing the Start-Up Scenario of Solid Oxide Fuel Cell Utilizing Transient Analyses.* Journal of the Electrochemical Society, 2008. **155**: p. B650-B659.

44. Li, M., J. Brouwer, J.D. Powers, and G.S. Samuelsen, *A Finite Volume SOFC Model For Coal-Based Integrated Gasification Fuel Cell System Analysis.* Journal of Fuel Cell Science and Technology, 2010.

45. Achenbach, E., *SOFC Stack Modeling, Final Report of Activity A2, Annex II: Modeling and Evaluation of Advanced Solid Oxide Fuel Cells, International Energy Agency Programme on R, D&D on Advanced Fuel Cells*. 1996, International Energy Agency: Juelich, Germany.

46. Maclay, J.D., J. Brouwer, and G.S. Samuelsen, *Diurnal Temperature and Pressure Effects on Axial Turbomachinery Stability in Solid Oxide Fuel Cell-Gas Turbine Hybrid Systems.* Journal of Fuel Cell Science and Technology, 2011. **8**: p. 031012-6.

47. Mueller, F., B. Tarroja, J. Maclay, F. Jabbari, J. Brouwer, and S. Samuelsen, *Design, Simulation and Control of a 100 MW-Class Solid Oxide Fuel Cell Gas Turbine Hybrid System.* Journal of Fuel Cell Science and Technology, 2010. **7**: p. 031007-11.

48. Trasino, F., M. Bozzolo, L. Magistri, and A.F. Massardo, *Modeling and Performance Analysis of the Rolls-Royce Fuel Cell Systems Limited: 1 MW Plant.* Journal of Engineering for Gas Turbines and Power, 2011. **133**: p. 021701-11.

49. Magistri, L., P. Costamagna, A.F. Massardo, C. Rodgers, and C.F. McDonald, *A Hybrid System Based on a Personal Turbine (5 kW) and a Solid Oxide Fuel Cell Stack: A Flexible and High Efficiency Energy Concept for the Distributed Power Market.* Journal of Engineering for Gas Turbines and Power, 2002. **124**: p. 850-857.

50. Roberts, R.A., J. Brouwer, and G.S. Samuelsen, *Fuel Cell/Gas Turbine Hybrid System Control for Daily Load Profile and Ambient Condition Variation.* Journal of Engineering for Gas Turbines and Power, 2010. **132**: p. 012302-7.

51. Ferrari, M.L., E. Liese, D. Tucker, L. Lawson, A. Traverso, and A.F. Massardo, *Transient Modeling of the NETL Hybrid Fuel Cell/Gas Turbine Facility and Experimental Validation.* Journal of Engineering for Gas Turbines and Power, 2007. **129**: p. 1012-1019.

52. Mueller, F., R. Gaynor, A.E. Auld, J. Brouwer, F. Jabbari, and G.S. Samuelsen, *Synergistic integration of a gas turbine and solid oxide fuel cell for improved transient capability.* Journal of Power Sources, 2008. **176**: p. 229-239.

53. Aguiar, P., C.S. Adjiman, and N.P. Brandon, *Anode-Supported Intermediate Temperature Direct Internal Reforming Solid Oxide Fuel Cell. I: Model-Based Steady-State Performance.* Journal of Power Sources, 2004. **138**: p. 120-136.

54. Costamagna, P., A. Selimovic, M. Del Borghi, and G. Agnew, *Electrochemical Model of the Integrated Planar Solid Oxide Fuel Cell (IP-SOFC).* Chemical Engineering Journal, 2004. **102**: p. 61-69.

55. Hernandez-Pacheco, E., M.D. Mann, P.N. Hutton, D. Singh, and K.E. Martin, *A Cell-Level Model for a Solid Oxide Fuel Cell Operated with Syngas from a Gasification Process.* International Journal of Hydrogen Energy, 2005. **30**: p. 1221-1233.

56. Yakabe, H., M. Hishinuma, M. Uratani, Y. Matsuzaki, and I. Yasuda, *Evaluation and Modeling of Performance of Anode-Supported Solid Oxide Fuel Cell.* Journal of Power Sources, 2000. **86**: p. 9.

57. Cayan, F.N., S.R. Pakalapati, F. Elizalde-Blancas, and I. Celik, *On Modeling Multi-Component Diffusion Inside the Porous Anode of Solid Oxide Fuel Cells Using Fick's Model.* Journal of Power Sources, 2009. **192**: p. 467-474.

58. Chan, S.H. and Z.T. Xia, *Anode Micro Model of Solid Oxide Fuel Cell.* Journal of the Electrochemical Society, 2001. **148**: p. A388-A394.

59. Campanari, S. and P. Iora, *Comparison of Finite Volume SOFC Models for the Simulation of a Planar Cell Geometry.* Fuel Cells, 2005. **5**: p. 34-51.

60. Sanchez, D., R. Chacartegui, A. Munoz, and T. Sanchez, *On the Effect of Methane Internal Reforming Modelling in Solid Oxide Fuel Cells.* International Journal of Hydrogen Energy, 2008. **33**: p. 1834-1844.

61. Aguiar, P., C.S. Adjiman, and N.P. Brandon, *Anode-Supported Intermediate-Temperature Direct Internal Reforming Solid Oxide Fuel Cell - II. Model-Based Dynamic Performance and Control.* Journal of Power Sources, 2005. **147**: p. 136-147.

62. Cao, H., Z. Deng, X. Li, J. Yang, and Y. Qin, *Dynamic Modeling of Electrical Characteristics of Solid Oxide Fuel Cells Using Fractional Derivatives.* International Journal of Hydrogen Energy, 2010. **35**: p. 1749-1758.

63. Xie, Y. and X. Xue, *Transient modeling of anode-supported solid oxide fuel cells.* International Journal of Hydrogen Energy, 2009. **34**: p. 6882-6891.

64. Ki, J. and D. Kim, *Computational model to predict thermal dynamics of planar solid oxide fuel cell stack during start-up process.* Journal of Power Sources, 2010. **195**: p. 3186-3200.

65. Lin, P.H. and C.W. Hong, *On the Start-Up Transient Simulation of a Turbo Fuel Cell System.* Journal of Power Sources, 2006. **160**: p. 1230-1241.

66. Leucht, F., W.G. Bessler, J. Kallo, K.A. Friedrich, and H. Müller-Steinhagen, *Fuel Cell System Modeling for Solid Oxide Fuel Cell/Gas Turbine Hybrid Power Plants, Part I: Modeling and Simulation Framework.* Journal of Power Sources, 2011. **196**: p. 1205-1215.

67. Sedghisigarchi, K. and A. Feliachi, *Dynamic and transient analysis of power distribution systems with fuel Cells-part I: fuel-cell dynamic model.* Energy Conversion, IEEE Transactions on, 2004. **19**: p. 423-428.

68. Damm, D.L. and A.G. Fedorov, *Reduced-order Transient Thermal Modeling for SOFC Heating and Cooling.* Journal of Power Sources, 2006. **159**: p. 956-967.

69. Ghigliazza, F., A. Traverso, A.F. Massardo, J. Wingate, and M. Ferrari, *Generic Real-Time Modeling of Solid Oxide Fuel Cell Hybrid Systems.* Journal of Fuel Cell Science and Technology, 2009. **6**: p. 021312-7.

70. Perry, R. and D. Green, *Perry's Chemical Engineer's Handbook*. 7th ed. 1997, New York, NY: McGraw-Hill.

71. Li, M., J. Brouwer, J.D. Powers, and G.S. Samuelsen, *A Finite Volume SOFC Model For Coal-Based Integrated Gasification Fuel Cell System Analysis*, in *ASME 7th International Fuel Cell Science, Engineering and Technology Conference*, ASME, Editor. 2009, ASME: Newport Beach, CA.

72. Noren, D.A. and M.A. Hoffman, *Clarifying the Butler-Volmer Equation and Related Approximations for Calculating Activation Losses in Solid Oxide Fuel Cell Models.* Journal of Power Sources, 2005. **152**: p. 175-181.

73. ThyssenKrupp, *Crofer22APU Material Data Sheet No. 4046*, ThyssenKrupp, Editor. 2010, ThyssenKrupp: Werdohl, Germany.

74. *JMatPro*. 2005, Sente Software Ltd., Surrey Technology Centre: United Kingdon.

75. Evans, N.D., P.J. Maziasz, J.P. Shingledecker, and Y. Yamamoto, *Microstructure evolution of alloy 625 foil and sheet during creep at 750 °C.* Materials Science and Engineering: A, 2008. **498**: p. 412-420.

76. Turns, S.R., *An Introduction to Combustion: Concepts and Applications*. Second ed. 2002: Mc-Graw Hill.